AD_____

Award Number: DAMD17-98-2-8019

TITLE: New Inhibitors of the Peripheral Site in Acetylcholinesterase that Specifically Block Organophosphorylation

PRINCIPAL INVESTIGATOR: Terrone Rosenberry, Ph.D.

CONTRACTING ORGANIZATION: Mayo Clinic Jacksonville
Jacksonville, Florida 32224

REPORT DATE: November 2001

TYPE OF REPORT: Final

PREPARED FOR: U.S. Army Medical Research and Materiel Command
Fort Detrick, Maryland 21702-5012

REPORT DOCUMENTATION PAGE

Form Approved
OMB No. 074-0188

1. AGENCY USE ONLY (Leave blank)	2. REPORT DATE	3. REPORT TYPE AND DATES COVERED
	November 2001	Final (1 Sep 98 - 31 Aug 01)

4. TITLE AND SUBTITLE
New Inhibitors of the Peripheral Site in Acetylcholinesterase that Specifically Block Organophosphorylation

5. FUNDING NUMBERS
DAMD17-98-2-8019

6. AUTHOR(S)
Terrone Rosenberry, Ph.D.

7. PERFORMING ORGANIZATION NAME(S) AND ADDRESS(ES)
Mayo Clinic Jacksonville
Jacksonville, Florida 32224

E-Mail: Rosenberry@mayo.edu

8. PERFORMING ORGANIZATION REPORT NUMBER

9. SPONSORING / MONITORING AGENCY NAME(S) AND ADDRESS(ES)
U.S. Army Medical Research and Materiel Command
Fort Detrick, Maryland 21702-5012

10. SPONSORING / MONITORING AGENCY REPORT NUMBER

11. SUPPLEMENTARY NOTES
Report contains color

12a. DISTRIBUTION / AVAILABILITY STATEMENT
Approved for Public Release; Distribution Unlimited

12b. DISTRIBUTION CODE

13. ABSTRACT *(Maximum 200 Words)*

Acetylcholinesterase (AChE) is one of the most efficient enzymes known. The AChE active site consists of a narrow gorge with two separate ligand binding sites: an *acylation site* at the bottom of the gorge where substrate hydrolysis occurs and a *peripheral site* at the gorge mouth. In recent studies, we showed that ligands which bind specifically to the peripheral site can slow the rates at which other ligands enter and exit the acylation site, a feature we denoted steric blockade. We also demonstrated that cationic substrates can form a low affinity complex at the peripheral site that accelerates catalytic hydrolysis at low substrate concentrations but results in substrate inhibition at high concentrations because of steric blockade of product release. AChE is inactivated by organophosphates in pesticides and chemical warfare agents because organophosphates can pass through the peripheral site and phosphorylate the catalytic serine in the acylation site. We are investigating the design of cyclic inhibitors that will bind specifically to the peripheral site and present a pronounced steric blockade to organophosphates while allowing selective passage of acetylcholine to the acylation site. Cyclic inhibitors with affinities for the peripheral site in the sub-micromolar range have been identified.

14. SUBJECT TERMS
Acetylcholinesterase, organophosphates, inhibitors, nonequilibrium, analysis, combinational libraries

15. NUMBER OF PAGES
161

16. PRICE CODE

17. SECURITY CLASSIFICATION OF REPORT	18. SECURITY CLASSIFICATION OF THIS PAGE	19. SECURITY CLASSIFICATION OF ABSTRACT	20. LIMITATION OF ABSTRACT
Unclassified	Unclassified	Unclassified	Unlimited

Table of Contents

INTRODUCTION

Acetylcholinesterase (AChE) hydrolyzes the neurotransmitter acetylcholine at extremely high catalytic rates (1). The activity of this enzyme is essential for normal cholinergic transmission and neuromuscular function. Organophosphates (OPs) in chemical warfare agents inactivate AChE and can lead to death through muscular paralysis and seizures. The goal of this project is to identify new drugs that will protect AChE from OP inactivation.

AChE structure. The three dimensional structure of *Torpedo* AChE (2) revealed several important features of the catalytic site (Fig. 1). This narrow gorge, lined with aromatic residues, is about 20 Å deep and penetrates nearly to the center of the 70 kDa catalytic subunit. At the base of the gorge is the *acylation site.* In this site, residue S*200* (italics: *Torpedo* numbering; non-italics: human numbering) is acylated and deacylated during substrate turnover, H*440* and E*327* participate with S*200* in a catalytic triad (E - H - S), and W*84* binds to the trimethylammonium group of acetylcholine as acyl transfer to S*200* is initiated. The *peripheral site* involves other residues including W*279* (3; 4; 5; 6; 7; 8). AChE, like other members of the α/β-hydrolase family, contains an ω loop with boundaries set by a disulfide bond (C*67* – C*94*) (9; 10). Residues from Y*70* through W*84* in this loop extend along one side of the gorge from the peripheral site to the acylation site. This segment includes residue D*72*, which is positioned near a constriction at the boundary between the peripheral site and the acylation site. Ligands can bind selectively to either the acylation or the peripheral sites, and ternary complexes with distinct ligands bound to each site can form (11). Peripheral site ligands that form these ternary complexes include the phenanthridinium derivative propidium and the fasciculins, a family of very similar snake venom neurotoxins comprised of 61-amino acid polypeptides (12;13).

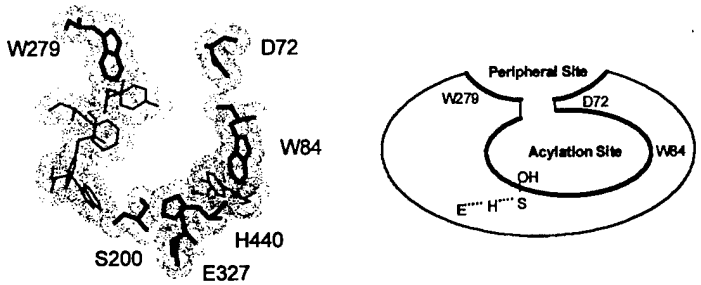

Figure 1. Structure of the AChE active site. *Left panel*, residues from crystal structure that line the active site gorge of *Torpedo* AChE. *Right panel*, schematic representation of the two regions for ligand association within the AChE active site, the acylation and peripheral sites.

Three dimensional structures have been invaluable in providing a framework for understanding AChE function. An excellent model of the transition state for acylation by acetylcholine was provided by (*m*-(N,N,N-trimethylammonio)trifluoroacetophenone (TMTFA). The crystal structure of the TMTFA-AChE complex showed a tetrahedral adduct that nearly superimposed on a calculated structure of acetylcholine in the active site (14). Structures also were obtained of AChE complexes with other ligands bound to the acylation site (15; 16), with fasciculin bound to the peripheral site (16; 14), and with bisquaternary as well as uncharged ligands that span the 12-15 Å distance between the two sites (15; 17). Key residues identified in these structures were altered by site-specific mutagenesis to identify their substrate interactions in the acylation site. For example, F*288* and F*290* form an "acyl pocket" that largely dictates the

acyl group specificity of a substrate (18; 19), and G*121* and G*122* contribute to an oxyanion hole that interacts with the substrate carbonyl group (20).

The catalytic mechanism. The hydrolysis of the neurotransmitter acetylcholine by AChE is one of the most efficient enzyme catalytic reactions known and proceeds at rates close to the limits of diffusion control (1). Despite the wealth of information on the AChE structure and the role of specific residues in catalysis, an understanding of the catalytic mechanism has lagged far behind. As might be expected for an enzyme built for speed, structure determinations have indicated no large conformational changes associated with ligand binding to the acylation site or with fasciculin binding to the peripheral site. In particular, AChE structures have failed to indicate any role for the peripheral site in catalysis, and we have turned to kinetic studies to clarify this role. Studies of AChE catalysis have often started with the classic acyl enzyme mechanism in Scheme 1 (see 21). In this scheme the initial enzyme-substrate complex ***E*S** proceeds to an acylated enzyme intermediate ***E*A** which is then hydrolyzed. However, with acetylcholine and many other cationic substrates, Scheme 1 does not explain a decline in AChE-catalyzed hydrolysis at high substrate concentrations that has long been referred to as substrate inhibition (see 21; Fig. 2A below). Most investigators currently analyze substrate inhibition data with Scheme 2 (*e.g.*, 5).

$$E + S \underset{k_{-S}}{\overset{k_S}{\rightleftharpoons}} ES \xrightarrow{k_2} EA \xrightarrow{k_3} E + \text{Products}$$

SCHEME 1

The **S*E*S** complex in Scheme 2 indicates simultaneous binding of two substrate molecules to the enzyme, and substrate inhibition is generally attributed to a decrease in the acylation rate constant in this ternary complex (*i.e.*, $b < 1$).

$$\begin{array}{ccccc} S + E & \overset{K_M}{\rightleftharpoons} & ES & \xrightarrow{k_{cat}} & E + \text{Products} \\ + & & + & & \\ S & & S & & \\ K_{SS} \Big\uparrow & & K_{SS} \Big\uparrow & & \\ S + SE & \overset{K_M}{\rightleftharpoons} & SES & \xrightarrow{bk_{cat}} & SE + \text{Products} \end{array}$$

SCHEME 2

BODY

Proposals about a role for the peripheral site in AChE catalysis have often been limited by the context presented by Schemes 1 and 2. Many peripheral site ligands inhibit substrate hydrolysis, and AChE inhibition by propidium has been attributed entirely to a conformational change at the acylation site induced by the binding of propidium to the peripheral site (22). As noted below, this conclusion is based on an analysis which assumes that all enzyme intermediates are in equilibrium, and this assumption cannot be justified (1; 23). Our evidence in support of an alternative steric blockade model is presented in the following sections.

A. *Steric blockade occurs with AChE* (24; 25; appendix reprints 1 and 3). AChE can form ternary complexes as shown in Scheme 3. To demonstrate steric blockade, we examined the binding of two reversible ligands (**L**) that equilibrate slowly with the acylation site in the presence and absence of the peripheral site ligand propidium (**I**). The relative association rate constants in the presence of propidium (k_{L2}/k_L) decreased 50- and 380-fold for huperzine A and TMTFA, respectively. The relative dissociation rate constants (k_{-L2}/k_{-L}) also decreased, respectively, by factors of 10 and 60. Thus, the primary effect of bound propidium was to slow the entrance and exit of these ligands from the acylation site.

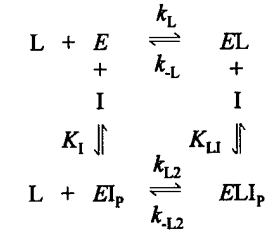

SCHEME 3

Propidium is a noncompetitive inhibitor of substrate hydrolysis by AChE. We next asked whether steric blockade could explain this inhibition. According to the classic mechanism in Scheme 1, the inhibitor (**I**) in principle can bind to each of the three enzyme species as modeled in Scheme 4. For example, $\boldsymbol{E}\mathbf{SI_P}$ represents a ternary complex with **S** at the acylation site and **I** at the peripheral site (denoted by the subscript P). The acylation rate constant k_2 is altered by a factor a in this ternary complex, and the deacylation rate constant k_3 is altered by a factor b in the $\boldsymbol{E}\mathbf{AI_P}$ complex. Unfortunately, for acetylcholine and other carboxylester substrates, these rate constants are too fast to permit direct measurement by any rapid kinetic technique. Consequently, investigations of Scheme 4 have employed steady-state kinetic analyses, and all reports prior to our work have been forced to assume that all the intermediates in Scheme 4 are in equilibrium. This assumption will generate equations that fit the inhibition data, but the approach is problematic. The fit requires that bound inhibitor decrease either acylation ($a < 1$) and/or deacylation ($b < 1$) rates even though there is no independent evidence of such a decrease. Furthermore, the equilibrium assumption is far too limiting. A ligand whose only effect is to induce a steric blockade of substrate association and dissociation ($k_{S2}/k_S = k_{-S2}/k_{-S} < 1$) would show no inhibition according to an equilibrium analysis! We introduced a nonequilibrium treatment of Scheme 4 with a program called SCoP (24). This simulation and curve-fitting program, developed at the NIH National Center for Research Resources, numerically solves differential equations that correspond to a model with a series of

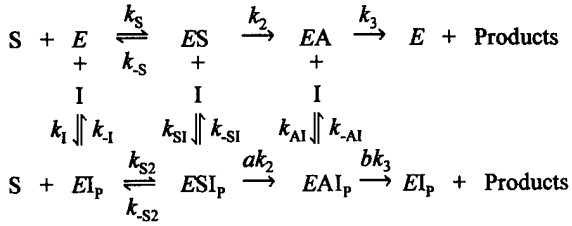

SCHEME 4

chemical reactions. Our steric blockade hypothesis assumes that bound peripheral site ligand in Scheme 4 has no effect on acylation or deacylation rate constants ($a = b = 1$) or on the affinity of ligands at the acylation site ($k_I = k_{SI} = k_{AI}$ and $k_{-I} = k_{-SI} = k_{-AI}$) but only lowers the substrate association and dissociation rate constants ($k_{S2}/k_S = k_{-S2}/k_{-S} = 0.015$). The value of 0.015 gave the best correspondence to the experimental data but also agreed well with the reductions in rate constants for TMTFA when propidium was bound. The simulations reproduced the data quite well at lower substrate concentrations but predicted larger hydrolysis rates than observed at higher substrate concentrations. Application of this steric blockade hypothesis to simulations of inhibition data with another substrate (phenyl acetate) and another peripheral site inhibitor (gallamine) gave similar results (24).

In considering extensions of the nonequilibrium solution to Scheme 4 to remedy this situation, we recognized that steric blockade should apply not only to substrate entry to and exit from the acylation site but also to the exit of product, particularly of an alcohol leaving group the size of thiocholine. For example, if bound propidium at the peripheral site also reduced this product dissociation rate constant k_{-P} to 1.5% of its initial value, then simulated hydrolysis rates agreed with the observed over the entire range of substrate concentrations (25). We concluded that steric blockade by a bound peripheral site ligand can decrease association and dissociation rate constants for substrates and their hydrolysis products and is sufficient to account for noncompetitive inhibition patterns.

B. *The steric blockade model reveals that substrate binding to the peripheral site initiates enzymatic catalysis.* (25; 26; appendix reprints 2 and 5). If substrate itself were to bind to the peripheral site, it occurred to us that this bound substrate could block the release of product and give rise to the substrate inhibition phenomenon noted in the introduction. Before testing this concept, we determined that substrate did in fact bind to the peripheral site by employing a fasciculin competition assay. In this assay, rate constants k_{on} for fasciculin binding were obtained during continuous hydrolysis of an essentially fixed concentration of acetylthiocholine ([S]). Plots of k_{on} *vs.* [S] revealed that k_{on} did decrease at higher [S] (see O in Fig. 2B) and indicated that acetylthiocholine competes with fasciculin. Additional tests confirmed that the competition resulted from acetylthiocholine binding to the peripheral site with an equilibrium dissociation constant (K_S) of 1 – 2 mM (25). To assess whether this binding could lead to substrate inhibition, we formulated a general scheme of substrate hydrolysis with AChE in which substrate can interact at both the acylation

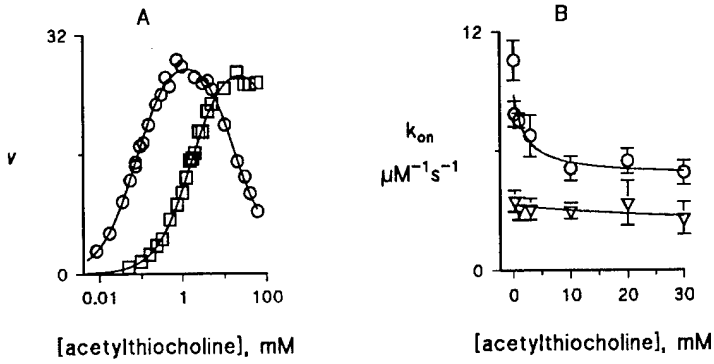

Figure 2. Acetylthiocholine binding to the peripheral site of human AChE (4). *Panel A*. Substrate inhibition with acetylthiocholine. Initial velocities v (uM/min) were measured with recombinant wild type (-O-) or D74G (-□-) AChE (80 pM). Lines were fitted with the SCoP program. *Panel B*: Inhibition of fasciculin 3 binding by acetylthiocholine. Association rate constants k_{on} for fasciculin 3 were measured with recombinant wild type (-O-) or D74G (-▽-) AChE. Lines were obtained by fixing K_S at the value obtained from substrate inhibition before fitting.

and the peripheral sites. This Scheme 5, which includes 9 enzyme intermediates and 22 rate constants, is presented in Appendix 1. By applying our steric blockade model to this scheme, we reduced the number of independent rate constants to 8, and further constraints outlined in Appendix 1 allowed us to fit substrate inhibition profiles with just 3 kinetic parameters, K_S, k_{-P} and k_2. For example, the profile of v *vs.* [S] for acetylthiocholine with wild type human AChE was fitted precisely to give fitted values of $K_S = 1.9 \pm 0.7$ mM and $k_{-P} = (6 \pm 1) \times 10^4$ s^{-1} (Fig. 2A). The fitted K_S and k_{-P} can be compared to independent experimentally predicted values. The predicted k_{-P} (1×10^5 s^{-1}) (25) agreed reasonably with the fitted k_{-P} value here, and the K_S predicted from fasciculin competition (1.3 ± 1.0 mM from Fig. 2B) also agreed well with the fitted K_S.

The quantitative agreement between the K_S obtained by fitting the substrate inhibition profile and that measured by fasciculin competition was reassuring, but we investigated whether such agreement would extend to other AChEs. We first constructed, expressed and examined the human D74G mutant, because D74 may be the key residue in defining peripheral site binding of acetylthiocholine. It is one of the few important residues in the peripheral site that does not make direct contact with bound fasciculin (16; 14), and space adjacent to D74 may accommodate acetylthiocholine in a ternary complex with fasciculin (26). If this idea is correct, K_S should increase dramatically in D74G mutants. With the human D74G enzyme in Fig. 2A, substrate inhibition in fact was decreased to such an extent that we were forced to fix k_2 to the value obtained for wild type human AChE and fit only K_S and k_{-P}. Average fitted values of $K_S = 33 \pm 8$ mM and $k_{-P} = (9 \pm 3) \times 10^4$ s^{-1} were obtained. The 20-fold increase in K_S with the D74G mutant was sufficient to nearly abolish substrate inhibition. Of particular importance, this increase in K_S was supported by the fasciculin competition data for the human D74G mutant in Fig. 2B. Values of k_{on} did not differ significantly as acetylthiocholine ranged from 0.1 to 30 mM, and the data was fitted by assigning a fixed K_S of 33 mM from the substrate inhibition data. Good correlations between K_S obtained by fitting substrate inhibition curves with K_S determined by competition with fasciculin also were obtained with purified AChEs from *Torpedo* (26). For wild type *Torpedo* AChE these respective K_S values were 0.5 ± 0.2 mM and 0.4 ± 0.2 mM, while for D72G *Torpedo* AChE these respective K_S values were 10 ± 1 mM and 4 ± 2 mM. The agreement between K_S values determined by the two procedures provides strong support for the application of the steric blockade model to substrate inhibition data.

C. *Steric blockade and organophosphorylation.* (27; 26; appendix reprints 3 and 5). A key feature of the steric blockade model is that ligand binding to the peripheral site results in significant inhibition only if substrate fails to reach equilibrium binding prior to reaction at the acylation site. According to this model, the reactions of substrates that are thought to form equilibrium complexes at the acylation site should be unaffected by peripheral site ligands and, therefore, provide a test of the model. Among these substrates are the organophosphates (OPs), a class of compounds that inactivate cholinesterases because they are poor substrates (28; 29; 30). OPs readily phosphorylate the active site serine of AChE, but very slow hydrolysis of this phosphoryl enzyme results in essentially irreversible inactivation of the enzyme (31). We monitored the AChE reactions of two fluorogenic OPs by the appearance of their fluorescent leaving groups with stopped flow fluorometry (27; 26). EMPC (7-[(methylethoxyphosphonyl)oxy]-4-methylcoumarin) is a neutral OP, and DEPQ (7-[(diethoxyphosphoryl)oxy]-1-methylquinolinium iodide) is cationic. The release of product

from each OP occurred primarily in one large phase that was fitted to an exponential time course with rate constant k (27). Data were analyzed according to Scheme 4, and the dependence of k on the OP concentration was fitted to eq. 1 to give k_{OP} and k_{OP}/K_{OP}, the respective first- and second-order rate constants of phosphorylation. In the presence of a saturating concentration of **I**, $k_{OP} = ak_2$ (27; 26), where the parameter a indicates the relative efficiency of first-order phosphorylation when **I** is bound to the peripheral site.

$$k = \frac{k_{OP}[OP]}{K_{OP} + [OP]} \quad \text{(eq. 1)}$$

The phosphorylation rate constants in fact were affected by the peripheral site ligands propidium and fasciculin (Table 1), in apparent conflict with our steric blockade model. One effect was that propidium increased K_{OP} for both EMPC and DEPQ by about an order of magnitude for both OPs. This effect was readily explained: Computer modeling revealed a clear unfavorable steric overlap between propidium in the peripheral site and the leaving group of either EMPC or DEPQ in the acylation site (27; 32). The steric blockade model assumes no interaction between ligands in the ternary complex, and adjustments to this model are required if steric or electrostatic interaction occurs. Ligand affinities should not affect k_{OP}, the first order phosphorylation constant and, in agreement with the model, bound propidium had no significant effect on k_{OP} for DEPQ. However, bound propidium had a pronounced effect on k_{OP} for EMPC, increasing a by at least a factor of 5. An acceleration of k_{OP} by bound peripheral site ligands also was recently reported by Radic and Taylor (33). It may be possible to reconcile this increase with the steric blockade model, but it raises the possibility of an additional mechanism of communication between the peripheral and acylation sites.

Table 1. Phosphorylation of wild type AChE by fluorogenic OPs

Structure	Inhibitor	k_{OP}		K_{OP}
		min^{-1}	a	μM
EMPC 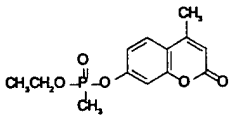	None	150 ± 11	—	224 ± 24
	Propidium	570 ± 140	5 ± 2	1260 ± 350
	Fasciculin	0.23 ± 0.08	0.002	220 ± 110
DEPQ 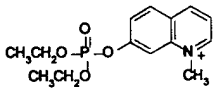	None	1600 ± 200	—	7.5 ± 1.3
	Propidium	1200 ± 400	0.7 ± 0.4	85 ± 30
	Fasciculin	0.66 ± 0.10	0.0003	700 ± 140

The consequences of fasciculin binding to the peripheral site of wild type AChE on phosphorylation kinetic parameters for EMPC and DEPQ were qualitatively different from those of propidium. Values of k_{OP}/K_{OP} were decreased by factors of 10^3 to 10^5, and k_{OP} was decreased by factors of 300 to 4000 (Table 1). We have shown that fasciculin presents a substantial steric blockade to the entrance and exit of ligands that bind to the acylation site: Association and dissociation rate constants for the binding of N-methylacridinium were decreased 8000- and 2000-fold, respectively, when fasciculin was bound (34). However, steric blockade of OP association and dissociation rate constants cannot account for these effects on the phosphorylation rate constants. The pronounced fasciculin inhibition of AChE phosphorylation requires an additional interaction between fasciculin and the acylation site. Since the three-dimensional structures of the fasciculin-AChE complexes show no penetration of the acylation site by fasciculin that would lead to unfavorable steric overlap with these OPs (8; 7), the additional interaction is likely to involve a conformational change in the acylation site induced by bound fasciculin .

D. *Recombinant AChE expression system.* (35; appendix reprint 6). Our progress has been aided by the success of this system, which utilizes the Schneider 2 (S2) *Drosophila* cell line and an expression vector with an actin promoter. With this system, stable transfectants of secretion constructs of dimeric *Drosophila* AChE were found to accumulate up to 50 μg/ml of AChE in media after 10-14 days of culture (36). Our ability to purify large quantities of this AChE (~ 100 mg) by affinity chromatography resulted in the establishment of a collaboration with the protein crystallography lab of Dr. Joel Sussman at the Wiezmann Institute in Israel. A structure has recently been obtained (35; appendix reprint 6). We have adapted this system for expression of a soluble dimeric form of recombinant human AChE. Several dozen mg of wild type human AChE, D74G and other mutant constructs have been purified for use in our current studies (27; 26), and the Sussman group is carrying out crystallization efforts with several of these constructs as noted in the Experimental Plan and Methods.

E. *Huprine X is a novel high affinity inhibitor of AChE.* (37; appendix reprint 5). Inhibitors of the enzyme acetylcholinesterase slow and sometimes reverse the cognitive decline experienced by individuals with Alzheimer's disease. Huperzine A, a natural product used in traditional Chinese herbal medicine, and tacrine (Cognex®) are among the potent acetylcholinesterase inhibitors used in this treatment, but the search for more selective inhibitors continues. We have synthesized and characterized (-)-12-amino-3-chloro-9-ethyl-6,7,10,11-tetrahydro-7,11-methanocycloocta[*b*]quinoline hydrochloride (huprine X), a hybrid that combines the carbobicyclic substructure of huperzine A with the 4-aminoquinoline substructure of tacrine. Huprine X inhibited human acetylcholinesterase with an inhibition constant K_I of 26 pM, indicating that it binds to this enzyme with one of the highest affinities yet reported. Under equivalent assay conditions, this affinity was 180 times that of huperzine A, 1200 times that of tacrine, and 40 times that of E2020 (donepezil, Aricept®), the most selective acetylcholinesterase inhibitor currently approved for therapeutic use. The association and dissociation rate constants for huprine X with acetylcholinesterase were determined, and the location of its binding site on the enzyme was probed in competition studies with the peripheral site inhibitor propidium and the acylation site inhibitor edrophonium. These data indicated that huprine X binds to the enzyme acylation site in the active site gorge but interferes slightly with the binding of peripheral site ligands. A high affinity inhibitor like huprine X also may be useful as a potential protective agent against OP inactivation, and future studies to examine this point may be warranted.

F. *Thioflavin T is a fluorescent probe of the acetylcholinesterase peripheral site that reveals conformational interactions between the peripheral site and the acylation site.*(38; appendix reprint 9). Changeux (39) was among the first to appreciate that AChE contained two distinct ligand binding sites and that allosteric interactions between ligands bound at these sites might involve conformational changes in the protein molecule. However, evidence for such conformational interactions has been difficult to obtain. We have found that thioflavin T, a fluorophore widely used to detect amyloid structure in proteins, binds selectively to the P site of AChE with an equilibrium dissociation constant of 1 μM. The fluorescence of the bound thioflavin T increased more than 1000-fold over that of unbound thioflavin T, making thioflavin T one of the best fluorescent probes of AChE yet discovered. Furthermore, when A site ligands like edrophonium or TMTFA formed ternary complexes with AChE and thioflavin T, the fluorescence was quenched by factors of 3 to 4. The observation of this partial quenching of

thioflavin T fluorescence is a major advance in the study of AChE for two reasons. First, it allows thioflavin T to be used as a reporter for ligand reactions at the A site. Second, it indicates that ligand binding to the A site initiates a change in the local AChE conformation at the P site that quenches the fluorescence of bound thioflavin T. The data provide the strongest evidence in support of a conformational interaction between the two AChE sites yet obtained.

G. *Cyclic ligands as selective inhibitors of organophosphorylation.* (40; appendix preprint 8). Our progress outlined above in demonstrating how peripheral site ligands inhibit AChE activity has led us to pursue a new strategy for protection against OP inactivation of AChE. This strategy is to design an inhibitor that will bind to the peripheral site and impose a steric blockade that is selective for OPs and thus protective against OP toxicity. Such an inhibitor must exclude OPs from the acylation site while interfering minimally with acetylcholine passage. Our search for such ligands has focused on cyclic peptide and pseudopeptide compounds. Cyclic molecules have a variety of advantages that we intend to exploit during the course of our studies. First, a cyclic molecule is a ring with a pore that in theory can be designed to exclude passage of bulky OPs while allowing smaller acetylcholine to pass. Relatively small cyclic compounds consisting of 6 to 8 amino acids possess the necessary space to permit passage of acetylcholine. Second, the incorporation of both natural and unnatural amino acids using combinatorial methods allows for synthesis of an enormous number of cyclic compounds in libraries of various size. Furthermore, cyclic peptides are conformationally constrained, an asset in molecular modeling studies.

Our initial efforts focused on large libraries of several hundred cyclic peptides with random amino acid sequences. We examined the effect of ring size (5- to 9-member cyclic peptides), peptide backbone (D- amino acids, L- amino acids, unnatural peptide linkages (thioether, aminosubstituted)), and amino acid side chain composition (charge, hydrophobicity, and aromaticity). Several sets of peptides indicated AChE binding at high total peptide concentrations (100 μM), and common features began to emerge. First, most of the libraries that gave positive results possessed amino acid sequences with positively charged residues. Second, there was a clear preference in binding and inhibitory activity for libraries with 7- and 8-residue cyclic peptides. The diversity of libraries identified in this screening procedure was very encouraging, as it demonstrated that numerous different amino acid sequences have potential as AChE peripheral site specific inhibitors.

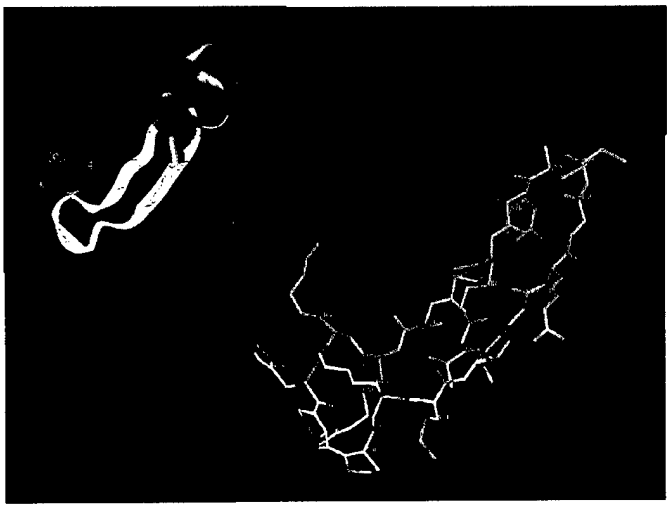

Figure 3. Structure of fasciculin and fasciculin loop II as taken from the AChE-fasciculin crystal structure. *Upper panel*, structure of fasciculin with individual loops colored in green (I), yellow (II), and red (III). *Lower panel*, structure of loop II of fasciculin with AChE contact residues colored to indicate degree of buried surface in the AChE-fasciculin interface (*red* being completely buried and *blue* being solvent exposed).

With the information gained from our initial screening of random peptide libraries, we initiated the directed design of the next series of cyclic compound libraries using fasciculin as a prototype. Fasciculin serves as an excellent example of the kind of AChE inhibitor that would be necessary for the protection of the enzyme from OPs. Fasciculin is specific for the peripheral site and displays an impressive affinity for the enzyme (K_D ~ 10 - 20 pM) (12; 41). Furthermore, the structure of fasciculin consists of three finger-like loops protruding from a central disulfide linked core (Fig. 3) (42). Previous studies have shown that disulfide linked cyclic peptides based on the loops of fasciculin could bind to AChE and inhibit enzyme activity, but with low affinities (~15 μM) that were 10^5 times smaller than the natural toxin (43). We have employed molecular modeling using the crystal structure of the AChE-fasciculin complex (7; 8) to design individual cyclic peptides and peptide mixtures based on the primary amino acid sequence of loop II of fasciculin (Fig. 3). This loop displays the greatest area of contact with the AChE peripheral site. Our initial efforts focused on cyclic peptides based on the fasciculin primary sequence of cyclo[Arg-Arg-His-Pro-Pro-Lys-Met-Xxx], where Xxx is the cyclization residue (Asp, Asn, Glu, or Gln). Closer examination of the AChE-fasciculin crystal structure indicated that Arg^2, Lys^6, and Xxx do not make direct contact with the enzyme surface. We varied these residues to evaluate the effect of different side chains or peptide linkages on cyclic peptide activity. In addition, novel amino acids (nor-leucine (Nle) and napthylalanine (Nal)) were inserted in an attempt to improve inhibitor potency by altering peptide hydrophobicity and conformational flexibility. To insure that we were accurately assessing peptide concentrations, we instituted routine amino acid analysis with the analyzer in our laboratory of all individual new peptides. These analyses allowed us to establish extinction coefficients for each peptide (*e.g.*, $\varepsilon_{224\,nm} = 90{,}000 - 110{,}000\ M^{-1}cm^{-1}$ for the compounds in Table 2) and thus use absorbance measurements to determine peptide concentrations. The amino acid analyses also served as a check on quality control of the peptides, as even trace amounts of extraneous amino acids can be detected, and complemented the mass spectrometry analysis initially used to characterize individual peptides. Inhibitory peptides identified as promising candidates from initial screening assays were analyzed to determine their K_I for AChE (Table 2). Results indicated that cyclic peptide structures with a net positive charge, a Gln cyclization residue and a napthylalanine residue at position 2 or 7 displayed the best inhibitory activity with AChE. Furthermore, cyclic peptides outperformed linear molecules, and our screening assay accurately predicted the rank-order of K_I values measured for active peptide inhibitors (Table 2).

Octapeptide Inhibitors at the AChE Peripheral Site

Peptide Sequence								Percent Inhibition, Initial Screen				KI
1	2	3	4	5	6	7	8	Activity		Fas Binding		
								10 μM	1 μM	10 μM	1 μM	μM
Fasciculin												
R	R	H	P	P	K	M						
cyclic peptides												
R	L-Nal	H	P	P	K	M	Q	79	40	52	14	0.2
R	A	H	P	P	K	L-Nal	Q	78	28	62	23	1
R	A	H	P	P	K	D-Nal	Q	68	21	50	7	1.5
R	D-Nal	H	P	P	K	M	Q	65	27	54	27	1.1
R	A	H	P	P	K	M	Q	51	16	53	36	2
R	A	H	P	P	K	M	N	29	5	15	0	6.4
linear peptide												
R	A	H	P	P	K	Nle	Q	18	12	20	26	14.4

Table 2. Summary data from the best cyclic and linear peptide compounds tested to date.

As shown in Table 2, by using information from fasciculin in the directed design of novel, cyclic peripheral site AChE inhibitors, we have generated a class of compounds with low

micromolar to high nanomolar affinity for the enzyme peripheral site. We continue to focus our efforts on improving peptide inhibitor affinity for AChE. Current efforts are directed toward the synthesis of individual peptides and peptide mixtures that incorporate alternate amino acid sequences and chemistries. These new peptides also include residues that allow chemical structures which are more conformationally restrained (using substituted amino acids or disulfide bonds). We will also include the use of positional scanning and library deconvolution to assess the effect of amino acid composition. These methods have been used previously to rediscover a naturally occurring peptide ligand from large combinatorial libraries (44). Proprietary

We are also interested in developing a supplemental strategy for studying our cyclic peptides that specifically focuses on the proper orientation of the peptides at the mouth of the gorge. Recently, Boyd et al., (45) have reported the use of cysteine substitution mutagenesis, followed by labeling the resulting reactive thiol with methanethiosulfonate (MTS) compounds or fluorescent probes, to identify and characterize functionally important residues in AChE. One of the AChE mutants that we have made is a cysteine substitution at the gorge rim (His^{287}) or H287C. An MTS substituent would provide a means of tethering the cyclic peptides through a linker to this cysteine residue. Therefore, if inhibition occurs we would have more confidence that our peptides were in the vicinity of the mouth of the gorge and not somewhere else on the enzyme. In preliminary kinetic experiments with H287C we found that the catalytic activity of acetylthiocholine hydrolysis is preserved. We have begun our testing of MTS modification of the H287C mutant and will evaluate the different MTS reagents available (see Fig.4) to determine the optimum compound for labeling H287C. Additionally, we have begun preliminary experiments establishing conditions for the introduction of MTS groups into the peptide molecule. Initial results indicate that the ε amino group of Lys could be a good candidate for the linker attachment. We have evaluated the interaction of N-succinimidyloxycarbonylethyl methanethiosulfonate (MTS-3-NHS) with Boc-Lys-OFm and also with Boc-Lys-NH_2. Both expected derivatives were confirmed by HPLC and MALDI-TOF-MS analysis and determined to be stable. Finally, we are developing a similar conversion of Lys containing cyclic peptides to their MTS derivatives through a similiar interaction with MTS-3-NHS.

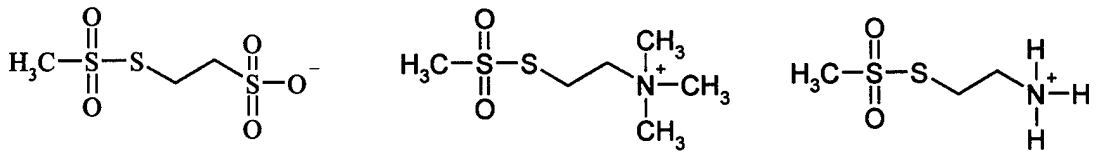

MTSES MTSET MTSEA

Figure 4. Structures of MTS compounds used in cysteine labeling: MTSES, sodium (2-sulfonatoethyl)-methanethiosulfonate; MTSET, 2-(trimethylammonium)ethyl methanethiosulfonate bromide; MTSEA, 2-aminoethyl methanethiosulfonate hydrobromide.

KEY RESEARCH ACCOMPLISHMENTS

- Expanded our nonequilibrium analysis of the effect of peripheral site ligands on organophosphorylation of AChE with experimentation and computational analysis with the SCoP numerical integration program.

- Completed our analysis of the D74 residue located near the peripheral site of AChE. Our results with the D74G mutant confirm our hypothesis that acetylcholine initially binds transiently to the peripheral site near residue D74.

- Demonstrated that D74 is important in conveying to the acylation site an inhibitory conformational effect induced by the binding of fasciculin to the peripheral site.

- Established of a productive collaboration with the protein crystallography laboratory of Dr. Joel Sussman. We have successfully produced large quantities of purified wild type and mutant AChE's from our Schneider 2 Drosophila cell line and provided these constructs to Dr. Sussman's group for crystallography studies.

- Characterized a novel AChE inhibitor, huprine X, which is a hybrid of huperzine A and tacrine. With a K_I = 26 pM it represents the most selective AChE inhibitor currently approved for therapeutic use. This inhibitor may be useful as a potential protective agent against OP activation and may provide an important tool for refining our models.

- Demonstrated for the first time that thioflavin T, a fluorophore widely used to detect amyloid structure in proteins, binds selectively to the AChE peripheral site. Bound thioflavin T exhibited a more than 1000-fold increase in fluorescence over that of unbound thioflavin T. In the presence of acylation site ligands, only partial quenching of fluorescence was observed.

- Continued our development of cyclic peptides that compete with fasciculin for binding at the peripheral site. To date we have synthesized and tested 124 peptides for competition with AChE and fasciculin. We have generated a class of compounds with low micromolar to high nanomolar affinity for the enzyme peripheral site.

- Initiated a supplemental strategy to localize cyclic peptides near the AChE peripheral site. We have expressed H287C, a mutation near the peripheral site, and designed cyclic peptides that incorporate a methanethiosulfonate (MTS) substituent. Reaction of the MTS peptides with H287C will tether the peptides and allow us to evaluate their blockade of the AChE active site.

REPORTABLE OUTCOMES

PAPERS

Szegletes, T., Mallender, W. D. and Rosenberry, T. L. (1998). Nonequilibrium analysis alters the mechanistic interpretation of inhibition of acetylcholinesterase by peripheral site ligands. *Biochemistry* **37**: 4206-4216

Romanovskis, P. and Spatola, A.F. (1998). Preparation of head-to-tail cyclic peptides via side chain attachment: Implications for library synthesis. *J. Peptide Res.* **52**, 356-374.

Szegletes, T., Mallender, W. D., Thomas, P. J. and Rosenberry, T. L. (1999). Substrate binding to the peripheral site of acetylcholinesterase initiates enzymatic catalysis. Substrate inhibition arises as a secondary effect. *Biochemistry* **38**: 122-133

Mallender, W. D., Szegletes, T. and Rosenberry, T. L. (1999). Organophosphorylation of acetylcholinesterase in the presence of peripheral site ligands: Distinct effects of propidium and fasciculin. *J. Biol. Chem.* **274**: 8491-8499

Camps, P., Cusack, B., Mallender, W.D., El Achab, R., Morral, J., Muñoz-Torrero, D., and Rosenberry, T.L. (2000). Huprine X is a novel high affinity inhibitor of acetylcholinesterase that is of interest for the treatment of Alzheimer's disease. *Mol. Pharmacol.* **57**, 409-417.

Mallender, W.D., Szegletes, T., and Rosenberry, T.L. (2000). Acetylthiocholine binds to Asp74 at the peripheral site of human acetylcholinesterase as the first step in the catlytic pathway. *Biochemistry* **39**, 7753-7763.

Harel, M., Kryger, G., Rosenberry, T.L., Mallender, W.D., Lewis, T., Fletcher, R.J., Guss, J.M., Silman, I., and Sussman, J.L. (2000). 3D Structure of Drosophila melanogaster acetylcholinesterase and of its complexes with putative insecticides. *Protein Science* **9,** 1063-1072.

Romanovskis, P. and Spatola, A.F. (2000). Head-to-Tail Cyclic Peptides and Cyclic Peptide Libraries, In: *The Amide Linkage: Significance in Chemistry, Biochemistry, and Materials Science*, Arthur Greenberg, Curt Breneman, and Joel F. Liebman, Editors, John Wiley, pp. 519-564.

Rosenberry, T.L., Mallender, W.D., Cusack, B., Szegletes, T., Romanovskis, P. and Spatola, A.F. (2000). In: *Proceedings of the Bioscience 2000 Medical Defense Review,* Hunt Valley, Maryland, June 4-9, 2000. In press.

De Ferrari, G.V., Mallender, W.D., Inestrosa, N.C., and Rosenberry, T.L. (2001). Thioflavin T is a fluorescent probe of the acetylcholinesterase peripheral site that reveals conformational interactions between the peripheral and the acylation sites. *J. Biol. Chem.,* **276**, 23282-23287.

Johnson J.L., Davies M.P., Venkatasubban K.S., Cusack B., Mallender W.D., Rosenberry, T.L. (2001). Characterization of a human acetylcholinesterase mutant that exhibits substrate activation kinetics. *Biophysical Journal.* **80:** (1) 1147 , Part 2.

ABSTRACTS

Mallender, W.D., Ma, W., Spatola, A.F., and Rosenberry, T.L. (1999) Directed design of novel high affinity, peripheral site acetylcholinesterase ligands to defend the enzyme against inactivation by organophosphates. *Biochemistry and Molecular Biology 99, American Society for Biochemistry and Molecular Biology*, May 1999.

Romanovskis, P. and Spatola, A.F. (1999) Cyclic peptides with α, α-isubstituted glycine derivatives. *16th American Peptide Symposium*, July 1999.

Mallender, W.D., Ma, W., Spatola, A.F., and Rosenberry, T.L. (1999). Directed design of novel high affinity, peripheral site acetylcholinesterase ligands to defend the enzyme against inactivation by organophosphates. *Faseb J.* **13**, A1350

Mallender, W.D., Romanovskis, P., Cusack, B., Ma, W., Spatola, A.F., and Rosenberry, T.L. Directed Design of novel high affinity, peripheral site acetylcholinesterase ligands to defend the enzyme against inactivation by organophosphates. *Mayo Research Forum* 1999.

Mallender, W.D., Cusack, B., Romanovskis, P., Spatola, A.F., and Rosenberry T.L. Design and screening of novel, high affinity peripheral site acetylcholinesterase ligands to prevent enzyme inactivation by organophosphate chemical warfare agents. *Bioscience 2000 Medical Defense Review*, June, 2000.

Rosenberry, T.L., Mallender, W.D., Cusack, B., Szegletes, T., Romanovskis, R., and Spatola, A.F. Inhibitors of the acetylcholinesterase peripheral site may protect against organophosphate toxicity. *Bioscience 2000 Medical Defense Review*, June, 2000.

Romanovskis, P., Rosenberry, T.L., Cusack, B., Spatola, A.F. Cyclic octapeptide inhibitors of the acetylcholinesterase peripheral site: Implications for inhibition of nerve toxins. *Institute for Molecular Diversity and Drug Design Symposium*, 2000.

Romanovskis, P., Rosenberry, T.L., Cusack, B., Spatola, A.F. Surprising by-product formation during SPPS of linear, cyclic, and novel bicyclic peptides as AChE inhibitors. 2001.

Johnson, J.L, Davies, M.P., Venkatasubban, K.S., Cusack, B., Mallender, W.D., Rosenberry, T.L. Characterization of a human acetylcholinesterase mutant that exhibits substrate activation kinetics. *Biophysical Society Annual Meeting,* February, 2001, Boston, MA.

Cusack, B.M., Mallender, W.D., Johnson, J.L., Romanovskis, P., Spatola, A.F. and Rosenberry, T.L.a novel class of cyclic peptides: possible protective agents for defense against organophosphate inactivation of acetylcholinesterase. *Enzyme 2001*, June, 2001. Orlando, FL.

Rosenberry, T. L., Johnson, J. L., Davies, M. P., Cusack, B. M., Mallender, W. D., and Szegletes, T. Unmasking tandem site cooperation in acetylcholinesterase. *Enzyme 2001*, June, 2001. Orlando, FL.

Romanovskis, P., Rosenberry, T.L., Cusack, B., and Spatola, A.F. Surprising by-product formation during SPPS of linear, cyclic, and novel bicyclic peptides as AchE inhibitors. *Peptides: The Wave of the Future.* 2nd International Peptide Symposium in conjunction with the 17th American Peptide Symposium, June 9-14, 2001 San Diego, California

Romanovskis, P., Rosenberry, T.L., Cusack, B., and Spatola, A.F. Cyclic octapeptide inhibitors of the acetylcholinesterase peripheral site: Implications for inhibition of nerve toxins. *Peptides: The Wave of the Future.* 2nd International Peptide Symposium in conjunction with the 17th American Peptide Symposium, June 9-14, 2001 San Diego, California

PATENTS

Spatola, A.R., Darlak, K., Wen, J.J., and Romanovskis, P. Cyclic peptide mixtures via side chain or backbone attachment and solid phase synthesis. US Patent # 6,008,058, 12/28/1999

FUNDING APPLIED FOR BASED ON THIS RESEARCH

NIH, Modular Research Grant , "Interactions in the Active Site of Acetylcholinesterase", PI: T.L. Rosenberry, Ph.D. Submitted November, 2001.

Muscular Dystrophy Association, "Assess the role of ligand binding to peripheral sites near the AChE active site gorge by kinetic analysis", PI: T.L. Rosenberry, Ph.D. Submitted July, 2000.

United States Army Medical Research and Material Command, "Acetylcholinesterase peripheral site and development of new inhibitors that specifically block organophosphorylation", PI: T.L. Rosenberry, Ph.D., Proposal submitted November, 2000.

EMPLOYMENT OPPORTUNITIES APPLIED FOR AND RECEIVED ON EXPERIENCE SUPPORTED BY THIS AWARD

William D. Mallendar, Ph.D., Scientist II, Enzymology-Assay Department, Millenium Pharmaceuitcal Co., September, 2000.

CONCLUSIONS

We have focused our efforts on the introduction and confirmation both by experimentation and computer simulation, of an alternative nonequilibrium analysis of the steady-state inhibition patterns of AChE. During the past year we have expanded our nonequilibrium analysis of the effect of peripheral site ligands on organophosphorylation of AChE. An examination of the binding of two reversible ligands (huperzine A and TMTFA) that equilibrate slowly with the acylation site in the presence and absence of the peripheral site ligand propidium, revealed a decrease in both the relative association and dissociation rate constants. We introduced a nonequilibrium treatment of the rate constants with the SCoP program. Using this simulation and curve-fitting program, we simulated the data quite well. However, we also investigated whether such agreement would extend to other AChEs. Since the D74 residue may be one of the few key residues in the peripheral site that does not make direct contact with bound fasciculin, we constructed, expressed and examined the D74G mutant in detail. Our results with the D74G mutant confirmed our hypothesis that acetylcholine initially binds transiently to the peripheral site near residue D74. Additionally, we observed that D74 is important in conveying (to the acylation site) an inhibitory conformational effect induced by the binding of fasciculin to the peripheral site. Our success with the expression of this mutant in the Schneider 2 *Drosophila* cell line has resulted in a productive collaboration with Dr. Joel Sussman. We have been able to provide his crystallography laboratory with mg quantities of this mutant as well as other AChE mutants and the wild type enzyme. This collaboration has already resulted in a major publication describing the 3D structure of *Drosophila* AChE (see reportable outcomes).

We have also been very fortunate to characterize a novel AChE inhibitor, huprine X. With a pM affinity, this inhibitor in not only the most potent and selective AChE inhibitor to date, but also may be useful as a potential protective agent against OP activation. Further experiments will be needed to completely define this role. Another major finding has been the work done with the fluorophore, thioflavin T, which has been used to detect amyloid structure in proteins. Surprisingly, we found that thioflavin T binds selectively to the AChE peripheral site. Even more interesting is the observation that in the presence of acylation site ligands, thioflavin T binding is only partially decreased.

Our work with the cyclic peptides has expanded to include more than 124 compounds. We have explored novel amino acids, positional changes, varied length and cyclization residues. To date, we have found that a naphthylalanine substitution in position 2 of a cyclic octapeptide provides mid-nanomolar affinity at AChE inhibition, and competes with fasciculin for binding at the peripheral site. Further modifications including rigidifying the molecule and modifying side chains are planned, in addition to the use of positional scanning and library deconvolution. Finally, we have begun preliminary experiments with the H287C mutant followed by labeling the resulting reactive thiol with MTS compounds. By attaching the cyclic peptides through a linker to the MTS moiety, we will have more confidence that our peptides are in the vicinity of the mouth of the gorge and not somplace else on the enzyme. This novel approach should provide for more accurate screening of compounds at the AChE peripheral site.

REFERENCES

1. Rosenberry, T. L. (1975). Acetylcholinesterase. In: **Advances in Enzymology, 43** (Meister, A., ed.), John Wiley & Sons, New York, pp. 103-218

2. Sussman, J. L., Harel, M., Frolow, F., Oefner, C., Goldman, A., Toker, L. and Silman, I. (1991). Atomic structure of acetylcholinesterase from *Torpedo californica*: A prototypic acetylcholine-binding protein. *Science* **253**: 872-879

3. Weise, C., Kreienkamp, H.-J., Raba, R., Pedak, A., Aaviksaar, A. and Hucho, F. (1990). Anionic subsites of the acetylcholinesterase from Torpedo californica: affinity labelling with the cationic reagent N,N-dimethyl-2-phenyl-aziridiuim. *EMBO J.* **9**: 3885-3888

4. Schalk, I., Ehret-Sabatier, L., Bouet, F., Goeldner, M. and Hirth, C. (1992). Structural analysis of acetylcholinesterase ammonium binding sites. In: **Multidisciplinary Approaches to Cholinesterase Functions** (Shafferman, A. and Velan, B., ed.), Plenum Press, New York, pp. 117-120

5. Radic, Z., Pickering, N. A., Vellom, D. C., Camp, S. and Taylor, P. (1993). Three distinct domains in the cholinesterase molecule confer selectivity for acetyl- and butyrylcholinesterase inhibitors. *Biochemistry* **32**: 12074-12084

6. Barak, D., Kronman, C., Ordentlich, A., Ariel, N., Bromberg, A., Marcus, D., Lazar, A., Velan, B. and Shafferman, A. (1994). Acetylcholinesterase peripheral anionic site degeneracy conferred by amino acid arrays sharing a common core. *J. Biol. Chem.* **269**: 6296-6305

7. Harel, M., Kleywegt, G. J., Ravelli, R. B. G., Silman, I. and Sussman, J. L. (1995). Crystal structure of an acetylcholinesterase-fasciculin complex: interaction of a three-fingered toxin from snake venom with its target. *Structure* **3**: 1355-1366

8. Bourne, Y., Taylor, P. and Marchot, P. (1995). Acetylcholinesterase inhibition by fasciculin: Crystal structure of the complex. *Cell* **83**: 503-512

9. Velan, B., Barak, D., Ariel, N., Leitner, M., Bino, T., Ordentlich, A. and Shafferman, A. (1996). Structural modifications of the ω loop in human acetylcholinesterase. *FEBS Lett.* **395**: 22-28

10. Ollis, D. L., Cheah, E., Cygler, M., Dijkstra, B., Frolow, F., Franken, S. M., Harel, M., Remington, S. J., Silman, I., Schrag, J., Sussman, J. L., Verschueren, K. H. G. and Goldman, A. (1992). The alpha/beta hydrolase fold. *Protein Eng.* **5**: 197-211

11. Taylor, P. and Lappi, S. (1975). Interaction of fluorescence probes with acetylcholinesterase. The site and specificity of propidium binding. *Biochemistry* **14**: 1989-1997

12. Karlsson, E., Mbugua, P. M. and Rodriguez-Ithurralde, D. (1984). Fasciculins, anticholinesterase toxins from the venom of the green mamba Dendroaspis angusticeps. *J. Physiol. (Paris)* **79**: 232-240

13. Marchot, P., Khelif, A., Ji, Y.-H., Masnuelle, P. and Bourgis, P. E. (1993). Binding of ^{125}I-fasciculin to rat brain acetylcholinesterase. The complex still binds diisopropyl fluorophosphate. *J. Biol. Chem.* **268**: 12458-12467

14. Harel, M., Quinn, D. M., Nair, H. K., Silman, I. and Sussman, J. L. (1996). The X-ray structure of a transition state analog complex reveals the molecular origins of the catalytic power and substrate specificity of acetylcholinesterase. *J. Am. Chem. Soc.* **118**: 2340-2346

15. Harel, M., Schalk, I., Ehret-Sabatier, L., Bouet, F., Goeldner, M., Hirth, C., Axelsen, P. H., Silman, I. and Sussman, J. L. (1993). Quaternary ligand binding to aromatic residues in the active-site gorge of acetylcholinesterase. *Proc. Natl. Acad. Sci. USA* **90**: 9031-9035

16. Raves, M. L., Harel, M., Pang, Y.-P., Silman, I., Kozikowski, A. P. and Sussman, J. L. (1997). Structure of acetylcholinesterase complexed with the nootropic alkaloid, (-)-huperzine A. *Nat. Struct. Biol.* **4**: 57-63

17. Kryger, G., Sillman, I. and Sussman, J. L. (1999). Structure of acetylcholinesterase complexed with E2020 (Aricept): implications for the design of new anti-Alzheimer drugs. *Structure* **7**: 297-307

18. Vellom, D. C., Radic, Z., Li, Y., Pickering, N. A., Camp, S. and Taylor, P. (1993). Amino acid residues controlling acetylcholinesterase and butyrylcholinesterase specificity. *Biochemistry* **32**: 12-17

19. Ordentlich, A., Barak, D., Kronman, C., Flashner, Y., Leitner, M., Segall, Y., Ariel, N., Cohen, S., Velan, B. and Shafferman, A. (1993). Dissection of the human acetylcholinesterase active center determinants of substrate specificity. Identification of residues constituting the anionic site, the hydrophobic site, and the acyl pocket. *J. Biol. Chem.* **268**: 17083-17095

20. Ordentlich, A., Barak, D., Kronman, C., Ariel, N., Segall, Y., Velan, B. and Shafferman, A. (1998). Functional characteristics of the oxyanion hole in human acetylcholinesterase. *J. Biol. Chem.* **273**: 19509-19517

21. Nachmansohn, D. and Wilson, I. B. (1951). Enzymic hydrolysis and synthesis of acetylcholine. *Adv. Enzymol.* **12**: 259-339

22. Barak, D., Ordentlich, A., Bromberg, A., Kronman, C., Marcus, D., Lazar, A., Ariel, N., Velan, B. and Shafferman, A. (1995). Allosteric modulation of acetylcholinesterase activity by peripheral ligands involves a conformational transition of the anionic subsite. *Biochemistry* **34**: 15444-15452

23. Quinn, D. M. (1987). Acetylcholinesterase: Enzyme structure, reaction dynamics, and virtual transition states. *Chem. Rev.* **87**: 955-979

24. Szegletes, T., Mallender, W. D. and Rosenberry, T. L. (1998). Nonequilibrium analysis alters the mechanistic interpretation of inhibition of acetylcholinesterase by peripheral site ligands. *Biochemistry* **37**: 4206-4216

25. Szegletes, T., Mallender, W. D., Thomas, P. J. and Rosenberry, T. L. (1999). Substrate binding to the peripheral site of acetylcholinesterase initiates enzymatic catalysis. Substrate inhibition arises as a secondary effect. *Biochemistry* **38**: 122-133

26. Mallender, W. D., Szegletes, T. and Rosenberry, T. L. (2000). Acetylthiocholine binds to Asp74 at the peripheral site of human acetylcholinesterase as the first step in the catalytic pathway. *Biochemistry* **39**: 7753-7763

27. Mallender, W. D., Szegletes, T. and Rosenberry, T. L. (1999). Organophosphorylation of acetylcholinesterase in the presence of peripheral site ligands: Distinct effects of propidium and fasciculin. *J. Biol. Chem.* **274**: 8491-8499

28. Burgen, A. S. V. (1949). The mechanism of action of anticholinesterase drugs. *Brit. J. Pharmacol.* **4**: 219-228

29. Wilson, I. B. (1951). Acetylcholinesterase. XI. Reversibility of tetraethyl pyrophosphate inhibiton. *J. Biol. Chem.* **190**: 111-117

30. Aldridge, W. N. and Reiner, E. (1972). Enzyme inhibitors as substrates. Interaction of esterases with esters of organophosphorus and carbamic acids. In: **Frontiers of Biology, 26** ed.), North Holland, Amsterdam, pp. 328

31. Froede, H. C. and Wilson, I. B. (1971). Acetylcholinesterase. In: **The Enzymes, 3rd Edition** (Boyer, P. D., ed.), **V**, Academic Press, New York, pp. 87-114

32. Albaret, C., Lacoutiere, S., Ashman, W. P., Foment, d. and Fortier, P.-L. (1997). Molecular mechanic study of nerve agent *O*-ethyl-*S*-[2-(diisopropylamino)ethyl]methylphosphonothioate (VX) bound to the active site of *Torpedo californica* acetylcholinesterase. *Proteins* **28**: 543-555

33. Radic, Z. and Taylor, P. (1999). The influence of peripheral site ligands on the reaction of symmetric and chiral organophosphates with wild type and mutant acetylcholinesterases. *Chem.-Biol. Interact.* **119-120**: 111-117

34. Rosenberry, T. L., Rabl, C. R. and Neumann, E. (1996). Binding of the neurotoxin fasciculin 2 to the acetylcholinesterase peripheral site drastically reduces the association and dissociation rate constants for N-methylacridinium binding to the active site. *Biochemistry* **35**: 685-690

35. Harel, M., Kryger, G., Rosenberry, T. L., Mallender, W. D., Lewis, T., Fletcher, R. J., Guss, J. M., Silman, I. and Sussman, J. L. (2000). 3D structure of *Drosophila Melanogaster* acetylcholinesterase and of its complexes with putative insecticides. *Protein Sci.* **9**: 1063-1072

36. Incardona, J. P. and Rosenberry, T. L. (1996). Construction and characterization of secreted and chimeric transmembrane forms of Drosophila acetylcholinesterase: A large truncation of the C-terminal signal peptide does not eliminate glycoinositol phospholipid anchoring. *Mol. Biol. Cell* **7**: 595-611

37. Camps, P., Cusack, B., Mallender, W. D., El Achab, R., Morral, J., Muñoz-Torrero, D. and Rosenberry, T. L. (2000). Huprine X is a novel high affinity inhibitor of acetylcholinesterase that is of interest for the treatment of Alzheimer's disease. *Mol. Pharmacol.* **57**: 409-417

38. De Ferrari, G. V., Mallender, W. D., Inestrosa, N. C. and Rosenberry, T. L. (2001). Thioflavin T is a fluorescent probe of the acetylcholinesterase peripheral site that reveals conformational interactions between the peripheral and acylation sites. *J. Biol. Chem.* **276**: 23282-23287

39. Changeux, J.-P. (1966). Responses of acetylcholinesterase from *Torpedo marmorata* to salts and curarizing drugs. *Mol. Pharmacol.* **2**: 369-392

40. Rosenberry, T. L., Mallender, W. D., Cusack, B., Szegletes, T., Romanovskis, P. and Spatola, A. P. (2000). Inhibitors of the acetylcholinesterase peripheral site may protect against organophosphate toxicity. In: **Bioscience 2000 Medical Defense Review** ed.), Hunt Valley, Maryland, pp. in press

41. Eastman, J., Wilson, E. J., Cervenansky, C. and Rosenberry, T. L. (1995). Fasciculin 2 binds to a peripheral site on acetylcholinesterase and inhibits substrate hydrolysis by slowing a step involving proton transfer during enzyme acylation. *J. Biol. Chem.* **270**: 19694-19701

42. le Du, J. H., Marchot, P., Bourgis, P. E. and Fontecilla-Camps, J. C. (1992). 1.9-A resolution of fasciculin 1, an anti-acetylcholinesterase toxin from green mamba snake venom. *J. Biol. Chem.* **267**: 22122-22130

43. Falkenstein, R. J. and Pena, C. (1997). Synthetic peptdies derived from the central loop of fasciculin: structural analysis and evaluation as inhibitors of acetylcholinesterase. *Biochem. Biophys. Acta* **1340**: 143-151

44. Spatola, A. F., Crozet, Y., deWit, D. and Yanagisawa, M. (1996). Rediscovering an endothelin antagonist (BQ-123): A self-deconvoluting cyclic pentapeptide library. *J. Med. Chem.* **39**: 3842-3846

45. Boyd, A. E., Marnett, A. B., Wong, L. and Taylor, P. (2000). Probing the active center gorge of acetylcholinesterase by fluorophores linked to substituted cysteines. *J. Biol. Chem.* **275**: 22401-22408

Appendix 1: Description of the steric blockade model.

Scheme 5 is a general formulation of substrate hydrolysis with AChE from which the steric blockade model is derived (*1*). *E*S, *E*A, *E*AP, and *E*P are intermediates involving only the acylation site, and S can bind to the peripheral site (designated by subscript P) in each of these intermediates as well as in the free enzyme *E*. In general, the 10 enzyme species specified in this scheme are related by 22 independent rate constants. The steric blockade model simplifies this scheme by assuming that the rate constants for substrate binding and reaction at one site are independent of additional ligand occupancy at either site (*i.e.*, $k_S = k_{SS} = k_{AS} = k_{PS} = k_{APS}$; $k_{-S} = k_{-AS} = k_{-SS} = k_{-PS} = k_{-APS}$; and $a = b = c = d = e = f$) with one exception: $k_{-P2} < k_{-P}$. These assumptions reduce the number of independent rate constants to 8. Direct measurements have been made only for the ratio of two rate constants (k_2/k_3), by a laborious stopped-flow acid quench method with [^{3}H]acetylcholine and [^{3}H]acetylthiocholine (*2*), with eel AChE. Ratios of 1.9 for acetylcholine and 1.3 for acetylthiocholine were obtained, and given a smaller k_{cat} for human AChE than for eel AChE, we have assumed a ratio of 1 in our fitting procedures. To obtain further reductions, certain approximations can be justified. Substrate inhibition profiles are relatively insensitive to four of the remaining independent rate constants when they are confined within expected ranges (see *1*; appendix reprint 5). The ratio k_{-P2}/k_{-P} sets the extent of steric blockade, and we have assigned this ratio as 0.01 based on the simulated k_{-S2}/k_{-S} of 0.015 for propidium inhibition of acetylthiocholine hydrolysis (*3*; *4*). However, fitting is insensitive to k_{-P2}/k_{-P} ratios between 0 and 0.05. Fitting is also insensitive to the absolute values of k_s, k_1 and k_{-1} as long as their relative values are consistent with the observed second order hydrolysis rate constant $k_{cat}/K_{app} = k_S k_1 k_2/(k_{-S}k_{-1} + k_{-S}k_2 + k_1 k_2)$. The association rate constant k_S must be greater than or equal to k_{cat}/K_{app}, and k_{cat}/K_{app} for acetylthiocholine with AChE approaches the limit of diffusion control (where $k_S = k_{cat}/K_{app}$), based on both visocisity (*5*) and D_2O isotope effect measurements (*6*; *7*). Fitting is relatively insensitive when the ratio of k_S to k_{cat}/K_{app} is assigned between 1 and 10. Finally, a value of k_{-1} can be assigned from D_2O effects on k_{cat}/K_{app} (*1*). This leaves only k_{-P}, k_2 and k_{-S} (in the form of K_S) as independent parameters in the fitting process (*e.g.*, Fig. 2A and *1* in appendix reprint 5).

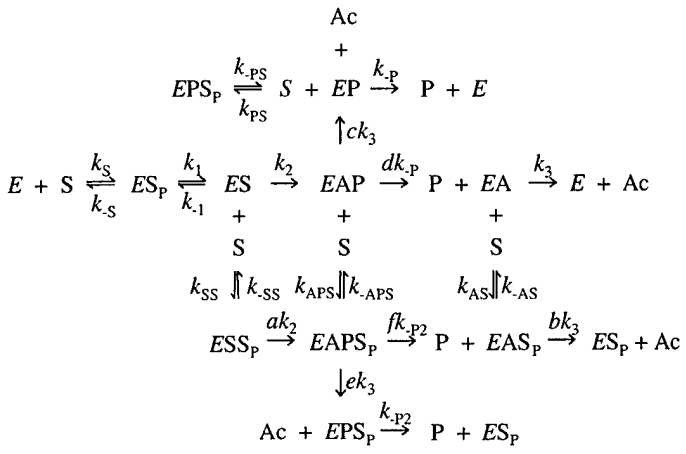

SCHEME 5

While a model based on Scheme 5 with 22 rate constants might appear hopelessly complex and the assumptions used to reduce it to our steric blockade model might seem arbitrary, from a mechanistic perspective this model is far more satisfactory than that in Scheme 2. Scheme 2 simply ignores (and therefore equates to zero) the concentrations of several of the intermediates in Scheme 5 that are known to occur. Scheme 5 acknowledges these intermediates, and in the absence of further information, makes one overall assumption that they reflect ternary ligand complexes in which binding and reaction at each site is independent of occupancy of the other site. We have also adapted Scheme 5 to studies of inhibition with peripheral site ligands by including additional intermediates in which the ligand is bound to the peripheral site (*4*).

References

1. Mallender, W. D., Szegletes, T. and Rosenberry, T. L. (2000). *Biochemistry* **39**: 7753-7763.
2. Froede, H. C. and Wilson, I. B. (1984). *J. Biol. Chem.* **259**: 11010-11013.
3. Szegletes, T., Mallender, W. D. and Rosenberry, T. L. (1998). *Biochemistry* **37**: 4206-4216.

4. Szegletes, T., Mallender, W. D., Thomas, P. J. and Rosenberry, T. L. (1999). *Biochemistry* **38**: 122-133.
5. Bazelyansky, M., Robey, E. and Kirsch, J. F. (1986). *Biochemistry* **25**: 125-130.
6. Rosenberry, T. L. (1975). *Proc. Nat. Acad. Sci. USA* **72**: 3834-3838.
7. Eastman, J., Wilson, E. J., Cervenansky, C. and Rosenberry, T. L. (1995). *J. Biol. Chem.* **270**: 19694-19701.

Biochemistry **1998,** *37,* 4206−4216

Nonequilibrium Analysis Alters the Mechanistic Interpretation of Inhibition of Acetylcholinesterase by Peripheral Site Ligands†

Tivadar Szegletes, William D. Mallender, and Terrone L. Rosenberry*

Department of Pharmacology, Mayo Foundation for Medical Education and Research, and Department of Research, Mayo Clinic Jacksonville, Jacksonville, Florida 32224

Received August 29, 1997; Revised Manuscript Received November 13, 1997

ABSTRACT: The active site gorge of acetylcholinesterase (AChE) contains two sites of ligand binding, an acylation site near the base of the gorge with a catalytic triad characteristic of serine hydrolases, and a peripheral site at the mouth of the gorge some 10−20 Å from the acylation site. Many ligands that bind exclusively to the peripheral site inhibit substrate hydrolysis at the acylation site, but the mechanistic interpretation of this inhibition has been unclear. Previous interpretations have been based on analyses of inhibition patterns obtained from steady-state kinetic models that assume equilibrium ligand binding. These analyses indicate that inhibitors bound to the peripheral site decrease acylation and deacylation rate constants and/or decrease substrate affinity at the acylation site by factors of up to 100. Conformational interactions have been proposed to account for such large inhibitory effects transmitted over the distance between the two sites, but site-specific mutagenesis has failed to reveal residues that mediate the proposed conformational linkage. Since examination of individual rate constants in the AChE catalytic pathway reveals that assumptions of equilibrium ligand binding cannot be justified, we introduce here an alternative nonequilibrium analysis of the steady-state inhibition patterns. This analysis incorporates a steric blockade hypothesis which assumes that the only effect of a bound peripheral site ligand is to decrease the association and dissociation rate constants for an acylation site ligand without altering the equilibrium constant for ligand binding to the acylation site. Simulations based on this nonequilibrium steric blockade model were in good agreement with experimental data for inhibition by the peripheral site ligands propidium and gallamine at low concentrations of either acetylthiocholine or phenyl acetate if binding of these ligands slows substrate association and dissociation rate constants by factors of 5−70. Direct measurements with the acylation site ligands huperzine A and *m*-(*N,N,N*-trimethylammonio)trifluoroacetophenone showed that bound propidium decreased the association rate constants 49- and 380-fold and the dissociation rate constants 10- and 60-fold, respectively, relative to the rate constants for these acylation site ligands with free AChE, in reasonable agreement with the nonequilibrium steric blockade model. We conclude that this model can account for the inhibition of AChE by small peripheral site ligands such as propidium without invoking any conformational interaction between the peripheral and acylation sites.

Acetylcholinesterase (AChE)[1] hydrolyzes its physiological substrate acetylcholine at one of the highest known catalytic rates (*1*), and the unique features of AChE structure that determine its catalytic power have been pursued for many years. A major advance occurred with the X-ray crystallographic determination of the three-dimensional structure of *Torpedo californica* AChE (TcAChE) (*2*). This structure revealed an active site gorge lined with aromatic residues that is about 20 Å deep. Two sites of ligand interaction in AChE were first demonstrated in ligand binding studies (*3*) and later confirmed by crystallography, site-specific mutagenesis, and molecular modeling: an *acylation site* at the base of the gorge and a *peripheral site* at its mouth. In the acylation site (Figure 1) residue S200 (TcAChE sequence numbering) is acylated and deacylated during substrate turnover, H440 and E327 participate with S200 in a catalytic triad (E−H−S), and W84 binds to the trimethylammonium group of acetylcholine as acyl transfer to S200 is initiated. The peripheral site involves other residues including W279 (*4*−*9*). Ligands can bind selectively to either the acylation or the peripheral sites, and ternary complexes with distinct ligands bound to each site can form (*3*). Peripheral site ligands that form these ternary complexes include the

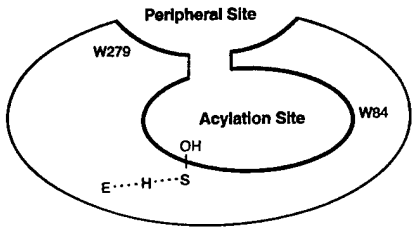

FIGURE 1: Schematic diagram of the sites for ligand binding in AChE.

† This work was supported by Grant NS-16577 from the National Institutes of Health and by grants from the Muscular Dystrophy Association of America. W.D.M. was supported by a Kendall-Mayo Postdoctoral Fellowship.

* To whom correspondence should be addressed.

[1] Abbreviations: AChE, acetylcholinesterase; TcAChE, acetylcholinesterase from *Torpedo californica*; DTNB, 5,5′-dithiobis(2-nitrobenzoic acid); TMTFA, *m*-(*N,N,N*-trimethylammonio)trifluoroacetophenone.

S0006-2960(97)02158-2 CCC: $15.00
Published on Web 03/05/1998

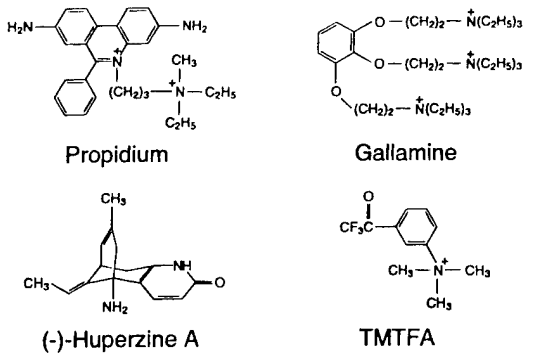

FIGURE 2: Structures of peripheral site and acylation site ligands.

phenanthridinium derivative propidium (Figure 2) and the fasciculins, a family of very similar snake venom neurotoxins composed of 61-amino acid polypeptides (*10*, *11*).

In this paper we address the question of how ligand binding to the peripheral site alters AChE catalytic activity. While it is well documented that ligand binding to this site can inhibit substrate hydrolysis, the mechanism of this inhibition is less clear. Specifically, an understanding of the inhibition mechanism may depend on whether the substrate and inhibitor are equilibrated with AChE. This point can be examined in the conventional pathway for the hydrolysis of acetylcholine (S) by AChE (*E*) in Scheme 1.[2] The initial

Scheme 1

$$E + S \underset{k_{-S}}{\overset{k_S}{\rightleftharpoons}} ES \xrightarrow{k_2} EA \xrightarrow{k_3} E + P$$

enzyme–substrate complex *ES* proceeds to an acylated enzyme intermediate *EA* which is then hydrolyzed to product P and *E* (see ref *12*). Under classical steady-state conditions (*13*), hydrolysis rates v vary with [S] according to the Michaelis–Menten equation (eq 1a) to give the maximum hydrolysis rate V_{max}, the apparent first-order rate constant k_{cat}, and the second-order rate constant k_{cat}/K_{app} (eqs 1b and 1c).

$$v = \frac{d[P]}{dt} = \frac{V_{max}[S]}{[S] + K_{app}} \quad (1a)$$

$$\frac{V_{max}}{[E]_{tot}} = k_{cat} = \frac{k_2 k_3}{k_2 + k_3} \qquad \frac{k_{cat}}{K_{app}} = \frac{k_S k_2}{k_{-S} + k_2} \quad (1b, 1c)$$

One way in which AChE has optimized these rate constants is by accelerating the acylation step k_2 so that it exceeds k_{cat} (eq 1b), which for AChE is about 10^4 s^{-1} (*1*). Of more importance to the arguments here, k_2 also exceeds k_{-S} (*1*, *14*). As a result, *ES* is not in equilibrium with *E* and S. The failure of *ES* to equilibrate with *E* and S is readily accommodated by eq 1c: k_{cat}/K_{app} approaches k_S, the substrate association rate constant. However, when an inhibitor binds to the nonequilibrated *ES* intermediate, the steady-state inhibition patterns present a greater challenge. The conventional interpretation of the classic noncompetitive inhibition pattern, for example, assumes that *ES* is equilibrated (see ref *15*). We avoid this equilibrium assumption here for the first time in the AChE literature by solving the appropriate differential rate equations with the simulation program SCoP. In particular, we examine the simple hypothesis that the only effect of peripheral site inhibitors such as propidium is to impose a steric blockade that decreases association and dissociation rate constants for substrates without altering their ratio, the equilibrium association constant. We test this hypothesis also by examining the effect of peripheral site ligands on the rate constants for the binding of acylation site inhibitors. Our results indicate that failure to achieve equilibrium can have a profound impact on the classical interpretation of AChE inhibition and indeed alter mechanistic conclusions.

EXPERIMENTAL PROCEDURES

Materials. Human erythrocyte AChE was purified as outlined previously and active site concentrations were determined by assuming 410 units/nmol (*16*, *17*). (−)-Huperzine A and propidium iodide were purchased from Calbiochem and gallamine triethiodide from Aldrich Chemical Co. Huperzine A concentrations were adjusted with an extinction coefficient[3] $\epsilon_{308\ nm} = 10400\ M^{-1}\ cm^{-1}$. TMTFA was kindly provided by Dr. Daniel Quinn (University of Iowa), and stock TMTFA concentrations were calibrated by titration with AChE.

Steady-State Measurements of AChE-Catalyzed Substrate Hydrolysis. Hydrolysis rates v were measured at various substrate (S) concentrations in buffer composed of 20 mM sodium phosphate and 0.02% Triton X-100 at pH 7.0 and 25 °C unless otherwise indicated. Acetylthiocholine assay solutions (1 mL) included 0.33 mM DTNB, and hydrolysis was monitored by formation of the thiolate dianion of DTNB at 412 nm ($\Delta\epsilon_{412\ nm} = 14.15\ mM^{-1}\ cm^{-1}$ (*18*)) for 1–5 min on a Varian Cary 3A spectrophotometer (*19*). Acetylthiocholine concentrations were low enough (<0.5 mM) in the absence of inhibitors (*20*) that compensation for substrate inhibition was unnecessary. Hydrolysis rates for phenyl acetate (0.2–5 mM, ≤1% methanol final) were measured in 1-ml assay solutions at 270 nm ($\Delta\epsilon_{270\ nm} = 1.40\ mM^{-1}\ cm^{-1}$) for 1–5 min (*21*). Reciprocal plots of v^{-1} vs $[S]^{-1}$ at all inhibitor (I) concentrations here were linear, and slopes and intercepts of these plots were calculated by weighted linear regression analyses which assumed that v has a constant percent error. Nonlinear regression analyses of these slopes and intercepts vs [I] were conducted with Fig.P (BioSoft, version 6.0) as described, with slope and intercept values weighted by the reciprocal of their variance (also see ref *22*).

Simulations of Kinetic Equations. When the reversible reactions in Scheme 2 below are not at equilibrium, the corresponding differential equations were solved with the program denoted SCoP (version 3.51) developed at the NIH National Center for Research Resources and available from Simulation Resources, Inc. (Berien Springs, MI). A model file was constructed with differential equations for each enzyme intermediate except *E* and with values of all rate constants. Mass conservation was introduced by substitution of $[E] = [E]_{tot} - \Sigma[M]$, where $[E]_{tot}$ is the total concentration

[2] Scheme 1 assumes substrate concentrations low enough that *ESS* or *EAS* species leading to substrate inhibition are negligible (see ref *1*).

[3] Personal communication from B. P. Doctor, Walter Reed Army Institute of Research, Washington, DC.

Table 1: Inhibition of AChE-Catalyzed Hydrolysis of Acetylthiocholine by Propidium[a]

case	k_S (μM^{-1} s^{-1})	k_{-S} (s^{-1})	k_2, k_3 (s^{-1})	k_I (μM^{-1} s^{-1})	k_{-I} (s^{-1})	k_{S2} (μM^{-1} s^{-1})	k_{-S2} (s^{-1})	K_{app}[b] (mM)	slope K_I[b] (μM)	slope α[b]	intercept β[b]
1	**200**	**3×10^3**	**1.4×10^4**	**200**	**200**	**3**	**45**	0.043	1.00	0.0197	0.09 ± 0.01
2	200	3×10^3	1.4×10^4	200	200	**0.3**	**4.5**	0.043	1.01	0.0033 ± 0.0001	0.030 ± 0.001
3	200	3×10^3	1.4×10^4	200	200	**200**	**3×10^3**	0.043		1.00	1.00
4	200	**3×10^5**	1.4×10^4	200	200	**3**	**4.5×10^3**	0.79	1.00	0.26	0.78 ± 0.05
5	200	**3×10^7**	1.4×10^4	200	200	3	**4.5×10^5**	75	1.00	0.97	1.00

[a] Simulations for cases 1−5 were generated as outlined in the text with indicated rate constant values. Bold entries indicate a change from the previous case. Values of K_{app}, K_I and α and β were calculated by weighted least-squares analysis of replots as in Figure 4. [b] Standard errors were less than 2% of the mean unless otherwise indicated.

of enzyme and Σ [M] is the sum of the concentrations of all enzyme intermediates. An analogous mass conservation was introduced for [S]. Simulation and curve-fitting files were generated by SCoP from the model file by employing the numerical solver clsoda. This solver for stiff and nonstiff sets of differential equations uses an improved Gear method (*23*, *24*).

Rate constants used in these simulations (see Tables 1 and 2) were justified as follows. For acetylthiocholine, direct estimates of k_2 and k_3 (available only for eel AChE) gave $k_2/k_3 = 1.3$ (*25*). Noting a 2-fold smaller k_{cat} of 7000 s^{-1} for human AChE (*26*) and assuming $k_2 = k_3$ for this enzyme, substitution into eq 1b gave $k_2 = k_3 = 1.4 \times 10^4$ s^{-1}. Solvent deuterium oxide (D_2O) isotope effects provided an estimate of k_{-S}: k_{cat} for acetylthiocholine was slowed by a factor of 2.03 ± 0.05 when H_2O was replaced by D_2O, a value close to a typical factor of 2.5 for enzyme-catalyzed steps that are rate limited by proton transfer (*14*), but k_{cat}/K_{app} decreased by a factor of only 1.21 ± 0.02 in D_2O (*22*). Inserting this value in eq 1c and assuming that k_2 decreased by a factor of 2.5 in D_2O while k_S and k_{-S} were unaffected, then $k_2/k_{-S} = 6$ and, from k_2 above, $k_{-S} = 3 \times 10^3$ s^{-1}. An estimate of $k_S = 2 \times 10^8$ M^{-1} s^{-1} was obtained by substitution of these values of k_2 and k_{-S} and the observed value of $K_{app} = 45$ μM (see Table 2) into eq 1c. For phenyl acetate, k_{cat} was assumed equal to that of acetylthiocholine (*1*) and the same value of 1.4×10^4 s^{-1} was assigned for k_2 and k_3. From observed D_2O isotope effects of 2.45 ± 0.08 for k_{cat} and 1.48 ± 0.05 for k_{cat}/K_{app} (*22*), k_2 was assumed to decrease by a factor of 2.5 in D_2O while k_S and k_{-S} were unaffected, yielding $k_2/k_{-S} = 2.1$ and $k_{-S} = 7 \times 10^3$ s^{-1}. These values together with the observed value of $K_{app} = 1.31$ mM (see Table 2) gave $k_S = 8 \times 10^6$ M^{-1} s^{-1} for phenyl acetate from eq 1c. For propidium and gallamine, an estimate of $k_I = 2 \times 10^8$ M^{-1} s^{-1} was based on association rate constants of 5×10^7 M^{-1} s^{-1} for the bisquaternary ligand ambenonium (*20*) and 4×10^8 M^{-1} s^{-1} for *N*-methylacridinium (*27*) with human AChE. Values for k_{-I} were then calculated from $k_{-I} = (k_I)(K_I)$, where K_I was the observed equilibrium inhibition constant for propidium or gallamine (see Table 2).

Slow Equilibration of an Acylation Site Ligand in the Presence of a Peripheral Site Inhibitor. The slow interaction of an acylation site ligand (L) with AChE in the presence of a peripheral site inhibitor I as shown in Scheme 3 in the Results was analyzed by procedures used previously (*22*) to describe the interaction of fasciculin 2 with AChE. Bovine serum albumin (1 mg/mL) was incubated overnight in buffer (20 mM sodium phosphate, 0.02% Triton X-100, pH 7.0) containing 0.33 mM 5,5′-dithiobis(2-nitrobenzoic acid) (DTNB), and association reactions were initiated by adding AChE, the inhibitor propidium, and the acylation site ligand (huperzine A or TMTFA) at 23 °C. Except where indicated, binding was measured under pseudo-first-order conditions in which the concentration of ligand was adjusted to at least 10 times the concentration of AChE. At various times a 1.0-mL aliquot was removed to a cuvette, 40 μL of acetylthiocholine and DTNB were added to final concentrations of 0.5 mM and 0.33 mM, respectively, and a continuous assay trace was immediately recorded at 412 nm. Background rates in the absence of AChE were subtracted. Dissociation reactions were measured by incubating ligand with AChE for 1−24 h, diluting ≥200-fold to the indicated final concentrations, and assaying 1.0-mL aliquots as above.

Assay rates v from association and dissociation reactions of huperzine A and TMTFA were divided by control assay rates in the absence of these ligands ($v_{H=0}$ or $v_{TMTFA=0}$) to give a normalized value $v_{(N)}$. For huperzine A these values were fitted by nonlinear regression analysis (Fig.P) to eq 2, where $v_{(N)initial}$ and $v_{(N)final}$ are the calculated values of $v_{(N)}$ at time zero and at equilibrium, respectively, and the observed

$$v_{(N)} = v_{(N)final} + (v_{(N)inital} - v_{(N)final})e^{-kt} \quad (2)$$

pseudo first-order rate constant k for the approach to equilibrium is given by eq 3.

$$k = k_{on}[L] + k_{off} \quad (3)$$

In eq 3,

$$k_{on} = \frac{k_L + k_{L2}\frac{[I]}{K_I}}{1 + \frac{[I]}{K_I}} \qquad k_{off} = \frac{k_{-L} + k_{-L2}\frac{[I]}{K_{LI}}}{1 + \frac{[I]}{K_{LI}}} \quad (4a, 4b)$$

Structure Analysis and Molecular Graphics. Construction and analysis of three-dimensional models were performed on a Silicon Graphics workstation Indigo2 IMPACT using QUANTA96 modeling software (Molecular Simulations, Inc.). Modeling of the ternary TcAChE enzyme−inhibitor complexes began with the crystal structure coordinates for the TcAChE−huperzine A complex [Protein Data Bank (PDB) file: 1VOT] (*28*) and the TcAChE−TMTFA complex (PDB file: 1AMN) (*29*). Propidium was manually docked into the peripheral site as previously described (*7*). Briefly, the aromatic and alkyl portions of propidium were positioned in the peripheral site and active site gorge by avoiding unfavorable contacts with the TcAChE structure. The resulting structures were optimized by energy minimization

Table 2: Observed and Simulated Inhibition of AChE-Catalyzed Hydrolysis of Acetylthiocholine and Phenyl Acetate by Peripheral Site Ligands[a]

substrate inhibitor	observed parameters				simulated parameters[b]			
	K_{app} (mM)	K_I (μM)	α	β	k_{S2}/k_S	K_I' (μM)	α'	β
acetylthiocholine	0.045 ± 0.003							
propidium		1.1 ± 0.1	0.019 ± 0.004	0.10 ± 0.01	0.015	1.00	0.0197	0.09 ± 0.01
gallamine		37 ± 2	0.019 ± 0.002	0.44 ± 0.03	0.015	35	0.0189	0.5 ± 0.1
phenyl acetate	1.31 ± 0.15							
propidium		0.8 ± 0.1	0.071 ± 0.008	0.46 ± 0.02	0.05	1.01	0.076	0.4 ± 0.1
gallamine		31 ± 5	0.25 ± 0.01	1.0 ± 0.1	0.2	39	0.27	0.95 ± 0.03

[a] Values of K_{app}, K_I, α, and β were calculated by analysis of replots as in Figures 3 and 4. The ratio of k_{S2}/k_S in each simulation was assigned to give optimal agreement between the observed and simulated parameters. [b] Simulations were conducted with the rate constants from case 1 in Table 1 except as follows: When gallamine replaced propidium, $k_{-1} = 6 \times 10^3$ s^{-1}; when phenyl acetate replaced acetylthiocholine, $k_S = 8$ μM^{-1} s^{-1} and $k_{-S} = 7 \times 10^3$ s^{-1}; with phenyl acetate and propidium, $k_{S2} = 0.4$ μM^{-1} s^{-1} and $k_{-S2} = 350$ s^{-1}; and with phenyl acetate and gallamine, $k_{S2} = 1.6$ μM^{-1} s^{-1} and $k_{-S2} = 1.4 \times 10^3$ s^{-1}. Simulated K_{app} values were identical to the experimental K_{app}, as expected from the assignment of rate constants in Table 1. [c] Standard errors were less than 2% of the mean.

using the CHARMm module of QUANTA96 (conjugate gradient). Initial structural refinement included only the propidium and gorge solvent molecules while final optimization added all amino acid side chains vicinal to propidium and the acylation site ligand.

RESULTS

Equilibrium Model of AChE Inhibition. When ligands bind to the peripheral site, AChE activity is often inhibited. The inhibitor (I) can bind to each of the three enzyme species from Scheme 1, as modeled in Scheme 2. For example, ESI_P

Scheme 2

$$\begin{array}{ccccccc} S + E & \underset{k_{-S}}{\overset{k_S}{\rightleftharpoons}} & ES & \xrightarrow{k_2} & EA & \xrightarrow{k_3} & E + P \\ + & & + & & + & & \\ I & & I & & I & & \end{array}$$

$$k_I \Big\updownarrow k_{-I} \qquad k_{SI} \Big\updownarrow k_{-SI} \qquad k_{AI} \Big\updownarrow k_{-AI}$$

$$S + EI_P \underset{k_{-S2}}{\overset{k_{S2}}{\rightleftharpoons}} ESI_P \xrightarrow{ak_2} EAI_P \xrightarrow{bk_3} EI_P + P$$

represents a ternary complex with S at the acylation site and I at the peripheral site (denoted by the subscript P). The acylation rate constant k_2 is altered by a factor a in this ternary complex, and the deacylation rate constant k_3 is altered by a factor b in the EAI_P complex. To characterize how a peripheral site ligand inhibits AChE, it is useful to know whether substrate affinities are altered and whether the relative rate constants a and b are less than 1 when the inhibitor is bound. Unfortunately, for acetylcholine and other carboxylester substrates, the acylation and deacylation rate constants are too fast to permit direct measurement by any rapid kinetic technique. Consequently, investigations of Scheme 2 have employed steady-state kinetic analyses based on extensions of the Michaelis–Menten expression. However, this approach is problematic. In contrast to the simple steady-state solution in the absence of inhibitor, the general steady-state solution for v in Scheme 2 is too complex for useful comparison to experimental data (*30*, *31*). To obtain a more tractable simplified solution, it has invariably been assumed with AChE that the reversible reactions in Scheme 2 are at equilibrium (i.e., $k_{-S} \gg k_2$; $k_{-S2} \gg ak_2$; $k_{-SI} \gg k_2$; $k_{-SI} \gg ak_2$; $k_{-AI} \gg k_3$; $k_{-AI} \gg bk_3$; *32*; *33*; see ref *22*). This solution is given in eq 5, where $K_X = k_{-X}/k_X$.

$$v^{-1} = \frac{1}{V_{max}}\left[\frac{k_{cat}\left(1+\frac{[I]}{K_{SI}}\right)}{k_2\left(1+\frac{a[I]}{K_{SI}}\right)} + \frac{k_{cat}\left(1+\frac{[I]}{K_{AI}}\right)}{k_3\left(1+\frac{b[I]}{K_{AI}}\right)} + \frac{K_{app}\left(1+\frac{[I]}{K_I}\right)}{[S]\left(1+\frac{a[I]}{K_{SI}}\right)}\right] \quad (5)$$

Many inhibition patterns observed with AChE are consistent with eq 5. For example, propidium inhibition of phenyl acetate and acetylthiocholine hydrolysis gave the steady-state kinetic data in Figure 3a,b and Figure 4a,b. The slopes of the reciprocal plots in Figure 3a increased with propidium concentration (Figure 3b), and analyses of these slopes by eq 6 allowed estimation of K_I, the equilibrium dissociation

$$\frac{\text{slope } (v^{-1} \text{ vs } [S]^{-1})}{K_{app}/V_{max}} = \frac{\left(1+\frac{[I]}{K_I}\right)}{\left(1+\frac{\alpha[I]}{K_I}\right)} \quad (6)$$

constant for I with E, and the *experimental* parameter α. At saturating concentrations of I ($[I] \gg K_I/\alpha$), the slope in eq 6 $= K_{app}/\alpha V_{max}$. Therefore, α is simply the ratio of the second-order rate constant with saturating I, which we denote k_{cat}'/K_{app}', to that in the absence of I. When equilibrium is assumed as in eq 5, $\alpha = aK_I/K_{SI} = aK_S/K_{S2}$. Within an equilibrium framework, the low values of $\alpha = 0.071$ for propidium and phenyl acetate in Figure 3b and 0.019 for propidium and acetylthiocholine in Figure 4b require either that ESI_P does not form ($K_S/K_{S2} \cong 0$) or that $a \cong 0$. While these two possibilities can in principle be distinguished by analysis of the intercepts of the reciprocal plots in Figures 3a and 4a, contributions from inhibition of both acylation and deacylation complicate the interpretation (eq 5). For example, the intercepts in Figure 4b also increased with propidium concentration but in a less linear fashion than the slopes. If we denote[4] βk_{cat} as the first-order hydrolysis rate constant for the pathway through the ternary complexes ESI_P and EAI_P, the intercept data in Figure 4b gave $\beta = 0.10$. Uncertainties in the ratio of k_2 to k_3 and in b make it difficult

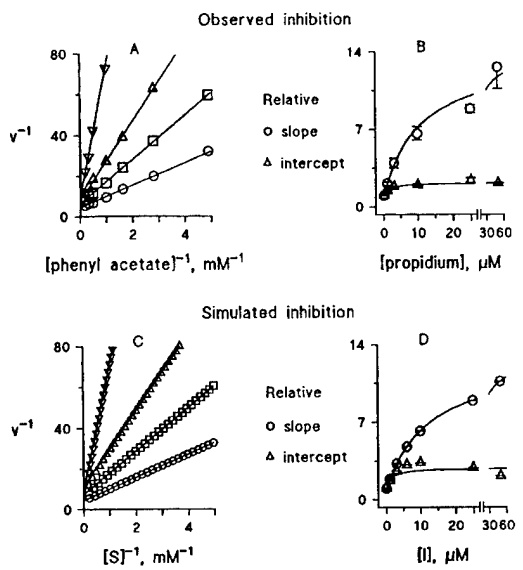

FIGURE 3: Observed and simulated inhibition of AChE-catalyzed phenyl acetate hydrolysis by propidium. Part A: Reciprocal plots of measured initial velocities (mM/min) and substrate concentrations were fitted by weighted linear regression analysis according to eq 5 at various fixed propidium concentrations ((○) 0 μM, (□) 1 μM, (△) 3 μM, (▽) 50 μM) and 0.5 nM E. Four additional points are offscale and not shown. Part B: Slopes of reciprocal plots including those in part A were normalized by dividing by K_{app}/V_{max} (the slope in the absence of propidium) and fitted by weighted nonlinear regression analysis to eq 6 to give $K_I = 0.8 \pm 0.1$ and $\alpha = 0.071 \pm 0.008$ (see Table 2). Normalized intercepts of the reciprocal plots were fitted to an equation of the same form as eq 6 to give $\beta = 0.46 \pm 0.02$ (see footnote 4 and Table 2). Part C: Plots of v^{-1} vs $[S]^{-1}$ at various [I] ((○) 0 μM; (□) 1 μM; (△) 3 μM; (▽) 50 μM) were generated by the SCoP simulation program with rate constant parameters listed for phenyl acetate and propidium in Table 2. Lines were extrapolated from linear regions of these plots encompassing $[S] = 0.02K_{app}$ to $0.2K_{app}$. Part D: Slopes and intercepts of lines calculated as in part C were analyzed by replot analysis as in part B to obtain the simulated estimates of K_I, α, and β in Table 2.

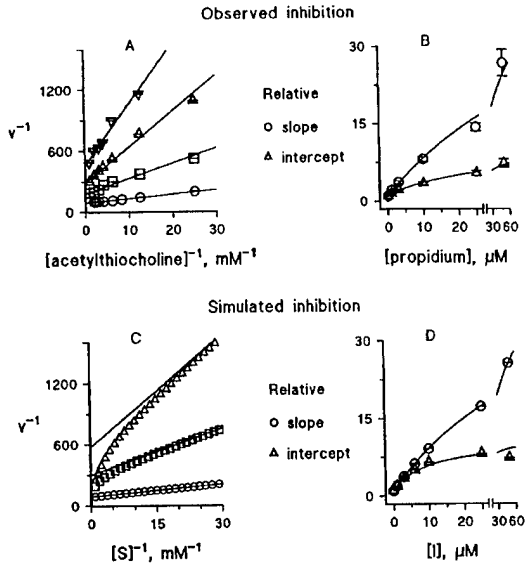

FIGURE 4: Observed and simulated inhibition of AChE-catalyzed acetylthiocholine hydrolysis by propidium. Analyses were conducted as in Figure 3. Part A: Reciprocal plots were obtained at fixed propidium concentrations ((○) 0 μM, (□) 3 μM, (△) 10 μM, (▽) 25 μM) and 25 pM E. Two additional points are offscale and not shown. Part B: Normalized slopes and intercepts of reciprocal plots including those in part A were analyzed to give $K_I = 1.1 \pm 0.1$, $\alpha = 0.019 \pm 0.004$, and $\beta = 0.10 \pm 0.01$ (see Table 1, Case 1). Part C: Plots of v^{-1} vs $[S]^{-1}$ at various [I] ((○) 0 μM; (□) 3 μM; (△) 10 μM) were generated by the SCoP simulation program with rate constant parameters listed for acetylthiocholine and propidium in Table 2. Lines were extrapolated from linear regions of these plots encompassing $[S] = 0.02K_{app}$ to $0.2K_{app}$. Part D: Slopes and intercepts of lines calculated as in part C were analyzed by replot analysis as in part B to obtain the simulated estimates of K_I, α, and β in Table 2.

to estimate a value of a from this value of β, and about all that can be concluded within this equilibrium model for propidium inhibition of acetylthiocholine hydrolysis is that a and/or b is at most 0.1. Values of β are useful, however, because they provide a basis for comparison of the experimental data with the simulated data below.

Nonequilibrium Analysis of AChE Inhibition. We noted in the Introduction that the equilibrium model assumes $k_{-S} \gg k_2$ and that this assumption does not hold for acetylthiocholine hydrolysis by AChE. Nevertheless, the rate equation in eq 5 which assumes equilibrium can still fit the observed inhibition in Figure 4. Are the mechanistic conclusions that $K_I/K_{SI} \cong 0$ or $a \cong 0$ with propidium bound to the peripheral site invalid? To address this question it is necessary to solve the rate equations for Scheme 2 without equilibrium assumptions. This solution has not been examined previously because the corresponding differential equations cannot be solved analytically. These equations can be solved numerically with the SCoP simulation program if reasonable estimates of all rate constants in Scheme 2 are available. Rate constant assignments for acetylthiocholine or phenyl acetate interaction alone with AChE were deduced as described in the Experimental Procedures and are shown in Table 1 (case 1, columns 2−4) or in Table 2. They are likely to be accurate within a factor of 2. Phenyl acetate hydrolysis by AChE also does not involve equilibrium substrate binding, and the primary difference between the assigned rate constants for acetylthiocholine and phenyl acetate was a lower value of k_S for phenyl acetate (see Experimental Procedures and footnote a in Table 2). Rate constants for propidium interaction with free AChE and the *E*S and *E*A intermediates in Scheme 2 are less certain, so we propose a simplifying hypothesis based on the location of the peripheral site at the mouth of the active site gorge. We hypothesize that the effect of propidium binding to this site is simply a steric blockade that decreases equally the association and dissociation rate constants for substrates without altering any other rate constants in Scheme 2. Thus, this steric blockade hypothesis postulates that bound propidium does not alter the thermodynamics of substrate interaction with AChE ($K_{S2} = K_S$). It also stipulates that bound propidium has no effect on acylation and deacylation rate constants ($a = b = 1$), and that bound substrate does not alter propidium interactions ($k_I = k_{SI} = k_{AI}$ and $k_{-I} = k_{-SI} = k_{-AI}$). In this case values for only the two rate constants k_I and k_{-I} for propidium interaction are required. The key feature of the hypothesis is that bound propidium slows substrate entry into and exit from the acylation site ($k_{S2} < k_S$ and $k_{-S2} < k_{-S}$). The only experimental indication to date of the extent of this slowdown involves the effect of fasciculin 2 binding to the peripheral

[4] β^{-1} is defined as the maximal factor by which the intercepts in Figure 3b increased at high concentrations of propidium. Within the equilibrium framework in eq 5, $\beta = ab(k_2 + k_3)/(ak_2 + bk_3)$ and $\beta k_{cat} = abk_2k_3/(ak_2 + bk_3)$.

site on *N*-methylacridinium binding to the acylation site: association and dissociation rate constants for *N*-methylacridinium decreased 8000- and 2000-fold, respectively, in the AChE−fasciculin 2 complex relative to those in free AChE (*27*). Steric blockade by the smaller propidium is likely to be less than that by fasciculin 2. In our simulations (Table 2 and Figures 3c and 4c) we assigned decreases in k_{S2} and k_{-S2} that gave optimal agreement with experimental data, but we also surveyed a range of decreases in these constants as described below.

The SCoP simulation procedure involved solving the set of differential equations corresponding to Scheme 2 to obtain $v = d[P]/dt$. By adjusting the total substrate and AChE amounts and the time, a series of calculated v and [S] pairs were generated as substrate was progressively converted to product at various fixed [I]. Transformation of these pairs to v^{-1} and $[S]^{-1}$ produced reciprocal plots analogous to the experimental data in Figures 3 and 4. Simulated propidium inhibition of phenyl acetate hydrolysis with k_{S2} and k_{-S2} assigned at 5% of k_S and k_{-S}, respectively, is illustrated in Figure 3c. The simulated reciprocal plots were nearly linear over a substrate concentration range corresponding to that accessible experimentally in Figure 3a. Simulated case 1 in Table 1 for propidium and acetylthiocholine, in which k_{S2} and k_{-S2} were 1.5% of k_S and k_{-S}, respectively, is illustrated in Figure 4c. The reciprocal plots were linear at low substrate concentrations, but they deviated downward at concentrations corresponding to the higher substrate concentrations examined experimentally in Figure 4a. These deviations can be eliminated if our steric blockade hypothesis is extended to include a decrease in product dissociation rate constant by bound peripheral site ligand[5] (see Discussion). However, simulations from our initial hypothesis can account for inhibition observed over the lower substrate concentrations typically employed in inhibition analyses of AChE, as the following comparisons indicate. The slopes and intercepts of the linear regions of the simulated reciprocal plots ($[S] < 0.2K_{app}$) increased as [I] became larger. The dependence of these slopes and intercepts on [I] was analyzed by nonlinear regression analyses (Figures 3d and 4d) exactly as done for the experimental data in Figures 3b and 4b. The corresponding curves (Figure 3b vs 3d and Figure 4b vs 4d) showed remarkable similarity, indicating that qualitatively our nonequilibrium hypothesis can account for inhibition of substrate hydrolysis by propidium. For a more quantitative comparison of the simulations with the experimental data, three parameters (K_I, α, and β) were examined for propidium inhibition of acetylthiocholine and phenyl acetate hydrolysis (Table 2). The K_I estimates agreed well, indicating that the K_I estimate from the simulated data still corresponds to the equilibrium constant despite the imposed nonequilibrium conditions. Furthermore, simulated α and β estimates were within about 10% of the corresponding experimental estimates for both substrates. Therefore, quantitatively as well as qualitatively, our nonequilibrium hypothesis can account for the inhibition of phenyl acetate and acetylthiocholine hydrolysis by propidium observed in Figures 3 and 4.

To demonstrate the sensitivity of the simulations to the input values, key simulation rate constants were varied and the effects on calculated values of α and β were assessed. When k_{S2} and k_{-S2} were reduced 10-fold to 0.15% of k_S and k_{-S}, estimates of α and β decreased by factors of three to six (Table 1, case 2). With k_{S2} and k_{-S2} set at 15% of k_S and k_{-S}, estimates of α and β increased to 0.18 and 0.7, respectively (data not shown), and when $k_{S2} = k_S$ and $k_{-S2} = k_{-S}$, α and β became 1.00 (Table 1, case 3). Case 3 demonstrates that, when propidium binding has no effect on any of the rate constants involving substrate hydrolysis, no inhibition is detected even though ligand binding is not at equilibrium.

Under equilibrium conditions our steric blockade hypothesis should result in no inhibition by peripheral site inhibitors. This is clear from eq 5, because the hypothesis stipulates no effect of inhibitor on either substrate binding ($K_{SI} = K_I$) or k_{cat} ($a = b = 1$). Equilibrium in Scheme 2 is approached when k_2/k_{-S} and ak_2/k_{-S2} become small. For example, if the rate constants in case 1 of Table 1 are assumed except for a 100-fold increase in k_{-S} and k_{-S2} ($k_2/k_{-S} = 0.047$ and $ak_2/k_{-S2} = 3.1$), α and β increase (Table 1, case 4) but still reflect some propidium inhibition. A further 100-fold increase in k_{-S} and k_{-S2} (to $k_2/k_{-S} = 0.00047$ and $ak_2/k_{-S2} = 0.031$) increases α to 0.97 and β to 1.00 (Table 1, case 5) and essentially abolishes the inhibition.

It is reassuring that the nonequilibrium model can account quantitatively for propidium inhibition of acetylthiocholine and phenyl acetate hydrolysis, but does this simulation model have any predictive value for the inhibition observed with other peripheral site inhibitors? Gallamine appears to bind exclusively to the peripheral site (*3*). The K_I for gallamine is 30- to 40-fold larger than the K_I for propidium (Table 2), and this lower affinity permits comparison of experimental and simulated values of α and β for a lower affinity inhibitor. The data with acetylthiocholine as substrate are shown in row 2 of Table 2, where the k_1 for gallamine was assumed to be the same as that for propidium and $k_{-1} = (k_1)(K_I)$ was 30 times greater than the k_{-1} for propidium. When k_{S2} and k_{-S2} were maintained at the same values found to be optimal for propidium inhibition of acetylthiocholine hydrolysis (1.5% of k_S and k_{-S}, respectively), the simulated estimates of α and β were again within about 10% of the respective observed values. Gallamine was a less effective inhibitor of phenyl acetate hydrolysis, and the experimental and simulated values were in best accord when the simulated values of k_{S2} and k_{-S2} were 15−20% of k_S and k_{-S}, respectively (Table 2, row 4). Thus the simulations indicate that propidium or gallamine binding to the peripheral site does not reduce the rate constants of substrate association and dissociation for the neutral substrate phenyl acetate as much as for the cationic substrate acetylthiocholine.

Slow Equilibration of Acylation Site Ligands when Propidium Is Bound to the Peripheral Site. The correlation of the simulation results with experimental data in Table 2 is impressive for steady-state inhibition of both acetylthiocholine and phenyl acetate hydrolysis by propidium or gallamine. However, it is important to design additional tests of the steric blockade hypothesis that do not incorporate unknown variables such as the relative magnitudes of k_{S2} and k_S. Reversible inhibitors that equilibrate slowly with the acylation site without interfering with the peripheral site offer such a test. The interaction of an acylation site ligand (L) with AChE (*E*) in the presence of propidium (I) is shown in

[5] T. Szegletes, P. Thomas, W. D. Mallender, and T. L. Rosenberry, manuscript in preparation.

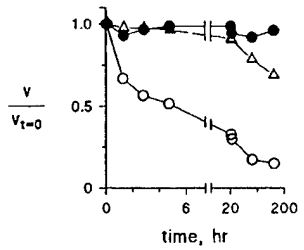

FIGURE 5: Stabilization of AChE-propidium complexes by bovine serum albumin. Incubations were conducted at 23 °C in 20 mM sodium phosphate, 0.02% Triton X-100, (pH 7.0) with (○) 1 nM AChE and 100 μM propidium; (●) 1 nM AChE, 100 μM propidium, and 1.0 mg/mL bovine serum albumin; or (△) 50 pM AChE. At the indicated times aliquots were assayed with acetylthiocholine as outlined in the Experimental Procedures. Assay points v were normalized to a control activity measured at time 0 ($v_{t=0}$). Since the inactivation was not strictly first order, lines simply connect the points. In curve (○), about 50% of the activity was lost after 6 h.

Scheme 3, where I binding to E and EL is assumed to reach equilibrium instantaneously with dissociation constants K_I

Scheme 3

$$\begin{array}{ccc} L + E & \underset{k_{-L}}{\overset{k_L}{\rightleftharpoons}} & EL \\ + & & + \\ I & & I \\ K_I \Big\Updownarrow & & K_{LI} \Big\Updownarrow \\ L + EI_P & \underset{k_{-L2}}{\overset{k_{L2}}{\rightleftharpoons}} & ELI_P \end{array}$$

and K_{LI}, respectively. Binding of L to E and EI_P is much slower and occurs with association rate constants k_L and k_{L2} and dissociation rate constants k_{-L} and k_{-L2}, respectively. Two acylation site ligands for which the rate constants in Scheme 3 can be measured without resorting to rapid kinetics instrumentation are huperzine A (*34*) and the transition state analogue TMTFA (*35*) (see structures in Figure 2). These ligands are also attractive because crystal structures of their complexes with AChE have been determined (see Discussion).

Before assessing the effects of propidium on the association and dissociation rate constants for these acylation site ligands, it was important to confirm AChE stability during incubation with propidium over periods of several days. Propidium in fact was observed to inactivate AChE slowly in 0.02% Triton X-100 and 20 mM sodium phosphate (pH 7.0) alone (Figure 5), but this inactivation was prevented by addition of bovine serum albumin at 1 mg/mL. It has long been known that added protein can stabilize AChE activity (e.g., gelatin; see ref *36*). However, to our knowledge this is the first report that a peripheral site ligand like propidium can promote the inactivation of AChE and that added protein can prevent this enhancement of inactivation. Bovine serum albumin was included in all subsequent experiments with acylation site ligands.

Association and dissociation rate constants for huperzine A were obtained by first determining the rate constant k for the approach to equilibrium binding at various concentrations of L and propidium according to eq 2, next resolving k_{on} and k_{off} from the dependence of k on [L] (eq 3), and then fitting k_{on} and k_{off} to eqs 4a and b. These steps are illustrated in Figure 6a–c. A family of curves showing the approach to equilibrium at several concentrations of huperzine A is shown in Figure 6a, and the k values obtained as in Figure 6a are graphed against the huperzine A concentration in Figure 6b. Estimates of k_{on} and k_{off} from plots such as that in Figure 6b at two fixed concentrations of propidium and in its absence were fitted to eqs 4a,b in Figure 6c. Rate constants obtained from this fitting procedure are given in Table 3. The decrease in the huperzine A association rate constant when propidium is bound at the peripheral site was indicated by the ratio of k_L to k_{L2}, a 49-fold decrease.

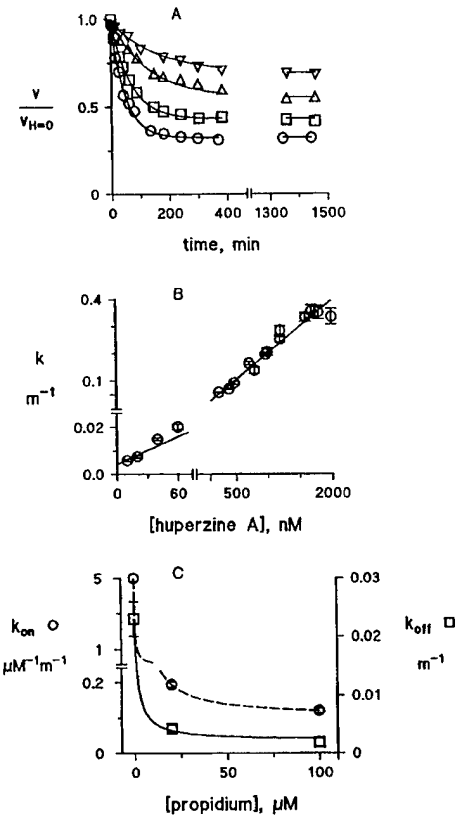

FIGURE 6: Determination of association and dissociation rate constants for huperzine A with both AChE and the AChE–propidium complex. Ligand binding was assumed to occur according to Scheme 3. Part A: Association reactions were initiated by mixing AChE (150 pM) with huperzine A ((○) 60 nM, (□) 40 nM, (△) 20 nM, (▽) 10 nM) and 20 μM propidium, and aliquots were assayed at the indicated times as outlined in the Experimental Procedures. Assay points v were normalized to a control 150 pM AChE activity with 20 μM propidium but without hyperzine A ($v_{H=0}$) and fitted to eq 2 to obtain a value of k for each curve. Part B: Values of k obtained from both part A and additional measurements at 20 μM propidium were plotted against the huperzine A concentration according to eq 3 to obtain $k_{on} = 0.195 \pm 0.007\ \mu M^{-1}m^{-1}$ and $k_{off} = 0.0043 \pm 0.0006\ m^{-1}$. In the absence of propidium, $k_{on} = k_L$ and $k_{off} = k_{-L}$ and a similar analysis was used to obtain the estimates of k_L and k_{-L} in Table 3. Part C: Values of k_{on} and k_{off} were plotted against the propidium concentration according to eqs 4a,b. The above k_L value was fixed in eq 4a, and the k_{on} estimates at 20 μM and 100 μM propidium were then fitted to this equation to obtain the estimates of k_{L2} and K_I in Table 3. Equation 4b was rearranged to the form $k_{off} = (k_{-L} + W[I]/K_I)/(1 + W[I]/K_I k_{-L2})$. The previously obtained k_{-L}, K_I, and $W = k_{L2}K_L$ were then fixed, and this equation was used to fit the k_{-L2} value in Table 3.

Table 3: Propidium Inhibition of Association and Dissociation Rate Constants for Acylation Site Ligands[a]

		acylation site ligand	
kinetic constant	units	huperzine A	TMTFA
k_L	$\mu M^{-1}\ m^{-1}$	5.0 ± 0.2	4.9 ± 0.1
k_{L2}	$\mu M^{-1}\ m^{-1}$	0.102 ± 0.009	0.013 ± 0.003
k_{-L}	m^{-1}	0.023 ± 0.003	$(2.4 \pm 0.1) \times 10^{-4}$
k_{-L2}	m^{-1}	0.0022 ± 0.0005	$(4.2 \pm 0.9) \times 10^{-6}$
K_L	nM	4.6 ± 0.7	0.049 ± 0.003
K_{L2}	nM	22 ± 5	0.32 ± 0.02
K_I	μM	0.39 ± 0.06	0.43 ± 0.05

[a] Values of kinetic constants were calculated as described in Figures 6 and 7.

Similarly, the decrease in the huperzine A dissociation rate constant when propidium is bound at the peripheral site, indicated by the ratio of k_{-L} to k_{-L2}, was about 10-fold. The steric blockade hypothesis is largely supported by these data, as both rate constants were reduced an order of magnitude or more when propidium was bound. A small thermodynamic effect of propidium binding on K_L for huperzine A, however, was also revealed by the fact that the two rate constants were not reduced equally.

The transition state analogue TMTFA has a much higher affinity for the acylation site than huperzine A. The apparent K_L of 49 pM in Table 3 is in reasonable agreement with previous estimates (*35*, *37*). This high affinity prevented application of eq 2, particularly for association reactions at low concentrations of TMTFA that were not in sufficient excess of AChE and for dissociation reactions where the free TMTFA concentration increased significantly over the course of the reaction. Therefore, several individual reaction profiles were fitted simultaneously with the SCoP program to obtain the rate and equilibrium constants in Table 3. Several of these simultaneous fits are shown in Figure 7. The reduction in TMTFA association and dissociation rate constants with propidium bound to the peripheral site was even more pronounced than for huperzine A. The association rate constant k_{L2} was 380-fold smaller than k_L with free AChE, and the dissociation rate constant k_{-L2} was 60-fold smaller than k_{-L} with free AChE. These data provide further support for the steric blockade hypothesis, again with a small thermodynamic effect of bound propidium on the TMTFA affinity.

DISCUSSION

We illustrate here a nonequilibrium alternative to the equilibrium analysis of AChE inhibition by peripheral site ligands. We have examined a very simple hypothesis that bound peripheral site inhibitors only decrease association and dissociation rate constants for acylation site ligands *without* effects on the thermodynamics of the binding of these ligands or the rate constants for substrate acylation and deacylation. In other words, the peripheral site inhibitor is proposed to act as a "permeable cork" at the mouth of the active site "bottle" and thus to slow ligand entry to and exit from the acylation site. This steric blockade hypothesis can account for most if not all of the observed steady-state inhibition. Within an equilibrium framework, AChE inhibition by propidium previously has been attributed entirely to a conformational change at the acylation site induced by the binding of propidium to the peripheral site (*38*). This would

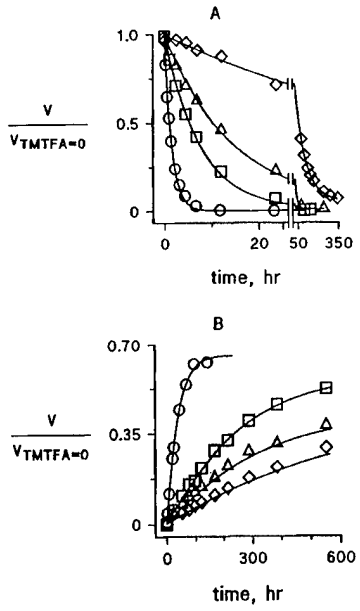

FIGURE 7: Determination of association and dissociation rate constants for TMTFA with both AChE and the AChE–propidium complex. AChE (50–800 pM) was incubated with TMTFA (0.03–320 nM) and propidium (0–100 μM) and aliquots were assayed for AChE activity at various times as outlined in the Experimental Procedures. Assay points (v) were normalized to parallel control assays ($v_{TMTFA=0}$) containing identical [AChE] and [propidium] but without TMTFA. Ligand binding was assumed to occur according to Scheme 3, and the SCoP fitting program was applied directly to the differential equations corresponding to Scheme 3. First, reaction time courses for six association and five dissociation reactions in the absence of propidium were simultaneously fit to give the values of k_L and k_{-L} in Table 3. These values were then fixed in the SCoP program and reaction time courses for five association reactions containing 100 μM propidium and eight dissociation reactions containing 20–100 μM propidium were simultaneously fit to give the values of k_{-L2}, K_{L2}, and K_I values in Table 3. Part A: Assay points and calculated fits to 4 association reactions containing 100 μM propidium, 800 pM AChE, and TMTFA (total concentration: (○) 320 nM, (□) 64 nM, (△) 33 nM, (◇) 6.4 nM). Part B: Assay points and calculated lines to four dissociation reactions containing propidium ((○) 0 μM; (□) 20 μM; (△) 40 μM; (◇) 100 μM), AChE (total concentration: (○) 62 pM, (□) 250 pM, (△) 620 pM, (◇) 620 pM), and TMTFA (total concentration: (○) 77 pM, (□) 310 pM, (△) 770 pM, (◇) 770 pM).

appear reasonable in view of the spatial separation between propidium in the peripheral site and acetylthiocholine in the acylation site. According to the equilibrium model in eq 5, the low values of α and β in Figures 3b and 4b can occur only if a (or b and K_I/K_{SI}) are much less than one, and these inhibitory effects would indeed appear to require a conformational interaction between the two sites. However, the conformational interaction hypothesis fails to provide a satisfactory explanation for several observations. First, propidium only partially inhibits the hydrolysis of *p*-nitrophenyl acetate, showing an α value of about 0.3 (*39*). It is unclear why a proposed conformational interaction would result in α values ranging from less than 0.02 for a good substrate like acetylthiocholine to 0.3 for *p*-nitrophenyl acetate, but this observation is readily accommodated by the steric blockade hypothesis: For *p*-nitrophenyl acetate, the estimated K_{app} is 35-fold higher and k_{cat} is 3-fold lower than the corresponding estimates for acetylthiocholine (*39*). These values indicate that the ratios k_2/k_{-S} and ak_2/k_{-S2} are smaller for *p*-nitrophenyl acetate than for either acetylthiocholine or

phenyl acetate, placing the AChE interactions of this substrate near equilibrium where the steric blockade hypothesis predicts little inhibition. Second, in some mutants (W84A and Y130A) the K_I for propidium inhibition of acetylthiocholine hydrolysis increases up to 100-fold, while the K_{eq} for propidium binding as determined by fluorescence titration remains unchanged (*38*). In these mutants the k_{cat} for acetylthiocholine decreased 10- to 50-fold and/or K_{app} increased by more than 2 orders of magnitude (*37*, *38*), again indicating decreases in k_2/k_{-S} and ak_2/k_{-S2} that should result in less inhibition according to the steric blockade hypothesis. In fact, case 5 in Table 1 predicts no inhibition when increases in k_{-S} and k_{-S2} result in a 2000-fold increase in K_{app}, an increase comparable to the 700-fold reported for acetylthiocholine with the W84A mutant (*38*).

The simulations of steady-state substrate hydrolysis in Tables 1 and 2 provide insight into the mechanism by which peripheral site inhibition can arise within the steric blockade hypothesis. First, the ratios k_2/k_{-S} and ak_2/k_{-S2} must be large enough that the ES and ESI_P complexes in Scheme 2 fail to achieve equilibrium. The k_2/k_{-S} ratio has been denoted C, the commitment to catalysis (*14*), and eq 1c shows that as C approaches and then exceeds unity the second-order substrate hydrolysis rate constant k_{cat}/K_{app} approaches k_S. According to Scheme 1, this reflects a change in the rate-limiting step from k_2 to k_S. At saturating levels of peripheral site inhibitor, the second-order substrate hydrolysis rate constant k_{cat}'/K_{app}' is given by eq 7 under equilibrium conditions and approximated by eq 7 under nonequilibrium conditions (*22*).

$$\frac{k_{cat}'}{K_{app}'} = \frac{k_{S2}ak_2}{k_{-S2} + ak_2} \tag{7}$$

As ak_2 exceeds k_{-S2} in the ESI_P complex, the rate-limiting step similarly becomes k_{S2}. Second, k_{S2} must be smaller than k_S. In this case, increasing saturation of the peripheral site slows the second-order hydrolysis rate constant from k_S to k_{S2}, and this slowdown is reflected in a value of $\alpha < 1$. No further restrictions on rate constants are necessary to obtain inhibition, but it is noteworthy that the relative magnitude of k_{-I} does influence the value of the inhibition parameter β, the relative value of k_{cat} in the ternary complex. The simulated β of 0.5 for gallamine inhibition of acetylthiocholine hydrolysis was significantly larger than the simulated β of 0.09 for propidium inhibition (Table 2). Since the only simulation rate constant that differed between propidium and gallamine was k_{-I}, it is clear that β was sensitive to this rate constant. For propidium k_{-I} was much less than k_2 and k_3, whereas for gallamine k_{-I} was comparable to k_2 and k_3. Thus with propidium the apparent k_{cat} is partially limited by k_{-I}, meaning that with a saturating concentration of propidium and intermediate concentrations of substrate (i.e., roughly between K_{app} and $K_{app}' \cong ak_2/k_{S2}$), most catalytic turnovers of EAI_P are followed by slow dissociation of the EI_P product before the next catalytic turnover. A similar effect of inhibitor dissociation rate constant on k_{cat} was noted previously for a simpler version of Scheme 2 in which EAI_P but not ESI_P can form (*1*, *20*). In contrast, for gallamine k_2 and k_3 alone remain largely rate limiting as in the equilibrium model in eq 5. When k_{-I} was set to a value at least 10 times k_2 or k_3 in case 1 of Table 1, β became 1.0 and k_{-I} had no influence on the relative value of k_{cat} (data not shown).

The nonequilibrium simulations in Tables 1 and 2 generated slope replots that fit eq 6 with high precision, as indicated by the low standard errors for α in Table 2. The intercept replots tended to be bell shaped rather than hyperbolic (see Figure 3d), and this led to greater uncertainty in the estimates of β. The bell-shaped curves arose from slight error that was introduced in the reciprocal plot intercepts by the curvature of the reciprocal plots that was noted in the Results in describing Figures 3c and 4c. Not all of the curvature was eliminated by restricting the simulation analyses to the low concentrations of substrate indicated. The curvature occurs because inhibition in our steric blockade model here arises exclusively from a decrease in the substrate association constant when inhibitor occupies the peripheral site ($k_{S2}/k_S \ll 1$). At high substrate concentrations with this model (i.e., as [S] approaches and exceeds $K_{app}' \cong ak_2/k_{S2}$), most catalytic turnovers of EAI_P are followed by substrate association with EI_P that is faster than the slow dissociation of EI_P. Hydrolysis rates approach those in the absence of inhibitor because ak_2 and bk_3 become rate limiting, and inhibitor does not affect these steps because the model sets $a = b = 1$. A logical extension of Scheme 2 consistent with the steric blockade model is to propose that bound peripheral site ligand not only reduces association and dissociation rate constants for substrate binding to the acylation site but also reduces the dissociation rate constant for product release from this site. If product affinity for the acylation site is sufficiently high, then product release may become partially rate-limiting when the peripheral site is occupied. We have found that this extension can eliminate the curvature in the reciprocal plots and give quantitative agreement between simulated and experimental data over the entire range of substrate concentrations. Furthermore, if substrate can form a low affinity complex at the peripheral site and block product dissociation from the acylation site, this extended model can account quantitatively for substrate inhibition.[5] The necessity for slight revision of the simplest version of the steric blockade hypothesis offered here also is indicated by consistent observations of small decreases in the affinity of ligands in ternary AChE complexes relative to the corresponding binary complex. In Table 3 this decrease, indicated by the ratio of K_{L2}/K_L, was a factor of 4.7 ± 1.4 for huperzine A and of 6.5 ± 0.6 for TMTFA in the AChE−propidium complex relative to the free enzyme. Other studies have shown an affinity decrease of about 5 for edrophonium (*22*) and 4 for methylacridinium (*27*) in the AChE−fasciculin 2 complex relative to free AChE. The consistent magnitude of these factors suggests that affinity decreases of cationic ligands in many AChE ternary complexes are governed by general properties such as electrostatic attraction rather than specific conformational interaction. Even though the steric blockade hypothesis here proposed no changes in equilibrium constants in AChE ternary complexes, a minor 5-fold decrease in ligand affinities in the ternary complexes can be incorporated into the hypothesis with virtually no effect on simulated values of α and β. For example, a 5-fold increase in k_{-S2} and k_{-SI} from their values in case 1 of Table 1 changes the simulated values of α and β by less than 8% (data not shown).

Despite the agreement of the simulated and experimental data for the two substrates and two inhibitors in Table 2, these data provide only a correlation and do not prove our

nonequilibrium steric blockade hypothesis. The predictive power of the hypothesis would be enhanced if *all* the rate constants in the simulations could be assigned independently, but independent estimates of k_{S2} and k_{-S2} for substrates are very difficult to obtain. Alternatively, the hypothesis predicts that not only substrates but also ligand inhibitors that bind to the acylation site should show decreased association and dissociation rate constants (k_{L2} and k_{-L2}) when a peripheral site ligand like propidium is bound. Most acylation site ligands equilibrate too rapidly to test this prediction. For example, *N*-methylacridinium has a K_I in the micromolar range and equilibrates with AChE in about a msec or less (*27*, *40*). However, huperzine A binds near the acylation site (*28*) and equilibrates slowly enough to allow measurement of association and dissociation rate constants (*34*). Furthermore, the AChE complex with the trifluoromethyl ketone TMTFA provides an excellent model of the transition state for acylation by acetylcholine. The crystal structure of the TMTFA−TcAChE complex shows a tetrahedral adduct that nearly superimposes on a calculated structure of acetylcholine in the active site (*29*). TMTFA has no leaving group, so it accumulates as the tetrahedral adduct. Molecular modeling of the ternary complexes of these ligands with TcAChE−propidium revealed that the bound propidium is separated by at least 1.6 Å from either bound huperzine A or bound TMTFA (Figure 8), indicating that no overlap occurs in the binding sites that could perturb equilibrium affinities in the ternary complexes. As noted above in support of this conclusion, the 4- to 7-fold decreases in ligand equilibrium affinities in these ternary complexes are comparable to those reported previously for ternary complexes involving fasciculin 2 in the peripheral site. Measured values of k_{L2} and k_{-L2} for huperzine A and TMTFA with the AChE−propidium complex provide compelling support for our steric blockade hypothesis. These rate constants are 49- and 10-fold lower for huperzine A and 380- and 60-fold lower for TMTFA than the respective rate constants k_L and k_{-L} for the interaction of these ligands with free AChE. It is particularly satisfying that the magnitude of these decreases for the acetylcholine analogue TMTFA agrees so well with the simulated k_S/k_{S2} ratio of about 70 that was found to provide the best correspondence to observed kinetic parameters for acetylthiocholine and propidium in Table 2.

Does the successful application of our steric blockade hypothesis in this report rule out any conformational interaction between the peripheral and acylation sites? We argue that it probably does when the peripheral site is occupied by small ligands such as propidium and gallamine. Proof of this conformational interaction now requires evidence beyond steady-state measurements of the extent of propidium inhibition. For example, with the larger ligand fasciculin 2 bound to the peripheral site, we previously reported not only steric blockade of ligand access to the acylation site (*27*) but also a conformational change in the acylation site that decreased the efficiency of the catalytic triad (*22*). This additional conformational effect of bound fasciculin is seen most clearly by comparing estimates of the dissociation rate constant k_{-L2} for TMTFA. In contrast to the 60-fold decrease in this rate constant observed here for the AChE−propidium−TMTFA complex relative to k_{-L} for AChE-TMTFA, a 20-fold *increase* in k_{-L2} relative to k_{-L} was reported for

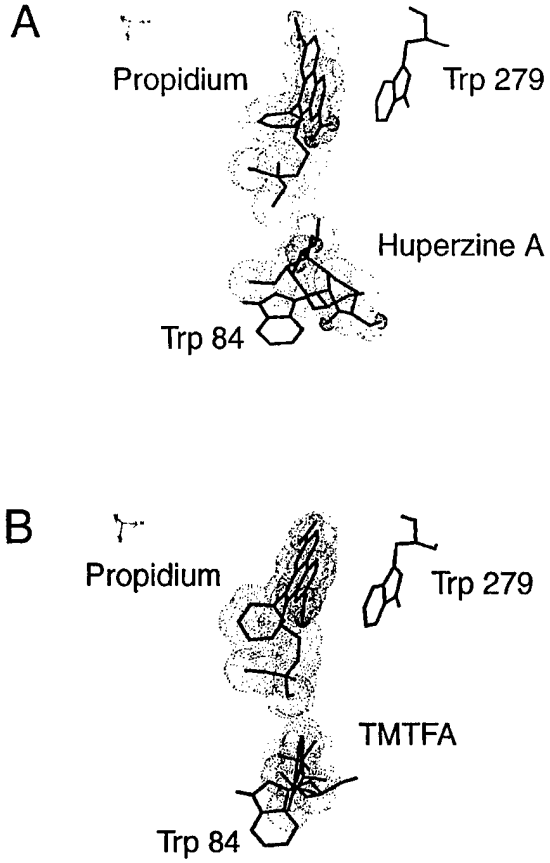

FIGURE 8: Molecular models of ternary complexes involving propidium and TcAChE. Residues are marked by a heavy line with propidium and acylation site ligand van der Waals spheres shown by a dotted surface. Nonpolar hydrogen atoms have been omitted for clarity. The conformation of propidium in the TcAChE−huperzine A complex (part A) was very similar to that in the TcAChE−TMTFA adduct (part B). The overall root mean square deviation between matched atoms in the two models was 0.25 Å. Atom to atom closest contacts between the propidium alkyl chain and the acylation site inhibitors are 1.6 Å (huperzine A) and 1.7 Å (TMTFA). Comparison of the propidium molecule between the two models revealed only minor changes in both the planarity of the aromatic ring and the position of the alkyl chain.

the AChE-fasciculin 2-TMTFA complex (*37*).[6] The increase results in conformational destabilization of the tetrahedral TMTFA adduct in this ternary complex ($K_{L2}/K_L \cong 200$), and the conformational effect predominates over steric blockade of TMTFA egress in determining the net change in k_{-L2}. Crystal structure analyses of fasciculin-AChE complexes (*8*, *9*) show that fasciculin 2 interacts not only with W279 in the peripheral site but also with residues on the outer surface of an ω-loop within 4 Å of W84 in the acylation site, well beyond the region of the peripheral site occupied by propidium (see Figures 7 and 8). These more extensive surface interactions provide a structural basis for an inhibitory conformational effect on the acylation site when fasciculin rather than propidium is bound to the peripheral site.

ACKNOWLEDGMENT

We express our gratitude to Dr. Michel Roux at the Ecole Normale Superieure in Paris, France, for bringing the SCoP

[6] J. Eastman, P. Thomas, G. Rogers, J. Yustein, and T. L. Rosenberry, unpublished observations.

program to our attention. We also acknowledge the technical assistance of Mr. Mark Frey in early measurements of propidium inhibition of substrate hydrolysis and thank Dr. Daniel Quinn in the Department of Chemistry at the University of Iowa for kindly supplying TMTFA.

REFERENCES

1. Rosenberry, T. L. (1975) Acetylcholinesterase, in *Advances in Enzymology* (Meister, A., Ed.) Vol. 43, pp 103−218, John Wiley & Sons, New York.
2. Sussman, J. L., Harel, M., Frolow, F., Oefner, C., Goldman, A., Toker, L., and Silman, I. (1991) *Science 253*, 872−879.
3. Taylor, P., and Lappi, S. (1975) *Biochemistry 14*, 1989−1997.
4. Weise, C., Kreienkamp, H.-J., Raba, R., Pedak, A., Aaviksaar, A., and Hucho, F. (1990) *EMBO J. 9*, 3885−3888.
5. Schalk, I., Ehret-Sabatier, L., Bouet, F., Goeldner, M., and Hirth, C. (1992) in *Multidisciplinary Approaches to Cholinesterase Functions* (Shafferman, A., and Velan, B., Eds.) pp 117−120, Plenum Press, New York.
6. Radic, Z., Pickering, N. A., Vellom, D. C., Camp, S., and Taylor, P. (1993) *Biochemistry 32*, 12074−12084.
7. Barak, D., Kronman, C., Ordentlich, A., Ariel, N., Bromberg, A., Marcus, D., Lazar, A., Velan, B., and Shafferman, A. (1994) *J. Biol. Chem. 269*, 6296−6305.
8. Harel, M., Kleywegt, G. J., Ravelli, R. B. G., Silman, I., and Sussman, J. L. (1995) *Structure 3*, 1355−1366.
9. Bourne, Y., Taylor, P., and Marchot, P. (1995) *Cell 83*, 503−512.
10. Karlsson, E., Mbugua, P. M., and Rodriguez-Ithurralde, D. (1984) *J. Physiol. (Paris) 79*, 232−240.
11. Marchot, P., Khelif, A., Ji, Y.-H., Masnuelle, P., and Bourgis, P. E. (1993) *J. Biol. Chem. 268*, 12458−12467.
12. Nachmansohn, D., and Wilson, I. B. (1951) *Adv. Enzymol. 12*, 259−339.
13. Briggs, G. E., and Haldane, J. B. S. (1925) *Biochem. J. 19*, 338−339.
14. Quinn, D. M. (1987) *Chem. Rev. 87*, 955−979.
15. Dixon, M., and Webb, E. C. (1958) *Enzymes*, pp 171−181, Academic Press, New York.
16. Rosenberry, T. L., and Scoggin, D. M. (1984) *J. Biol. Chem. 259*, 5643−5652.
17. Roberts, W. L., Kim., B. H., and Rosenberry, T. L. (1987) *Proc. Natl. Acad. Sci. U.S.A. 84*, 7817−7821.
18. Riddles, P. W., Blakeley, R. L., and Zerner, B. (1979) *Anal. Biochem. 94*, 75−81.
19. Ellman, G. L., Courtney, K. D., Andres, J. V., and Featherstone, R. M. (1961) *Biochem. Pharmacol. 7*, 88−95.
20. Hodge, A. S., Humphrey, D. R., and Rosenberry, T. L. (1992) *Mol. Pharmacol. 41*, 937−942.
21. Rosenberry, T. L. (1975) *Proc. Natl. Acad. Sci. U.S.A. 72*, 3834−3838.
22. Eastman, J., Wilson, E. J., Cervenansky, C., and Rosenberry, T. L. (1995) *J. Biol. Chem. 270*, 19694−19701.
23. Hindmarsh, A. C. (1983) in *Scientific Computing* (Stepleman, R. S., et al., Eds.) pp 55−64, North-Holland, Amsterdam.
24. Petzhold, L. R. (1983) *SIAM J. Sci. Stat. Comput. 4*, 136−148.
25. Froede, H. C., and Wilson, I. B. (1984) *J. Biol. Chem. 259*, 11010−11013.
26. Gnagey, A. L., Forte, M., and Rosenberry, T. L. (1987) *J. Biol. Chem. 262*, 13290−13298.
27. Rosenberry, T. L., Rabl, C. R., and Neumann, E. (1996) *Biochemistry 35*, 685−690.
28. Raves, M. L., Harel, M., Pang, Y.-P., Silman, I., Kozikowski, A. P., and Sussman, J. L. (1997) *Nat. Struct. Biol. 4*, 57−63.
29. Harel, M., Quinn, D. M., Nair, H. K., Silman, I., and Sussman, J. L. (1996) *J. Am. Chem. Soc. 118*, 2340−23346.
30. Botts, J., and Morales, M. (1953) *Trans. Faraday Soc. 49*, 696−707.
31. Bernhard, S. A. (1968) The Structure and Function of Enzymes, in *Biology Teaching Monograph Series* (Levinthal, C., Ed.) pp 80−85, W. A. Benjamin, Inc., New York.
32. Krupka, R. M., and Laidler, K. J. (1961b) *J. Am. Chem. Soc. 83*, 1454−1458.
33. Barnett, P., and Rosenberry, T. L. (1977) *J. Biol. Chem. 252*, 7200−7206.
34. Ashani, Y., Grunwald, J., Kronman, C., Velan, B., and Shafferman, A. (1994) *Mol. Pharmacol. 45*, 555−560.
35. Nair, H. K., Lee, K., and Quinn, D. M. (1993) *J. Am. Chem. Soc. 115*, 9939−9941.
36. Wilson, I. B., and Bergmann, F. (1950) *J. Biol. Chem. 185*, 479−489.
37. Radic, Z., Quinn, D. M., Vellom, D. C., Camp, S., and Taylor, P. (1995) *J. Biol. Chem. 270*, 20391−20399.
38. Barak, D., Ordentlich, A., Bromberg, A., Kronman, C., Marcus, D., Lazar, A., Ariel, N., Velan, B., and Shafferman, A. (1995) *Biochemistry 34*, 15444−15452.
39. Ordentlich, A., Barak, D., Kronman, C., Flashner, Y., Leitner, M., Segall, Y., Ariel, N., Cohen, S., Velan, B., and Shafferman, A. (1993) *J. Biol. Chem. 268*, 17083−17095.
40. Rosenberry, T. L., and Neumann, E. (1977) *Biochemistry 16*, 3870−3878.

BI972158A

Biochemistry **1999,** *38,* 122−133

Substrate Binding to the Peripheral Site of Acetylcholinesterase Initiates Enzymatic Catalysis. Substrate Inhibition Arises as a Secondary Effect†

Tivadar Szegletes,‡ William D. Mallender,‡ Patrick J. Thomas,§ and Terrone L. Rosenberry*,‡

Department of Pharmacology, Mayo Foundation for Medical Education and Research, Department of Research, Mayo Clinic Jacksonville, Jacksonville, Florida 32224, and Department of Pharmacology, Case Western Reserve University School of Medicine, Cleveland, Ohio 44120-4965

Received June 9, 1998; Revised Manuscript Received October 13, 1998

ABSTRACT: Two sites of ligand interaction in acetylcholinesterase (AChE) were first demonstrated in ligand binding studies and later confirmed by crystallography, site-specific mutagenesis, and molecular modeling: an acylation site at the base of the active site gorge and a peripheral site at its mouth. We recently introduced a steric blockade model which demonstrated how small peripheral site ligands such as propidium may inhibit substrate hydrolysis [Szegletes, T., Mallender, W. D., and Rosenberry, T. L. (1998) *Biochemistry 37,* 4206−4216]. In this model, the only effect of a bound peripheral site ligand is to decrease the association and dissociation rate constants for an acylation site ligand without altering the equilibrium constant for ligand binding to the acylation site. Here, we first provide evidence that not only rate constants for substrates but also dissociation rate constants for their hydrolysis products are decreased by bound peripheral site ligand. Previous reaction schemes for substrate hydrolysis by AChE were extended to include product dissociation steps, and acetylthiocholine hydrolysis rates in the presence of propidium under nonequilibrium conditions were simulated with assigned rate constants in the program SCoP. We next showed that cationic substrates such as acetylthiocholine and 7-acetoxy-*N*-methylquinolinium (M7A) bind to the peripheral site as well as to the acylation site. The neurotoxin fasciculin was used to report specifically on interactions at the peripheral site. Analysis of inhibition of fasciculin association rates by these substrates revealed K_S values of about 1 mM for the peripheral site binding of acetylthiocholine and 0.2 mM for the binding of M7A. The AChE reaction scheme was further extended to include substrate binding to the peripheral site as the initial step in the catalytic pathway. Simulations of the steric blockade model with this scheme were in reasonable agreement with observed substrate inhibition for acetylthiocholine and M7A and with mutual competitive inhibition in mixtures of acetylthiocholine and M7A. Substrate inhibition was explained by blockade of product dissociation when substrate is bound to the peripheral site. However, our analyses indicate that the primary physiologic role of the AChE peripheral site is to accelerate the hydrolysis of acetylcholine at low substrate concentrations.

The hydrolysis of the neurotransmitter acetylcholine by acetylcholinesterase (AChE)[1] is one of the most efficient enzyme catalytic reactions known (*1*). The basis of this high efficiency has been investigated with ligand binding studies interpreted in the context of the AChE three-dimensional structure determined by X-ray crystallography (*2*). The long and narrow active site gorge is about 20 Å deep and includes two sites of ligand interaction: an *acylation site* at the base of the gorge and a *peripheral site* at its mouth. In the acylation site, residue S200 (TcAChE sequence numbering) is acylated and deacylated during substrate turnover, H440 and E327 participate with S200 in a catalytic triad, and W84 binds to the trimethylammonium group of acetylcholine as acyl transfer to S200 is initiated. The peripheral site involves other residues including W279 (*3*−*8*). Ligands can bind selectively to either the acylation or the peripheral sites, and ternary complexes with distinct ligands bound to each site can form (*9*). Ligands that bind specifically to the peripheral site include the phenanthridinium derivative propidium and the fasciculins, a family of very similar snake venom neurotoxins comprised of 61-amino acid polypeptides (*7*, *8*, *10*, *11*).

Despite its prominence, the role of the peripheral site in the AChE catalytic pathway has remained obscure. From analysis of the effect of ionic strength on k_{cat}/K_{app}, we proposed several years ago that acetylthiocholine binding to the active site is controlled by a high net negative charge near the active site that can electrostatically attract cationic substrates and inhibitors (*12*). Molecular modeling calculations (*13*, *14*) from the three-dimensional structure support this notion by suggesting that the AChE catalytic subunit has a dipole moment aligned with the active site gorge that can accelerate association rate constants for cationic ligands. The extent of this acceleration, measured as a ratio of the

† This work was supported by Grant NS-16577 from the National Institutes of Health and by grants from the Muscular Dystrophy Association of America. W.D.M. was supported by a Kendall-Mayo Postdoctoral Fellowship.

* To whom correspondence should be addressed.

‡ Mayo Clinic Jacksonville.

§ Case Western Reserve University School of Medicine.

[1] Abbreviations: AChE, acetylcholinesterase; TcAChE, acetylcholinesterase from *Torpedo californica*; DTNB, 5,5′-dithiobis(2-nitrobenzoic acid); TMTFA, *m*-(*N,N,N*-trimethylammonio)trifluoroacetophenone; M7A, 7-acetoxy-*N*-methylquinolinium; M7H, 7-hydroxy-*N*-methylquinolinium.

10.1021/bi9813577 CCC: $18.00
Published on Web 12/12/1998

association rate constant at low ionic strength to that at high ionic strength, depends on the cationic ligand and the species of AChE, but it appears to be about a factor of 7.5 for the cation TMTFA with mouse AChE at zero ionic strength (*15*). However, mutation of up to seven negatively charged residues at or near the peripheral site on the gorge rim reduced this factor by less than 60% (*15*, *16*), indicating that the peripheral site makes only a modest contribution to the electrostatic field at the active site. A second possibility is that ligand binding to the peripheral site results in a conformational change that promotes catalysis. Many peripheral site ligands inhibit substrate hydrolysis, and AChE inhibition by propidium has been attributed entirely to a conformational change at the acylation site induced by the binding of propidium to the peripheral site (*17*). If substrate interacted with the peripheral site on entering the active site gorge, this interaction in principle could induce a conformational change that might promote substrate hydrolysis. However, we recently introduced a steric blockade model which demonstrated how small peripheral site ligands such as propidium may inhibit substrate hydrolysis without inducing a conformational change in the acylation site (*18*). This model includes the simple hypothesis that the only effect of a bound peripheral site ligand is to decrease the association and dissociation rate constants for an acylation site ligand without altering the equilibrium constant for ligand binding to the acylation site. This hypothesis was generally supported by our direct demonstration that bound propidium decreased the association and dissociation rate constants for the acylation site ligands huperzine A and TMTFA by factors of 10−400. Therefore, there is little evidence that the binding of substrates and other small ligands to the peripheral site induces a conformational change that is significant with respect to catalysis.

In this paper, we show that further examination of our steric blockade model leads directly to a proposed new role for the peripheral site, namely, the initial binding of substrate on the AChE catalytic pathway. A similar role has been suggested for a peripheral site in the closely related enzyme butyrylcholinesterase (*19*). The first step in clarifying this role in AChE was to analyze further the inhibition of substrate hydrolysis by peripheral site ligands. We conducted nonequilibrium simulations that accounted quantitatively for inhibition by peripheral site ligands at low substrate concentrations but diverged from experimental data at higher substrate concentrations (*18*). The discordance prompted us here to extend the model to include steric blockade of product dissociation as well as of substrate association and dissociation by a bound peripheral site ligand. The extended model not only brought the simulations into quantitative agreement with experimental data at all substrate concentrations but also suggested that substrate binding to the peripheral site could block product release and account for the well-known phenomenon of substrate inhibition with AChE. With a competition assay for fasciculin binding to quantify the affinity of substrates for the peripheral site, we then demonstrated a satisfactory correspondence of the simulated and observed substrate inhibition data. The complete model indicates that the peripheral site serves as an initial binding site for substrate entry to the acylation site and that this initial binding accelerates the rate constant (k_{cat}/K_{app}) for substrate hydrolysis at low substrate concentrations.

EXPERIMENTAL PROCEDURES

Materials. Human erythrocyte AChE was purified as outlined previously, and active site concentrations were determined by assuming 410 units/nmol (*20*, *21*). Propidium iodide was purchased from Calbiochem. M7H iodide and some stocks of M7A iodide were obtained from Molecular Probes, while other stocks of M7A iodide were synthesized by the Mayo Clinic Jacksonville Organic Synthesis Core Facility. Fasciculin was the fasciculin 2 form obtained from C. Cervenansky at the Instituto de Investigaciones Biologicas (Clemente Estable, Montevideo, Uruguay) (*22*).

Steady State Measurements of AChE-Catalyzed Substrate Hydrolysis. Hydrolysis rates v were measured at various substrate (S) concentrations in 1 mL assay solutions with buffer (20 mM sodium phosphate and 0.02% Triton X-100 at pH 7.0) at 25 °C. To maintain a constant ionic strength with protocols in which the acetylthiocholine concentration exceeded 1 mM, NaCl was added such that the sum of the acetylthiocholine and NaCl concentrations was 60 mM. Acetylthiocholine assay solutions included 0.33 mM DTNB, and hydrolysis was monitored by formation of the thiolate dianion of DTNB at 412 nm [$\Delta\epsilon_{412nm} = 14.15$ mM^{-1} cm^{-1} (*23*)] for 1−5 min on a Varian Cary 3A spectrophotometer (*24*). Hydrolysis of M7A was followed by formation of M7H at 406 nm ($\Delta\epsilon_{406nm} = 9.2$ mM^{-1} cm^{-1} at pH 7.0), and nonenzymatic hydrolysis rates were deducted (*25*, *26*).

At high concentrations of acetylthiocholine and M7A, v declined below the maximal hydrolysis rates observed at lower S concentrations. The dependence of v on [S] was fitted to the Haldane equation for substrate inhibition (*27*) as shown in eq 1.

$$v = \frac{V_{max}[S]}{[S]\left(1 + \frac{[S]}{K_{SS}}\right) + K_{app}} \quad (1)$$

In eq 1, $V_{max} = k_{cat}[E]_{tot}$ where $[E]_{tot}$ is the total concentration of AChE active sites. Data were fitted with Fig.P (BioSoft, version 6.0) to eq 1 by nonlinear regression analyses; with experimental data, weighting assumed that v has a constant percent error.

At low concentrations of acetylthiocholine and M7A, reciprocal plots of v^{-1} vs $[S]^{-1}$ were linear. Competitive inhibition constants (K_I) for inhibitors I were obtained by either (1) analysis of replots of reciprocal plot slopes obtained over a range of fixed concentrations of I (*18*) or (2) direct measurements of the second-order hydrolysis rate constants z in the presence and absence of I at low S concentrations. When I was a competing substrate, z was measured as an initial velocity at low S concentrations (i.e., $[S] < 0.1K_{app}$). The extent of acetylthiocholine hydrolysis in the presence of M7A was measured with 20 μM pyridine disulfide (2,2′-dithiobispyridine; Acros) in place of DTNB. Absorbance of pyridine thiol was monitored at 347 nm [$\Delta\epsilon_{341nm} = 8.1$ mM^{-1} cm^{-1} (*28*)] because 347 nm corresponded to the isosbestic point of M7H and M7A. The extent of M7A hydrolysis in the presence of acetylthiocholine was measured on a Perkin-Elmer LS 50B luminescence spectrometer [excitation at 400 nm, emission at 500 nm (*25*)]. When I was an inhibitor that

was not metabolized, z was determined as a pseudo-first-order rate constant from eq 2 (*22*).

$$[S] = [S]_0 e^{-zt} \quad (2)$$

Equation 2 is valid when the initial substrate concentration $[S]_0$ is low (i.e., $[S]_0 \ll K_{SS}$ and $[S]_0 <$ about $0.2K_{app}$). In the absence of I, z is denoted $z_{I=0} = V_{max}/K_{app}$ and eq 2 corresponds to the integrated form of eq 1. Measured z values at various I concentrations were fitted to eq 3 to obtain K_I and the constant α (*18*).

$$\frac{z}{z_{I=0}} = \frac{\left(1 + \frac{[I]}{K_I}\right)}{\left(1 + \frac{\alpha[I]}{K_I}\right)} \quad (3)$$

For inhibitors that bind to the peripheral site and form ternary complexes ESI_P (see Scheme 1 below), α is a measure of the acylation rate constant through the ternary complex at low substrate concentrations relative to k_{cat}/K_{app} (*18*). In contrast, for inhibitors that bind preferentially to the acylation site, α is essentially zero.

Slow Equilibration of Fasciculin in the Presence of Peripheral Site Inhibitors. The rates of fasciculin binding to the AChE peripheral site were analyzed by an extension of procedures used previously (*22*). Association reactions (2 mL) were initiated by adding small volumes of AChE and acetylthiocholine to final concentrations of 0.5−10 nM fasciculin and 0.1 mM DTNB in buffer (with [NaCl] = 60 mM − [S] as above) at 25 °C. Some reaction mixtures also included 20 μM propidium. The extent of fasciculin binding was measured under approximate first-order conditions in which the concentrations of all ligands were adjusted to at least 8 times the concentration of AChE and the acetylthiocholine level was not significantly depleted (<20%). Acetylthiocholine hydrolysis was monitored by continuous spectrophotometric assay as outlined above, and assay rates v over 2 s intervals were fitted by nonlinear regression analysis (Fig.P) to eq 4. In eq 4, $v_{initial}$ and v_{final} are the calculated values of v at time zero and at the final steady state when fasciculin binding has reached equilibrium, and k is the observed first-order rate constant for the approach to equilibrium.

$$v = v_{final} + (v_{initial} - v_{final})\, e^{-kt} \quad (4)$$

Each series of binding measurements included reactions at a fixed acetylthiocholine (S) concentration and at least four fasciculin concentrations [F]. The observed k for each reaction was given by eq 5, and k_{on}, the apparent association rate constant, was determined by weighted linear regression analysis in which k was assumed to have a constant percent error.

$$k = k_{on}[F] + k_{off} \quad (5)$$

If ligand binding to the peripheral site is unaffected by the presence of ligands or an acyl group at the acylation site, then only three sets of enzyme species need be considered: ΣE, ΣES_P, and ΣEI_P. These are the sums of the concentrations of all enzyme species in which nothing, S, or propidium (I), respectively, is bound to the peripheral site. Assuming that fasciculin (F) reacts only with species in ΣE and ΣES_P, k_{on} is given by eq 6.

$$k_{on} = \frac{k_F + k_{FP}\frac{[S]}{K_S}}{1 + \frac{[S]}{K_S} + \frac{[I]}{K_I}} \quad (6)$$

In eq 6, k_F is the intrinsic association rate constant for E and F, k_{FP} is the intrinsic association rate constant for ES_P and F, and K_S and K_I are the equilibrium dissociation constants for S and I, respectively, at the peripheral site. When eq 6 was employed, mean values of k_{on} obtained at each S concentration were fitted with Fig.P by nonlinear regression analysis with the reciprocals of the variances as weighting factors to give apparent K_S estimates. If ligand binding to the peripheral site is altered by the presence of a ligand at the acylation site, then k_{on} in eq 6 in principle must be extended by additional terms (*26*, *29*). We will assume that these additional terms can be grouped in ΣEX_A as shown in eq 7, where the specific terms in each sum are given in Scheme 5 in the Appendix and k_{FA} is the intrinsic association rate constant for species in ΣEX_A and F.

$$k_{on} = \frac{k_F([E] + [EA]) + k_{FP}\sum ES_P + k_{FA}\sum EX_A}{[E] + [EA] + \sum ES_P + \sum EX_A + \sum EI_P} \quad (7)$$

Equation 7 cannot be solved analytically, but it can be solved numerically with the SCoP simulation program as outlined in the text.

The value of K_S for M7A was obtained by a modification of the above procedure in which fasciculin association reactions were measured at 412 nm with 2 nM fasciculin, 0.25 mM acetylthiocholine, and 0−300 μM M7A in 1.0 mL of buffer without added NaCl. Observed k values were assumed to approximate k_{on}, and K_S was calculated from eq 6 (with [I] and k_{FP} set to 0).

Simulations of Kinetic Equations and Assignment of Simulation Rate Constants. The calculation of substrate hydrolysis rates from AChE reaction pathways in which reversible reactions are not at equilibrium is difficult because solutions to the corresponding differential equations are too complex for useful comparison to experimental data. We previously described our application of the program denoted SCoP (version 3.51), developed through the NIH National Center for Research Resources and available from Simulation Resources, Inc. (Redlands, CA), to solve these equations numerically (*18*). To obtain the simulated solutions to reaction schemes with the SCoP program, values for all reaction rate constants must be assigned or fitted. For Scheme 1, the second-order rate constant for substrate hydrolysis in the absence of inhibitor is given by eq 8.

$$\frac{k_{cat}}{K_{app}} = \frac{k_S k_2}{k_{-S} + k_2} \quad (8)$$

We previously showed (*18*) that values of k_S and k_{-S} in eq 8 could be assigned if (1) estimates of k_{cat}, K_{app}, and k_2 were

Table 1: Rate Constants for Simulated Substrate Hydrolysis and Substrate Inhibition with AChE[a]

substrate	k_S (μM^{-1} s^{-1})	k_{-S} (s^{-1})	k_1[b] (s^{-1})	k_{-1}[b] (s^{-1})	k_2, k_3 (s^{-1})	k_{-P}[c] (s^{-1})	k_{-P2}/k_{-P} (s^{-1})	a–f, i
acetylthiocholine	150[d]	2×10^5	3×10^6	4×10^4	1.4×10^4	1.3×10^5	0.01	1
M7A	200	4×10^4	8×10^4	4×10^3	1.4×10^4	1.3×10^3	0.01	1

[a] Simulations for both substrates were generated as outlined in the text with the indicated values of rate constants defined in Scheme 5 in the Appendix. [b] Calculated from eq 9 or 10 with an R_S that was assumed to be 1.0 (see Experimental Procedures). [c] Assigned from measured values for K_P of 0.66 ± 0.03 mM for thiocholine or 6.4 ± 0.6 μM for M7H as outlined in Experimental Procedures. [d] The extent of substrate inhibition with acetylthiocholine was measured at a constant ionic strength slightly higher than that in other experiments (see Experimental Procedures). Ionic strength affects primarily K_{app} but not k_{cat} (*12*); k_S, assumed to be the only rate constant sensitive to ionic strength, was recalculated from K_{app}.

available and (2) the solvent deuterium oxide isotope effects R, R_S, and R_2 were known, where R, R_S, and R_2 are the respective ratios of k_{cat}/K_{app}, k_S, and k_2 in H_2O to that in D_2O. When R_2 was assigned a typical value of 2.5 and R_S was assumed to be 1.0, for example, $k_S = 1.5(k_{cat}/K_{app})/(2.5 - R)$.

The second-order substrate hydrolysis rate constant in Scheme 3 in the Results is given by eq 9.

$$\frac{k_{cat}}{K_{app}} = \frac{k_S k_1 k_2}{k_{-S} k_{-1} + k_2 (k_{-S} + k_1)} \quad (9)$$

Assuming again that k_2 and k_S are the only intrinsic rate constants in this equation that are altered when H_2O is replaced by D_2O and that $R_2 = 2.5$, eq 10 may be derived.

$$\frac{k_S}{1 + \frac{k_{-S}}{k_1}} = \frac{1.5 k_{cat}}{K_{app}\left(2.5 - \frac{R}{R_S}\right)} \quad (10)$$

To assign the intrinsic rate constants in eq 9, we inserted independent estimates of k_{cat} and K_{app} into eq 10. For example, for acetylthiocholine and human AChE, we previously estimated that $k_{cat} = 7000$ s^{-1} and $k_2 = k_3 = 1.4 \times 10^4$ s^{-1} (*18*). With a measured value for K_{app} of 58 μM (Table 2 below), eq 10 requires that $k_S > k_{cat}/K_{app} = 120$ μM^{-1} s^{-1}. For M7A, we obtained k_{cat}/K_{app} from parallel measurements of V_{max}/K_{app} (as the constant $z_{I=0}$ in eq 2) for M7A and acetylthiocholine. The k_{cat}/K_{app} for M7A was 82 ± 2% of the k_{cat}/K_{app} for acetylthiocholine (data not shown). From our measured values of K_S [1.5 mM for acetylthiocholine (Figure 2B below) and 0.18 ± 0.01 mM for M7A (data not shown)], k_{-S} values were calculated from $k_{-S} = K_S k_S$. Assignments of k_1 and k_{-1} become problematic when R approaches 1.0 because of uncertainty in R_S. R_S has been considered to be as high as 1.25, the ratio of the viscosities of D_2O to H_2O at 25 °C (see, e.g., refs *30* and *31*). For acetylthiocholine, R = 1.21 ± 0.02 (*22*), and for M7A, $R = 1.09 \pm 0.05$ (data not shown); k_1 calculated from eq 10 was very sensitive to the values of both k_S and R_S. In practical terms, the simulations were not sensitive to the absolute values of k_S, k_1, and k_{-1} as long as k_1 was calculated from eq 10 and k_{-1} from eq 9. For example, simulated substrate inhibition curves for acetylthiocholine (Figure 3A below) were fitted to the Haldane equation (eq 1) by varying k_S from 120 to 500 μM^{-1} s^{-1} and calculating the corresponding values of k_{-S}, k_1, and k_{-1} (with all other rate constants fixed). The resulting fitted K_{app} and K_{SS} values varied by less than 5% (data not shown). We assigned k_S values of 200 μM^{-1} s^{-1} (at the ionic strength of buffer alone) to correspond to the general ligand association rate constant used in our previous simulations (*18*). The assigned values of k_2 and k_3 for M7A were the same as those for acetylthiocholine because (1) the k_3 reaction is identical with both substrates and (2) the simulations were quite insensitive to k_2 when k_2 exceeded k_{-P}; 8-fold increases or decreases in k_2 resulted in less than a factor of 2 change in fitted parameters when simulated v versus [S] curves were analyzed with the Haldane equation.

For all substrates, we obtained estimates of k_{-P} (Schemes 2 and 3) from $k_{-P} = K_I k_P$, where $K_I = K_P$ was the competitive inhibition constant for reaction product P measured with a different substrate. Since estimates of k_P are unavailable for any of the substrates used in this study, k_P was assumed to have the same value as k_S. The steric blockade parameter k_{-P2}/k_{-P} was assumed to be 0.01–0.04, consistent with our previous observations that ligand binding to the peripheral site decreases ligand dissociation rate constants from the acylation site by 10–100-fold (*18*). Assigned intrinsic rate constants for acetylthiocholine and M7A are summarized in Table 1.

RESULTS

Expansion of Our Steric Blockade Model To Include Inhibition of Product Dissociation. When a ligand binds to the peripheral site of AChE, the ensuing inhibition of substrate hydrolysis is often interpreted according to Scheme 1.

Scheme 1

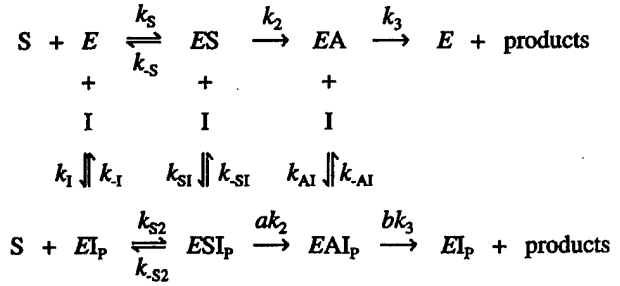

Inhibitor (I) can bind to each of the three enzyme species E, ES, and EA. For example, ESI_P represents a ternary complex with substrate (S) at the acylation site and I at the peripheral site (denoted by the subscript P). The acylation rate constant k_2 is altered by a factor a in this ternary complex, and the deacylation rate constant k_3 is altered by a factor b in the EAI_P complex. To obtain a tractable solution to the steady state substrate hydrolysis rate v that corresponds to Scheme 1, it has often been assumed that the reversible reactions are at equilibrium (with $k_{-X}/k_X = K_X$). Although this assumption cannot be justified for AChE (*1*), the mixed, partial inhibition patterns that are often observed with peripheral site inhibitors of AChE can be fitted to the equilibrium solution (*18*). These fits require that a (or b and

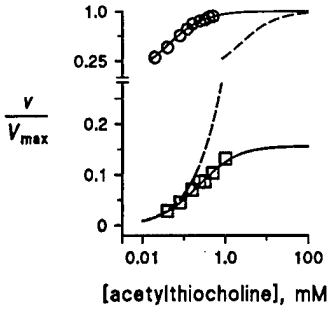

FIGURE 1: Propidium inhibition of the AChE-catalyzed hydrolysis of acetylthiocholine. Points represent initial velocities measured as outlined in Experimental Procedures at 25 pM AChE and the indicated acetylthiocholine concentrations with (□) or without (○) 50 μM propidium. Lines were generated by the SCoP simulation program for rate constants in Scheme 1 (○—○ and - - -) or Scheme 4 (□—□). Rate constant values assigned previously (*18*) were as follows: $k_S = k_I = k_{SI} = k_{AI} = 200\ \mu M^{-1}\ s^{-1}$; $k_{S2} = 3\ \mu M^{-1}\ s^{-1}$; $k_{-S} = 3 \times 10^3\ s^{-1}$; $k_{-S2} = 45\ s^{-1}$; $k_{-I} = k_{-SI} = k_{-AI} = 200\ s^{-1}$; $k_2 = k_3 = 1.4 \times 10^4\ s^{-1}$; and $a = b = 1$. New rate constants required to extend Scheme 1 to Scheme 4 were assigned as follows: $k_{-P} = 6 \times 10^4\ s^{-1}$; $k_{-P2} = 9 \times 10^2\ s^{-1}$; and $c = d = e = f = i = 1$.

K_S/K_{S2}) be much less than 1, and interpretation of such low values would appear to indicate a conformational interaction between the two sites.

To avoid assumptions of equilibrium in Scheme 1, we introduced a nonequilibrium analysis that involved numerical solution of the rate equations that arise from Scheme 1 with the SCoP program (*18*). The analysis required assignment of all the rate constants in Scheme 1 and generated simulated values of v. We simplified these assignments by proposing our steric blockade model in which the only effect of bound peripheral site ligand is to decrease k_{S2} relative to k_S and k_{-S2} relative to k_{-S} while maintaining $K_S = K_{S2}$ and $a = b = 1$. Since k_S is rate-limiting at low substrate concentrations without inhibitor and k_{S2} becomes rate-limiting at low substrate concentrations and saturating concentrations of inhibitor, the model with Scheme 1 correctly predicts that increasing concentrations of inhibitor should progressively decrease the second-order hydrolysis rate measured at low substrate concentrations (*18*). However, at high substrate concentrations, neither k_S nor k_{S2} remains rate-limiting, and the model with Scheme 1 predicts that inhibitor should have no effect on the V_{max} obtained at high substrate concentrations. This prediction is not supported experimentally, as illustrated in Figure 1. This figure shows v as a function of acetylthiocholine concentration. In the absence of propidium, the observed v (○) were fitted well by the line simulated with the steric blockade model. With the peripheral site occupied by a saturating concentration of propidium (50 μM), the simulated v (dashed line) corresponded well with the observed v (□) at low substrate concentrations but increased much more than the observed v at higher substrate concentrations. Near 100 mM acetylthiocholine, the simulated lines for v with and without propidium converged. Therefore, the steric blockade model with Scheme 1 fails to incorporate an inhibition component that becomes apparent at high substrate concentrations. This inhibition component might involve substrate inhibition, a phenomenon observed with some cationic substrates such as acetylthiocholine that is addressed below. However, the experimental acetylthiocholine concentrations in Figure 1 are below the range where substrate inhibition is observed. Furthermore, the divergence in Figure 1 between simulated and observed v values in the presence of propidium is also seen with other substrates such as phenyl acetate that do not exhibit substrate inhibition (*18*).

Schemes 2 and 4 incorporate a logical extension of Scheme 1 which, as we now show, can eliminate disagreement between the steric blockade model and observed v at the higher substrate concentrations investigated experimentally in Figure 1. Scheme 2 makes explicit the dissociation rate constant k_{-P} for the first product P, the alcohol leaving group (e.g., thiocholine) generated by acylation of the active site serine. For simplicity, inclusion of a peripheral site inhibitor is deferred to Scheme 4 in the Appendix.

Scheme 2

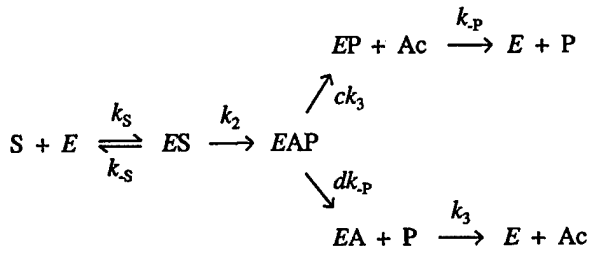

The first intermediate following enzyme acylation in Scheme 2 is *E*AP. To maintain generality, P may dissociate before (dk_{-P}) or after (k_{-P}) the deacylation step. *E*AP has not been included explicitly in most catalytic pathways previously considered for AChE because dk_{-P} has been assumed to be sufficiently fast to render any accumulation of *E*AP negligible. This appears to be a good assumption for most AChE substrates. For example, we estimated k_{-P} for acetylthiocholine to be $1.3 \times 10^5\ s^{-1}$ from the relationship $k_{-P} = k_P K_P$, where a K_P of 0.66 mM was measured as the competitive inhibition constant for thiocholine inhibition of M7A hydrolysis (data not shown) and the association rate constant k_P for thiocholine was assigned the same value assumed for acetylthiocholine ($200\ \mu M^{-1}\ s^{-1}$). Since this k_{-P} is nearly 1 order of magnitude larger than k_2 or k_3, its inclusion in the model has little effect on the experimental kinetic parameters; calculations based on Schemes 1 and 2 (with $d = 1$) show that k_{cat} is decreased by less than 1% and k_{cat}/K_{app} is unaltered.

We extend our steric blockade hypothesis with Scheme 4 (Appendix) by proposing that a bound peripheral site inhibitor not only reduces association and dissociation rate constants for substrate binding to the acylation site but also reduces the dissociation rate constant for release of P. In this case, a simulated nonequilibrium analysis demonstrates that product dissociation rate constants can become important. A key rate constant in this analysis was k_{-P2}, the rate constant for dissociation of P from the *E*PI$_P$ ternary complex, since our steric blockade model proposes that the only consequences of ligand binding to the peripheral site are low ratios of k_{S2}/k_S, k_{-S2}/k_{-S}, and k_{-P2}/k_{-P}. For example, if bound propidium at the peripheral site reduced k_{-P2} in Scheme 4 to 1.5% of k_{-P}, the same reduction previously deduced for k_{-S2} relative to k_{-S} for acetylthiocholine (*18*), then thiocholine dissociation does contribute to a reduction in v. With a k_{-P} of $1.3 \times 10^5\ s^{-1}$ as calculated above, most of the divergence between the experimental points with 50 μM propidium and the corresponding simulated line in Figure 1 was eliminated. Assigning just a 2-fold lower value of k_{-P} ($6 \times 10^4\ s^{-1}$) completely eliminated this divergence and gave the simulated

lower line shown in Figure 1. Therefore, if product affinity for the acylation site is sufficiently high, product release may become partially rate-limiting when the peripheral site is occupied. Specifically, v will be affected when the product dissociation rate constant k_{-P2} falls within the range of the acylation (k_2) and deacylation (k_3) rate constants. Thiocholine, a cationic leaving group P, illustrates this point in Figure 1. In contrast, the acetate product (Ac) of acetylthiocholine hydrolysis has an affinity for the acylation site that is too low (K_I > 100 mM) to contribute any rate limitation even with propidium bound to the peripheral site. The analysis in Figure 1 completes our demonstration that the steric blockade can explain AChE inhibition by peripheral site ligands. Specifically, direct measurement of association and dissociation rate constants for the acylation site ligands huperzine A and TMTFA revealed decreases of 10−380-fold when propidium was bound to the peripheral site (*18*), and decreases in these rate constants alone for substrates and their hydrolysis products are sufficient to account for inhibition by bound peripheral site ligands at both low (*18*) and high (Figure 1) substrate concentrations.

Acetylcholine Can Bind to the Peripheral Site. We turn next to the questions of whether acetylthiocholine, a close analogue of the physiological substrate acetylcholine, can bind to the peripheral site and whether this binding is of significance on the catalytic pathway. Scheme 3 defines an initial complex ES_P of substrate with the peripheral site and incorporates this species into the previous catalytic pathway from Scheme 2.

Scheme 3

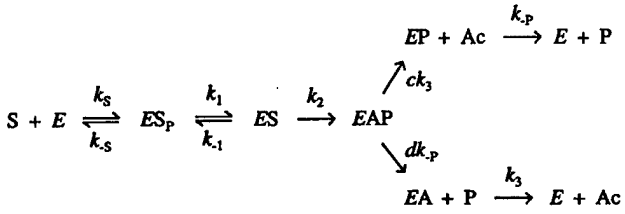

ES_P can reversibly proceed to ES, the complex of substrate with the acylation site, where acylation occurs. For simplicity, we have not included the additional complexes ESS_P, $EAPS_P$, EAS_P, and EPS_P in Scheme 3, but they are made explicit in Scheme 5 in the Appendix. These complexes are important in the phenomenon of substrate inhibition considered below, and they also must be considered in any measurement of substrate affinity for the peripheral site.

A direct way of measuring substrate affinity for the peripheral site is to measure the effect of substrate on the association rate constant k_{on} for a slowly equilibrating ligand that binds exclusively to the peripheral site. Fasciculin is such a ligand, and we previously confirmed the affinity of propidium for the peripheral site by measuring its inhibition constant K_I during fasciculin binding (*22*). The analysis was straightforward with an inhibitor like propidium (I) that competes with fasciculin, because only a single complex EI_P is formed to alter the observed k_{on}. If our steric blockade model is correct and ligand binding to the peripheral site is unaffected by the presence of ligands or an acyl group at the acylation site, then this analysis can be extended directly to include substrate. Only species with S bound to the peripheral site are relevant, and the resulting analysis should

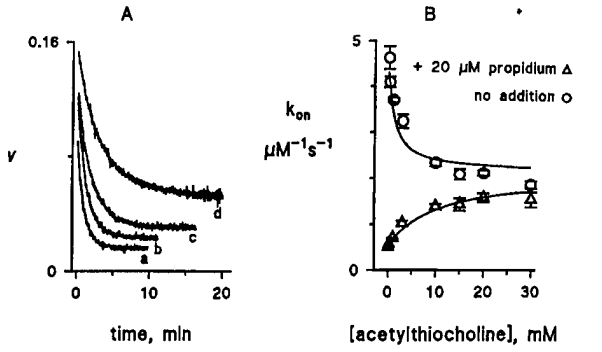

FIGURE 2: Acetylthiocholine binding to the AChE peripheral site. (A) The hydrolysis rate v (ΔA_{412nm} per minute) for the approach to equilibrium fasciculin (F) binding was measured with 10 mM acetylthiocholine, 50 pM AChE, F (a, 5 nM; b, 3 nM; c, 2 nM; and d, 1 nM), and buffered 50 mM NaCl by continuous spectrophotometric assay as outlined in Experimental Procedures. Rate constants (k) obtained from eq 4 were then plotted against the fasciculin concentration (eq 5) to obtain k_{on} (plot not shown). (B) The dependence of k_{on} on the acetylthiocholine concentration was analyzed with eqs 6 and 7. Indicated points representing the average of three or four k_{on} measurements (except at 15 mM) were fitted with eq 6 to give apparent K_S estimates of 3.6 ± 1.0 mM in the absence of propidium (O) and 0.6 ± 0.1 mM with 20 μM propidium (Δ). (This fitting is not shown here but is given in Figure 2B of ref *45*.) A mean K_S of 1.5 mM was used to assign k_{-S} in Table 1 and to generate *both* lines representing the simulated dependence of k_{on} on [S] from eq 7. The simulations were based on Scheme 5 as outlined in the text with the rate constant assignments in Table 1 except that $k_{-P} = 6 \times 10^4$ s^{-1}; in addition, k_{-I} and k_{-P2} for propidium were the same as in Figure 1 but $k_I = 70\ \mu M^{-1}\ s^{-1}$ (due to the change in ionic strength from Figure 1). The simulated lines also were fitted well by eq 6 with a K_S value of 1.36 ± 0.01 mM both in the absence of propidium and with 20 μM propidium.

be compatible with eq 6. However, in the presence of both S and I, Scheme 5 includes 14 liganded enzyme species as noted in the Appendix. It is certainly possible that our model is oversimplified and that ligands bound to the acylation site will alter ligand binding to the peripheral site. We can address this possibility by simulation analysis of the more general eq 7. We began our experimental analysis by measuring the observed rate constants k for fasciculin binding during continuous substrate hydrolysis as shown in Figure 2A. Apparent association rate constants k_{on} were then calculated from a series of k values obtained at fixed acetylthiocholine concentrations [S] according to eq 5. Plots of k_{on} versus [S] in the absence of propidium revealed that k_{on} did decrease at higher S concentrations and reasonably conformed to eq 6 (O in Figure 2B). This decrease suggested that acetylthiocholine competes with fasciculin at the peripheral site, but to our surprise, the competition was only partial. Values of k_{on} at high S concentrations leveled off at about one-half of the k_{on} extrapolated to zero S concentration. According to eq 6, this observation indicates that k_{FP} for fasciculin binding to ES_P is about one-half of k_F, the intrinsic association rate constant for fasciculin binding to the peripheral site in free AChE. In contrast, k_{on} for fasciculin was observed previously to decrease to near zero at high propidium concentrations, and the absence of any detectable k_{FP} for fasciculin with the propidium−AChE complex was taken as evidence that fasciculin and propidium were completely competitive (*22*). Our immediate concern was that the partial acetylthiocholine inhibition of fasciculin binding did not reflect an interaction

of acetylthiocholine at the peripheral site but instead was an indirect effect of acetylthiocholine bound at the acylation site. Three points argued against this interpretation. First, the apparent K_S for the acetylthiocholine that competes with fasciculin according to eq 6 was in the low millimolar range (Figure 2B). This value was nearly 2 orders of magnitude higher than K_{app} for acetylthiocholine, which roughly indicates the affinity of substrate complexes at the acylation site. Second, inclusion of edrophonium, an inhibitor specific for the acylation site, at high concentrations (90 times its K_I) with acetylthiocholine and fasciculin only slightly altered the upper plot in Figure 2B (data not shown). Third, when in contrast a high concentration of propidium (nearly 10 times its K_I) was included, progressively higher S concentrations actually increased the observed k_{on} substantially (Δ in Figure 2B). Since propidium affinity for the peripheral site is at most slightly affected by the binding of ligands to the acylation site (*9*, *18*), this observation appears to require that acetylthiocholine and propidium compete at the peripheral site and that displacement of propidium by acetylthiocholine result in an increased rate of fasciculin association.

To confirm this indication of acetylthiocholine binding to the peripheral site, we conducted nonequilibrium simulations in which k_{on} was calculated from eq 7. Differential equations corresponding to the rate expressions from Scheme 5 were solved numerically by the SCoP program with rate constants (Table 1 and Figure 2B) assigned as outlined in Experimental Procedures. The geometric mean of the apparent K_S estimates from eq 6 with and without propidium was about 1.5 mM (Figure 2B), and from this value and the previously estimated k_S, a k_{-S} of 2×10^5 s^{-1} was assigned. Two other key assignments involved the relative values of k_{FP}/k_F and k_{FA}/k_F in eq 7. The decision to limit the 14 possible fasciculin association rate constants to only these three in the numerator in eq 7 was largely based on the close conformity of the data in Figure 2B to eq 6. This conformity indicated that fasciculin associated with several enzyme species with identical rate constants. We sorted these enzyme species into four groups. The first consisted of those with no bound cationic ligands (i.e., $[E] + [EA]$) with a fasciculin association rate constant of k_F. The second contained those in which substrate was bound to the peripheral site ($\sum ES_P$) and was characterized by a relative rate constant of k_{FP}/k_F. The third included those in which the peripheral site was free but substrate or its thiocholine product was bound to the acylation site ($\sum EX_A$), and these were given a relative rate constant of k_{FA}/k_F. The fourth involved those with propidium bound to the peripheral site ($\sum EI_P$) and with a relative rate constant of zero. We first simulated our steric blockade model, in which ligand binding to the peripheral site is unaffected by the presence of ligands or an acyl group at the acylation site. Fasciculin association was assumed to be partially blocked by substrate bound at the peripheral site ($k_{FP}/k_F = 0.5$) but unaffected by substrate or product bound at the acylation site ($k_{FA}/k_F = 1$). In support of the latter assignment, previous data (*22*) and our results above indicated that fasciculin association rate constants are not affected by edrophonium bound to the acylation site. With these assignments, the simulation program calculated the concentrations of all the enzyme intermediates in Scheme 5, with and without propidium, and solved eq 7 for k_{on} as a function of S concentration. The simulated values of k_{on} are shown as the lines in Figure 2B. They superimposed well with the original fits of the experimental data to eq 6, and they confirmed that eq 6 provides an excellent approximation when fasciculin association is affected only by substrate bound to the peripheral site. The K_S of 1.4 mM calculated from the simulations agreed with the assigned K_S. In contrast, when both k_{FP}/k_F and k_{FA}/k_F were assigned a value of 0.5, the simulated K_S with 20 μM propidium was unchanged but the simulated K_S without propidium decreased 5-fold. This trend was the opposite of that observed experimentally in Figure 2B. We also examined whether a small decrease in the relative fasciculin association rate with substrate or product bound to the acylation site ($k_{FA}/k_F = 0.5$) could be superimposed on complete competition between substrate and fasciculin at the peripheral site ($k_{FP}/k_F = 0$). In this case, the simulations showed that k_{on} with 20 μM propidium did not change significantly with increased S concentrations, again in contrast to the observations in Figure 2B. These simulations confirmed the indication in the previous paragraph that acetylthiocholine and propidium must compete at the peripheral site for acetylthiocholine to accelerate fasciculin association in the presence of propidium.

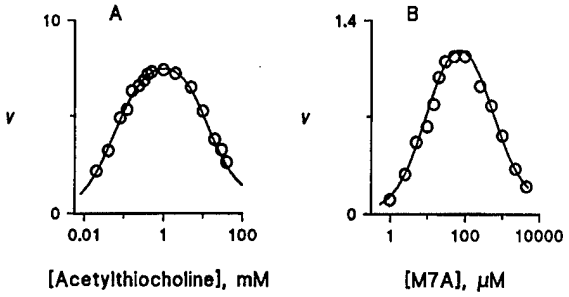

FIGURE 3: Substrate inhibition with acetylthiocholine and M7A. Points represent initial velocities (μM min^{-1}) measured at the indicated substrate concentrations as outlined in Experimental Procedures. (A) Reaction mixtures with acetylthiocholine and 20 pM AChE were supplemented with NaCl such that [S] + [NaCl] = 60 mM to maintain a constant ionic strength. The line was generated by the SCoP simulation program with assigned rate constants in Table 1 except that $k_{-P} = 6 \times 10^4$ s^{-1}. When fitted to the Haldane equation (eq 1), the simulated line corresponded to a K_{app} of 57.9 $\pm$ 0.4 μM and a K_{SS} of 17.9 $\pm$ 0.1 mM. (B) Initial velocities for M7A in 20 mM sodium phosphate buffer with the experimental AChE concentrations (20−2000 pM) were normalized to 20 pM AChE for comparison to Figure 3A. The line was generated by the SCoP simulation program with assigned rate constants in Table 1 except that k_{-P} was slightly increased to 1.5×10^3 s^{-1} and thermodynamic interaction between sites was allowed, with $i = 4$, $k_{-S} = 2 \times 10^4$ s^{-1}, $k_i = 4 \times 10^4$ s^{-1}, and $k_{-P2}/k_{-P} = 0.04$. When fitted to the Haldane equation, the simulated line corresponded to a K_{app} of 9.3 $\pm$ 0.1 μM and a K_{SS} of 640 $\pm$ 3 μM.

Since the individual rate constants on the catalytic pathway in Scheme 3 in general are too high to measure by rapid kinetic techniques, there are relatively few phenomena involving substrate hydrolysis by AChE that allow us to obtain experimental evidence to support Schemes 3 and 5 and the rate constant assignments in Figure 2B. Two pertinent phenomena are substrate inhibition and mixed substrate hydrolysis, and these are examined in the following sections.

Substrate Inhibition. When rates of acetylthiocholine hydrolysis with AChE are measured as a function of acetylthiocholine concentration [S], the profile in Figure 3A is observed. This profile does not correspond to a simple

Table 2: Simulated and Observed Kinetic Parameters for Substrate Hydrolysis and Substrate Inhibition with AChE[a]

substrate	k_{cat} (s^{-1})	K_{app} (μM)	K_{SS} (mM)
	Observed Values		
acetylthiocholine	7000[b]	58 ± 2	18.6 ± 0.7
M7A	1300 ± 160[c]	10 ± 1	0.7 ± 0.1
	Simulated Values		
acetylthiocholine	*d*	*d*	44.4 ± 0.1
M7A	1120 ± 30[c]	8.8 ± 0.04	0.25 ± 0.001

[a] Kinetic parameters were determined by fitting the dependence of v on the substrate concentration to the Haldane equation (eq 1). Simulated values were obtained with Scheme 5 (Appendix) and the rate constants in Table 1. [b] From previous literature values (see ref *18*). [c] Calculated from the product of $k_{cat}/K_{app} \times K_{app}$. [d] Matched to observed parameters by rate constant assignments.

Michealis–Menten kinetic pattern, and the bell-shaped curve with the decline at high S concentrations has long been referred to as substrate inhibition (*32*). This curve can be fitted to the Haldane equation (eq 1), which contains three experimental parameters: V_{max} (= $k_{cat}[E]_{tot}$), K_{app}, and the substrate inhibition constant K_{SS}. Since the Haldane equation is not restricted to any mechanistic scheme, it provides a useful quantitative standard for assessing data simulated from our nonequilibrium analysis of Scheme 5 with the rate constant assignments in Table 1. It is important to note that these rate constants were assigned from data unrelated to the substrate inhibition phenomenon itself.

For acetylthiocholine K_{SS} was the only parameter independently obtained from this fitting procedure, as known values of k_{cat} and K_{app} were incorporated into the rate constant assignments. The simulation in fact generated a curve exhibiting substrate inhibition with a K_{SS} value of 44.4 mM, about twice the observed K_{SS} of 18.6 mM (Table 2). We assessed changes in assigned rate constants that could reconcile this difference. Although substrate inhibition results from a low value of k_{-P2}/k_{-P}, the value of K_{SS} obtained from the simulation was only moderately sensitive to the k_{-P2}/k_{-P} assignment (e.g., changing k_{-P2}/k_{-P} from 0.01 to 0 only decreased the simulated K_{SS} to 28 mM). In contrast, the simulated K_{SS} value was more sensitive to the assigned value of k_{-P}, with the two values appearing virtually proportional. For example, decreasing the assigned k_{-P} from 1.3×10^5 to 6×10^4 s^{-1} decreased the K_{SS} obtained from the simulation to 17.9 mM and gave an excellent fit of the simulated curve to the experimental data, as shown in Figure 3A. Since the original assignment of k_{-P} assumed that $k_P = k_S$, an assumption that cannot be tested experimentally with available techniques, the agreement between the observed and simulated substrate inhibition data appears to be quite reasonable.

We next turned to M7A, a substrate that previously exhibited substrate inhibition with eel AChE (*26*, *33*) and also showed this inhibition pattern with human AChE (Figure 3B). This substrate is of particular interest in testing our steric blockade model because it binds to the peripheral site (K_S = 0.18 ± 0.01 mM from competition with fasciculin, data not shown), and its hydrolysis product M7H has a high affinity for AChE and a consequent low calculated k_{-P} of 1.3×10^3 s^{-1} (Table 1). Analysis of the simulated v versus [S] curve with the Haldane equation and the constants for M7A in Table 1 gave independent estimates of K_{SS} and k_{cat}, since only the ratio k_{cat}/K_{app} was incorporated into the rate constant assignments. The simulated K_{SS} of 0.25 mM was nearly 3 times smaller than the observed K_{SS} of 0.7 mM, but the simulated k_{cat} was within 20% of that observed (Table 2). The reasonably close agreement supported our steric blockade model. In particular, the observed k_{cat} for M7A was only 19% of the k_{cat} for acetylthiocholine (Table 2), and this low relative k_{cat} was explained in the steric blockade model by the low k_{-P} for the M7H product. In contrast to the interaction of acetylthiocholine with AChE, the most abundant simulated intermediate with M7A at concentrations below K_{SS} was *E*P, the AChE complex with the M7H product, and dissociation of this complex was the step that limited the value of k_{cat}. As a consequence, a slight increase in k_{-P} resulted in an almost proportionate increase in k_{cat} but in almost no effect on K_{SS}. The most straightforward way to achieve agreement between the simulated and observed K_{SS} values[2] was to relax the stringent assumption in our steric blockade model that the affinity of ligands for the peripheral and acylation sites was unchanged when both sites were occupied simultaneously in a ternary complex (see Discussion). Good agreement was then observed in Figure 3B, where the affinities of M7A and M7H in ternary complexes were assigned to be 25% of their affinities in binary complexes (e.g., $i = 4$). The simulation in Figure 3B also assumed that the apparent K_S of 0.18 mM for M7A was an average of the actual K_S and of iK_S, where iK_S is the dissociation constant for M7A binding to the peripheral site when the acylation site is occupied by M7A or M7H.

Mixed Substrate Hydrolysis. When two substrates are mixed with AChE, each substrate inhibits the hydrolysis of the other. We measured the extent of competitive inhibition of acetylthiocholine hydrolysis by M7A and, conversely, the extent of competitive inhibition of M7A hydrolysis by acetylthiocholine by monitoring the hydrolysis of each substrate independently. Competitive inhibition was assessed from relative second-order hydrolysis rate constants z by plotting the data according to eq 3. If none of the enzyme intermediates generated by the competing substrate can react with the monitored substrate, then the K_I for the competing substrate should equal its K_{app}. This is typically the case for simple models of substrate competition, and it is also the case when M7A is the competing substrate during acetylthiocholine hydrolysis. In Figure 4A, the solid line represents the inhibition calculated from eq 3 when K_I for M7A equals its K_{app} from Figure 3B. The observed points were within experimental error of this line. Furthermore, simulation of this competition with the steric blockade model applied to Scheme 5 and the assigned rate constants in panels A and B of Figure 3 generated the dashed line that also closely followed the solid line. The data indicate that acetylthiocholine does not initiate its catalytic pathway with any

[2] Assigned rate constants could also be adjusted in the following way to obtain agreement of the simulated and observed K_{SS} for M7A in Figure 3B. A 7-fold decrease in k_2 combined with a 3-fold increase in k_{-P}, relative to the assignments in Table 1, shifted the rate-limiting step in k_{cat} from product dissociation to acetylation and gave a simulated curve virtually identical to the one in Figure 3B. These adjustments were not a very attractive option because they seem to run counter to observations that the M7H leaving group promotes excellent acylation of AChE. For example, dimethylcarbamoylated M7H shows a higher acylation rate constant than dimethylcarbamoylated choline (*25*, *34*). Furthermore, these adjustments gave a less than satisfactory fit of the simulated curve to the experimental points in Figure 4B.

in Figure 2B and the simulated data were then fitted with eq 6, a higher K_S was obtained without propidium than with propidium. This appears to be an improvement, because a similar divergence in K_S values was seen in our experimental fits in Figure 2B. However, these simulations for acetylthiocholine also require small adjustments in other assigned rate constants, and we have not attempted to find a self-consistent set of adjustments that would retain the agreement of the simulations to the observed data for acetylthiocholine in Figures 1, 2B, 3A, and 4 noted above.

The steric blockade model in Schemes 3 and 5 resolves a long controversy over the mechanistic interpretation of substrate inhibition with AChE. The controversy involved two alternative mechanisms. One proposal was that substrate inhibition arises from S binding to the anionic site of acetylated AChE to give an *E*AS complex in which deacylation is blocked (*26, 35*−*37*). This proposal predicted that the substrate inhibition constant K_{SS} fitted by the Haldane equation (eq 1) will depend not only on the substrate affinity in *E*AS but also on the relative amount of *E*A. It was supported by observations that uncompetitive inhibition constants as well as K_{SS} increased for substrates with a lower k_{cat} (since these formed less *E*A). Alternatively, it was proposed that substrate inhibition arises from binding of two molecules of S in an *E*SS complex in which enzyme acetylation is blocked. Either the two S molecules could bind in the acylation site (*38*), or one S could bind in the acylation site and one in the peripheral site (*39, 40*). This proposal predicted that K_{SS} from the Haldane equation should equal the dissociation constant for the lower-affinity S site in the *E*SS complex. It was supported when values for K_S of 15−25 mM for acetylcholine or acetylthiocholine binding to the peripheral site, determined by competition in a fluorescence titration of propidium with DFP-inactivated AChE, were the same as the corresponding K_{SS} estimates (*40*). It is unclear why these K_S estimates are so much higher than those we have determined from acetylthiocholine inhibition of the association reactions of ambenonium (*29*) or fasciculin (Figure 2B) with the peripheral site.[3] Our steric blockade model combines features from both of these proposals and extends them in a nonequilibrium context. The complex responsible for inhibition is neither *E*AS nor *E*SS but instead is *E*PS$_P$. This intermediate accumulates because S binding to the peripheral site blocks the dissociation of P, a feature that agrees with the contention in the second proposal that substrate bound to the peripheral site is responsible for substrate inhibition. Furthermore, for a series of substrates with similar K_S and k_{-P} values but varying k_2 values, K_{SS} will increase as k_{cat} decreases. Thus, our steric blockade model can account for the variations in K_{SS} which originally led to the first proposal.

Some previous reports (*5*) have noted that measured v values at high S concentrations fall above the overall substrate inhibition curve fitted to the Haldane equation (eq 1). Such deviations have been attributed to a low acetylation activity in the ESS complex. While no significant deviations of this type were observed over the range of S concentrations investigated in our experiments, it is worth noting that such deviations can be accounted for within our steric blockade model. As k_{-P2}/k_{-P} increases from the low value of 0.01 assumed in Table 1, simulated values of v at high S concentrations fall above the curve predicted by the Haldane equation because the rate of product dissociation even with S bound to the peripheral site makes a significant contribution to v.

Our observation in Figure 2B that acetylthiocholine and fasciculin were only partially competitive in binding to the peripheral site was unexpected. From our analyses with eqs 6 and 7, k_{FP} for fasciculin binding to the *E*S$_P$ complex was nearly 50% of the k_F for fasciculin binding to the free enzyme. However, these equations do not address the stability of the *E*S$_P$F$_P$ complex in which both acetylthiocholine and fasciculin are bound to the peripheral site. To explore the stability of this complex, we considered an extension of Schemes 4 and 5 in which a set of 20 complete time courses for fasciculin binding in the presence of acetylthiocholine (e.g., like those in Figure 2A) were fitted with the SCoP program (see examples involving TMTFA binding in ref *18*). Only rough approximations were attempted because fasciculin exerts a conformational effect on the acylation site in addition to its steric blockade (i.e., $a < 1$; *18, 22*). However, the fitting procedure indicated a 2−3 order of magnitude decrease in the affinities of acetylthiocholine and fasciculin in this *E*S$_P$F$_P$ ternary complex relative to the affinities of either ligand in the binary complexes with the free enzyme. To rationalize the formation of this ternary complex, we reviewed the kinetic properties of previously reported AChE mutants and examined the crystal structures of the fasciculin−AChE complexes (*7, 8*) to identify a potential acetylthiocholine binding site that largely overlaps with that of propidium but only slightly overlaps with that of fasciculin. D72 is a residue midway along the active site gorge that some reports have included in the peripheral site, and its mutation decreases k_{cat}/K_m for acetylthiocholine about 50-fold (*5*). D72 appears to be important in the initial binding of TMTFA, because mutation to D72N reduced the overall TMTFA association rate constant at high ionic strengths more than 20-fold without an effect on the corresponding rate constant for the neutral analogue of TMTFA (*15*). D72 also was shown to be responsible for the enhanced reactivity of cationic organophosphates relative to their uncharged counterparts (*41*). Since D72 does not make contact with fasciculin in the crystal structures, it appears to be possible that acetylthiocholine could interact with D72 and still allow a nearly normal association rate constant for the binding of fasciculin to the remainder of the peripheral site to form the ternary complex. Studies with D72 mutants are currently underway to examine this possibility.

Our discussion of the steric blockade model has focused entirely on the point that ligand binding to the peripheral site can have an inhibitory effect on substrate turnover at the acylation site. However, inhibitor binding to the peripheral site is not apparent in vivo and thus is not suspected to play any regulatory role under physiological conditions of acetylcholine hydrolysis by AChE. Furthermore, the concentrations of acetylcholine itself are not high enough to give rise to any significant substrate inhibition during synaptic

[3] Preliminary measurement of K_S for *Torpedo* AChE gave a value of about 0.5 mM with techniques identical to those in Figure 2 (T. Szegletes, W. D. Mallender, and T. L. Rosenberry, manuscript in preparation), indicating that the higher affinity of acetylthiocholine for the peripheral site reported here is not unique to human AChE. We suspect that the lower affinities in the previous reports were subject to technical limitations.

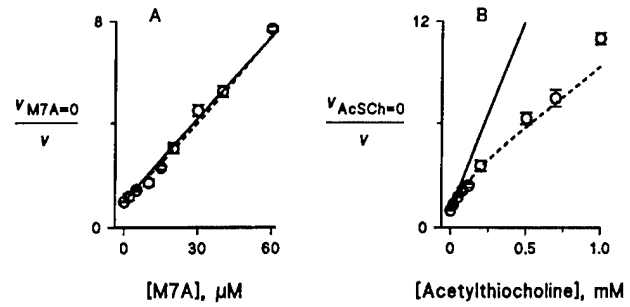

FIGURE 4: Inhibition of hydrolysis of one substrate by a second substrate. (A) Points denote second-order rate constants z for acetylthiocholine (AcSCh) measured in the presence of competing M7A as the inhibitor (see Experimental Procedures). The points were normalized to $z_{M7A=0}$ for acetylthiocholine in the absence of M7A and plotted according to eq 3. (B) Points denote second-order rate constants z for M7A in the presence of competing acetylthiocholine (AcSCh) normalized to $z_{AcSCh=0}$ for M7A in the absence of acetylthiocholine. M7A hydrolysis was monitored by spectrofluorometry. In each panel, indicated points represent averages of two to four measurements. The solid line is the extent of calculated inhibition if the K_I for the competing substrate were equal to its K_{app}. The dashed line is the extent of inhibition simulated for the steric blockade model with Scheme 5 and the assigned rate constants in panels A and B of Figure 3. New rate constants resulting from mixed ternary complexes (e.g., $i_{ST} = i_{TS} = 1$, see Appendix) were assigned assuming no thermodynamic interaction between the bound ligands in these complexes.

enzyme intermediate produced by M7A. However, when acetylthiocholine is the competing substrate during M7A hydrolysis, the observed inhibition points fell below the solid line expected if K_I for acetylthiocholine were equal to its K_{app} (Figure 4B). A similar pattern of inhibition of M7A hydrolysis by acetylthiocholine was observed previously with eel AChE (*26*). The level of inhibition in Figure 4B corresponded well to the level of inhibition simulated with Scheme 5 (dashed line in Figure 4B), thereby supporting our steric blockade model. The simulation was particularly sensitive to two parameters, k_{-S} for M7A and k_{-P2}/k_{-P} for thiocholine product dissociation when M7A was bound to the peripheral site. A decrease in k_{-S} or an increase in this k_{-P2}/k_{-P} resulted in less inhibition by acetylthiocholine. This pattern indicates that an M7A molecule can initiate its catalytic pathway by binding to the peripheral site when acetylthiocholine is bound to the acylation site. The dissociation of this M7A is sufficiently slow that it will *wait* at the peripheral site while acetylation by the acetylthiocholine and deacetylation occur and the thiocholine product dissociates from the enzyme. This M7A then will proceed to the acylation site. A corresponding phenomenon is not seen during M7A inhibition of acetylthiocholine hydrolysis because acetylthiocholine dissociates too rapidly from the peripheral site and product M7H dissociates too slowly from the acylation site. These data provide the most direct evidence in support of our proposal in Schemes 3 and 5 that initial substrate binding to the peripheral site occurs on the catalytic pathway. This pathway does not require release of substrate from the peripheral site to the solution and its direct reassociation with the acylation site for catalysis to occur.

DISCUSSION

A key observation in this report is that acetylthiocholine can bind to the AChE peripheral site with an equilibrium dissociation constant K_S of about 1 mM. This value was determined from the effect of the acetylthiocholine concentration on the rate at which fasciculin associates with the peripheral site. The approach to equilibrium fasciculin binding was monitored by continuous spectrophotometric assay of acetylthiocholine hydrolysis. We employed this method previously with the high-affinity bisquaternary inhibitor ambenonium and found that acetylthiocholine inhibited ambenonium association by binding to a site on AChE with a K_S of about 1 mM (*29*), in good agreement with our current estimate. However, since ambenonium binds to both the acylation and peripheral sites simultaneously, it was difficult to assign this acetylthiocholine binding to the peripheral site. Our current assay has the advantages that fasciculin binds only to the peripheral site and that its slower rate of binding allows greater precision. Noise levels with the Cary 3A spectrophotometer are low enough to allow velocity estimates over 2 s intervals, and rate constants (k) for the approach to equilibrium fasciculin binding (Figure 3A) were fitted with typical standard errors of 1−5%.

When acetylthiocholine binding to the peripheral site is incorporated into our steric blockade model, a wide range of kinetic data, including substrate inhibition, can be explained. To keep the model conceptually simple, we have examined the very limited hypothesis that the only effect of substrates or inhibitors bound to the peripheral site is to decrease association and dissociation rate constants for acylation site ligands without changing their ratio, the equilibrium dissociation constant. Thus, we hypothesize that a bound peripheral site ligand has no effect on the thermodynamics of binding of acylation site ligands or on their reactivity at the acylation site. Even with this assumption, some of the rate constants in Schemes 3 and 5 cannot be assigned uniquely. The simulations revealed that an important assignment is the rate constant for product dissociation k_{-P}. This rate constant has not been measured directly for either thiocholine or M7H, the hydrolysis products of the substrates examined here. It is therefore reassuring that a single assignment for k_{-P} of 6×10^4 s^{-1} for thiocholine results in excellent agreement of the simulations with the observed data for propidium inhibition of acetylthiocholine hydrolysis (Figure 1), acetylthiocholine competition with fasciculin and propidium (Figure 2B), and substrate inhibition with acetylthiocholine (Figure 3A). While we are convinced that the steric blockade model offers the best understanding to date of ligand interactions with AChE, further refinements can be made. For example, we noted previously that association rate constants were decreased more than dissociation rate constants for both huperzine A and TMTFA when propidium was bound to the peripheral site (*18*). The difference corresponded to about a 5-fold decrease in affinity for the ligands in the ternary complex relative to the affinities of either ligand in the binary complexes with the free enzyme. We suggested that this difference might reflect an electrostatic interaction between these cationic ligands in the ternary complexes, and we do not view it as a serious challenge to the general steric blockade model. In terms of Scheme 4 or 5, this refinement would dictate a larger value of k_{-S2}/k_{-S} than of k_{S2}/k_S and in turn require thermodynamically that i be greater than 1. Increasing i to 4 gave the best agreement of the simulated and the observed data for M7A in Figures 3B and 4. Furthermore, when similar changes were incorporated into the simulations for acetylthiocholine with eq 7

transmission at the neuromuscular junction (*42*). Therefore, it is important to note that our model indicates a key role for the peripheral site under physiological conditions in which AChE is not saturated with acetylcholine. The hydrolysis rate v under these conditions is proportional to the second-order rate constant k_{cat}/K_{app} as given by eq 9, and initial binding of the substrate to the peripheral site increases this rate constant in several ways. It increases k_S because the peripheral site enlarges the enzyme surface and increases the frequency of productive substrate encounters; it decreases k_{-S} and thus allows a greater proportion of substrate molecules initially associated with the peripheral site to proceed to the acylation site, and it may well accelerate k_1 by optimally positioning substrate to diffuse rapidly into the acylation site.

Most previous kinetic analyses of AChE have employed equilibrium interpretations of reaction schemes similar to that in Scheme 1. Under what conditions do the conclusions from these analyses remain valid? We offer three guidelines. (1) If the intent is only to obtain an estimate of an inhibition constant K_I, an equilibrium analysis of Scheme 1 will provide an accurate estimate of the thermodynamic affinity of an inhibitor for either the acylation site or the peripheral site in free AChE (*18*). (2) If a substrate under investigation essentially equilibrates with AChE during reaction, an equilibrium analysis of Scheme 1 can be applied. Many slowly reacting substrates such as organophosphates (*43*) fall into this category. (3) If, however, one is investigating ligand binding to the peripheral site with substrates that do not equilibrate with AChE, kinetic parameters can be misinterpreted with an equilibrium analysis. In particular, K_{app} and K_{SS} (eq 1) will not reflect equilibrium values, and a and b (Scheme 1) will not be relative acylation and deacylation rate constants.

APPENDIX

Scheme 4 is an extension of Scheme 2 in which all complexes involving bound peripheral site inhibitor (I) are included. Our steric blockade model postulates that peripheral site binding is unaffected by acylation site ligands (i.e., $i = 1$ and the same association rate constant k_I and the same dissociation rate constant k_{-I} characterize I binding in the EI_P, ESI_P, $EAPI_P$, EAI_P, and EPI_P complexes) and that bound peripheral site ligand has no effect on acylation and deacylation rate constants (i.e., $a = b = 1$). Our current treatment of Scheme 5 also assumes for simplicity that product P bound to the acylation site does not alter the rate constant for deacetylation ($c = e = 1$) and that P dissociation rate constants for dissociation from the acetylated enzyme are identical to those from free enzyme ($d = f = 1$). These assumptions may require future refinement in view of reported interactions between ligands and acyl groups at the acylation site (*25*, *44*). The important feature of the steric blockade model here is that $k_{S2}/k_S = k_{-S2}/k_{-S} < 1$ and that $k_{-P2}/k_{-P} < 1$.

In Scheme 3, we proposed a more detailed model of AChE catalysis in which the first step involved the formation of an ES_P complex at the peripheral site. Scheme 5 is an extension of Scheme 3 in which all other complexes

Scheme 4

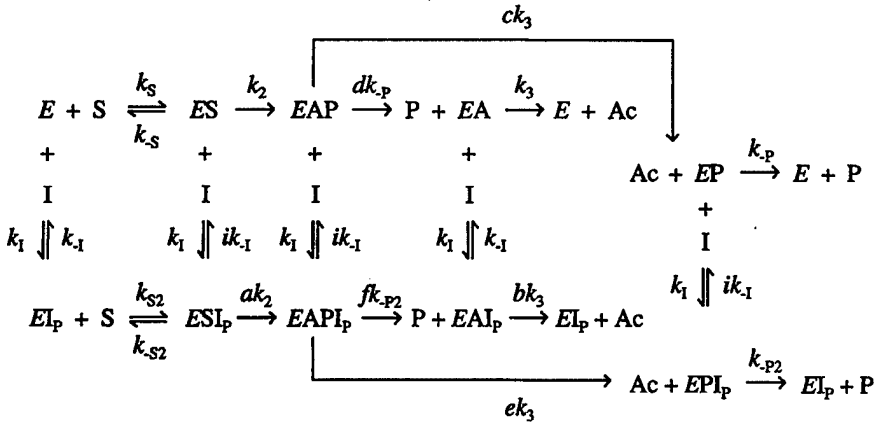

Scheme 5

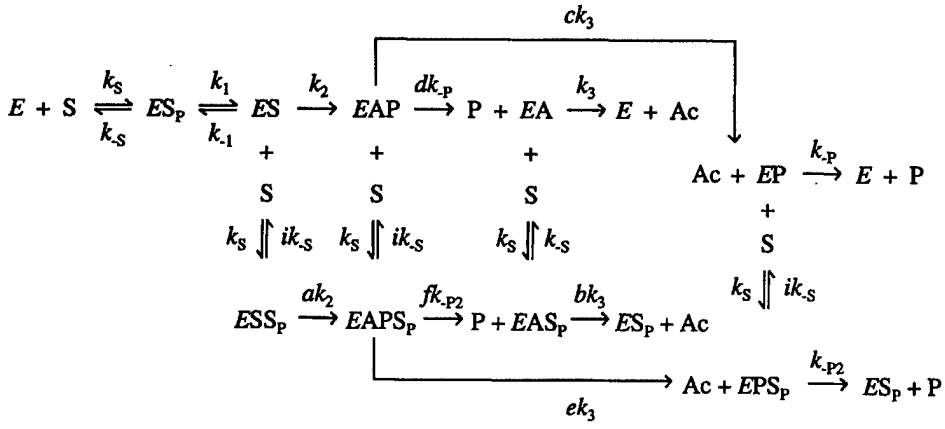

involving bound peripheral site substrate are included. As in Scheme 4, our steric blockade model postulates that $a = b = i = 1$ and that $k_{S2}/k_S = k_{-S2}/k_{-S} < 1$ and $k_{-P2}/k_{-P} < 1$, and again for simplicity, we assume that $c = d = e = f = 1$. When both S and I are present and compete for binding to the peripheral site (i.e., no enzyme species involving S_PI_P can form, such as ES_PI_P), then the five enzyme species involving I_P in Schcme 4 (EI_P, ESI_P, $EAPI_P$, EAI_P, and EPI_P) must be added to Scheme 5 to describe the complete system. While we do not show the scheme corresponding to this system, in eqs 6 and 7 we define the following combinations of enzyme species: $\sum ES_P = [ES_P] + [ESS_P] + [EAPS_P] + [EAS_P] + [EPS_P]$, $\sum EI_P = [EI_P] + [ESI_P] + [EAPI_P] + [EAI_P] + [EPI_P]$, and $\sum EX_A = [ES] + [EAP] + [EP]$. Furthermore, in the text description of eq 6, $\sum E = [E] + [EA] + \sum EX_A$. When acetylthiocholine (S) and M7A (T) are substrates simultaneously, 17 liganded species from Scheme 5 for the substrates must be considered (EA is common to both substrates) as well as six additional species representing mixed complexes (e.g., EST_P). New rate constants also are introduced by these mixed complexes (e.g., $i_{ST}k_{-T}$ is the rate constant for dissociation of T from EST_P).

ACKNOWLEDGMENT

We express our gratitude to Dr. Michel Roux at the Ecole Normale Superieure in Paris, France, for bringing the SCoP program to our attention. We also thank Dr. Abdul Fauq (Director of the Organic Synthesis Core Facility at Mayo Clinic Jacksonville) for synthesis of M7A iodide.

REFERENCES

1. Rosenberry, T. L. (1975) Acetylcholinesterase, in *Advances in Enzymology* (Meister, A., Ed.) Vol. 43, pp 103−218, John Wiley & Sons, New York.
2. Sussman, J. L., Harel, M., Frolow, F., Oefner, C., Goldman, A., Toker, L., and Silman, I. (1991) *Science 253*, 872−879.
3. Weise, C., Kreienkamp, H.-J., Raba, R., Pedak, A., Aaviksaar, A., and Hucho, F. (1990) *EMBO J. 9*, 3885−3888.
4. Schalk, I., Ehret-Sabatier, L., Bouet, F., Goeldner, M., and Hirth, C. (1992) in *Multidisciplinary Approaches to Cholinesterase Functions* (Shafferman, A., and Velan, B., Eds.) pp 117−120, Plenum Press, New York.
5. Radic, Z., Pickering, N. A., Vellom, D. C., Camp, S., and Taylor, P. (1993) *Biochemistry 32*, 12074−12084.
6. Barak, D., Kronman, C., Ordentlich, A., Ariel, N., Bromberg, A., Marcus, D., Lazar, A., Velan, B., and Shafferman, A. (1994) *J. Biol. Chem. 269*, 6296−6305.
7. Harel, M., Kleywegt, G. J., Ravelli, R. B. G., Silman, I., and Sussman, J. L. (1995) *Structure 3*, 1355−1366.
8. Bourne, Y., Taylor, P., and Marchot, P. (1995) *Cell 83*, 503−512.
9. Taylor, P., and Lappi, S. (1975) *Biochemistry 14*, 1989−1997.
10. Karlsson, E., Mbugua, P. M., and Rodriguez-Ithurralde, D. (1984) *J. Physiol. (Paris) 79*, 232−240.
11. Marchot, P., Khelif, A., Ji, Y.-H., Masnuelle, P., and Bourgis, P. E. (1993) *J. Biol. Chem. 268*, 12458−12467.
12. Nolte, H. J., Rosenberry, T. L., and Neumann, E. (1980) *Biochemistry 19*, 3705−3711.
13. Ripoll, D. R., Faerman, C. H., Axelsen, P. H., Silman, I., and Sussman, J. L. (1993) *Proc. Natl. Acad. Sci. U.S.A. 90*, 5128−5132.
14. Antosiewicz, J., McCammon, J. A., Wlodek, S. T., and Gilson, M. K. (1995) *Biochemistry 34*, 4211−4219.
15. Radic, Z., Kirchhoff, P. D., Quinn, D. M., McCammon, J. A., and Taylor, P. (1997) *J. Biol. Chem. 272*, 23265−23277.
16. Shafferman, A., Ordentlich, A., Barak, D., Kronman, C., Ber, R., Bino, T., Ariel, N., Osman, R., and Velan, B. (1994) *EMBO J. 13*, 3448−3455.
17. Barak, D., Ordentlich, A., Bromberg, A., Kronman, C., Marcus, D., Lazar, A., Ariel, N., Velan, B., and Shafferman, A. (1995) *Biochemistry 34*, 15444−15452.
18. Szegletes, T., Mallender, W. D., and Rosenberry, T. L. (1998) *Biochemistry 37*, 4206−4216.
19. Masson, P., Legrand, P., Bartels, C. F., Froment, M.-T., Schopfer, L. M., and Lockridge, O. (1997) *Biochemistry 36*, 2266−2277.
20. Rosenberry, T. L., and Scoggin, D. M. (1984) *J. Biol. Chem. 259*, 5643−5652.
21. Roberts, W. L., Kim., B. H., and Rosenberry, T. L. (1987) *Proc. Natl. Acad. Sci. U.S.A. 84*, 7817−7821.
22. Eastman, J., Wilson, E. J., Cervenansky, C., and Rosenberry, T. L. (1995) *J. Biol. Chem. 270*, 19694−19701.
23. Riddles, P. W., Blakeley, R. L., and Zerner, B. (1979) *Anal. Biochem. 94*, 75−81.
24. Ellman, G. L., Courtney, K. D., Andres, J. V., and Featherstone, R. M. (1961) *Biochem. Pharmacol. 7*, 88−95.
25. Rosenberry, T. L., and Bernhard, S. A. (1971) *Biochemistry 10*, 4114−4120.
26. Rosenberry, T. L., and Bernhard, S. A. (1972) *Biochemistry 11*, 4308−4321.
27. Haldane, J. B. S. (1930) *Enzymes*, p 84, Longmans, Green, New York.
28. Stuchbury, T., Shipton, M., Norris, R., Malthouse, J. P. G., and Brocklehurst, K. (1975) *Biochem. J. 151*, 417−432.
29. Hodge, A. S., Humphrey, D. R., and Rosenberry, T. L. (1992) *Mol. Pharmacol. 41*, 937−942.
30. Bazelyansky, M., Robey, E., and Kirsch, J. F. (1986) *Biochemistry 25*, 125−130.
31. Kasianowicz, J. J., and Bezrukov, S. M. (1995) *Biophys. J. 69*, 94−105.
32. Nachmansohn, D., and Wilson, I. B. (1951) *Adv. Enzymol. 12*, 259−339.
33. Prince, A. K. (1966) *Arch. Biochem. Biophys. 113*, 195−204.
34. Kitz, R. J., Ginsburg, S., and Wilson, I. B. (1967) *Biochem. Pharmacol. 16*, 2201−2209.
35. Krupka, R. M., and Laidler, K. J. (1961) *J. Am. Chem. Soc. 83*, 1445−1447.
36. Krupka, R. M., and Laidler, K. J. (1961) *J. Am. Chem. Soc. 83*, 1448−1454.
37. Froede, H. C., and Wilson, I. B. (1971) in *The Enzymes* (Boyer, P. D., Ed.) 3rd ed., Vol. V, pp 87−114, Academic Press, New York.
38. Zeller, E. A., and Bissegger, A. (1943) *Helv. Chim. Acta 26*, 1619−1630.
39. Aldridge, W. N., and Reiner, E. (1969) *Biochem. J. 115*, 147−162.
40. Radic, Z., Reiner, E., and Taylor, P. (1991) *Mol. Pharmacol. 39*, 98−104.
41. Hosea, N. A., Radic, Z., Tsigelny, I., Berman, H. A., Quinn, D. M., and Taylor, P. (1996) *Biochemistry 35*, 10995−11004.
42. Rosenberry, T. L. (1979) *Biophys. J. 26*, 263−290.
43. Mallender, W. D., Szegletes, T., and Rosenberry, T. L. (1999) *J. Biol. Chem.* (in press).
44. Barnett, P., and Rosenberry, T. L. (1977) *J. Biol. Chem. 252*, 7200−7206.
45. Rosenberry, T. L., Mallender, W. D., Thomas, P. J., and Szegletes, T. (1999) *Chem.-Biol. Interact.* (in press).

BI9813577

THE JOURNAL OF BIOLOGICAL CHEMISTRY
Vol. 274, No. 13, Issue of March 26, pp. 8491–8499, 1999
Printed in U.S.A.

Organophosphorylation of Acetylcholinesterase in the Presence of Peripheral Site Ligands

DISTINCT EFFECTS OF PROPIDIUM AND FASCICULIN*

(Received for publication, October 6, 1998, and in revised form, December 17, 1998)

William D. Mallender‡, Tivadar Szegletes, and Terrone L. Rosenberry§

From the Department of Pharmacology, Mayo Foundation for Medical Education and Research, and the Department of Research, Mayo Clinic Jacksonville, Jacksonville, Florida 32224

Structural analysis of acetylcholinesterase (AChE) has revealed two sites of ligand interaction in the active site gorge: an acylation site at the base of the gorge and a peripheral site at its mouth. A goal of our studies is to understand how ligand binding to the peripheral site alters the reactivity of substrates and organophosphates at the acylation site. Kinetic rate constants were determined for the phosphorylation of AChE by two fluorogenic organophosphates, 7-[(diethoxyphosphoryl)oxy]-1-methylquinolinium iodide (DEPQ) and 7-[(methylethoxyphosphonyl)oxy]-4-methylcoumarin (EMPC), by monitoring release of the fluorescent leaving group. Rate constants obtained with human erythrocyte AChE were in good agreement with those obtained for recombinant human AChE produced from a high level *Drosophila* S2 cell expression system. First-order rate constants k_{OP} were 1,600 ± 300 min^{-1} for DEPQ and 150 ± 11 min^{-1} for EMPC, and second-order rate constants k_{OP}/K_{OP} were 193 ± 13 μM^{-1} min^{-1} for DEPQ and 0.7–1.0 ± 0.1 μM^{-1} min^{-1} for EMPC. Binding of the small ligand propidium to the AChE peripheral site decreased k_{OP}/K_{OP} by factors of 2–20 for these organophosphates. Such modest inhibitory effects are consistent with our recently proposed steric blockade model (Szegletes, T., Mallender, W. D., and Rosenberry, T. L. (1998) *Biochemistry* 37, 4206–4216). Moreover, the binding of propidium resulted in a clear increase in k_{OP} for EMPC, suggesting that molecular or electronic strain caused by the proximity of propidium to EMPC in the ternary complex may promote phosphorylation. In contrast, the binding of the polypeptide neurotoxin fasciculin to the peripheral site of AChE dramatically decreased phosphorylation rate constants. Values of k_{OP}/K_{OP} were decreased by factors of 10^3 to 10^5, and k_{OP} was decreased by factors of 300–4,000. Such pronounced inhibition suggested a conformational change in the acylation site induced by fasciculin binding. As a note of caution to other investigators, measurements of phosphorylation of the fasciculin-AChE complex by AChE inactivation gave misleading rate constants because a small fraction of the AChE was resistant to inhibition by fasciculin.

Acetylcholinesterase (AChE)[1] terminates neurotransmission by catalyzing hydrolysis of the neurotransmitter acetylcholine at rates near that of a diffusion-controlled process (1). The x-ray crystal structure of AChE reveals that despite the impressive turnover rate of the enzyme, substrate molecules must penetrate 20 Å into a deep active site gorge to be hydrolyzed (2–4). This gorge contains two sites of ligand interaction: a peripheral site at the surface of the enzyme and an acylation site at the base of the gorge where the substrate acyl group is first transferred to residue Ser^{200} (*Torpedo californica* AChE sequence numbering) and then hydrolyzed. In the acylation site, a catalytic triad consisting of residues Ser^{200}, His^{440}, and Glu^{327} promotes the acyl transfers, and Trp^{84} binds the acetylcholine trimethylammonium group, positioning the substrate for hydrolysis. Certain ligands can bind selectively to either the acylation site or the peripheral site, and ternary complexes can be formed in which ligands are bound to both sites simultaneously (5, 6). Ligands specific for the peripheral site include the small aromatic compound propidium and the snake venom neurotoxin fasciculin, both of which are potent inhibitors of the hydrolysis of the chromogenic acetylcholine analog, acetylthiocholine.

The AChE peripheral site is an attractive target for the design of new classes of therapeutic agents, so it is important to understand how ligand binding to the peripheral site affects substrate hydrolysis. We recently provided evidence for a steric blockade model which proposes that small peripheral site ligands like propidium inhibit substrate hydrolysis by decreasing the association and dissociation rate constants for an acylation site ligand without significantly altering their ratio, the ligand equilibrium constant (7, 8). Cationic substrates like acetylthiocholine also were shown to bind to the peripheral site as the first step in their catalytic pathway, and steric blockade arising from this substrate binding accounted for the well known phenomenon of substrate inhibition for AChE at very high concentrations of substrate (8). A key feature of the steric blockade model is that ligand binding to the peripheral site results in significant inhibition only if substrate fails to reach equilibrium binding prior to reaction at the acylation site. Substrates that are thought to form equilibrium complexes at the acylation site can be examined to test this prediction. Among these substrates are the organophosphates (OPs), a class of compounds that inactivate cholinesterases because they are poor substrates (9–11). OPs readily phosphorylate the active site serine of AChE, but very slow hydrolysis of this

* This work was supported in part by National Institutes of Health Grant NS-16577, United States Army Medical Research Acquisition Activity Grant DAMD 17-98-2-8019, and by grants from the Muscular Dystrophy Association of America. The costs of publication of this article were defrayed in part by the payment of page charges. This article must therefore be hereby marked "*advertisement*" in accordance with 18 U.S.C. Section 1734 solely to indicate this fact.

‡ Supported by a Kendall-Mayo postdoctoral fellowship.

§ To whom correspondence should be addressed. Tel.: 904-953-7375; Fax: 904-953-7370; E-mail: rosenberry@mayo.edu.

[1] The abbreviations used are: AChE, acetylcholinesterase; DTNB, 5,5′-dithiobis-(2-nitrobenzoic acid); OP, organophosphate; EMPC, 7-[(methylethoxyphosphonyl)oxy]-4-methylcoumarin; 7HMC, 7-hydroxy-4-methylcoumarin; DEPQ, 7-[(diethoxyphosphoryl)oxy]-1-methylquinolinium iodide; 7HMQ, 7-hydroxy-1-methylquinolinium iodide; TMTFA, *m*-(*N,N,N*-trimethylammonio)trifluoroacetophenone.

DEPQ

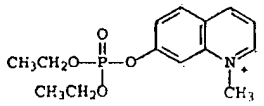

EMPC

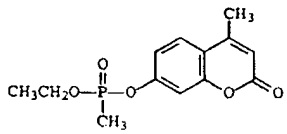

7HMQ

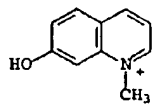

7HMC

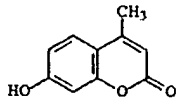

FIG. 1. **Chemical structures of OPs and their fluorescent hydrolysis products in these studies.**

phosphoryl enzyme results in essentially irreversible inactivation of the enzyme (12). In this paper we examine the effects of ligand binding to the peripheral site on OP phosphorylation of AChE in the context of the steric blockade model. Rate constants of phosphorylation are measured in two ways. The classical method involves periodic measurements of AChE activity toward substrates as the enzyme becomes inactivated. The second method involves continuous assay of the phosphorylation reactions either with mixtures of acetic acid ester substrates and OPs (13, 14) or by monitoring loss of a fluorogenic OP leaving group (15, 16). This method can be adapted to stopped-flow kinetic techniques to allow determination of both first- and second-order phosphorylation rate constants (13, 14). Here we monitor the reactions of two fluorogenic OPs, EMPC and DEPQ (Fig. 1), with erythrocyte and recombinant human AChE. Phosphorylation rate constants obtained directly by fluorescence measurement of their AChE-mediated hydrolysis products 7HMC and 7HMQ, respectively (Fig. 1), are compared with those obtained by enzyme inactivation.

EXPERIMENTAL PROCEDURES

Materials—Human erythrocyte AChE was purified as outlined previously, and active site concentrations were determined by assuming 410 units/nmol (17, 18).[2] DEPQ (15, 19) and EMPC were synthesized by established procedures (see Ref. 16). [(Methylethoxyphosphonyl)oxy]-chloride was reacted with 7HMC (Molecular Probes, Inc.) to give EMPC, and [(diethoxyphosphoryl)oxy]chloride was linked to 7-hydroxyquinoline (Acros Organics) and quaternized by methylation to form DEPQ. Structures were confirmed by ^{1}H NMR and ^{31}P NMR, and stock concentrations were determined by absorbance ($\epsilon_{310\ nm}$ = 11.0 mM^{-1} cm^{-1} for EMPC, and $\epsilon_{317\ nm}$ = 8.3 mM^{-1} cm^{-1} for DEPQ). Fasciculin was the fasciculin 2 form obtained from Dr. Carlos Cervenansky at the Instituto de Investigaciones Biologicas, Clemente Estable, Montevideo, Uraguay (6). Propidium iodide was purchased from Calbiochem.

Recombinant Human AChE—The full-length cDNA for human G_4 AChE was obtained from Dr. Avigdor Shafferman in the vector pACHE10 (20). To obtain a secreted dimeric form of human AChE, a 96-base pair truncation sequence including a stop codon was synthesized and inserted just downstream from the exon 4/5 boundary (see Ref. 21). Insertion of the modified exon 4/5 sequence (corresponding to ^{544}ASEAPSTC-DGDSS-stop, human AChE sequence numbering) resulted in a partial duplication of the 3′-end of the exon 4 region of the gene. To remove this duplicated segment, the *Not*I-*Nhe*I 3′- segment of the gene was cloned into *Not*I-*Nhe*I-digested pCIneo (Promega Corp.). This construct, pCIneo3′-AChE, contained an *Esp*I site in both the original and modified sections of exon 4. The unwanted duplicated gene segment was removed by digestion with *Esp*I followed by cloning of the resolved *Not*I-*Nhe*I fragment back into the AChE gene cassette. The final gene construct was confirmed by DNA sequencing carried out at the Mayo Clinic Rochester Molecular Biology Core Facility. The modified human AChE cDNA was moved into the pPac vector for transfection into and expression from *Drosophila* S2 cells in tissue culture (21). S2 cells were maintained in Schneider's *Drosophila* medium (Life Technologies, Inc.) with 10% fetal bovine serum and appropriate antibiotics at 28 °C. S2 cells were cotransfected with pPac carrying the hygromycin phosphotransferase gene for selection of cells with hygromycin B. After selection with 0.2 mg/ml hygromycin B, monoclonal cell lines were isolated from colonies formed using a modified soft agar cloning protocol (21). Briefly, 10^4 to 10^5 selected cells were suspended in complete medium with 0.3% low melting temperature agarose. This mixture was plated onto a base layer of solidified 1.5% low melting temperature agarose (in complete medium with 0.15 M NaCl) in 12-well tissue culture plates. After cell/medium layer solidification, a layer of complete medium was placed on top of the agarose. Colonies (>2 mm) were picked and grown in 24-well plates until confluence. At this point clones were assayed for AChE activity, and lines with high activity were kept for large scale culturing and long term propagation. AChE was purified from culture medium by two cycles of affinity chromatography on acridinium resin (17). Purified recombinant AChE samples analyzed by SDS-polyacrylamide gel electrophoresis (22) showed no contaminants. In the absence of disulfide reducing agents, a prominent band of 140-kDa dimer and a minor band of 70-kDa monomer were apparent, whereas in the presence of reducing agents a single 70-kDa band was observed. Comparison of the recombinant AChE with purified human erythrocyte AChE showed no differences in k_{cat}, K_{app}, or K_{SS} for acetylthiocholine hydrolysis (8), in K_I for propidium inhibition, in k_{on}, the fasciculin association rate constant (8), or in phosphorylation rate constants (see Table I below).

AChE Phosphorylation Determined with Fluorogenic OPs—Direct reaction of AChE with EMPC or DEPQ was followed by formation of their respective fluorescent leaving groups 7HMC or 7HMQ on a Perkin-Elmer LS-50B luminescence spectrometer in 20 mM sodium phosphate buffer and 0.02% Triton X-100 at 23 °C. Because these groups are fluorescent only when their 7-OH substituents are deprotonated (7HMC, pK_a = 7.8 (catalog from Molecular Probes, Inc.); 7HMQ, pK_a = 5.9 (23)), measurements were conducted at pH 8.0 for EMPC and pH 7.0 for DEPQ. Ratios of OP to AChE concentrations were adjusted to at least 20 for EMPC and 9 for DEPQ in all cases to prevent significant depletion of OP during the course of the reaction. Formation of 7HMC ($\epsilon_{360\ nm}$ = 19.0 mM^{-1} cm^{-1} at pH 9.0; catalog of Molecular Probes, Inc.) was monitored with excitation at 360 nm and emission at 450 nm, and 7HMQ formation was monitored with excitation at 400 nm and emission at 500 nm (for 7HMQ, $\epsilon_{405\ nm}$ = 10.0 mM^{-1} cm^{-1} at pH 9.0). For reactions that were completed in less than 1 min, a Hi-Tech SFA 20 stopped-flow apparatus was used to mix equal volumes (300 μl) of AChE (or AChE with inhibitor) and OP solutions rapidly, and fluorescence was recorded at fixed intervals as short as 20 ms. Formation of 7HMC or 7HMQ did not follow a simple exponential time course. Nonenzymatic hydrolysis of EMPC under all conditions and of DEPQ in the presence of propidium or fasciculin as inhibitors was significant, and under these conditions data were fitted by nonlinear regression analysis (Fig. P version 6.0, BioSoft, Inc.) to Equation 1.

$$f = f_{initial} + \Delta f(1 - e^{-kt}) + Ct \qquad \text{(Eq. 1)}$$

In Equation 1, $f_{initial}$ is the fluorescence at time zero, Δf is the fluorescence change corresponding to an amount of fluorescent product equal to the AChE concentration (23), C is the nonenzymatic hydrolysis rate, and k is the rate constant for the approach to the steady-state level of phosphorylation. With DEPQ in the absence of inhibitors the release of 7HMQ occurred in two phases, a large rapid phase and a small slower phase (see "Results") for both erythrocyte and recombinant AChE. These data were fitted to Equation 2, where Δf_2 and k_2 were the respective amplitude and the rate constant for the slower phase, and the other parameters were as defined in Equation 1.

$$f = f_{initial} + \Delta f(1 - e^{-kt}) + \Delta f_2(1 - e^{-k_2 t}) \qquad \text{(Eq. 2)}$$

The rate constants k were analyzed according to the catalytic pathway in Scheme 1. In this Scheme, OPX is the intact OP with leaving group X; *E*OPX is the initial complex of the OP with AChE, characterized by the equilibrium dissociation constant $K_S = k_{-S}/k_S$; and *E*OP is the phosphorylated enzyme. The inhibitor I can bind to the peripheral site in each of the enzyme species (as denoted by the subscript P). This scheme is identical to a general pathway for substrate hydrolysis by AChE considered elsewhere (7). Kinetic analysis of this scheme was simplified here in two ways. First, dephosphorylation rate constants (k_3 in Scheme 1), which appeared consistent with a value of 2–4 × 10^{-4}

[2] One unit corresponds to 1 μmol of acetylthiocholine hydrolyzed/min under standard pH-stat assay conditions (3.67 $\Delta A_{412\ nm}$/min in our standard spectrophotometric assay (17)).

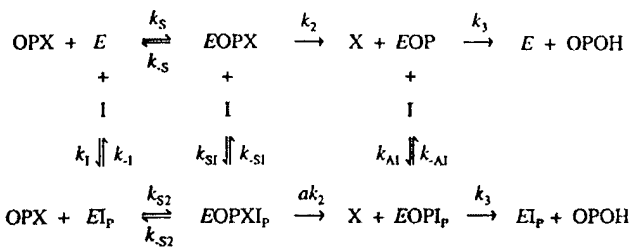

SCHEME I

min^{-1} reported previously for diethoxyphosphorylated eel AChE (24, 15; data not shown), were assumed to be negligible in all our experiments. Second, OPs were assumed to equilibrate with the AChE acylation site even when inhibitors were bound to the peripheral site. This assumption was supported by nonequilibrium kinetic simulations with the program SCoP, as noted under "Results,"[3] and it obviated the need for more complex mechanistic schemes that apply to substrates that do not equilibrate with AChE (8). With these assumptions, the dependence of k evaluated from either Equation 1 or Equation 2 on the OP concentration was analyzed by weighted nonlinear regression analysis (assuming constant percent error in k) according to Equation 3 to give k_{OP} and k_{OP}/K_{OP}, the respective first- and second-order rate constants of phosphorylation.

$$k = \frac{k_{OP}[OP]}{K_{OP} + [OP]} \qquad \text{(Eq. 3)}$$

These rate constants are related to the intrinsic rate constants in Scheme 1 as shown Equations 4 and 5.

$$k_{OP} = \frac{k_2\left(1 + \frac{a[I]}{K_{SI}}\right)}{\left(1 + \frac{[I]}{K_{SI}}\right)} \qquad \text{(Eq. 4)}$$

$$\frac{k_{OP}}{K_{OP}} = \frac{k_2\left(1 + \frac{a[I]}{K_{SI}}\right)}{K_S\left(1 + \frac{[I]}{K_I}\right)} \qquad \text{(Eq. 5)}$$

In the absence of I, $k_{OP} = k_2$ and $K_{OP} = K_S$. In the presence of I, K_{OP} is given by Equation 6.

$$K_{OP} = \frac{K_S\left(1 + \frac{[I]}{K_I}\right)}{\left(1 + \frac{[I]}{K_{SI}}\right)} \qquad \text{(Eq. 6)}$$

Assays with the peripheral site inhibitors propidium (30 μM) or fasciculin (0.5–10 μM) were conducted at inhibitor concentrations at least 30 times their respective K_I values to ensure that most of the AChE was complexed with inhibitor. Values of K_I were taken as 1.0 ± 0.1 μM for propidium (7), 11 ± 0.2 pM for fasciculin (6), and 100 pM for fasciculin in the presence of DTNB and acetylthiocholine in the standard assay (6, 8). Measurements that included fasciculin were modified in several ways. First, the enzyme was incubated with fasciculin for 5–10 min to generate equilibrated complex before the addition of OP. Second, the reaction buffer with EMPC was adjusted to pH 7.0 to reduce nonenzymatic hydrolysis of the OP. Finally, a four-cell cuvette changer was employed (except where noted) for reaction times as long as 4 h. This device minimized fluorophore photobleaching because the sample was cycled in and out of the light path. Each reaction was measured in parallel with cuvettes corresponding to an air blank and a nonenzymatic hydrolysis control devoid of AChE.

AChE Phosphorylation Determined by OP Inactivation of AChE-catalyzed Substrate Hydrolysis—AChE activity was monitored by a modified acetylthiocholine assay (25). Standard assays were conducted in 3.0 ml of 20 mM sodium phosphate, 0.02% Triton X-100, 0.33 mM DTNB, and 0.5 mM acetylthiocholine (pH 7.0) at 25 °C. Enzyme hydrolysis was monitored by formation of the thiolate dianion of DTNB at 412 nm ($\Delta\epsilon_{412\ nm}$ = 14.15 $mM^{-1}\ cm^{-1}$ (26)) for 1–5 min on a Varian Cary 3A spectrophotometer.[4] The inactivation of AChE by an OP was initiated by mixing AChE and OP at 23 °C in 20 mM phosphate buffer and 0.02% Triton X-100 (pH = 7.0). At various times a 1.0-ml aliquot was removed to a cuvette, 40 μl of acetylthiocholine and DTNB were added to final concentrations of 0.5 mM and 0.33 mM, respectively, and a continuous assay trace was recorded immediately at 412 nm. Background hydrolysis rates in the absence of AChE were subtracted. To assess the effects of peripheral site inhibitors on OP inactivation rates, propidium (30 μM) or fasciculin (50–250 nM) was incubated with AChE for at least 10–30 min prior to the addition of the OP. In some cases, DEPQ was also added (to 10–60 nM) for 60–120 min after incubation of fasciculin with AChE to eliminate a minor population of AChE which was refractory to normal fasciculin inhibition (see "Results"). Titrations of AChE activity with substoichiometric amounts of DEPQ were conducted by procedures similar to those in other inactivation measurements except that initial incubation mixtures contained higher concentrations of AChE (28–260 nM) and fasciculin (0–2 μM) and that after 90–120 min small aliquots of the mixtures (15–20 μl) were diluted into the standard acetylthiocholine assay solution.

OP inactivation reactions were measured under pseudo first-order conditions in which the ratio of OP to AChE concentrations was adjusted to at least 5. Assay rates v during inactivation were divided by the control assay rate in the absence of OP to give a normalized value $v_{(N)}$, and these values were fitted by nonlinear regression analysis (Fig. P) to Equation 7, where $v_{(N)initial}$ and $v_{(N)final}$ are the calculated values of $v_{(N)}$ at time zero and in the final steady state, respectively.

$$v_{(N)} = v_{(N)final} + (v_{(N)initial} - v_{(N)final})e^{-kt} \qquad \text{(Eq. 7)}$$

OP concentrations also were sufficiently low that the observed inactivation rate constant k was proportional to [OP]. The second-order rate constant for inactivation k_{OP}/K_{OP} was fitted by weighted linear regression analysis of the relationship $k = (k_{OP}/K_{OP})[OP]$ (see Equation 3), assuming a constant percent error in k.

RESULTS

Direct Fluorometric Measurement of AChE Phosphorylation by OPs in the Presence and Absence of Peripheral Site Ligands—The rapid reactions of EMPC and DEPQ with AChE require the use of stopped-flow methods if both first- and second-order phosphorylation rate constants are to be measured. Fig. 2*A* illustrates the measurement of an individual k value for the reaction of DEPQ with AChE. The release of the fluorescent product 7HMQ occurred largely with a single rapid exponential time course, but a slower phase corresponding to about 10% of the overall reaction also was apparent. The amplitude, or amount of product released, in the predominant faster reaction phase equaled the AChE concentration (Equations 1 and 2) and thus corresponded to a fluorescence titration of the enzyme normality which reacted rapidly with DEPQ (15, 23). Fitted k values for the rapid phase were analyzed according to Equation 3 (Fig. 2*B*) to obtain the first-order phosphorylation rate constant k_{OP} and the second-order rate constant k_{OP}/K_{OP}. A second, slower phase was not apparent in reactions of EMPC with AChE or in reactions of either OP in the presence of the pe-

[3] To ensure that EMPC and DEPQ were close enough to equilibrium with AChE in the presence of 30 μM propidium or 0.5–10 μM fasciculin to justify application of Equations 4–6, we applied the SCoP simulation program (7) to Scheme 1 with the following rate constant assignments: $k_S = 1 \times 10^7\ M^{-1}\ s^{-1}$ for EMPC and $2 \times 10^8\ M^{-1}\ s^{-1}$ for DEPQ, values similar to those assigned previously for neutral and cationic acetic acid ester substrates (7); $k_I = k_{SI} = 2 \times 10^8\ M^{-1}\ s^{-1}$ for propidium (7); $k_I = k_{SI} = 3 \times 10^7\ M^{-1}\ s^{-1}$ for fasciculin with free AChE, and $k_I = k_{SI} = 1 \times 10^7\ M^{-1}\ s^{-1}$ for fasciculin with AChE in the presence of DTNB and acetylthiocholine (6); $k_3 = 5 \times 10^{-6}\ s^{-1}$; k_{-S}, k_{-I}, k_2, and a from Table I and "Experimental Procedures" (with $k_{-X} = K_X k_X$); k_{-SI} from K_{SI} from Equation 6; and $k_{-S2} = k_{S2}\ K_S\ K_{SI}/K_I$. Simulated values of k_{OP} and k_{OP}/K_{OP} were then compared for complete equilibrium ($k_{S2}/k_S = 1$) and pronounced steric blockade ($k_{S2}/k_S = 0.00001$) and found to differ by less than 10%, justifying the equilibrium assumption.

[4] Enzyme activities were standardized to 0.1 $\Delta A_{412\ nm}$/min by applying the observed relationship $v_{std} = 0.1(v/0.1)^{1/R}$, where v was the measured activity, v_{std} was the standardized activity, and r = 0.95. R was the slope of a plot of log measured activity *versus* log enzyme concentration over a 200-fold range of enzyme dilution.

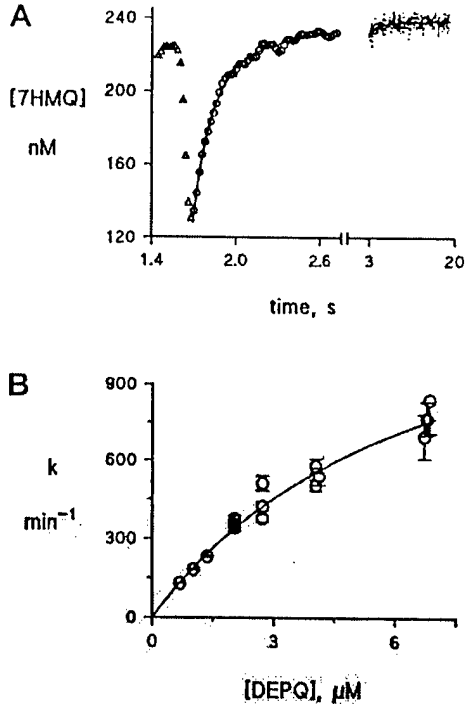

FIG. 2. **Reaction of DEPQ with recombinant AChE.** *Panel A*, equal volumes of DEPQ and AChE were mixed rapidly with the stopped-flow accessory to final concentrations of 2 μM and 100 nM, respectively, and generation of 7HMQ was monitored by spectrofluorometry as outlined under "Experimental Procedures." Prior to the reaction, the stopped-flow cuvette was washed extensively with the DEPQ stock solution alone; fluorescence in this wash solution results from about 5% contamination of the stock DEPQ with 7HMQ. In this recording, data collection on the spectrometer was triggered manually at time zero, and mixing was initiated at 1.6 s. Points observed for the reaction from 1.7 to 19 s (O and *dotted line*) were fitted to Equation 2 (*solid line*), with approximately 90% of the reaction amplitude corresponding to a reaction rate constant of 356 ± 13 min^{-1} and 10% to a rate constant of 24 ± 2 min^{-1}. Fluorescence units were converted to 7HMQ product formed (nM) by comparison with a 7HMQ standard solution. *Panel B*, rate constants for the faster phase of the reaction of DEPQ with AChE obtained as in *panel A* were plotted against the DEPQ concentration according to Equation 3 to obtain first- and second-order rate constants of 1,600 ± 200 min^{-1} and 205 ± 11 μM^{-1} min^{-1}, respectively (Table I).

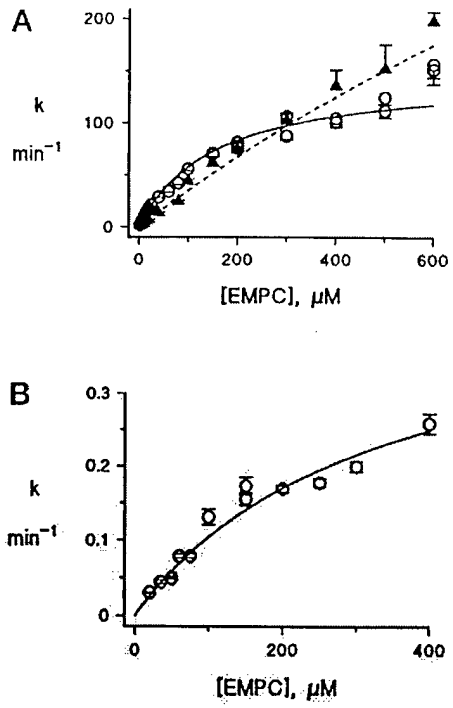

FIG. 3. **Phosphorylation of erythrocyte AChE by EMPC in the presence and absence of peripheral site ligands.** Rate constants k, measured by spectrofluorometric detection of 7HMC as outlined under "Experimental Procedures" (see also Fig. 2*A*), were plotted against the EMPC concentration and fitted to Equation 3 (*lines*) to obtain k_{OP} and k_{OP}/K_{OP} (Table I). *Panel A*, O indicates no inhibitor; $k_{OP} = k_2 = 149 \pm 9$ min^{-1} and $k_{OP}/K_{OP} = k_2/K_S = 0.95 \pm 0.04$ μM^{-1} min^{-1}. ▲ indicates plus 30 μM propidium; $k_{OP} = 900 \pm 500$ min^{-1} and $k_{OP}/K_{OP} = 0.37 \pm 0.02$ μM^{-1} min^{-1}. Points for [EMPC] ≥ 200 μM are shown as means of two to nine k measurements. *Panel B*, O indicates plus 1.3 μM fasciculin; $k_{OP} = 0.46 \pm 0.09$ min^{-1} and $k_{OP}/K_{OP} = 0.0013 \pm 0.0001$ μM^{-1} min^{-1}.

ripheral site inhibitors propidium or fasciculin. These reaction time courses, however, were superimposed upon significant nonenzymatic OP hydrolysis rates that were incorporated into the curve fitting of the k values. Estimates of k_{OP} and k_{OP}/K_{OP} were obtained from these k values by analyses similar to that in Fig. 2*B* (Table I). Purified recombinant human AChE expressed in *Drosophila* S2 cells gave rate constants for both OPs and relative amplitudes for DEPQ which were in good agreement with those for purified human erythrocyte AChE. Furthermore, our k_{OP}/K_{OP} value for DEPQ ($1.9–2.1 \times 10^8$ M^{-1} min^{-1}) agreed with previous estimates of this second-order phosphorylation rate constant determined by inactivation of eel AChE (15, 27; see below and Table I). No previous estimates of k_{OP} for either DEPQ or EMPC or of k_{OP}/K_{OP} for EMPC have been reported. We observe that k_{OP}/K_{OP} is about 200–300 times larger for DEPQ than for EMPC and that k_{OP} is about 10 times larger for DEPQ than for EMPC. These differences are consistent with previous expectations that the cationic nature of DEPQ and the lower pK_a of its leaving group relative to neutral EMPC should result in higher rates of AChE phosphorylation (14, 27, 28).

The effects of the small peripheral site ligand propidium on phosphorylation of AChE by OPs have not been widely studied. In Fig. 3*A* we show that propidium decreased k_{OP}/K_{OP} but increased k_{OP} for the phosphorylation of AChE by EMPC. The decrease in k_{OP}/K_{OP} was small (2.6- and 1.5-fold, for the erythrocyte and recombinant enzymes, respectively (Table I)) and consistent with those reported previously for neutral OPs with *T. californica* AChE (29). This small decrease appears consistent with the prediction of our steric blockade model that small peripheral site inhibitors like propidium will have little effect on the reaction of substrates that equilibrate with AChE (7; see Footnote 3 and Discussion). The extent of the increase in k_{OP} for EMPC when propidium is bound was less clear because the very slight curvature of the plot with propidium in Fig. 3*A* made extrapolation to k_{OP} problematic. Inclusion of 30 μM propidium increased the K_{OP} for EMPC by factors of 15 ± 9 and 6 ± 2 for the two AChEs to a value greater than 1 mM, and increased signal to noise prevented us from extending the EMPC concentration into the mM range to improve the precision of these factors. Insertion of these factors into Equation 6 and calculation from Equation 5 indicated that both K_S/K_I and α in Scheme 1 were on the order of 10 (Table I), indicating both lower affinity and higher reactivity of EMPC in the ternary complex with AChE and propidium. Propidium (30 μM) had a more pronounced effect on k_{OP}/K_{OP} for DEPQ, producing 18- and 14-fold decreases for the two AChEs (Table I). These factors again are consistent with those reported previously for cationic OPs with *T. californica* AChE (29). As observed for EMPC, bound propidium also increased K_{OP} for DEPQ to the point where it became technically difficult to measure the corresponding k_{OP}. It appeared that k_{OP} for DEPQ with propidium was at least as large as k_{OP} for DEPQ alone (Table I), but more

TABLE I

Rate constants for the phosphorylation of AChE by OPs

Rate constants were calculated from the dependence of k on [OP] as outlined under "Experimental Procedures."

Enzyme, OP, and inhibitor	Fluorescent product release				Enzyme inactivation	
	k_{OP}		k_{OP}/K_{OP}		k_{OP}/K_{OP}	
	min^{-1}	a	$\mu M^{-1}\ min^{-1}$	Relative decrease (fold)	$\mu M^{-1}\ min^{-1}$	Relative decrease (fold)
Erythrocyte						
EMPC						
None	149 ± 9		0.95 ± 0.04		0.82 ± 0.03	
Propidium	900 ± 500[a]	11 ± 12	0.37 ± 0.02	2.6	0.30 ± 0.01	2.7
Fasciculin	0.46 ± 0.09	0.003	0.0013 ± 0.0001	730	0.18 ± 0.01	4.6
Fasiculin + DEPQ[b]					0.0013 ± 0.0001	630
DEPQ						
None	1,600 ± 300		193 ± 13		151 ± 8	
Propidium	1,100 ± 500	≥1	11 ± 1	18	6.0 ± 0.2	25
Fasciculin	0.45 ± 0.09[a]	0.0003	0.0016 ± 0.0001	120,000	63 ± 10	2.4
Recombinant						
EMPC						
None	150 ± 11		0.67 ± 0.03		0.83 ± 0.02	
Propidium	570 ± 140[a]	4.4 ± 1.5	0.45 ± 0.02	1.5	0.31 ± 0.02	2.7
Fasciculin	0.23 ± 0.08	0.002	0.0011 ± 0.0002	600	0.24 ± 0.02	3.5
Fasiculin + DEPQ[b]					0.0019 ± 0.0002	440
DEPQ						
None	1,600 ± 200		205 ± 11		99 ± 3	
Propidium	1,200 ± 400	≥1	15 ± 1	14	5.2 ± 0.4	19
Fasciculin	0.66 ± 0.10[a]	0.0003	0.0010 ± 0.0001	220,000	32 ± 17	3.0

[a] The maximum [OP] employed did not exceed 80% of the estimated K_{OP}, and therefore estimates of k_{OP} are approximate.

[b] AChE was first preincubated with fasciculin then with DEPQ to eliminate the fasciculin-resistant AChE population (see "Results").

precise estimates were not possible.

Unlike propidium, the binding of fasciculin to the AChE peripheral site had a drastic effect on the phosphorylation of AChE by OPs (Fig. 3*B*). At saturating fasciculin concentrations (10^4 to 10^6 times greater than its K_I), k_{OP}/K_{OP} was decreased about 700-fold for EMPC and by about 10^5 for DEPQ. Bound fasciculin also decreased k_{OP} for both OPs by factors of 300–4,000 (Table I). The amplitudes of the OP reactions with the fasciculin-AChE complex again were consistent with the AChE normality, indicating that most of the enzyme was involved in the slowly reacting complex. A previous report of the effects of bound fasciculin on the reaction of AChE with the OPs echothiophate and paraoxon found only modest decreases of less than an order of magnitude for either k_{OP}/K_{OP} or k_{OP} (30). These relative changes in rate constants, however, were determined from rates of enzyme inactivation monitored by progressive reductions in the residual activity of the fasciculin-AChE complex, not from the release of the OP leaving group. To assess whether there were discrepancies between these methods, we repeated measurements of EMPC and DEPQ reaction rate constants by following enzyme inactivation.

Measurement of AChE Phosphorylation by OPs by Enzyme Inactivation—We measured AChE inactivation by EMPC and DEPQ without the use of stopped-flow kinetic methods, and our determinations were limited to the second-order phosphorylation rate constants k_{OP}/K_{OP}. With either OP alone or in the presence of propidium, values of k_{OP}/K_{OP} determined by inactivation were in agreement with those from spectrofluorometric assays within about a factor of 2 (Table I). However, when the reaction of either OP was measured in the presence of fasciculin, a striking discrepancy between the two methods became apparent. Bound fasciculin decreased k_{OP}/K_{OP} determined by inactivation only 2–5-fold (Table I), in agreement with the above report by Radic *et al.* (30) but in contrast to the decreases of up to 10^5-fold determined by spectrofluorometry (Table I). The discrepancy raised a concern that the enzyme activity observed during inactivation by OPs did not arise from the fasciculin-AChE complex. Because fasciculin binding reduces the activity of human AChE preparations to a residual 0.1–1% of the activity of the free enzyme (6), a tiny fraction of the AChE preparation resistant to fasciculin inhibition for any reason could become the dominant activity during the OP inactivation measurements. To examine this possibility, we altered the ratio of the OP to the AChE concentrations for the inactivation reaction in the presence of saturating fasciculin. When the DEPQ/AChE ratio was a typical value of 8, about 80% of the residual fasciculin-AChE activity was inactivated with a rate constant k consistent with the k_{OP}/K_{OP} of $6.2 \times 10^7\ M^{-1}\ min^{-1}$ in Table I (*lower trace*, Fig. 4). The inactivation reaction was then repeated at the same concentration of DEPQ but with 50 times as much AChE (*i.e.* [AChE]/[DEPQ] = 6). If all of the fasciculin-AChE complex could react with DEPQ at the previous rate, only about 17% of the residual activity should have been inactivated before DEPQ was completely depleted; in fact we continued to observe 80% inactivation with about the same k value (data not shown). Repeating the inactivation reaction again with a ratio [AChE]/[DEPQ] = 60 finally did result in depletion of the DEPQ but not before more than 40% of the residual fasciculin-AChE activity was inactivated (*upper trace*, Fig. 4). These data indicated that only a few percent of the total AChE concentration was involved in the observed inactivation reaction.

To quantify this point, we titrated several AChE stocks with DEPQ in the presence and absence of fasciculin by measuring inactivation. Examples of these titrations are shown in Fig. 5. As expected in the absence of fasciculin, the stoichiometric amount of DEPQ required for complete inactivation was within about 15% of the AChE active site concentration calculated from the initial activity (Fig. 5*A*). In the presence of saturating fasciculin, however, less than 100% of the residual activity was rapidly inactivated (Fig. 5, *B* and *C*). We fitted these titration data to a model with two enzyme populations, one that was relatively rapidly inactivated by DEPQ and the other that reacted with DEPQ at the very low rate constants measured by the fluorescence assays in Table I. The rapidly inactivated population corresponded to 5% of the total AChE concentration in Fig. 5*B* and 40% in Fig. 5*C*. These percentages varied among AChE stocks, with erythrocyte AChE typically giving about 5%

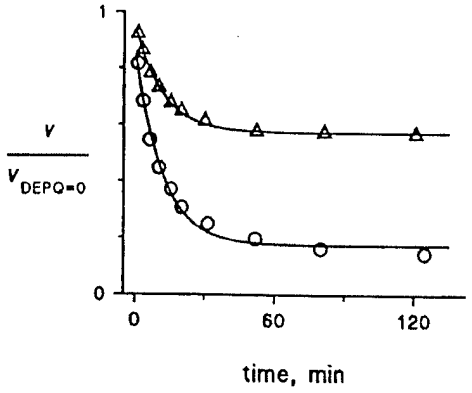

FIG. 4. **Inactivation of the residual activity of the fasciculin-AChE complex by DEPQ at two ratios of the DEPQ to AChE concentrations.** Erythrocyte AChE at 0.16 nM (○) and 80 nM (△) was incubated for 10 min with fasciculin at 50 nM (○) and 500 nM (△), and inactivation was initiated by the addition of DEPQ to a final concentration of 1.4 nM. Aliquots were assayed at the indicated times as outlined under "Experimental Procedures." Assay points v were normalized to corresponding control residual activities with fasciculin but without DEPQ (v_{DEPQ-0}) and fitted to Equation 7 (*lines*) to obtain a value of k for each curve.

and two preparations of recombinant AChE exhibiting 2 and 40%, respectively. These data thus are consistent with the assignment of a small but variable fraction of the AChE as a population that is largely resistant to fasciculin inhibition.

We next confirmed that the residual activity remaining after the rapid inactivation by DEPQ in Fig. 5, *B* and *C*, in fact did correspond to the fasciculin-AChE complex. This involved demonstrating that this residual activity was slowly inactivated by OPs at the same low rate constants determined with the fluorescence assays in Table I. AChE was incubated with fasciculin, and activity from the fasciculin-resistant population was removed by rapid inactivation with 10–60 nM DEPQ (see "Experimental Procedures"). The activity remaining after this treatment (*e.g.* the activity remaining after 60 min in the *lower trace* of Fig. 4) was then progressively inactivated by further incubation with EMPC, and k_{OP}/K_{OP} was determined as above. These values of k_{OP}/K_{OP} from inactivation were now in good agreement with the values of k_{OP}/K_{OP} obtained for the reaction of EMPC with the fasciculin-AChE complexes by fluorescence assay (*e.g.* 1.3×10^3 M^{-1} min^{-1} for erythrocyte AChE in Table I).

Detection of More Than One Population of AChE in the Presence of Fasciculin by Fluorometry—As our last demonstration of the consistency between the fluorescence- and inactivation-based assays, we reexamined the release of fluorescent 7HMQ from the reaction of DEPQ with AChE when fasciculin was present. Because this method does not depend on residual enzyme activity, the fasciculin-resistant population can be monitored separately from the fasciculin-AChE complex simply by altering the time of measurement and the concentration of DEPQ (Fig. 6). In Fig. 6*A*, DEPQ was 7–14-fold in excess of the expected fasciculin-resistant population of AChE. A burst of 7HMQ was released in the initial minute of reaction, and the amplitude of this burst indicated that approximately 2–3% of the recombinant AChE concentration had reacted. This percentage agreed with the percentage of rapidly inactivated AChE obtained by an inactivation titration like those in Fig. 5 for this recombinant AChE sample (data not shown). When the DEPQ concentration was increased by a factor of 25 (Fig. 6*B*), the initial burst in Fig. 6*A* became too fast to measure, but the slower reaction of DEPQ with the fasciculin-AChE complex became apparent. As expected, the amplitude of this reaction corresponded to the total AChE concentration, and the k value

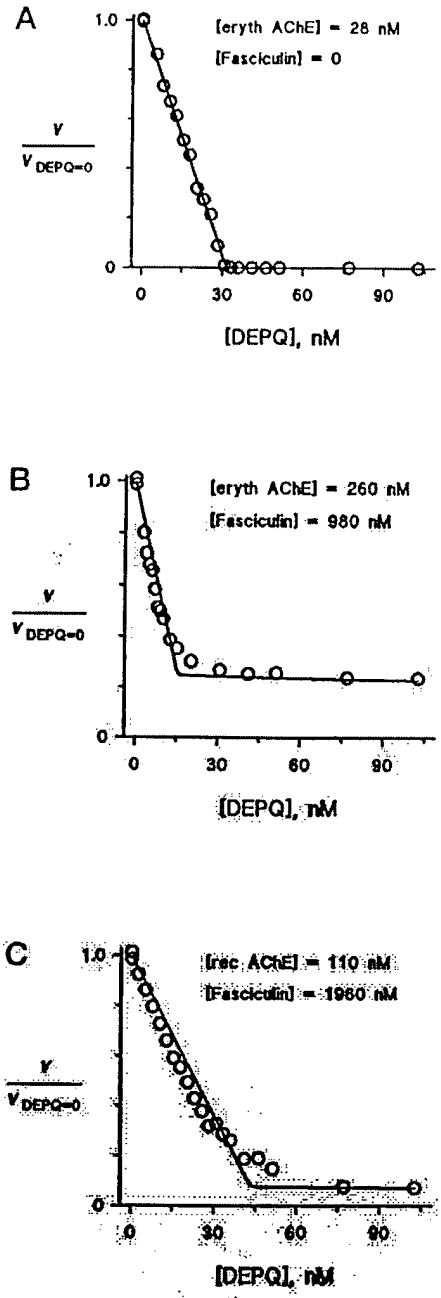

FIG. 5. **Titration of AChE with DEPQ in the presence and absence of fasciculin.** Erythrocyte (*eryth*) or recombinant (*rec*) AChE was incubated with or without fasciculin for 10–30 min and mixed with an equal volume of DEPQ for 90–120 min as outlined under "Experimental Procedures." Each point represents one mixture with the indicated final concentrations of DEPQ, AChE, and fasciculin. Aliquots (15–20 μl) were then diluted 50-fold (*panels B* and *C*) or 200-fold (*panel A*) into the standard acetylthiocholine solution for assay. Observed v were normalized to v_{DEPQ-0} obtained in the absence of DEPQ, and titration lines fitting the stoichiometric amount of DEPQ required to give complete rapid inactivation were calculated with the SCoP program. The calculated concentrations of rapidly inactivated AChE were 32 nM (*panel A*), 13 nM (*panel B*), and 43 nM (*panel C*) and correspond closely to the intersections of the *lines* in the plots. [The SCoP simulation program (7) was applied to two populations of AChE which reacted with DEPQ according to Scheme 1 to fit the data in Fig. 5, *B* and *C*. Rate constant assignments for the fasciculin-inhibited population were taken from Footnote 3; k_{OP}/K_{OP} for DEPQ with the fasciculin-resistant population was assigned as 1×10^8 M^{-1} min^{-1}, and the measured nonenzymatic DEPQ hydrolysis rate was 1.4×10^{-4} min^{-1} (data not shown). The fitted variables were the ratio of the concentrations of the two populations and the ratio of their acetylthiocholine hydrolysis rates.]

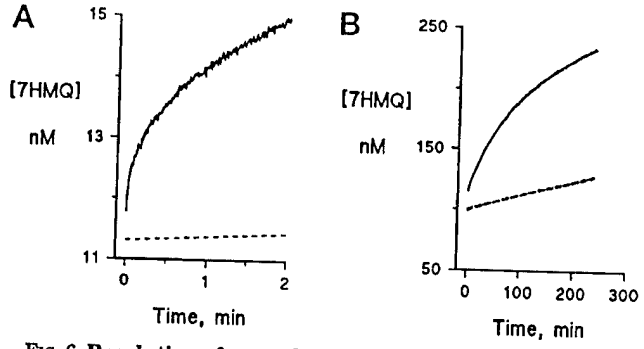

FIG. 6. **Resolution of more than one population of AChE in the presence of fasciculin by fluorometric assay with DEPQ.** *Panel A*, recombinant AChE (200 nM) was preincubated with fasciculin (1.0 μM) before mixing with an equal volume of 380 nM DEPQ in the stopped-flow accessory, and generation of 7HMQ was monitored by spectrofluorometry as in Fig. 2. *Panel B*, recombinant AChE (200 nM) was preincubated with fasciculin (1.0 μM) before conventional mixing with an equal volume of 10 μM DEPQ, and generation of 7HMQ was monitored as in *panel A*. A value of $k = 0.01$ min^{-1} was estimated by fitting the data in *panel B* with Equation 1. *Dashed lines* indicate blank DEPQ hydrolysis rates measured in the absence of AChE.

was consistent with the k_{OP}/K_{OP} determined by fluorometry for the reaction of DEPQ with AChE in the presence of fasciculin (Table I).

DISCUSSION

In this paper, we report kinetic parameters for the phosphorylation of AChE by two fluorogenic OPs, EMPC and DEPQ (Fig. 1). Both human erythrocyte AChE and recombinant human AChE produced from a high level *Drosophila* S2 cell expression system were examined. Because this expression system yields more than 20 mg of purified AChE from 2 liters of medium after 10 days of continuous culture, it is attractive for the preparation of wild type and site-specific mutants of AChE for comparative kinetic analyses and x-ray crystallography. The agreement of the phosphorylation kinetic parameters in Table I for the two AChEs provides important confirmation that the recombinant enzyme retains the catalytic properties of endogenous AChEs. EMPC and DEPQ were particularly useful organophosphorylation reagents because their reactions with AChE were observed both directly by fluorometry and indirectly by enzyme inactivation, their high phosphorylation rate constants approximated those for OPs used in chemical warfare applications, and their charges differed, allowing comparison of neutral EMPC with cationic DEPQ. We focused specifically on the effects of bound peripheral site ligands on AChE phosphorylation by OPs. Characterization of these effects is of great interest because it may be possible to design a peripheral site ligand that will block OP inactivation of AChE specifically while allowing sufficient acetylcholine hydrolysis activity to maintain synaptic transmission.

To pursue this goal we first compared the effects on AChE phosphorylation of two ligands that bind specifically to the peripheral site, the small phenanthridinium derivative propidium and the 61-residue polypeptide fasciculin. Propidium is a potent inhibitor of substrate hydrolysis by AChE, decreasing the second-order rate constant k_{cat}/K_{app} for acetylthiocholine and phenyl acetate by factors of 15–50 and the first-order rate constant k_{cat} by factors of 2–10 (7). To account for this inhibition, we proposed a steric blockade model in which the primary effect of a small peripheral site ligand like propidium is to slow the association and dissociation rate constants for ligand binding to the acylation site without significantly altering their ratio, the equilibrium constant (7, 8). One objective in proposing this model was to demonstrate that inhibition by peripheral site ligands could be explained without invoking a conformational change in the acylation site induced by the binding of ligand to the peripheral site. Our steric blockade model was supported by direct measurements with the acylation site ligands huperzine A and TMTFA: bound propidium decreased the association rate constants 49- and 380-fold and the dissociation rate constants 10- and 60-fold, respectively, relative to the rate constants for these acylation site ligands with free AChE (7). The model also was supported by computer simulations of substrate hydrolysis based on Scheme 1. When the binding of substrate to the acylation site failed to reach equilibrium, the observed level of propidium inhibition could be reproduced (7). On the other hand, the model predicts that propidium should have little effect on the reaction of a substrate that essentially equilibrates with the acylation site. Few reports in the literature include data that allow this prediction to be examined, but it is supported by a recent investigation of aryl acylamidase activity in AChE (31). The peripheral site ligands propidium and gallamine failed to inhibit AChE-catalyzed hydrolysis of aryl acylamides, which are hydrolyzed slowly by AChE and thus should equilibrate with the acylation site (32), but gave typical inhibition of acetylthiocholine hydrolysis.

The reaction of OPs, including EMPC and DEPQ, with AChE appears to involve equilibration of the OP with the acylation site (see Footnote 3). Table I indicates that propidium did have modest effects on k_{OP} and k_{OP}/K_{OP} for both EMPC and DEPQ. Do these observations invalidate our steric blockade model and require that the binding of propidium induce a conformational change in the acylation site? We argue that they do not, if the model is extended to allow an unfavorable electrostatic interaction or a steric overlap between propidium at the peripheral site and an OP at the acylation site in the AChE ternary complex. The need for such an extension in fact has been recognized in our previous studies because small decreases in the affinity of ligands in ternary AChE complexes relative to the corresponding binary complex are observed consistently (7). For example, from the rate constants noted above one can calculate that the affinities of huperzine A and TMTFA for the acylation site decreased by factors of 5–6 when propidium was bound to the peripheral site. Computer modeling revealed no steric overlap between the ligands in these ternary complexes (7), so the decreased affinity must result from unfavorable electrostatic interaction between these cationic ligands. Extending these observations to the OPs, a decrease in affinity for EMPC and DEPQ also was apparent when propidium was bound to the peripheral site. Insertion of data from Table I into Equation 6 indicated that this decrease (given by $K_{SI}/K_I = K_{S2}/K_S$) was about an order of magnitude for both OPs. There was also a clear increase in the k_{OP} for EMPC ($\alpha > 1$ in Table I) and a possible increase in k_{OP} for DEPQ when propidium was bound, consistent with an acceleration of first-order phosphorylation rate constants by bound peripheral site ligands reported recently by Radic (33, 34). It has long been known that k_{OP}/K_{OP} for the reaction of neutral OPs with AChE varies smoothly and monotonically with the pK_a of the leaving group (27). This suggests that cleavage of the leaving group ester bond of the OP is prominent in the rate-limiting step for phosphorylation of AChE. Computer modeling revealed a clear unfavorable steric overlap between propidium in the peripheral site and the leaving group of either EMPC or DEPQ in the acylation site (data not shown; 35). This steric overlap could contribute to the decrease in affinity for both neutral EMPC and cationic DEPQ, and it could induce molecular or electronic strain caused by the proximity of propidium to the OP in the ternary complex to increase k_{OP}. This increase would not require an induced conformational change in the acylation si

when propidium alone is bound but would result from a change in ligand configuration or overall conformation in the ternary complex.

The consequences of fasciculin binding to the peripheral site of AChE on phosphorylation kinetic parameters for EMPC and DEPQ were qualitatively different from those of propidium. Values of k_{OP}/K_{OP} were decreased by factors of 10^3 to 10^5, and k_{OP} was decreased by factors of 300–4,000 (Table I). Fasciculin has been shown to present a substantial steric blockade to the entrance and exit of ligands that bind to the acylation site: association and dissociation rate constants for the binding of *N*-methylacridinium were decreased 8,000- and 2,000-fold, respectively, when fasciculin was bound (36). However, steric blockade of OP association and dissociation rate constants cannot account for the effects of fasciculin on the phosphorylation rate constants. Because OPs essentially equilibrate with the acylation site, a steric blockade of OPs by fasciculin that resulted in even a 100,000-fold decrease in association rate constant ($k_{S2}/k_S = 10^{-5}$) would result in less than a 10% decrease in k_{OP}/K_{OP} and no change in k_{OP} (see Footnote 3). The pronounced fasciculin inhibition of AChE phosphorylation requires an additional interaction between fasciculin and the acylation site. One possibility might be an unfavorable steric overlap between fasciculin at the peripheral site and an OP at the acylation site in the AChE ternary complex, but the three-dimensional structure of the fasciculin-AChE complex shows no penetration of the acylation site by fasciculin which would lead to such an interaction. Therefore, the additional interaction must involve a conformational change in the acylation site induced by bound fasciculin. Crystal structure analyses of fasciculin-AChE complexes (3, 4) show that fasciculin 2 interacts not only with Trp^{279} in the peripheral site but also with residues on the outer surface of an ω-loop within 4 Å of Trp^{84} in the acylation site, well beyond the region of the peripheral site occupied by propidium (7, 37). These more extensive surface interactions provide a structural basis for an inhibitory conformational effect on the acylation site when fasciculin but not when propidium is bound to the peripheral site.

Second-order phosphorylation rate constants k_{OP}/K_{OP} obtained for EMPC or DEPQ alone or in the presence of propidium were in good agreement when measured either by release of the fluorescent leaving group or by enzyme inactivation (Table I). In the presence of fasciculin, however, k_{OP}/K_{OP} values determined by enzyme inactivation were 100-fold greater for EMPC and 10^4-fold greater for DEPQ than the corresponding values measured fluorometrically. Through a series of titrations like those in Fig. 5, this discrepancy was shown to arise from misleading inactivation measurements caused by a small fraction of the total AChE (less than 5%, except for one preparation) which remained largely resistant to inhibition by fasciculin. This fraction thus accounted for most of the enzyme activity in the presence of fasciculin and was inactivated by both OPs much more rapidly than the fasciculin-AChE complex was phosphorylated. In support of this explanation, reexamination of the release of fluorescent 7HMQ from DEPQ in the presence of fasciculin revealed a small initial burst that was in stoichiometric agreement with the fraction of AChE that was rapidly inactivated (Fig. 6*A*). The population of AChE resistant to fasciculin inhibition may itself be heterogeneous. The titration curves in Fig. 5, *B* and *C*, were not fit precisely by a model with two forms of AChE, and the deviation suggested a third form with somewhat less resistance to fasciculin inhibition. In addition, the initial burst of 7HMQ release in Fig. 6*A* could not be fit to a single exponential release of 7HMQ but instead corresponded to two release reactions, the faster of which corresponded to the k_{OP}/K_{OP} initially observed for fasciculin inhibition of inactivation by DEPQ (Table I). Other uncertainties involve the source of the population of fasciculin-resistant AChE or the process whereby it was produced. Each AChE preparation we examined, whether erythrocyte or recombinant, showed this resistant population, but its extent varied among different affinity chromatography preparations. This population may represent a portion of the AChE which has undergone an undefined chemical modification that alters the affinity of fasciculin for the peripheral site and/or the catalytic efficiency of the fasciculin-AChE complex. Estimates of k_{OP}/K_{OP} for this population in the presence of fasciculin from the inactivation data in Table I were only 2–5-fold lower than k_{OP}/K_{OP} for AChE alone, and these estimates were relatively insensitive to the saturating fasciculin concentration (data not shown). Furthermore, calculations from the titration data in Fig. 5 indicated an acetylthiocholine turnover rate for this population which was about 30% of that for free AChE (data not shown). These comparisons suggest that catalysis at the acylation site is only slightly less efficient in the fasciculin-resistant population than in the predominant conventional AChE. Fasciculin does appear to interact weakly with this resistant population, resulting in 3–5-fold decreases in k_{OP}/K_{OP} for EMPC and DEPQ (Table I). A fasciculin-resistant population also may dominate the activity of recombinant mouse AChE in the presence of fasciculin: the addition of fasciculin induced biphasic phosphorylation rates and only modest decreases in phosphorylation rate constants and TMTFA association and dissociation rate constants (less than 20-fold; 30). It is possible that the population of AChE resistant to fasciculin can be distinguished even in the absence of fasciculin as the fraction of AChE that underwent a slower reaction with DEPQ in Fig. 2. The amount of this fraction (about 10% of the total AChE) and its phosphorylation rate constant (about 10% of the k for the faster phase) are roughly consistent with the data for the fasciculin-resistant population.

Regardless of the origin of the fasciculin-resistant population, it is significant because it obscures the kinetic properties of the actual fasciculin-AChE complex measured by enzyme inactivation, both in our measurements (Table I) and apparently in those of Radic *et al.* (30). We overcame this problem by exploiting the relatively high sensitivity of the fasciculin-resistant population to DEPQ. Incubation of small amounts of AChE (3–20 nM) in the presence of fasciculin with 10–60 nM DEPQ was sufficient to inactivate this population in 60 min, and the kinetic parameters of the fasciculin-AChE complex then could be measured by inactivation. For example, measurement of k_{OP}/K_{OP} for EMPC after this treatment gave good agreement with the k_{OP}/K_{OP} values determined for EMPC with the fasciculin-AChE complex by fluorometry (Table I). In addition to phosphorylation kinetic parameters, it may be necessary to employ DEPQ inactivation to reevaluate kinetic parameters for the reaction of substrates (6) and TMTFA (30) with fasciculin-AChE complexes.

Acknowledgments—We express our gratitude to Dr. Abdul Fauq of the Mayo Clinic Jacksonville Organic Synthesis Core Facility for preparation of EMPC and DEPQ used in these studies. We thank Dr. Harvey Berman of the State University of New York at Buffalo and Dr. Yacov Ashani of the Israel Institute for Biological Research at Ness-Ziona for initial samples of EMPC and DEPQ, respectively. We also thank Dr. Avigdor Shafferman of the Israel Institute for Biological Research at Ness-Ziona for the cDNA for AChE in pACHE10 and Dr. Carlos Cervenansky for fasciculin 2. We acknowledge the technical assistance of Dr. John Incardona, Jean Eastman, Dr. Robert Haas, and Pat Thomas in the initial phases of construction and cloning the recombinant human AChE gene cassette.

REFERENCES

1. Rosenberry, T. L. (1975) *Adv. Enzymol.* **43**, 103–218
2. Sussman, J. L., Harel, M., Frolow, F., Oefner, C., Goldman, A., Toker, L., and

Silman, I. (1991) *Science* **253**, 872–879
3. Bourne, Y., Taylor, P., and Marchot, P. (1995) *Cell* **83**, 503–512
4. Harel, M., Kleywegt, G. J., Ravelli, R. B. G., Silman, I., and Sussman, J. L. (1995) *Structure* **3**, 1355–1366
5. Taylor, P., and Lappi, S. (1975) *Biochemistry* **14**, 1989–1997
6. Eastman, J., Wilson, E. J., Cervenansky, C., and Rosenberry, T. L. (1995) *J. Biol. Chem.* **270**, 19694–19701
7. Szegletes, T., Mallender, W. D., and Rosenberry, T. L. (1998) *Biochemistry* **37**, 4206–4216
8. Szegletes, T., Mallender, W. D., Thomas, P. J., and Rosenberry, T. L. (1999) *Biochemistry* **38**, 122–133
9. Burgen, A. S. V. (1949) *Br. J. Pharmacol.* **4**, 219–228
10. Wilson, I. B. (1951) *J. Biol. Chem.* **190**, 111–117
11. Aldridge, W. N., and Reiner, E. (1972) in *Frontiers of Biology*, 26th Ed., p. 328, Elsevier, North Holland, Amsterdam
12. Froede, H. C., and Wilson, I. B. (1971) in *The Enzymes* (Boyer, P. D., ed.) 3rd Ed., Vol. 5, pp. 87–114, Academic Press, New York
13. Hart, G. D., and O'Brien, R. D. (1973) *Biochemistry* **12**, 2940–2945
14. Berman, H. A., and Leonard, K. (1989) *J. Biol. Chem.* **264**, 3942–3950
15. Gordon, M. A., Carpenter, D. E., Barrett, H. W., and Wilson, I. B. (1978) *Anal. Biochem.* **85**, 519–527
16. Levy, D., and Ashani, Y. (1986) *Biochem. Pharmacol.* **35**, 1079–1085
17. Rosenberry, T. L., and Scoggin, D. M. (1984) *J. Biol. Chem.* **259**, 5643–5652
18. Roberts, W. L., Kim., B. H., and Rosenberry, T. L. (1987) *Proc. Natl. Acad. Sci. U. S. A.* **84**, 7817–7821
19. Ginsburg, S., Kitz, R. J., and Wilson, I. B. (1966) *J. Med. Chem.* **9**, 632–633
20. Kronman, C., Velan, B., Gozes, Y., Leitner, M., Flashner, Y., Lazar, A., Marcus, D., Sery, T., Papier, Y., Grosfeld, H., Cohen, S., and Shafferman, A. (1992) *Gene (Amst.)***121**, 295–304
21. Incardona, J. P., and Rosenberry, T. L. (1996) *Mol. Biol. Cell* **7**, 595–611
22. Laemmli, U. K. (1970) *Nature* **227**, 680–685
23. Rosenberry, T. L., and Bernhard, S. A. (1971) *Biochemistry* **10**, 4114–4120
24. Maglothin, J. A., Wins, P., and Wilson, I. B. (1975) *Biochim. Biophys. Acta* **403**, 370–387
25. Ellman, G. L., Courtney, K. D., Andres, J., V., and Featherstone, R. M. (1961) *Biochem. Pharmacol.* **7**, 88–95
26. Riddles, P. W., Blakeley, R. L., and Zerner, B. (1979) *Anal. Biochem.* **94**, 75–81
27. Kitz, R. J., Ginsburg, S., and Wilson, I. B. (1967) *Mol. Pharmacol.* **3**, 225–232
28. Hosea, N. A., Radic, Z., Tsigelny, I., Berman, H. A., Quinn, D. M., and Taylor, P. (1996) *Biochemistry* **35**, 10995–11004
29. Berman, H., and Leonard, K. (1990) *Biochemistry* **29**, 10640–10649
30. Radic, Z., Quinn, D. M., Vellom, D. C., Camp, S., and Taylor, P. (1995) *J. Biol. Chem.* **270**, 20391–20399
31. Costagli, C., and Galli, A. (1998) *Biochem. Pharmacol.* **55**, 1733–1737
32. Barlow, P. N., Acheson, S. A., Swanson, M. L., and Quinn, D. M. (1987) *J. Am. Chem. Soc.* **109**, 253–257
33. Radic, Z., and Taylor, P. (1999) *Chem.-Biol. Interact.*, in press
34. Radic, Z., and Taylor, P. (1998) in *Structure and Function of Cholinesterases and Related Proteins* (Doctor, B. P., Taylor, P., Quinn, D. M., Rotundo, R. L., and Gentry, M. K., eds) pp. 211–214, Plenum Press, New York
35. Albaret, C., Lacoutiere, S., Ashman, W. P., Foment, D., and Fortier, P.-L. (1997) *Proteins* **28**, 543–555
36. Rosenberry, T. L., Rabl, C. R., and Neumann, E. (1996) *Biochemistry* **35**, 685–690
37. Barak, D., Kronman, C., Ordentlich, A., Ariel, N., Bromberg, A., Marcus, D., Lazar, A., Velan, B., and Shafferman, A. (1994) *J. Biol. Chem.* **269**, 6296–6305

0026-895X/00/020409-09$3.00/0

MOLECULAR PHARMACOLOGY, 57:409–417 (2000).

Huprine X is a Novel High-Affinity Inhibitor of Acetylcholinesterase That Is of Interest for Treatment of Alzheimer's Disease

PELAYO CAMPS, BERNADETTE CUSACK, WILLIAM D. MALLENDER, RACHID EL ACHAB, JORDI MORRAL, DIEGO MUÑOZ-TORRERO, and TERRONE L. ROSENBERRY

Department of Pharmacology, Mayo Foundation for Medical Education and Research and the Department of Research, Mayo Clinic Jacksonville, Jacksonville, Florida (B.C., W.D.M., T.L.R.); and Laboratori de Química Farmacèutica, Facultat de Farmàcia, Universitat de Barcelona, Barcelona, Spain (P.C., R.E.A., J.M., D.M.-T.)

Received August 23, 1999; accepted November 3, 1999

This paper is available online at http://www.molpharm.org

ABSTRACT

Inhibitors of the enzyme acetylcholinesterase (AChE) slow and sometimes reverse the cognitive decline experienced by individuals with Alzheimer's disease. Huperzine A, a natural product used in traditional Chinese herbal medicine, and tacrine (Cognex) are among the potent AChE inhibitors used in this treatment, but the search for more selective inhibitors continues. We report herein the synthesis and characterization of (−)-12-amino-3-chloro-9-ethyl-6,7,10,11-tetrahydro-7,11-methanocycloocta[*b*]quinoline hydrochloride (huprine X), a hybrid that combines the carbobicyclic substructure of huperzine A with the 4-aminoquinoline substructure of tacrine. Huprine X inhibited human AChE with an inhibition constant K_i of 26 pM, indicating that it binds to this enzyme with one of the highest affinities yet reported. Under equivalent assay conditions, this affinity was 180 times that of huperzine A, 1200 times that of tacrine, and 40 times that of E2020 (donepezil, Aricept), the most selective AChE inhibitor currently approved for therapeutic use. The association and dissociation rate constants for huprine X with AChE were determined, and the location of its binding site on the enzyme was probed in competition studies with the peripheral site inhibitor propidium and the acylation site inhibitor edrophonium. Huprine X showed no detectable affinity for the edrophonium-AChE complex. In contrast, huprine X did form a ternary complex with propidium and AChE, although its affinity for the free enzyme was found to be 17 times its affinity for the propidium-AChE complex. These data indicated that huprine X binds to the enzyme acylation site in the active site gorge but interferes slightly with the binding of peripheral site ligands.

Alzheimer's disease is associated with a selective loss of cholinergic neurons in the brain (Davies and Maloney, 1976; Whitehouse et al., 1981). The losses are accompanied by decreases in the neurotransmitter acetylcholine as well as in the respective enzymes that synthesize and degrade acetylcholine, choline acetyltransferase and acetylcholinesterase (AChE) (Perry et al., 1977; Bowen et al., 1982). These observations stimulated a cholinergic hypothesis of Alzheimer's disease (Bartus et al., 1982), which postulates that at least some of the cognitive decline experienced by patients with the disease results from a deficiency in acetylcholine and thus in cholinergic neurotransmission. This hypothesis suggested that inhibitors of AChE might elevate levels of acetylcholine in the brains of these patients and reverse the cognitive decline (Muramoto et al., 1979), and experimental evidence has supported this suggestion. The first, and thus far the only, two drugs approved by the U.S. Food and Drug Administration (FDA) for treatment of the cognitive deficit in Alzheimer's disease are both reversible inhibitors of AChE (Fig. 1). Tacrine (Cognex) was approved in 1993 and E2020 (donepezil, Aricept) in 1996. A third potent reversible AChE inhibitor, huperzine A (Fig. 1), is a natural product isolated from the club moss Lycopodium *Huperzia serrata* used in traditional Chinese herbal medicine (Kozikowski et al., 1992).

A number of efforts have been undertaken to synthesize

This work was supported by Grant NS-16577 from the National Institutes of Health, DAMD 17-98-2-8019 from the U.S. Army Medical Research Acquisition Activity, and by grants from the Muscular Dystrophy Association of America. Financial support from the Comisión Interministerial de Ciencia y Tecnología (Programa Nacional de Tecnología de los Procesos Químicos, Project QUI96–0828), Fundació "La Marató de TV3" (Project 3004/97), Comissionat per a Universitats i Recerca of the Generalitat de Catalunya (Project 1997-SGR-00140), and Medichem, S.A., and fellowships from Comissió Interdepartamental de Recerca i Innovació Tecnològica of the Generalitat de Catalunya to J. Morral and from Agencia Española de Cooperación Internacional (Instituto de Cooperación con el Mundo Arabe, Mediterráneo y Países en Desarrollo) to R.E.A. are gratefully acknowledged.

ABBREVIATIONS: AChE, acetylcholinesterase; MPLC, medium-pressure liquid chromatography; DTNB, 5,5′-dithiobis-(2-nitrobenzoic acid); TcAChE, *Torpedo californica* acetylcholinesterase; TMTFA, *m*-(*N, N,N* trimethylammonio)trifluoroacetophenone; COSY, correlation spectroscopy; HMQC, heteronuclear multiple-quantum coherence.

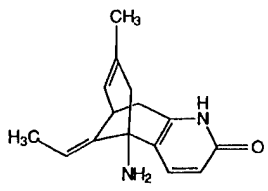

(-)-Huperzine A

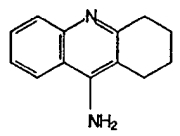

Tacrine

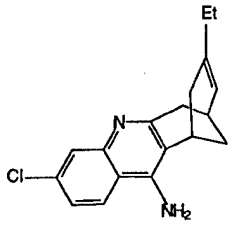

Huprine X

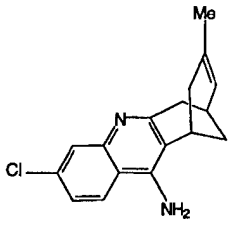

Huprine Y

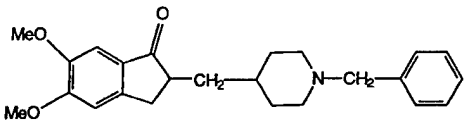

E2020

Fig. 1. Structures of inhibitors of AChE.

even more selective AChE inhibitors as potential therapeutic agents in Alzheimer's disease. Although the highest affinity reversible AChE inhibitors identified to date contain quaternary amine group(s), these efforts have focused on compounds which, like the approved drugs, contain nonquaternary amines and are more likely to pass from the circulation to the brain across the blood-brain barrier. Some new inhibitors have been modeled on tacrine, including bifunctional or bis-tacrine analogs with alkylene linked tacrine moieties (Pang et al., 1996). Other inhibitors have been designed that combine the carbobicyclic substructure of huperzine A with the 4-aminoquinoline substructure of tacrine (Badia et al., 1998). These initial tacrine-huperzine A hybrids, for which we suggest the name huprines, had slightly higher affinity for AChE than tacrine itself. Herein, we introduce a huprine with an ethyl group at position 9 and a chlorine atom at position 3. We designate this compound huprine X (Fig. 1) and show that it inhibits AChE by binding to the enzyme with an affinity that is among the highest yet reported for a reversible inhibitor of AChE.

We also estimate the location of huprine X binding in AChE by reference to the structures of AChE and AChE-inhibitor complexes determined by X-ray crystallography. These structures reveal a deep active site gorge with two sites of ligand interaction: a peripheral site at the surface of the enzyme and an acylation site at the base of the gorge where the substrate acyl group is first transferred to residue S200[1] (Sussman et al., 1991; Harel et al., 1993; Bourne et al., 1995; Harel et al., 1995). Certain ligands can bind selectively to either the acylation site or the peripheral site, and ternary complexes can be formed in which ligands are bound to both sites simultaneously (Taylor and Lappi, 1975; Eastman et al., 1995). X-ray crystallography has shown that edrophonium, huperzine A, and tacrine all are specific for the acylation site, although their contacts with the enzyme surface do not completely overlap (Harel et al., 1993; Raves et al., 1997). Ligands specific for the peripheral site include the small aromatic compound propidium. By examining inhibition of AChE by huprine X in the presence of either propidium or edrophonium, we show that huprine X appears to bind to the acylation site of AChE.

Experimental Procedures

Materials

Human erythrocyte AChE (Rosenberry and Scoggin, 1984; Roberts et al., 1987) and recombinant human AChE (Mallender et al., 1999) were purified as outlined previously. Analyses were conducted with human erythrocyte AChE except where noted, and active site AChE concentrations for both enzymes were determined by assuming 410 U/nmol.[2] Recombinant *Drosophila* AChE was the SEC1 variant (Incardona and Rosenberry, 1996). Human butyrylcholinesterase was purified from plasma (Lockridge, 1990) and was a gift from Dr. Oksana Lockridge, University of Nebraska Medical Center. Propidium iodide was obtained from Calbiochem (La Jolla, CA), and propidium concentrations were assigned with an extinction coefficient $\epsilon_{493\ nm} = 5900\ M^{-1}\ cm^{-1}$ (Taylor and Lappi, 1975). Tacrine was purchased from Sigma Chemical Co. (St. Louis, MO) and E2020 was a gift from Yoshiyuki Kawakami, Ph.D., Eisai Co., Ltd., Ibaraki, Japan.

General Chemistry Methods

Melting points were determined in open capillary tubes with a MFB 595010 M Gallenkamp melting point apparatus. ^1H NMR spectra were recorded at 500 MHz on a Varian VXR 500 spectrometer and ^{13}C NMR spectra were recorded at 75.4 MHz on a Varian Gemini 300 spectrometer. The chemical shifts are reported in parts per million (δ scale) relative to internal trimethylsilane and coupling constants are reported in Hertz. Correlation spectroscopy (COSY) $^1H/^1H$ experiments were performed with standard procedures and COSY $^1H/^{13}C$ experiments with the ^1H-detected heteronuclear multiple-quantum coherence (HMQC) sequence and an indirect detection probe. Infrared (IR) spectra were run on a Perkin Elmer model 1600 Fourier transform/infrared spectrometer. Absorption values are expressed as wavenumbers (cm^{-1}). Optical rotations were measured on a Perkin Elmer model 241 polarimeter. Chiral HPLC analyses were performed on a Waters model 600 liquid chromatograph provided with a Waters model 486 variable λ detector, with a CHIRALCEL OD-H column (25 × 0.46 cm) containing the chiral stationary phase cellulose tris(3,5-dimethylphenylcarbamate). Conditions A: mixture of hexane/EtOH in the ratio of 75:25, containing

[1] Throughout this paper, we number residues according to the TcAChE sequence. For example, W84 and S200 in this sequence correspond to W86 and S203, respectively, in mammalian AChE.

[2] One unit of AChE activity corresponds to 1 μmol of acetylthiocholine hydrolyzed per minute under standard pH-stat assay conditions, and these conditions correspond to maximal AChE activity at pH 8 (Rosenberry and Scoggin, 1984). Our conventional spectrophotometric assay at 412 nm is conducted in pH 7 buffer with 0.5 mM acetylthiocholine, conditions that result in 4.5 $\Delta A_{412\ nm}$/min with 1 nM AChE or ~76% of the maximal activity.

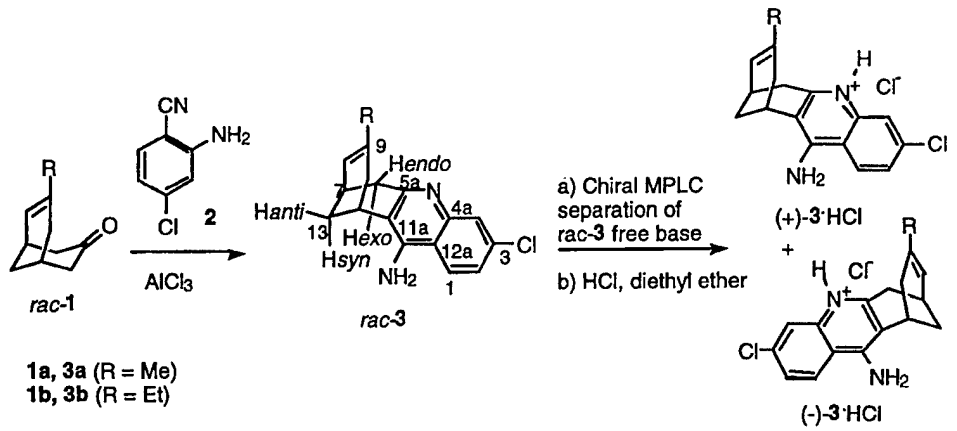

Fig. 2. Synthesis strategy for huprine derivatives. Compound *rac*-**3a** and its enantiomers (huprine Y is the HCl salt of (−)-*rac* **3a**) were prepared as described (Camps et al., 1998, 1999; for the synthesis of related compounds, see Badia et al., 1998). *Rac*-**3b** (huprine X is the HCl salt of (−)-*rac* **3b**) was prepared in a similar way from the known enone *rac*-**1b** (Camps et al., 1996) by Friedländer reaction with 4-chloro-2-aminobenzonitrile, **2** (Camps P, Muñoz-Torrero D, Görbig D, Contreras J, Simon M, Morral J, El Achab R, Badia A, Baños JE, Vivas N. WO patent application 97/13754). Separation of *rac*-**3b** was carried out in a similar manner to that described for *rac*-**3a** (see *Experimental Procedures*). Although the absolute configuration of (−)-**3a** was established by X-ray diffraction analysis, that of (−)-**3b** was assigned by analogy with (−)-**3a** (Camps et al., 1998).

0.1% diethylamine, as eluent, flow 0.20 ml/min, λ = 235 nm. Chiral medium-pressure liquid chromatography (MPLC) separation was carried out on equipment that consisted of a pump (Büchi 688), a variable UV detector (Büchi) and a column (25 × 2.5 cm) containing microcrystalline cellulose triacetate (15–25 μm) as the chiral stationary phase. Column chromatography was performed on silica gel 60 A C.C. (70–200 mesh; SDS, ref. 2100027). For the thin-layer chromatography, aluminum-backed sheets with silica gel 60 F_{254} (Merck; ref. 1.05554) were used. $AlCl_3$ and 2-amino-4-chlorobenzonitrile were purchased from Aldrich Chemical (Milwuakee, WI). Analytical grade solvents were used for recrystallizations, whereas pure for synthesis solvents were used in the reactions and column chromatography. Elemental analyses were carried out at the Mycroanalysis Service of the Centro de Investigación y Desarrollo, C.I.D., Barcelona, Spain.

Synthesis of Huprine X and Huprine Y

The synthesis strategy for these compounds is outlined in Fig. 2.

***rac*-12-Amino-3-chloro-9-ethyl-6,7,10,11-tetrahydro-7,11-methanocycloocta[*b*]quinoline Hydrochloride (*rac*-3b.HCl).** To a suspension of anhydrous $AlCl_3$ (3.00 g, 22.5 mmol) and 2-amino-4-chlorobenzonitrile (2.33 g, 15.3 mmol) in 1,2-dichloroethane (20 ml), a solution of 7-ethylbicyclo[3.3.1]non-6-en-3-one *rac*-**1b** (1.80 g, 11.0 mmol) in 1,2-dichloroethane (115 ml) was added dropwise. The reaction mixture was stirred under reflux for 7 h, allowed to cool to room temperature, diluted with water (80 ml) and tetrahydrofuran (80 ml), made basic by addition of 5 N NaOH, and stirred at room temperature for 30 min. The organic solvents were removed under reduced pressure, and the residue was filtered. The yellowish solid residue (4.20 g) was submitted to column chromatography [silica gel (125 g), hexane/AcOEt, gradient elution]. On elution with hexane/AcOEt 40:60, *rac*-**3b** (1.35 g, 41% yield) was isolated. Subsequent treatment with a solution of HCl (0.37 N solution in MeOH, 3 equiv.), evaporation, and recrystallization of the resulting solid (1.54 g) from MeOH/H_2O 3:10 (26 ml), afforded pure *rac*-**3b**.HCl.2/3H_2O (0.96 g, 25% overall) as a white solid: mp 202–206°C (dec.); IR 3500–2000 (max. at 3333, 3177, 2816, 2671) (CH, NH, and NH^+), 1652, 1634, and 1585 (ar-C-C and ar-C-N) cm^{-1}. ^1H NMR (500 MHz, CD_3OD) δ: 0.89 (t, J = 7.5 Hz, 3 H, CH_2-CH_3), 1.86 (m, 2H, CH_2-CH_3), 1.95 (dm, J = 12.5 Hz, 1 H, 13-H_{syn}), 2.00 (broad d, J = 17.5 Hz, 1 H, 10-H_{endo}), 2.07 (dm, J = 12.5 Hz, 1 H, 13-H_{anti}), 2.53 (broad dd, J = 17.5 Hz, J' = 4.5 Hz, 1 H, 10-H_{exo}), 2.80 (m, 1 H, 7-H), 2.87 (broad d, J = 18.0 Hz, 1 H, 6-H_{endo}), 3.20 (dd, J = 18.0 Hz, J' = 5.5 Hz, 1 H, 6-H_{exo}), 3.38 (m, 1 H, 11-H), 4.82 (s, NH_2 + NH), 5.56 (broad d, J = 5.5 Hz, 1 H, 8-H), 7.56 (dd, J = 9.0 Hz, J' = 1.5 Hz, 1 H, 2-H), 7.75 (d, J = 1.5 Hz, 1 H, 4-H), 8.34 (d, J = 9.0 Hz, 1 H, 1-H). ^{13}C NMR (75.4 MHz, CD_3OD) δ: 12.6 (CH_3, CH_2-CH_3), 27.6 (CH, C11), 28.1 (CH, C7), 29.4 (CH_2, C13), 30.9 (CH_2, CH_2-CH_3), 34.2 (CH_2, C10), 36.1 (CH_2, C6), 115.4 (C) and 115.5 (C) (C11a and C12a), 119.4 (CH, C4), 123.3 (CH, C8), 126.3 (CH, C1), 127.6 (CH, C2), 139.7 (C, C4a), 140.4 (2 C, C3 and C9), 153.2 (C) and 156.6 (C) (C5a and C12). Anal. Calcd. for $C_{18}H_{19}ClN_2$.HCl.2/3H_2O: C, 62.25; H, 6.20; N, 8.07; Cl, 20.42. Found: C, 61.95; H, 6.12; N, 8.08; Cl, 20.44.

Preparative Resolution of *rac*-3b by Chiral MPLC: (+)-(7*R*,11*R*)-3b and (−)-(7*S*,11*S*)-3b (Huprine X). The chromatographic resolution of *rac*-**3b** was carried out with MPLC equipment provided with a column containing microcrystalline cellulose triacetate (15–25 μm), pretreated with a 0.1% solution of Et_3N in ethanol, as the chiral stationary phase. The sample of *rac*-**3b** (1.59 g) was introduced as free base in three portions (1 × 90 mg + 1 × 500 mg + 1 × 1000 mg) with 96% ethanol (2 ml/min) as the sole eluent and solvent. The chromatographic fractions (5 ml) were analyzed by chiral HPLC under conditions A [(−)-**3b**, r.t. 23.87 min, k'_1 = 0.523; (+)-**3b**, r.t. 27.15 min, k'_2 = 0.733; α = 1.40, Res. = 1.75] and combined conveniently. In this way, (−)-**3b** (650 mg, 98% e.e.) and (+)-**3b** (390 mg, 94% e.e.) were obtained. The remaining product consisted of mixtures of both enantiomers with lower e.e. values.

A solution of (−)-**3b** (650 mg) in MeOH (40 ml) was treated with 0.77 N HCl in Et_2O (15 ml). The organic solvents were removed under reduced pressure and the yellowish solid residue (673 mg) was recrystallized from AcOEt/MeOH 3:1 (20 ml) to afford (−)-**3b**.HCl.H_2O {310 mg, $[\alpha]_D^{20}$ = −280 (c = 1.00, MeOH), 99% e.e. by chiral HPLC on the liberated base}: mp 271–273°C (dec.); IR 3500–2500 (max. at 3332, 3171, 2961, 2929, 2818, 2688) (CH, NH, and NH^+), 1651, 1636, and 1587 (ar-C-C and ar-C-N) cm^{-1}. Anal. Calcd. for $C_{18}H_{19}ClN_2$.HCl.H_2O: C, 61.19; H, 6.28; N, 7.93. Found: C, 61.12; H, 6.16; N, 7.80. A pK_a of 8.9 ± 0.1 for (−)-**3b** was determined from relative UV absorbances in sodium phosphate and sodium carbonate buffers (20 mM) at reference wavelengths of 251 and 326 nm and isosbestic points at 256 and 317 nm, respectively.

Similarly, a solution of (+)-**3b** (390 mg) in MeOH (10 ml) was treated with 0.77 N HCl in Et_2O (10 ml). The organic solvents were removed under reduced pressure and the yellowish solid residue (410 mg) was recrystallized from AcOEt/MeOH 3:1 (10 ml) to afford (+)-**3b**.HCl.5/4H_2O {180 mg, $[\alpha]_D^{20}$ = +260 (c = 1.00, MeOH), 97% e.e. by chiral HPLC on the liberated base}: mp 289–291°C (dec.); IR 3500–2500 (max. at 3380, 3186, 2929, 2826, 2683) (CH, NH, and NH^+), 1651, 1635, and 1586 (ar-C-C and ar-C-N) cm^{-1}. Anal. Calcd. for $C_{18}H_{19}ClN_2$.HCl.5/4H_2O: C, 60.42; H, 6.34; N, 7.83. Found: C, 60.40; H, 6.15; N, 7.89.

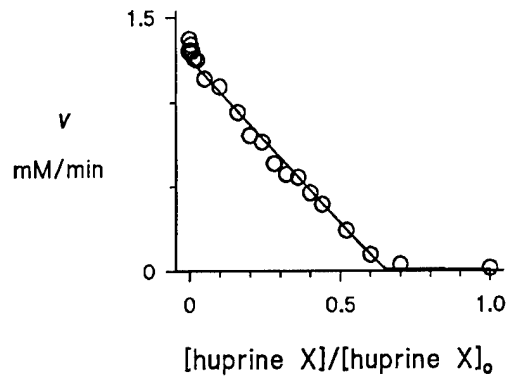

Fig. 3. Titration of recombinant human AChE with huprine X. Each point represents one mixture with a final concentration of 1.21 μM AChE and the indicated concentration of huprine X relative to the maximal concentration [huprine X]$_0$ incubated for 3 h at 23°C. Aliquots (10 μl) were then diluted 300- to 15,000-fold into assay solution containing 0.5 mM acetylthiocholine. Points represent observed v (mM/min) normalized to a 300-fold dilution into assay solution. The line was fitted to the points in a nonequilibrium analysis with the program SCoP, assuming that huprine X interacted with AChE according to Scheme 1 with rate constants $k_I = k_{AI}$ and $k_{-I} = k_{-AI}$ given in Fig. 5. The fitted value of [huprine X]$_0$ = 1.87 μM was used to determine an apparent extinction coefficient for huprine X.

Calibration of Huprine Concentrations by Titration with AChE

AChE active site concentrations can be estimated to an accuracy of better than 10% from the AChE activity assay described below, and stock concentrations of inhibitors can be determined by stoichiometric titration with the enzyme (Eastman et al., 1995; Mallender et al., 1999). Titration of AChE with huprine X gave a linear decrease in AChE activity with increasing concentrations of huprine X (Fig. 3), consistent with the formation of an inactive huprine X-AChE complex. However, the stock concentration of huprine X calculated by assuming 1:1 stoichiometry in this complex was about half of that calculated directly from the dry weight. Because there is no crystallographic or kinetic evidence that a high-affinity inhibitor binds with >1:1 stoichiometry to the AChE active site, we calculated an apparent extinction coefficient of 18 ± 1 mM^{-1} cm^{-1} for huprine X from the absorbance at 326 nm and the concentration determined by the titration in duplicate experiments. This extinction coefficient also was used to estimate concentrations of huprine Y.

Steady-State Inhibition of Enzyme-Catalyzed Substrate Hydrolysis

Inhibitor was preincubated with AChE or butyrylcholinesterase in buffer (20 mM sodium phosphate and 0.02% Triton X-100 at pH 7.0) for 30 min, except for 1 to 6 h preincubations of huprine X and Y with human AChE. Substrate hydrolysis rates v were measured at 25°C after addition of small aliquots of acetylthiocholine and DTNB (to a final concentration of 0.33 mM) in a total volume of 1.0–3.0 ml. Hydrolysis was monitored in an Ellman assay by formation of the thiolate dianion of 5,5′-dithiobis-(2-nitrobenzoic acid) (DTNB) at 412 nm ($\Delta\epsilon_{412\ nm}$ = 14.15 mM^{-1} cm^{-1}; Riddles et al., 1979) for 1 to 3 min on a Varian Cary 3A spectrophotometer (Ellman et al., 1961), and substrate concentrations were corrected for substrate depletion resulting from hydrolysis during this interval. It was assumed that acetylthiocholine concentrations were maintained at low enough values (<1.0 mM) to ignore substrate inhibition in the absence of inhibitors (Szegletes et al., 1999) and that inhibitors that bind exclusively to the acylation site in AChE are unable to form ternary complexes with substrate. These assumptions allow analysis of the inhibition data to be based on Scheme 1.

In Scheme 1, the initial enzyme-substrate complex ***ES*** can form an acyl enzyme intermediate ***EA*** with the rate constant k_2. The inhibitor (**I**) can bind to the free enzyme ***E*** or to ***EA*** with respective

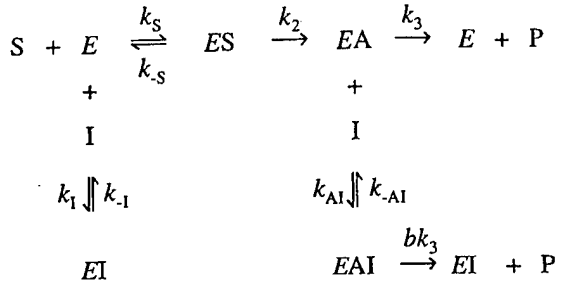

Scheme 1.

equilibrium constants K_I ($=k_{-I}/k_I$) and K_{AI} ($=k_{-AI}/k_{AI}$), and the deacylation rate constant k_3 is altered by a factor b in the ***EAI*** complex. According to Scheme 1, v is given by eq. 1.

$$v^{-1} = \frac{1}{V_{max}}\left[1 + \frac{[I]}{K_U} + \frac{K_{app}}{[S]}\left(1 + \frac{[I]}{K_I}\right)\right] \quad (1)$$

In this equation, V_{max} and K_{app} have been defined previously (Szegletes et al., 1998) and K_U is defined below. Consistent with eq. 1, reciprocal plots of v^{-1} versus $[S]^{-1}$ at all inhibitor (**I**) concentrations were linear with a slope of K_{app}/V_{max} in the absence of inhibitor. Slopes and intercepts of these plots were the respective reciprocals of the second- and first-order rate constants for substrate hydrolysis at a given concentration of **I** and were calculated by a weighted linear regression analysis (Fig. P, version 6.0; Biosoft, Milltown, NJ) that assumed that v has a constant percentage of error. The slopes were normalized by K_{app}/V_{max} as in eq. 2, and values of K_I were determined by linear regression analyses of these normalized slopes versus [I] according to eq. 2, with slope values weighted by the reciprocal of their variance (Eastman et al., 1995).

$$\frac{\text{slope}(v^{-1}\text{ vs }[S]^{-1})}{K_{app}/V_{max}} = \left(1 + \frac{[I]}{K_I}\right) \quad (2)$$

A similar analysis of the intercepts of the reciprocal plots gave K_U in eq. 1, where $K_U = k_3(K_R + b[I])/(k_{cat}(1 - b + (bk_3/k_{-I})))$, $K_R = (k_{-AI} + bk_3)/k_{AI}$, and $k_{cat} = k_2k_3/(k_2 + k_3)$ (Rosenberry, 1975). When the intercepts increase linearly with [I], K_U is a constant that corresponds to k_3K_{AI}/k_{cat} (when $bk_3 \ll k_{-AI}$) or to $k_3k_{-I}/k_{cat}k_{AI}$ (when $k_{-I} \ll bk_3$). For acetylthiocholine hydrolysis by human AChE, k_3 is ~10^4 s^{-1} and k_{cat} is about one-half of k_3 (Szegletes et al., 1999).

When an inhibitor (**I1**) specific to the acylation site is incubated with AChE together with varying concentrations of a second inhibitor (**I2**) specific for the AChE peripheral site, ternary complexes with both inhibitors bound simultaneously to the enzyme can occur (Taylor and Lappi, 1975; Szegletes et al., 1998). At equilibrium, the residual concentration of free enzyme [***E***] in the presence of both inhibitors relative to the concentration of free enzyme $[E]_{[I2]=0}$ when only **I1** is present is given by eq. 3.

$$\frac{[E]}{[E]_{[I2]=0}} = \frac{K_{I2}\left(1 + \frac{[I1]}{K_{I1}}\right)}{K_{I2}\left(1 + \frac{[I1]}{K_{I1}}\right) + [I2]\left(1 + \frac{[I1]}{K_{I12}}\right)} \quad (3)$$

In this equation, K_{I1} is the equilibrium dissociation constant for **I1** with ***E***, K_{I2} is the equilibrium dissociation constant for **I2** with ***E***, and K_{I12} is the equilibrium dissociation constant for **I1** with the ***EI2*** complex. The concentrations [***E***] and $[E]_{[I2]=0}$ are proportional to the second-order rate constants for substrate hydrolysis noted under eq. 1, and their ratio herein was estimated from the relative v for acetylthiocholine hydrolysis.

Slow Equilibration of an Inhibitor with AChE

Association rate constants were determined from the progressive inhibition of AChE with time as the inhibitor approached equilibrium binding (Eastman et al., 1995; Szegletes et al., 1998). Binding was initiated at 23°C in buffer, in most cases under pseudo first-order conditions in which the concentration of **I** in the incubation mixture was adjusted to at least four times the concentration of AChE. At various times t, a 1.0-ml aliquot was removed to a cuvette, and 40 μl of acetylthiocholine and DTNB was added to a final concentration of 0.5 and 0.33 mM, respectively. The initial hydrolysis rate v was immediately recorded at 412 nm, and the series of v at various t was fitted to eq. 4 by a weighted nonlinear regression analyses (Fig. P), which assumed that v has a constant percentage of error.

$$v = v_{\text{final}} + (v_{\text{initial}} - v_{\text{final}})e^{-kt} \quad (4)$$

In eq. 4, k is the observed pseudo first-order rate constant for the approach to equilibrium, and v_{initial} and v_{final} are the calculated values of v at time zero and at equilibrium, respectively. The dependence of k on [I] was analyzed by weighted linear regression analysis according to eq. 5, with k values weighted by the reciprocal of their variance.

$$k = k_1[\text{I}] + k_{-1} \quad (5)$$

Equation 5 assumes a simple bimolecular reaction of **I** with AChE, where k_1 is the association rate constant and k_{-1} is the dissociation rate constant (Eastman et al., 1995).

In some cases, hydrolysis rates v were fitted directly to a general steady-state solution of Scheme 1 with the program SCoP (version 3.51; Simulation Resources, Inc., Redlands CA) (Szegletes et al., 1998, 1999). This program solves rate equations numerically and allows fitting of v at times before inhibitor equilibrium.

AChE Peripheral Site Binding Affinity Determined by Fluorescence Titration

Binding of propidium to the AChE peripheral site was monitored by enhancement of the propidium fluorescence on a Perkin-Elmer LS-50B luminescence spectrometer in 1 mM sodium phosphate buffer and 0.02% Triton X-100 at 23°C (Taylor and Lappi, 1975). Measurements were performed in a low ionic strength buffer to increase the affinity of propidium (Taylor and Lappi, 1975). Propidium fluorescence was monitored with excitation at 500 nm and emission from 590 to 630 nm. Fluorescence contributions from scatter in the buffer and enzyme were subtracted. Total areas under the fluorescence emission curves (f) were fitted by nonlinear regression analysis (Fig. P) to eq. 6.

$$\text{F} = f_a\text{L}_{\text{tot}} + 0.5(f_b - f_a)[\text{D} - \sqrt{\text{D}^2 - 4E_{\text{tot}}\text{L}_{\text{tot}}}] \quad (6)$$

In eq. 6, f_a is the fluorescence intensity coefficient for free propidium, f_b is the fluorescence intensity coefficient for bound propidium, E_{tot} is the total enzyme concentration, L_{tot} is the total propidium concentration, K_D is the equilibrium dissociation constant, and $\text{D} = E_{\text{tot}} + \text{L}_{\text{tot}} + K_D$. Estimates of K_D are obtained with greatest accuracy from eq. 6 when $\text{L}_{\text{tot}} < K_D$. Data were fitted to eq. 6 with the calculated E_{tot} as the independent variable and L_{tot} at a fixed propidium concentration (0.2 and 2 μM for the binding to AChE and the huprine X-AChE complex, respectively) to give f_a, f_b, and K_D.

Molecular Modeling of Ternary Complex of AChE with Huprine X and Propidium

Construction and analyses of three-dimensional models were performed on a Silicon Graphics workstation Indigo2 IMPACT with QUANTA98 (Molecular Simulations, Inc., Waltham, MA). Modeling of the ternary complex of *Torpedo californica* AChE (TcAChE) with propidium and huprine X began with the crystal structure coordinates for the TcAChE-tacrine complex (Protein Data Bank file: 1ACJ) (Harel et al., 1993). Propidium was manually docked into the peripheral site with the same procedure as described previously (Barak et al., 1994; Szegletes et al., 1998). Huprine X was built from atomic coordinates of 9-methyl huprine (provided by Dr. Javier Luque, Departament de Fisicoquímica, Universitat de Barcelona) and manually docked into the acylation site to maximize the molecular overlap with the aminoquinoline portion of tacrine (Fig. 1). The resulting structure was optimized by energy minimization with CHARMm module of QUANTA98 (conjugate gradient) starting with refinement of the propidium, huprine X and gorge solvent molecules. Subsequent molecular optimization added all amino acid side residues in proximity to the propidium and huprine X ligands.

Results and Discussion

Comparison of Inhibition Constants for Various Inhibitors with AChE. Scheme 1 provides a framework for the analysis of inhibitors that bind to the acylation site of AChE. Steady-state inhibition data for huprine X and two other inhibitors in Fig. 1 is shown in Fig. 4. The reciprocal plots for all three inhibitors (Fig. 4, A–C) show both increasing slopes and increasing intercepts with higher inhibitor concentration. This pattern is often termed "mixed inhibition," and in Scheme 1, it is consistent with significant inhibitor interaction with both the free enzyme E and the acetyl enzyme EA. Replots of the normalized slopes versus the inhibitor concentrations (Fig. 4, D and F) gave estimates of K_I, the dissociation constant for inhibitor binding to E, as reported in Table 1. The K_I of 26 pM for huprine X indicates that it is one of the highest affinity reversible inhibitors for AChE yet reported. The peptide neurotoxin fasciculin, with a K_I for human AChE of ~10 pM under these buffer conditions (Eastman et al., 1995), has a slightly higher affinity. This K_I for huprine X was comparable with that for the bisquaternary inhibitor ambenonium (Hodge et al., 1992) and the transition state analog *m*-(*N,N,N*-trimethylammonio)trifluoroacetophenone (TMTFA) (Szegletes et al., 1998).[3] As shown in Table 1, the affinity of huprine X was 180 times higher than that of huperzine A and 1200 times higher than that of tacrine, the two well known inhibitors of AChE upon which the hybrid structure of huprine X was based. Furthermore, the huprine X affinity was 40 times higher than that of E2020. Huprine Y, the analog of huprine X in which a methyl group replaces the ethyl group at position 9, gave a K_I similar to that of huprine X (Table 1). The high affinity of huprine X also was very selective for vertebrate AChE relative to other cholinesterases. K_I values for the inhibition of human butyrylcholinesterase and *Drosophila* AChE were 120 ± 12 and 55 ± 10 nM, respectively, more than three orders of magnitude higher than that for human AChE.

The reciprocal plots in Fig. 4A show that intercepts as well as slopes were increased in the presence of huprine X. According to eq. 1, an increase in intercepts occurs when the inhibitor can bind to the acetyl enzyme EA and cause the parameter K_U to become significant. It is less straightforward to interpret K_U in the context of Scheme 1 than K_I, but K_U for huprine X with acetylthiocholine as substrate appears approximately equal to k_{-I}/k_{AI}, a ratio similar to the equilib-

[3] The K_I determined for TMTFA (50 pM; Szegletes *et al.*, 1998) was based on the total concentration of TMTFA and its hydrate in solution. Because the hydrate is not an AChE inhibitor but is present in 10^5-fold excess over TMTFA (Nair *et al.*, 1993), the intrinsic equilibrium dissociation constant K_D for TMTFA itself with AChE is about 10^{-15} M.

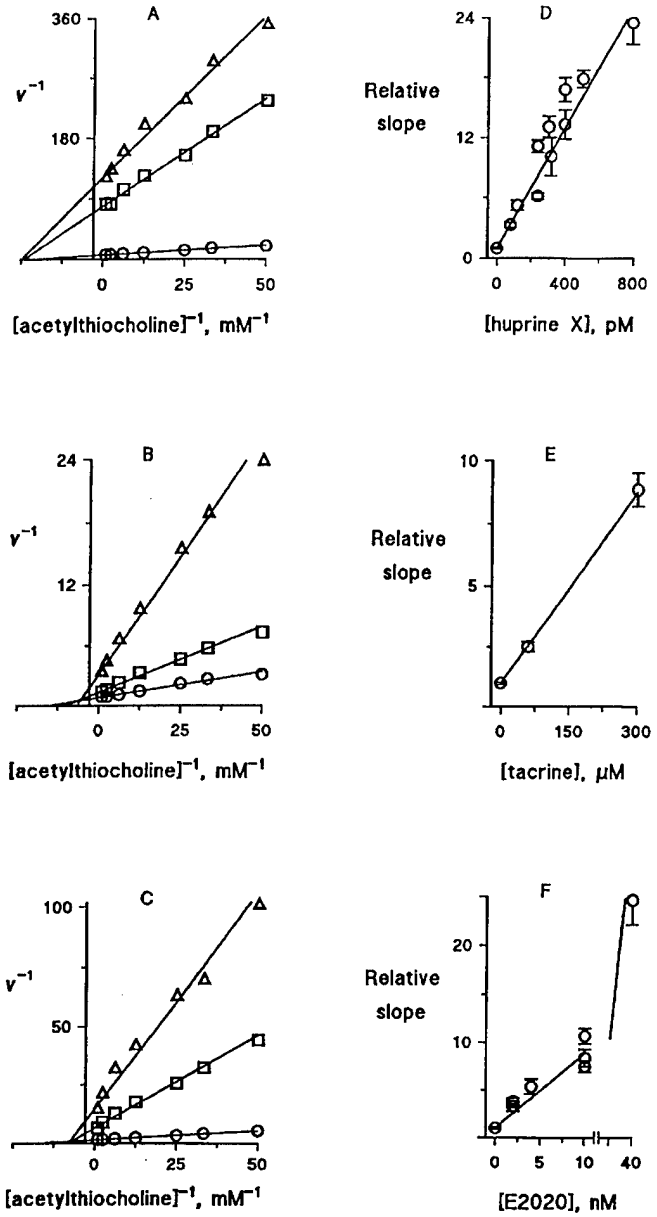

Fig. 4. Steady-state inhibition of AChE hydrolysis of acetylthiocholine. A–C, reciprocal plots of initial velocities ($\Delta A_{412\ nm}$/min) and substrate concentrations were analyzed according to eq. 1. Huprine X concentrations in *A* were 0 (○), 240 (□), and 400 pM (△). Tacrine concentrations in *B* were 0 (○), 60 (□), and 300 nM (△). E2020 concentrations in C were 0 (○), 10 (□), and 40 nM (△). D–F, slopes of plots in A–C were normalized by dividing by the slope in the absence of inhibitor and plotted against the inhibitor concentration according to eq. 2 to derive K_I values (Table 1). Additional points from data not shown in A and C were included in D and F, respectively.

rium constants for the binding of huprine X to *E* and *EA*. This interpretation is based on three conditions outlined in *Experimental Procedures*: The intercepts in Fig. 4A increased linearly with [huprine X] (data not shown); the dissociation rate constant k_{-I} for huprine X was several orders of magnitude smaller than the deacylation rate constant k_3 (see the next section); and k_3 and k_{cat} have similar values (Szegletes et al., 1998). Values of K_U also were obtained for tacrine and E2020 (Table 1), and these values were roughly three times the corresponding K_I values, as has been observed previously for

TABLE 1
Inhibition constants for several inhibitors of AChE.[a]

Inhibitor	K_I	K_U	k_I
	nM	*nM*	$\mu M^{-1}\ min^{-1}$
Tacrine	31 ± 3	104 ± 12	ND
E2020	1.1 ± 0.1	3.6 ± 0.4	ND
Huperzine A	4.6 ± 0.7[b]	ND	5.0 ± 0.2[b]
Huprine X	0.026 ± 0.002	0.024 ± 0.001	440 ± 30
Huprine Y	0.033 ± 0.003	0.038 ± 0.003	400

ND, not determined.
[a] Values of K_I, K_U, and k_I were obtained as outlined in *Experimental Procedures*.
[b] From reference Szegletes et al. (1998) under identical buffer conditions.

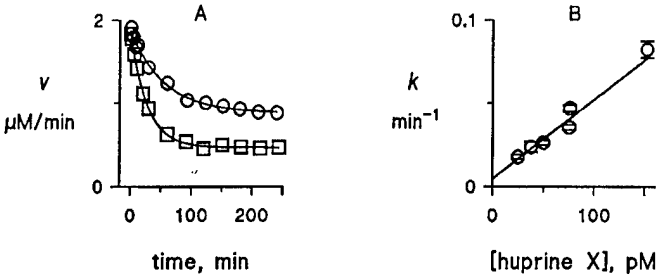

Fig. 5. Association and dissociation rate constants for huprine X and AChE. A, progressive inhibition of AChE (6 pM) with time as huprine X binding approached equilibrium was measured by removing 1-ml aliquots of the reaction mixture and immediately adding DTNB and the substrate acetylthiocholine for assay as outlined in *Experimental Procedures*. Hydrolysis rates v obtained with 25 (○) and 75 (□) pM huprine X were fitted to eq. 4 to obtain a value of k for each curve. B, values of k obtained at several concentrations of huprine X as in A were plotted against [huprine X]. Although the plot was nearly linear, the concentration of huprine X in some cases was not sufficiently in excess of the concentration of AChE to justify analysis with eq. 5. The SCoP fitting program was applied directly to all the association rate data (Szegletes et al., 1998) to obtain k_I = 440 ± 30 $\mu M^{-1}min^{-1}$ and k_{-I} = 0.009 ± 0.003 min^{-1}.

other AChE inhibitors (Rosenberry and Bernhard, 1972). The fact that K_U is comparable with K_I for huprine X and huprine Y arises from the high affinities of these compounds and their consequent slow reequilibration when substrate is added to the assay mixtures. Analysis of v versus time with the program SCoP demonstrated that K_I decreased ~20% and K_U increased by nearly a factor of 2 when v was adjusted for inhibitor equilibration.

Determination of Association and Dissociation Rate Constants for Huprine X and AChE. AChE inhibitors with K_I values in the subnanomolar range often have very low dissociation rate constants that permit measurement of the kinetics of inhibitor association. This was the case with huprine X and huprine Y, as demonstrated in Fig. 5 and Table 1. Rate constants for the approach to equilibrium binding at a fixed concentration of huprine X were estimated as in Fig. 5A, and from the time course of these reactions values of $k_I = 4.4 \pm 0.3 \times 10^8\ M^{-1}min^{-1}$ and $k_{-I} = 0.009 \pm 0.003\ min^{-1}$ were obtained (Fig. 5B). The value of k_I we previously reported for huperzine A in the same buffer (Szegletes et al., 1998) is also shown in Table 1, and this value is only ~1% of the k_I value for either huprine X or huprine Y. In fact, the difference in k_I accounts for almost all of the difference in K_I between huperzine A and the two hybrid compounds, as the k_{-I} values were nearly comparable. However, the k_I value reported herein for huprine X still remained <20% of that previously reported for the bisquaternary AChE inhibitor ambenonium (Hodge et al., 1992) and <1% of that for the

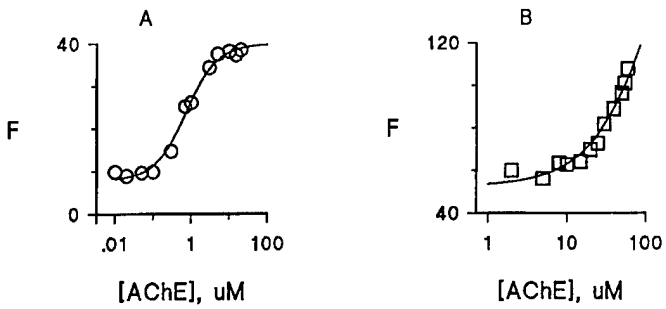

Fig. 6. Fluorescence titration of recombinant human AChE with propidium in the absence (A) and presence (B) of huprine X. A total of three fluorescence spectra was collected and averaged for each AChE titration point as outlined in *Experimental Procedures*, and total areas under the fluorescence emission curves (F) were plotted against the final AChE concentration in the assay sample. A, propidium was added to a total concentration of 0.2 μM to AChE and then successively diluted with a solution of 0.2 μM propidium. The data were fitted to eq. 6 to give f_a = 39 ± 4, f_b = 200 ± 4, and K_D = 0.63 ± 0.10 μM. B, because of the shift in the binding curve for propidium in the presence of huprine X, propidium was added to a higher total concentration of 2 μM to AChE preincubated with 100 μM huprine X and then successively diluted with a solution of 2 μM propidium and 100 μM huprine X. In the presence of huprine X, a plateau in the fluorescence enhancement indicating propidium saturation in the ternary complex was not obtained. However, if the same degree of fluorescence enhancement was assumed for propidium in the ternary complex as in the propidium-AChE binary complex (f_b/f_a = 5.1), the data fitted to eq. 6 gave f_a = 26 ± 1 and K_D = 190 ± 25 μM. This assumption is not necessarily valid, because some disruption of the propidium environment occurs in the presence of huprine X (Fig. 8).

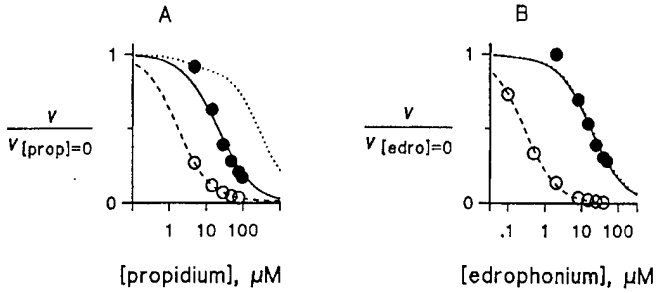

Fig. 7. Determination of the relative affinity of huprine X in the propidium-AChE complex (A) or the edrophonium-AChE complex (B) by inhibition of substrate hydrolysis. AChE (○, 25 pM; ●, 1200 pM) was incubated without (○) or with (●) huprine X (4 nM) and the indicated concentration of propidium or edrophonium for 6 h at 23°C, and a 2.9-ml aliquot was mixed with 100 μl of DTNB and 12 μl of acetylthiocholine to give final concentrations of 0.33 mM DTNB and 20 μM acetylthiocholine. Points represent v observed over a 2- to 5-min interval normalized by the corresponding v obtained at the same [huprine X] in the absence of propidium ($v_{[prop]=0}$) or edrophonium ($v_{[edro]=0}$). Lines correspond to normalized v obtained by fitting the experimental data to a complete nonequilibrium reaction scheme with the program SCoP, with kinetic rate constants previously determined for acetylthiocholine and propidium or edrophonium (Eastman et al., 1995; Szegletes et al., 1999) and those in Table 1 for huprine X. The dashed lines correspond to the absence of huprine X and the solid lines, to 4 nM huprine X. The dotted lines correspond to the curves calculated when no ternary complex forms ($1/K_{I12}$ = 0). Based on data with 4 nM huprine X as well as with 1 and 2 nM huprine X (data not shown) with both propidium and edrophonium, the procedure in A gave K_{I2} = 1.4 μM for propidium, K_{I1} = 20 pM for huprine X, and K_{I12}/K_{I1} = 17 ± 3. The procedure in B gave K_{I2} = 0.2 μM for edrophonium, K_{I1} = 29 pM for huprine X, and K_{I12}/K_{I1} > 1000. Lines also were fitted with the much simpler analysis scheme in eq. 3, which required the approximations that v reflects the true second-order rate constant, that the free huprine X concentration remains unchanged through the entire range of propidium or edrophonium concentrations, and that no slow reequilibration occurs in the presence of substrate. Although these approximations held only approximately at best, ratios of K_{I12}/K_{I1} of 12 ± 2 with propidium and >200 with edrophonium were in reasonable agreement with those from the SCoP program.

monoquaternary inhibitor *N*-methylacridinium (Rosenberry et al., 1996). We measured a pK_a of 8.9 for huprine X, indicating that the ring N should be largely protonated at pH 7, so huprine X should be cationic. Thus, the lower k_I for huprine X relative to ambenonium or *N*-methylacridinium appears to indicate some remaining steric or conformational restraints on its rapid association with the AChE active site.

Huprine X Binds to Acylation Site but Slightly Interferes with Binding of Propidium to Peripheral Site. Because crystal structures of AChE show that both tacrine and huperzine A bind to the acylation site (Harel et al., 1993; Raves et al., 1997), we anticipated that huprine X also would bind to the acylation site. To explore this point, we used propidium, a ligand specific for the AChE peripheral site (Taylor and Lappi, 1975). If huprine X binding is confined to the acylation site, a ternary complex of AChE with huprine X and propidium should be able to form. In principle, such a complex can be detected by equilibrium titration or by kinetic analyses. For example, kinetic studies have shown that propidium and huperzine A form a ternary complex with AChE (Szegletes et al., 1998).

We first examined the formation of an equilibrium ternary complex by direct fluorometric measurement of propidium binding to the AChE-huprine X complex. The binding of propidium to the AChE peripheral site results in significant enhancement of propidium fluorescence, a property that has been used to determine the binding affinity of this ligand for the peripheral site (Taylor and Lappi, 1975). Figure 6 illustrates the results of a titration experiment where AChE concentrations were varied in the presence of fixed concentrations of propidium alone or propidium plus huprine X. The 100 μM of huprine X used in this experiment was more than six orders of magnitude higher than the K_I for this compound reported above, ensuring that any detectable propidium binding would have to involve formation of a ternary complex. In the absence of huprine X, the fluorescence of bound propidium was enhanced ~5-fold relative to free ligand (Fig. 6A). A K_D value of 0.63 ± 0.10 μM was obtained, in reasonable agreement with propidium inhibition constants of 0.4 to 1.1 μM obtained previously at a somewhat higher ionic strength (Szegletes et al., 1998). When AChE was saturated with huprine X during the titration, the propidium binding curve was shifted (Fig. 6B). A qualitative increase in propidium fluorescence at higher AChE concentrations was apparent, but values of K_D as well as of the fluorescence intensity coefficient f_b for propidium with huprine X-bound AChE were uncertain. If the fluorescence enhancement for propidium bound to the huprine X-AChE complex was assumed to be the same as that for propidium bound to free AChE, the affinities of propidium and huprine X in the ternary complex decreased about two orders of magnitude relative to those with the free enzyme.

An alternative procedure for measuring the formation of ternary complexes of AChE with huprine X and propidium is to examine the steady-state inhibition of the enzyme in the presence of both inhibitors as illustrated in Fig. 7A. The concentration of huprine X was fixed, and the change in the enzyme activity v as propidium was added to the mixture was analyzed by two methods. One method assumed that the concentration of free AChE [*E*] was given by eq. 3 and was proportional to the substrate hydrolysis rate v at the low

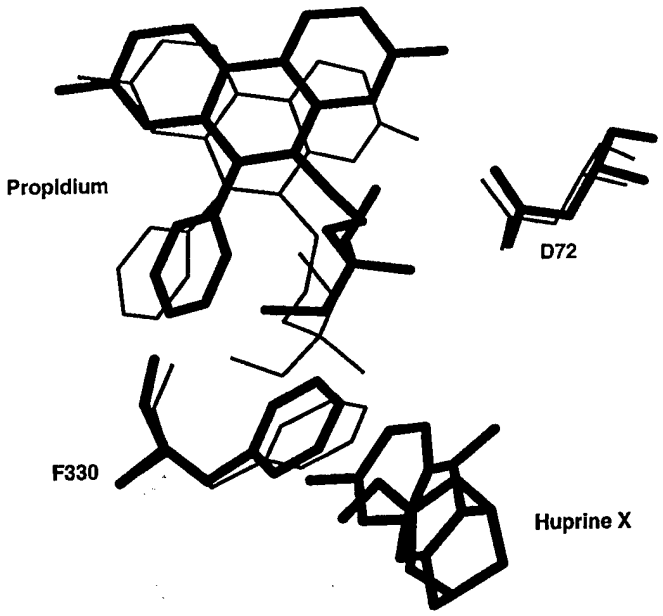

Fig. 8. Molecular modeling of the ternary complex of AChE with huprine X and propidium (see *Experimental Procedures*). AChE ligands and amino acids in the vicinity of the ligands are displayed with all other residues, solvent molecules and water omitted. The thin line indicates the orientations of propidium and amino acids in the propidium-TcAChE complex. The thick line indicates the effect of huprine X in the acylation site on the orientation of propidium, F330, and D72.

substrate concentration (20 μM) used in the assay. The other method avoided these assumptions by fitting v directly in the general steady-state solution with the program SCoP. As indicated in the legend to Fig. 7, the two methods gave reasonable agreement. When huprine X was omitted, increasing concentrations of propidium resulted in the decrease in v indicated by the dashed line and the open symbols in Fig. 7A. If no ternary complex could form, huprine X and propidium would be completely competitive and the decrease in v would correspond to the dotted line in Fig. 7A. Complete competition of huprine X is observed with edrophonium (Fig. 7B), a known acylation site inhibitor (Harel et al., 1993). However, the data for huprine X and propidium fall between the dashed and the dotted lines as indicated by the closed symbols in Fig. 7A, indicating that the ternary complex can form. Fitting this observed data gave an estimate of $K_{I12}/K_{I1} = 17 \pm 3$, indicating that the affinity of huprine X for free AChE was ~17-fold higher than its affinity for the propidium-AChE complex and providing a more accurate measure of the relative affinity than the fluorescence titration above.

Molecular modeling of the ternary complexes of either huperzine A or TMTFA with propidium-TcAChE revealed that the bound propidium does not make close contact with either of these two acylation site inhibitors (Szegletes et al., 1998). In fact, only minimal molecular adjustments were necessary for the propidium molecule to dock into the TcAChE peripheral site in the presence or absence of huperzine A or TMTFA, suggesting little or no interaction between the bound ligands. This was consistent with thermodynamic data showing a reduction of only 5- to 7-fold in the affinity of these ligands in the ternary complex relative to their affinity for free AChE. Most of this reduction could well represent an unfavorable electrostatic interaction between ligands in the ternary complex (Szegletes et al., 1998). Similar modeling of the ternary complex of TcAChE with huprine X and propidium indicated a more unfavorable interaction between the ligands (Fig. 8). Huprine X manually docked within the TcAChE acylation site occupied the position of the aminoquinoline portion of tacrine as observed in the tacrine-TcAChE crystal structure (Harel et al., 1993). This orientation resulted in a high degree of overlap of the carbobicyclic ring portion of huprine X with the position of huperzine A as indicated in the huperzine A-TcAChE crystal structure (Raves et al., 1997). In contrast to the binding of either TMTFA or huperzine A alone, however, insertion of huprine X between F330 and W84 in the acylation site resulted in movement of the F330 side chain away from W84 and up into the gorge toward D72 (Fig. 8). This movement was accompanied by a significant rotation of the phenyl ring of the F330 side chain. As a result of this rearrangement, propidium could not be fit as deeply in the TcAChE peripheral site when huprine X was bound, and portions of the propidium structure were displaced out toward bulk solvent by almost 2Å. Molecular modeling thus supports the experimental data and indicates that although a ternary complex of propidium and huprine X can form with AChE, the binding geometry and added molecular volume of huprine X will result in significant decreases in the affinities of the ligands in the ternary complex.

Other energy minimization analyses of docked huprine-TcAChE complexes result in a very similar huprine X orientation in the AChE active site (Camps et al., 1999). More extensive molecular dynamics calculations also support this orientation (Camps et al., 1999; Barril et al., 1999). Of particular interest are molecular dynamics simulations of the binding of 3-fluoro-9-methyl huprine to TcAChE, which show that the fluorine atom fills a hydrophobic pocket formed by L333, M436, I439, and W432 (Barril et al., 1999). Ligand interactions with this pocket have not been reported previously, and they may account for increases in huprine affinity for AChE of about one order of magnitude in the 3-fluoro and two to three orders of magnitude in the 3-chloro derivatives relative to unsubstituted 9-methyl or 9-ethyl huprines (Camps et al., 1999; present article).

Huprine X May Be Useful in the Treatment of Alzheimer's Disease. The selectivity of an inhibitor of AChE in treating patients with Alzheimer's disease appears to parallel the affinity of the inhibitor for the AChE active site. Thus, E2020, with an affinity some 30 times higher than that of tacrine, is administered at a daily dose of only one-tenth that of tacrine.[4] The lower dosage regimen results in fewer undesirable side effects with E2020 than with tacrine. If this trend is extended by huprine X, which has an AChE affinity yet 40 times higher than that of E2020, huprine X may prove to be an even more attractive drug for the treatment of Alzheimer's disease. Such optimization of the AChE inhibitor of therapeutic choice may provide the most effective treatment until other classes of drugs become available that target the basic cause of Alzheimer's disease.

Acknowledgments

We thank Dr. Javier Luque of the Department de Fisicoquímica, Universitat de Barcelona, for providing atomic coordinates of 9-methyl huprine overlaid on the configuration of AChE-bound ta-

[4] See the Physicians' Desk Reference (1999), Medical Economics Co., Montvale, New Jersey.

crine as well as of a final structure obtained from molecular dynamic simulations of the complex of huprine X with TcAChE.

References

Badia A, Baños JE, Camps P, Contreras J, Görbig DM, Muñoz-Torrero D, Simón M and Vivas NM (1998) Synthesis and evaluation of tacrine-huperzine A hybrids as acetylcholinesterase inhibitors of potential interest for the treatment of Alzheimer's disease. *Bioorg Med Chem* **6**:427–440.

Barak D, Kronman C, Ordentlich A, Ariel N, Bromberg A, Marcus D, Lazar A, Velan B and Shafferman A (1994) Acetylcholinesterase peripheral anionic site degeneracy conferred by amino acid arrays sharing a common core. *J Biol Chem* **269**:6296–6305.

Barril X, Orozco M and Luque FJ (1999) Predicting relative binding free energies of tacrine-huperzine A hybrids as inhibitors of acetylcholinesterase. *J Med Chem* **42**:5110–5119.

Bartus R, Dean R, Beer B and Lippa A (1982) The cholinergic hypothesis of geriatric memory dysfunction. *Science (Wash DC)* **217**:408–417.

Bourne Y, Taylor P and Marchot P (1995) Acetylcholinesterase inhibition by fasciculin: Crystal structure of the complex. *Cell* **83**:503–512.

Bowen DM, Benton JS, Spillane JA, Smith CC and Allen SJ (1982) Choline acetyltransferase activity and histopathology of frontal neocortex from biopsies of demented patients. *J Neurol Sci* **57**:191–202.

Camps P, Contreras J, Font-Bardia M, Morral J, Muñoz-Torrero D and Solans X (1998) Enantioselective synthesis of tacrine-huperzine A hybrids. Preparative chiral MPLC separation of their racemic mixtures and absolute configuration assignments by X-ray diffraction analysis. *Tetrahedron: Asymmetry* **9**:835–849.

Camps P, El Achab R, Font-Bardia M, Görbig D, Morral J, Muñoz-Torrero D, Solans X and Simon M (1996) Easy synthesis of 7-alkylbicyclo[3.3.1]non-6-en-3-ones by silica gel-promoted fragmentation of 3-alkyl-2-oxaadamant-1-yl mesylates. *Tetrahedron* **52**:5867–5880.

Camps P, El Achab R, Görbig DM, Morral J, Muñoz-Torrero D, Badia A, Baños JE, Vivas NM, Barril X, Orozco M and Luque FJ (1999) Synthesis, in vitro pharmacology, and molecular modeling of very potent tacrine-huperzine A hybrids as acetylcholinesterase inhibitors of potential interest for the treatment of Alzheimer's disease. *J Med Chem* **42**:3227–3242.

Davies P and Maloney AJF (1976) Selective loss of central cholinergic neurons in Alzheimer's disease. *Lancet* **2**:1403.

Eastman J, Wilson EJ, Cervenansky C and Rosenberry TL (1995) Fasciculin 2 binds to a peripheral site on acetylcholinesterase and inhibits substrate hydrolysis by slowing a step involving proton transfer during enzyme acylation. *J Biol Chem* **270**:19694–19701.

Ellman GL, Courtney KD, Andres JV and Featherstone RM (1961) A new and rapid colorimetric determination of acetylcholinesterase activity. *Biochem Pharmacol* **7**:88–95.

Harel M, Kleywegt GJ, Ravelli RBG, Silman I and Sussman JL (1995) Crystal structure of an acetylcholinesterase-fasciculin complex: Interaction of a three-fingered toxin from snake venom with its target. *Structure* **3**:1355–1366.

Harel M, Schalk I, Ehret-Sabatier L, Bouet F, Goeldner M, Hirth C, Axelsen PH, Silman I and Sussman JL (1993) Quaternary ligand binding to aromatic residues in the active-site gorge of acetylcholinesterase. *Proc Natl Acad Sci USA* **90**:9031–9035.

Hodge AS, Humphrey DR and Rosenberry TL (1992) Ambenonium is a rapidly reversible noncovalent inhibitor of acetylcholinesterase with one of the highest known affinities. *Mol Pharmacol* **41**:937–942.

Incardona JP and Rosenberry TL (1996) Construction and characterization of secreted and chimeric transmembrane forms of *Drosophila* acetylcholinesterase: A large truncation of the C-terminal signal peptide does not eliminate glycoinositol phospholipid anchoring. *Mol Biol Cell* **7**:595–611.

Kozikowski AP, Thiels E, Tang X-C and Hanin I (1992) Huperzine A—A possible lead structure in the treatment of Alzheimer's disease. *Adv Med Chem* **1**:175–205.

Lockridge O (1990) Genetic variants of human serum cholinesterase influence metabolism of the muscle relaxant succinylcholine. *Pharmacol Ther* **47**:35–60.

Mallender WD, Szegletes T and Rosenberry TL (1999) Organophosphorylation of acetylcholinesterase in the presence of peripheral site ligands: Distinct effects of propidium and fasciculin. *J Biol Chem* **274**:8491–8499.

Muramoto O, Sugishita M, Sugita H and Toyokura Y (1979) Effect of physostigmine on constructional and memory tasks in Alzheimer's disease. *Arch Neurol* **36**:501–503.

Nair HK, Lee K and Quinn DM (1993) *m*-(*N,N, N*-Trimethylammonio)trifluoroacetophenone: A femtomolar inhibitor of acetylcholinesterase. *J Am Chem Soc* **115**:9939–9941.

Pang Y-P, Quiram P, Jelacic T, Hong F and Brimijoin S (1996) Highly potent selective and low cost bis-tetrahydroaminacrine inhibitors of acetylcholinesterase. *J Biol Chem* **271**:23646–23649.

Perry EK, Perry TH, Blessed G and Tomlinson BE (1977) Necropsy evidence of central cholinergic deficits in senile dementia. *Lancet* **1**:189.

Raves ML, Harel M, Pang Y-P, Silman I, Kozikowski AP and Sussman JL (1997) Structure of acetylcholinesterase complexed with the nootropic alkaloid (−)-huperzine A. *Nat Struct Biol* **4**:57–63.

Riddles PW, Blakeley RL and Zerner B (1979) Ellman's reagent: 5, 5′-dithiobis-(2-nitrobenzoic) acid—A reexamination. *Anal Biochem* **94**:75–81.

Roberts WL, Kim BH and Rosenberry TL (1987) Differences in the glycolipid membrane anchors of bovine and human erythrocyte acetylcholinesterases. *Proc Natl Acad Sci USA* **84**:7817–7821.

Rosenberry TL (1975) Acetylcholinesterase, in *Advances in Enzymology 43* (Meister A ed) pp 103–218, John Wiley & Sons, New York.

Rosenberry TL and Bernhard SA (1972) Studies on catalysis by acetylcholinesterase: Synergistic effects of inhibitors during hydrolysis of acetic acid esters. *Biochemistry* **11**:4308–4321.

Rosenberry TL, Rabl CR and Neumann E (1996) Binding of the neurotoxin fasciculin 2 to the acetylcholinesterase peripheral site drastically reduces the association and dissociation rate constants for *N*-methylacridinium binding to the active site. *Biochemistry* **35**:685–690.

Rosenberry TL and Scoggin DM (1984) Structure of human erythrocyte acetylcholinesterase. Characterization of intersubunit disulfide bonding and detergent interaction. *J Biol Chem* **259**:5643–5652.

Sussman JL, Harel M, Frolow F, Oefner C, Goldman A, Toker L and Silman I (1991) Atomic structure of acetylcholinesterase from *Torpedo californica*: A prototypic acetylcholine-binding protein. *Science (Wash DC)* **253**:872–879.

Szegletes T, Mallender WD and Rosenberry TL (1998) Nonequilibrium analysis alters the mechanistic interpretation of inhibition of acetylcholinesterase by peripheral site ligands. *Biochemistry* **37**:4206–4216.

Szegletes T, Mallender WD, Thomas PJ and Rosenberry TL (1999) Substrate binding to the peripheral site of acetylcholinesterase initiates enzymatic catalysis. Substrate inhibition arises as a secondary effect. *Biochemistry* **38**:122–133.

Taylor P and Lappi S (1975) Interaction of fluorescence probes with acetylcholinesterase: The site and specificity of propidium binding. *Biochemistry* **14**:1989–1997.

Whitehouse PJ, Price DL, Clark AW, Coyle JT and DeLong MR (1981) Alzheimer disease: Evidence for selective loss of cholinergic neurons in the nucleus basalis. *Ann Neurol* **10**:122–126.

Send reprint requests to: Terrone L. Rosenberry, Department of Pharmacology, Mayo Clinic Jacksonville, 4500 San Pablo Rd., Jacksonville, FL 32224. E-mail: rosenb@mayo.edu

Biochemistry **2000,** *39,* 7753−7763

Acetylthiocholine Binds to Asp74 at the Peripheral Site of Human Acetylcholinesterase as the First Step in the Catalytic Pathway†

William D. Mallender, Tivadar Szegletes, and Terrone L. Rosenberry*

Department of Pharmacology, Mayo Foundation for Medical Education and Research, and Department of Research, Mayo Clinic Jacksonville, Jacksonville, Florida 32224

Received February 1, 2000; Revised Manuscript Received April 10, 2000

ABSTRACT: Studies of ligand binding to acetylcholinesterase (AChE) have demonstrated two sites of interaction. An acyl−enzyme intermediate is formed at the acylation site, and catalytic activity can be inhibited by ligand binding to a peripheral site. The three-dimensional structures of AChE−ligand complexes reveal a narrow and deep active site gorge and indicate that ligands specific for the acylation site at the base of the gorge must first traverse the peripheral site near the gorge entrance. In recent studies attempting to clarify the role of the peripheral site in the catalytic pathway for AChE, we showed that ligands which bind specifically to the peripheral site can slow the rates at which other ligands enter and exit the acylation site, a feature we called steric blockade [Szegletes, T., Mallender, W. D., and Rosenberry, T. L. (1998) *Biochemistry 37*, 4206−4216]. We also demonstrated that cationic substrates can form a low-affinity complex at the peripheral site that accelerates catalytic hydrolysis at low substrate concentrations but results in substrate inhibition at high concentrations because of steric blockade of product release [Szegletes, T., Mallender, W. D., Thomas, P. J., and Rosenberry, T. L. (1999) *Biochemistry 38*, 122−133]. In this report, we demonstrate that a key residue in the human AChE peripheral site with which the substrate acetylthiocholine interacts is D74. We extend our kinetic model to evaluate the substrate affinity for the peripheral site, indicated by the equilibrium dissociation constant K_S, from the dependence of the substrate hydrolysis rate on substrate concentration. For human AChE, a K_S of 1.9 ± 0.7 mM obtained by fitting this substrate inhibition curve agreed with a K_S of 1.3 ± 1.0 mM measured directly from acetylthiocholine inhibition of the binding of the neurotoxin fasciculin to the peripheral site. For *Torpedo* AChE, a K_S of 0.5 ± 0.2 mM obtained from substrate inhibition agreed with a K_S of 0.4 ± 0.2 mM measured with fasciculin. Introduction of the D72G mutation (corresponding to D74G in human AChE) increased the K_S to 4−10 mM in the *Torpedo* enzyme and to about 33 mM in the human enzyme. While the turnover number k_{cat} was unchanged in the human D74G mutant, the roughly 20-fold decrease in acetylthiocholine affinity for the peripheral site in D74G resulted in a corresponding decrease in k_{cat}/K_{app}, the second-order hydrolysis rate constant, in the mutant. In addition, we show that D74 is important in conveying to the acylation site an inhibitory conformational effect induced by the binding of fasciculin to the peripheral site. This inhibitory effect, measured by the relative decrease in the first-order phosphorylation rate constant k_{OP} for the neutral organophosphate 7-[(methylethoxyphosphonyl)oxy]-4-methylcoumarin (EMPC) that resulted from fasciculin binding, decreased from 0.002 in wild-type human AChE to 0.24 in the D74G mutant.

The primary physiological role acetylcholinesterase (AChE)[1] is to hydrolyze the neurotransmitter acetylcholine at cholinergic synapses (*1*). AChE is one of the most efficient enzymes known (*2*), and recent studies have focused on the structural basis of its high catalytic efficiency. Ligand binding studies (*3*) and X-ray crystallography (*4*) revealed a narrow active site gorge some 20 Å deep with two separate ligand binding sites. The acylation site at the bottom of the gorge contains residues involved in a catalytic triad (H*440*, E*327*, and S*200*)[2] and W*84*, which binds to the trimethylammonium group of acetylcholine. The peripheral site at the mouth of the gorge includes, among others, residue W*279*. AChE, like other members of the α/β-hydrolase family, contains an ω-loop with boundaries set by a disulfide bond (C*67*−C*94*) (*5*, *6*). Residues from Y*70* through W*84* in this loop extend along one side of the gorge from the peripheral site to the acylation site. This segment includes residue D*72*, which is positioned near a constriction at the boundary between the peripheral site and the acylation site.

† This work was supported by Grant NS-16577 from the National Institutes of Health, Grant DAMD 17-98-2-8019 from the United States Army Medical Research Acquisition Activity, and by grants from the Muscular Dystrophy Association of America. W.D.M. was supported by a Kendall-Mayo Postdoctoral Fellowship.

* To whom correspondence should be addressed. Telephone: (904) 953-7375. Fax: (904) 953-7370. E-mail: rosenberry@mayo.edu.

[1] Abbreviations: AChE, acetylcholinesterase; TcAChE, acetylcholinesterase from *Torpedo californica*; BChE, butyrylcholinesterase; DTNB, 5,5′-dithiobis(2-nitrobenzoic acid); OP, organophosphate; EMPC, 7-[(methylethoxyphosphonyl)oxy]-4-methylcoumarin; DEPQ, 7-[(diethoxyphosphoryl)oxy]-1-methylquinolinium iodide; TMTFA, *m*-(*N*,*N*,*N*-trimethylammonio)trifluoroacetophenone.

[2] Throughout this paper, italicized residue numbers refer to the *Torpedo* AChE sequence. D74 in the human and mouse AChE sequences corresponds to D72 in *Torpedo* AChE and D70 in mammalian BChE.

10.1021/bi000210o CCC: $19.00
Published on Web 06/08/2000

In a series of recent publications, we have focused on clarifying the role of the peripheral site in the catalytic pathway for AChE (*7*−*9*). The three-dimensional structure indicates that ligands specific for the acylation site must first pass through the peripheral site on their way to the acylation site. Other cationic ligands, including the phenanthridium derivative propidium and the fasciculins, a family of nearly identical snake venom neurotoxins, are specific for the peripheral site and do not proceed further. Cationic substrates such as the acetylcholine analogue acetylthiocholine partially competed with fasciculin for binding to the peripheral site (*8*). This discovery revealed that acetylthiocholine had a modest affinity for the peripheral site, and further kinetic analysis indicated that the binding of acetylthiocholine to the peripheral site accelerated hydrolysis rates at low substrate concentrations. The acceleration is probably the most important contribution of the peripheral site to the catalytic process. Additional information about the peripheral site was obtained by studying the formation of ternary complexes with AChE. Such complexes, involving the binding of different ligands to the acylation and peripheral sites, exhibited little thermodynamic interaction between the bound ligands (*3*). However, the binding of small cationic ligands such as propidium to the peripheral site slowed the rate constants for ligand entry into and exit from the acylation site by factors of up to 400 (*7*). We termed this effect steric blockade and demonstrated that it was responsible for pronounced propidium inhibition when substrate hydrolysis is near diffusion-controlled. Steric blockade also was shown to be involved in the phenomenon of substrate inhibition (*10*), a decrease in hydrolysis rates at high substrate concentrations. Our analysis revealed that substrate inhibition occurs because the binding of acetylthiocholine in the peripheral site also slows the rate of dissociation of product thiocholine from the acylation site, making it rate-limiting at high substrate concentrations (*8*). Steric blockade by a peripheral site ligand is predicted to result in little inhibition of substrates, like organophosphates, that equilibrate with the acylation site before reacting, and experimental data confirmed this point (*9*).

In this report, we examine the location of acetylthiocholine binding in the AChE peripheral site. A clue to this location was provided when acetylthiocholine was observed to only partially compete with fasciculin for binding to the peripheral site (*8*). This finding was unexpected, since propidium appears to be completely competitive with both fasciculin (*11*) and acetylthiocholine (*8*) at the peripheral site, and crystal structures of the fasciculin−AChE complex show direct fasciculin contacts with W*279* and most other residues in the peripheral site (*12*, *13*). However, the crystal structures also showed that D*72* was a little too deep in the gorge to make direct contact with fasciculin, and it appears possible that acetylthiocholine could bind near D*72* and still allow a nearly normal fasciculin association reaction with the remainder of the peripheral site. Furthermore, site-directed mutagenesis has identified D*72* as an important residue in the catalytic pathway. The mouse and human D74N[2] AChE mutants showed significant reductions in both k_{cat}/K_{app} for acetylthiocholine (*14*, *15*) and the second-order phosphorylation rate constant k_{OP}/K_{OP} for cationic organophosphates (*16*) relative to those of wild-type AChE, and substrate inhibition was nearly abolished in this mouse mutant (*14*). D70G[2] is a naturally occurring mutation in human butyrylcholinesterase (BChE), a close relative of AChE, that results in large increases in K_{app} for butyrylthiocholine and succinyldithiocholine relative to that of wild-type BChE (*17*). Individuals with this BChE mutation have severe difficulty in metabolizing the muscle relaxant succinyldicholine (*18*, *19*).

To examine the possibility that acetylthiocholine binds near D*72*, we constructed the human D74G mutant and assessed its ability to bind acetylthiocholine at the peripheral site both from the substrate inhibition profile and with the fasciculin competition assay. Similar analyses were carried out with wild-type *Torpedo* AChE and its D*72*G mutant to assess the importance of D*72* in acetylthiocholine binding at the peripheral site in AChE from another species. We also measured the effects of bound fasciculin on the organophosphorylation of human D74G. Fasciculin is the only peripheral site ligand identified to date that inhibits reactions at the acylation site by a mechanism in addition to steric blockade or simple steric overlap in the ternary complex. This mechanism, which appears to involve a conformational change in the acylation site, is best revealed by determination of the organophosphorylation rate constants (*9*), and we examined the extent to which it is disrupted in the D74G mutant.

EXPERIMENTAL PROCEDURES

Materials. Recombinant human "wild-type" AChE was expressed as a secreted dimeric form in *Drosophila* S2 cells in culture (*9*) and purified by two cycles of affinity chromatography on acridinium resin (*20*). AChE from *Torpedo* (type H), modified by site-directed mutagenesis as described previously (*21*) and produced by transfection of COS-7 cells with the pEF-Bos vector (*22*), was provided by S. Bon and J. Massoulié at the Ecole Normale Supérieure in Paris, France. The free cysteine (C231) was replaced by a serine, and a stop codon was introduced at position 540, thus deleting the GPI addition signal but retaining a C-terminal cysteine that results in a soluble disulfide-linked dimeric enzyme. In this study, this enzyme is denoted wild-type *Torpedo* AChE and is compared to its D*72*G derivative. *Torpedo* wild-type and D*72*G AChEs also were purified by affinity chromatography on acridinium resin except where noted. Purification did not alter the fitted substrate inhibition parameters for the *Torpedo* D*72*G enzyme (data not shown). Fasciculin 2 was obtained from C. Cervenansky at the Instituto de Investigaciones Biologicas, Clementa Estable, Montevideo, Uruguay (*11*), while fasciculin 3 was obtained from P. Marchot at the Laboratoire de Biochimie, Faculté de Médicine, Université d'Aix-Marseille II, Marseille, France (*23*). The concentration of purified fasciculin 2 was determined by absorbance (ϵ_{276} = 4900 M^{-1} cm^{-1}; *24*), while the fasciculin 3 concentration was determined by titration with a known amount of human erythrocyte AChE as described in ref *11*. DEPQ and EMPC were synthesized as previously described (*9*). Propidium iodide was purchased from Calbiochem.

Mutagenesis of Recombinant Human AChE. The secreted dimeric form of human AChE with a truncation sequence, including a stop codon inserted just downstream from the exon 4−5 boundary, was used as a template for mutagenesis (*9*). D74G AChE was constructed using the Alter Sites II *in vitro* Mutagenesis System (Promega Corp., Madison, WI). Briefly, the gene cassette encoding human AChE was cloned

from the *Drosophila* expression vector pPac into the cloning and mutagenesis vector pALTER to make $pALT_{human}$. DNA was transformed into JM109 *Escherichia coli* cells for preparation of phagemid ssDNA using R408 helper phage. dsDNA was synthesized *in vitro* using the AChE vector ssDNA template, DNA polymerase, DNA ligase, and three site-specific oligonucleotides. The first two oligonucleotides (provided in the Altered Sites II kit) were annealed with antibiotic resistance genes on the $pALT_{human}$ plasmid, switching the antibiotic resistance encoded on the synthesized DNA strand and allowing for selection of *E. coli* with mutant plasmids. The third oligonucleotide (synthesized by the Mayo Clinic Rochester Molecular Biology Core Facility) was annealed with AChE DNA corresponding to amino acid residues *67*−*76* to introduce the D74G mutation (GAC → GGC). The mutagenic oligonucleotide also contained a silent mutation that removed a Van91I restriction endonuclease site as a marker to confirm the presence of the mutation. The pool of mutant and wild-type dsDNA was transformed into ES 1301 mutS *E. coli*, and cultures were grown in liquid media with the appropriate antibiotic for mutant DNA selection. Plasmid DNA was prepared from these cultures and propagated in JM109 *E. coli*. Mutant plasmids from JM109 colonies were identified (after further antibiotic selection) by Van91I endonuclease digestion of purified DNA. The D74G AChE sequence was confirmed by DNA sequencing carried out at the Mayo Clinic Rochester Molecular Biology Core Facility. The modified human AChE D74G cassette was returned to the pPac vector for transfection into and expression from *Drosophila* S2 cells in tissue culture (*9*). D74G AChE was purified from culture medium by two cycles of affinity chromatography on acridinium resin (*20*). The affinity chromatography procedure was modified in that NaCl concentrations used during the washing steps did not exceed 100 mM and the Triton X-100 level was reduced to 0.02% to prevent excess stripping of bound protein off the column. Purified recombinant AChE samples analyzed by SDS−PAGE (*25*) showed no contaminants.

Steady-State Measurements of AChE-Catalyzed Substrate Hydrolysis. Hydrolysis of acetylthiocholine was monitored with a spectrophotometric Ellman assay (*26*). Assay solutions included 0.33 mM DTNB, and hydrolysis was monitored by formation of the thiolate dianion of DTNB at 412 nm [$\Delta\epsilon_{412} = 14.15\ mM^{-1}\ cm^{-1}$ (*27*)]. Hydrolysis rates v were measured at various substrate (S) concentrations in 20 mM sodium phosphate and 0.02% Triton X-100 (pH 7.0) at 25 °C, and the constant ionic strength was maintained with 0−100 mM NaCl (*8*). The dependence of v on S concentration was fitted to eq 1, the Haldane equation for substrate inhibition (*28*), by weighted nonlinear regression analysis (assuming constant percent error in v) with Fig.P (BioSoft, version 6.0). In eq 1, $V_{max} = k_{cat}[E]_{tot}$, where k_{cat} is the maximal substrate turnover rate, $[E]_{tot}$ is the total concentration of AChE active sites, K_{SS} is the substrate inhibition constant, and K_{app} is the apparent Michaelis constant. Active site concentrations were determined from V_{max}/k_{cat}, and k_{cat} was established in titrations with DEPQ monitored by fluorometric or inactivation assays (*9*). Measurements of k_{cat} at pH 7.0 for human erythrocyte AChE [$(5.78 \pm 0.38) \times 10^3\ s^{-1}$, $n = 3$], wild-type recombinant human AChE [$(6.61 \pm 0.32) \times 10^3\ s^{-1}$, $n = 3$], and D74G human AChE [$(6.53 \pm 0.27) \times 10^3\ s^{-1}$, $n = 3$] were not significantly different, and a mean k_{cat} value of $6.3 \times 10^3\ s^{-1}$ was assumed. This value agrees with a previously assigned k_{cat} of $7 \times 10^3\ s^{-1}$ at pH 8.0 (*8*) and a pK_a of 6.3 for k_{cat} (*20*). Determinations of k_{cat} at pH 7.0 for wild-type recombinant *Torpedo* AChE [$(4.18 \pm 0.20) \times 10^3\ s^{-1}$, $n = 3$] and D72G *Torpedo* AChE [$(5.33 \pm 0.17) \times 10^3\ s^{-1}$, $n = 3$] also were averaged to give a mean k_{cat} value of $4.8 \times 10^3\ s^{-1}$.

$$v = \frac{V_{max}[S]}{[S]\left(1 + \frac{[S]}{K_{SS}}\right) + K_{app}} \quad (1)$$

Determination of Rate Constants in Scheme 3. We have recently presented substantial evidence which shows that catalysis of acetylthiocholine hydrolysis by human AChE proceeds according to Scheme 3 in the Results (*8*). To estimate key rate constants in Scheme 3, we solved the corresponding steady-state rate equations numerically with the program SCoP (version 3.51) (*7*, *8*). This solution avoids equilibrium assumptions and allows examination of Scheme 3 in the context of our steric blockade model, which postulates that $k_{-P2} < k_{-P}$ and $a = b = 1$. To allow the fitting of rate constants from data, our current treatment also simplifies Schemes 2 and 3 from their more general format (see ref *8*) by postulating that product P bound to the acylation site does not alter the rate constant for deacetylation, that rate constants for P dissociation from the acetylated enzyme are identical to those from free enzyme, and that peripheral site binding is unaffected by the binding of ligands to the acylation site. These assumptions still leave eight rate constants in Scheme 3 to be assigned or determined. On the basis of previous experimental data, we assigned $k_2 = k_3$ (*7*, *29*) and $k_{-P2}/k_{-P} = 0.01$ (*7*, *8*). Additional constraints placed upon the remaining parameters are given by the following three equations. The second-order substrate hydrolysis rate constant k_{cat}/K_{app} for Schemes 2 and 3 is given by eq 2.

$$\frac{k_{cat}}{K_{app}} = \frac{k_S k_1 k_2}{k_{-S}k_{-1} + k_2(k_{-S} + k_1)} \quad (2)$$

An adjustable constant B is defined in eq 3 to set the ratio of k_S equal to k_{cat}/K_{app}.

$$B = \frac{k_S K_{app}}{k_{cat}} \quad (3)$$

Another adjustable constant R/R_S is defined in eq 4.

$$\frac{R}{R_S} = 1 + \frac{1.5\,(B - 1)}{B\left(1 + \frac{k_2}{k_{-1}}\right)} \quad (4)$$

To solve for the parameters in Scheme 3, k_{cat} was set to the

human or *Torpedo* AChE value determined above and K_{app} and $[E]_{tot}$ were obtained by an initial fit of data to eq 1. Values of B and R/R_S were assigned, and the dependence of v on [S] was then fitted in the SCoP program for the three remaining parameters in Scheme 3: $K_S = k_{-S}/k_S$, k_{-P}, and k_2. The three other rate constants (k_1, k_{-1}, and k_{-S}) were calculated iteratively from eqs 2−4 during the fitting of these parameters.

The constants B and R/R_S were defined for the fitting procedure outlined here because they are constrained within a narrow range of values (*8*). According to eq 2, $B \geq 1$. When $B \cong 1$, $k_{cat}/K_{app} \cong k_S$ and the second-order reaction is diffusion-controlled (i.e., $k_{-S}/k_1 \cong 0$). For acetylthiocholine, the relatively high value of k_{cat}/K_{app} ($>10^8$ M^{-1} s^{-1}; see ref *8*) and its viscosity dependence (*30*) argue that B is close to 1, and it is very unlikely to exceed 10. According to eq 4, $1 \leq R/R_S \leq 2.5$. This range places no restriction on the value of k_2/k_{-1}, but via assignment of B and R/R_S, the value of k_2/k_{-1} is set by eq 4 and that of k_{-S}/k_1 by eqs 2 and 3. R and R_S are introduced because they represent observed solvent deuterium oxide isotope effects for AChE. If k_2 and k_S are the only intrinsic rate constants in eq 2 that are altered when H_2O is replaced with D_2O, and R, R_S, and R_2 are defined as the respective ratios of k_{cat}/K_{app}, k_S, and k_2 in H_2O to that in D_2O, then R/R_S is given by eq 4 when R_2 is assigned a typical value of 2.5 (*8*). For all data fitting here, B was estimated to be 1.2 and R/R_S was set at the observed value of 1.1 (*8*). However, varying these constants over their entire range ($1 \leq B \leq 10$ and $1 \leq R/R_S \leq 2.5$), while producing large changes in calculated k_2/k_{-1}, resulted in no more than 40% changes in the fitted parameters K_S, k_{-P}, and k_2 for wild-type AChE.[3] Depending on the initial values of these three parameters, simultaneous fitting of wild-type AChE activities as in Figure 1A converged on one of two alternative solutions. The solution where $k_{-P} > k_2$ was selected, consistent with previous estimates of k_{-P} (*8*).

Slow Equilibration of Fasciculin in the Presence of Peripheral Site Inhibitors. Apparent association rate constants k_{on} for fasciculin binding to the AChE peripheral site were measured by a procedure used previously (*8*, *11*). In brief, stock solutions of fasciculin 2 (140 μM) and fasciculin 3 (20 nM) were prepared in buffer [20 mM sodium phosphate and 0.02% Triton X-100 (pH 7.0)] and contained 0.1% bovine serum albumin (*11*). Association reactions (0.1 mL for fasciculin 3 and 1−2 mL for fasciculin 2) were initiated by adding small volumes of AChE and acetylthiocholine to final concentrations of 0.1−1.8 nM fasciculin 2 (*Torpedo* AChE) or 1−5 nM fasciculin 3 (human AChE) and 0.1−30 mM acetylthiocholine. The reaction mixtures also included 0.1 mM DTNB and NaCl (with a NaCl concentration of 60 mM − [S]) in buffer at 25 °C. Fasciculin binding was assessed under approximate first-order conditions in which the fasciculin concentration was at least 7 times higher than the concentration of AChE and acetylthiocholine was not significantly depleted (<20%). Acetylthiocholine hydrolysis rates v determined over 2 s intervals were fitted by nonlinear regression analysis (BioSoft Fig.P) to eq 5.

$$v = v_{final} + (v_{initial} - v_{final})\ e^{-kt} \quad (5)$$

In eq 5, $v_{initial}$ and v_{final} are the calculated values of v at time zero and at the final steady state when fasciculin binding has reached equilibrium, respectively, and k is the observed first-order rate constant for the approach to the final steady state. Each series of binding measurements included reactions at a fixed acetylthiocholine (S) concentration and four to ten fasciculin concentrations [F]. The observed k for each reaction was given by eq 6, and k_{on}, the apparent association rate constant, was determined by linear regression analysis in which k values were weighted by the reciprocal of their variance.

$$k = k_{on}[F] + k_{off} \quad (6)$$

If ligand binding to the peripheral site is unaffected by the presence of ligands or an acyl group at the acylation site, then only two sets of enzyme species in Scheme 3 below need be considered, $\Sigma E[S_P]$ and ΣE (*8*). These are the sums of the concentrations of all enzyme species in which S or nothing, respectively, is bound to the peripheral site. Assuming that fasciculin reacts with species in ΣE with an intrinsic association rate constant k_F and with species in $\Sigma E[S_P]$ with an intrinsic association rate constant k_{FP}, k_{on} is given by eq 7, where K_S is the equilibrium dissociation constant for S at the peripheral site (*8*).

$$k_{on} = \frac{k_F + k_{FP}\dfrac{[S]}{K_S}}{1 + \dfrac{[S]}{K_S}} \quad (7)$$

To obtain estimates of K_S, values of k_{on} obtained at each S concentration were fitted to eq 7 by nonlinear regression analysis (BioSoft Fig.P) in which k_{on} values were weighted by the reciprocal of their variance.

Phosphorylation of Human D74G AChE by Fluorogenic OPs. Reaction of recombinant human D74G AChE with EMPC or DEPQ was monitored by the appearance of their fluorescent leaving groups by stopped flow fluorometry as described previously for wild-type human AChEs (*9*). We have shown that direct fluorescence monitoring of the leaving group during phosphorylation avoids misinterpretations of fasciculin inhibition that arise when phosphorylation is assessed by enzyme inactivation (*9*). The misinterpretation resulted from a small population of AChE that was resistant to normal fasciculin inhibition and dominated the enzyme activity during OP inactivation measurements in the presence of fasciculin. Measurements of inactivation of the D74G mutant by EMPC and DEPQ in the absence of fasciculin again indicated more than one population of enzyme. Stoichiometric titration of the D74G stock with DEPQ in the presence of fasciculin (*9*) indicated that less than 10% corresponded to the fasciculin-resistant population (data not shown).

Fluorogenic phosphorylation reactions were conducted in 20 mM sodium phosphate and 0.02% Triton X-100 at 23

[3] Values of B and R/R_S have a greater effect on the fitted parameters when little substrate inhibition is observed. When k_2 was fixed for the human D74G data sets in Table 1, fitted values of K_S and k_{-P} remained within a factor of 2 of those shown over most of the range of B and R/R_S values. However, in certain narrow ranges (e.g., $1.00 < R/R_S < 1.02$ and $1.3 < B < 1.8$, or $2 < R/R_S$ and $4 < B < 8$), fitted values of K_S and k_{-P} differed by up to a factor of 10.

°C (pH 8.0 for EMPC and pH 7.0 for DEPQ). The release of product from each OP occurred in two phases, a large rapid phase and a small slower phase, and was fitted to an equation with two exponential terms (*9*). Some reactions included the peripheral site inhibitors propidium (150 μM) or fasciculin 2 (10 μM). A two-exponential fit also was required with DEPQ in the presence of propidium. Additional precautions were taken with fasciculin (*9*). The rate constants k for the rapid phase were analyzed according to Scheme 1.

Scheme 1

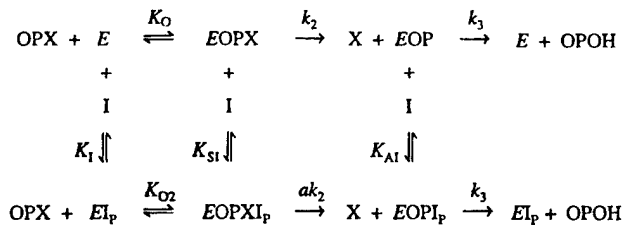

In this scheme, OPX is the intact OP with leaving group X, *E*OPX is the initial complex of the OP with AChE, characterized by the equilibrium dissociation constant K_O which equals k_{-O}/k_O (*9*) and *E*OP is the phosphorylated enzyme. The ligand I can bind to the peripheral site in each of the enzyme species (as denoted by the subscript P). OPs were assumed to equilibrate with the AChE acylation site even when inhibitors were bound to the peripheral site, and the dephosphorylation rate constant k_3 was assumed to be negligible. The dependence of k on the OP concentration was analyzed by weighted nonlinear regression analysis (assuming constant percent error in k) according to eq 8 to give k_{OP} and k_{OP}/K_{OP}, the respective first- and second-order rate constants of phosphorylation, respectively.

$$k = \frac{k_{OP}[OP]}{K_{OP} + [OP]} \quad (8)$$

In the absence of I, $k_{OP} = k_2$ and $K_{OP} = K_O$. In the presence of I, the relative intrinsic first-order rate constant a for phosphorylation in Scheme 1 was calculated from k_{OP}, K_{OP}, and the competitive inhibition constant K_I for the inhibitor as outlined previously (*9*). Values of K_I were obtained in the pH 7.0 buffer with acetylthiocholine as the substrate. The K_I for propidium was calculated from the slopes of $1/v$ versus $1/[S]$ plots over a range of fixed concentrations of inhibitor, while the K_I for fasciculin 2 was estimated from relative v measurements in the presence and absence of inhibitor at low S concentrations (*7*).

RESULTS

A Mechanistic Model for Substrate Inhibition of AChE. Traditional catalytic pathways for AChE propose the binding of an ester substrate S to the acylation site to form an *E*S complex, followed by formation of the acylated enzyme intermediate *E*A and deacylation to regenerate the free enzyme *E*. We recently obtained evidence that the catalytic pathway for AChE should be extended by making explicit two new classes of intermediates (*8*). One class includes enzyme species with the initial product of hydrolysis, the alcohol leaving group P (e.g., thiocholine), still bound to the acylation site. These intermediates are denoted *E*AP and *E*P in Scheme 2.

Scheme 2

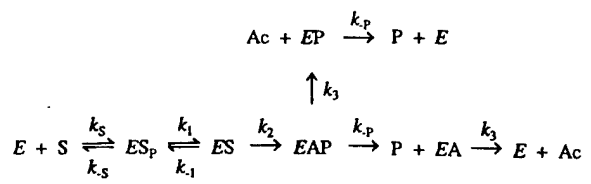

The second includes intermediates in which S is bound to the AChE peripheral site, indicated by the subscript P as in ES_P in Scheme 2. The substrate initially binds in ES_P and then slides into the acylation site to give *E*S.. Previous schemes that ignore intermediates such as *E*AP and *E*P can sometimes be justified. For example, with acetylthiocholine, the product dissociation rate constant k_{-P} is estimated to be nearly an order of magnitude greater than the acylation rate constant k_2 or deacylation rate constant k_3, and explicit inclusion of *E*AP, *E*P, and k_{-P} changes calculated values of k_{cat} by less than 1% (*8*). According to Scheme 2, a plot of the substrate hydrolysis rates v against the substrate concentration [S] should fit the familiar Michaelis–Menten expression. However, AChE shows substrate inhibition and thus requires a model in which a second molecule of substrate interacts with at least one of the intermediates in Scheme 2. Our recent evidence supports Scheme 3 (*8*).

Scheme 3

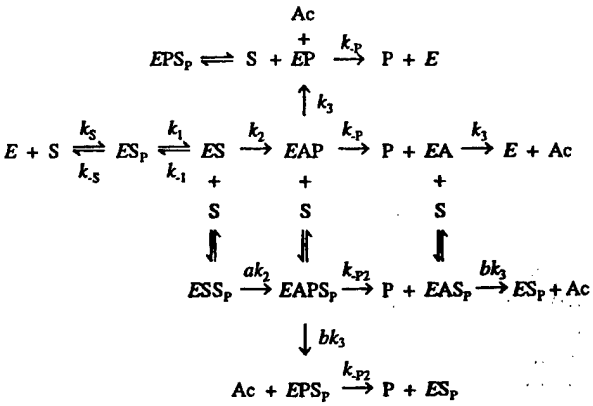

In this scheme, the second molecule of substrate can bind to the peripheral site in the *E*S, *E*A, *E*AP, and *E*P intermediates in Scheme 2 with an association rate constant k_S and a dissociation rate constant k_{-S}. In theory, substrate inhibition could arise from inhibition of acylation ($a < 1$) or of deacylation ($b < 1$) when S binds to the peripheral site, but there is no evidence that the binding of a small ligand like acetylthiocholine to the peripheral site can inhibit these steps. However, it has been directly shown that the binding of the small peripheral site ligands propidium or gallamine decreases the association and dissociation rate constants for ligand binding to the acylation site by factors of 10–400 (*7*). Substrate binding to the peripheral site then would be expected to slow the rate constant for product dissociation ($k_{-P2} < k_{-P}$) in Scheme 3. If k_{-P2} falls within the range of k_2 and k_3, then EPS_P can accumulate at high substrate concentrations and result in substrate inhibition. We recently

Table 1: Comparison of K_S Values Obtained from Substrate Inhibition Curves and from Fasciculin Competition[a]

AChE	rate constants from substrate inhibition				K_S from fasciculin competition (mM)
	n	K_S (mM)	k_{-P} (s^{-1})	k_2 (s^{-1})	
human wild type	3	1.9 ± 0.7[b]	$(6 \pm 1) \times 10^4$[b]	$(1.28 \pm 0.02) \times 10^4$	1.3 ± 1.0
human D74G	3	33 ± 8[c]	$(9 \pm 3) \times 10^4$[c]	1.28×10^4[d]	–
Torpedo wild type	2	0.51 ± 0.16	$(16 \pm 3) \times 10^4$	$(0.97 \pm 0.01) \times 10^4$	0.40 ± 0.21
Torpedo D72G	3	10 ± 1[b]	$(4 \pm 0.3) \times 10^4$	0.97×10^4[d]	4 ± 2

[a] Rate constants from substrate inhibition were the means of n measurements obtained by data fitting with the SCoP program and eqs 2–4. Estimates of K_S from fasciculin competition were obtained with eq 7 as shown in Figures 1B and 2B. [b] The mean includes one experiment in which the sum of [NaCl] and [S] was 40 mM. The K_S obtained from this experiment was normalized to 60 mM prior to calculating the mean by assuming that ionic strength affected only k_S (*31*) and that k_S was inversely proportional to K_{app} (eq 3). [c] The mean includes experiments in which the sum of [NaCl] and [S] was fixed at 40, 60, or 100 mM. K_S values obtained from the experiments at 40 and 100 mM were normalized to 60 mM prior to calculating the mean as in footnote b. [d] For the fitting of K_S and k_{-P}, this k_2 was fixed at the k_2 value observed for the wild-type AChE.

examined whether this scheme could account quantitatively for substrate inhibition profiles with human erythrocyte AChE by measuring the affinity of S for the peripheral site in a fasciculin competition assay (*8*; see Figure 1B below). The value of K_S ($=k_{-S}/k_S$) obtained for acetylthiocholine was about 1 mM. This value was then combined with our steric blockade model of Scheme 3, which postulates that $k_{-P2} < k_{-P}$ but that $a = b = 1$, to construct a nonequilibrium simulation of the substrate inhibition profile that was in excellent agreement with the observed profile (*8*).

Estimation of the Acetylthiocholine Affinity for the AChE Peripheral Site Directly from the Substrate Inhibition Profile. While our previous work demonstrated that experimental estimates of some of the remaining rate constants allowed reasonable simulation of substrate inhibition plots, our goal here was to actually fit the two key kinetic parameters in Scheme 3, K_S and k_{-P}, with substrate inhibition data. To achieve this, we reduced the 11 rate constant variables in Scheme 3 to three that could be fitted, as outlined in Experimental Procedures. Briefly, the assumptions in our steric blockade model together with previous data from inhibition of substrate hydrolysis by bound peripheral site ligands (*7*) decreased the number of variables to the seven rate constants in Scheme 2. Assigning $k_3 = k_2$ (*29*) and invoking eqs 2–4 further reduced the system to three fitted parameters (K_S, k_{-P}, and k_2). The profile of v versus [S] for acetylthiocholine with recombinant wild-type human AChE exhibited the bell shape that is the hallmark of pronounced substrate inhibition, and this profile was fitted precisely by the procedure (Figure 1A). Fitted values of K_S (1.9 ± 0.7 mM) and k_{-P} [$(6 \pm 1) \times 10^4$ s^{-1}] averaged from this experiment and two others (Table 1) agreed to within 40% of the corresponding values assigned previously to simulate substrate inhibition for human erythrocyte AChE (*8*).

We selected K_S and k_{-P} as parameters to be fitted because they can be compared to independent experimentally predicted values. The predicted k_{-P} was calculated indirectly from the relationship $k_{-P} = K_P k_P$, where K_P is the measured equilibrium dissociation constant for thiocholine inhibition of AChE and the association rate constant k_P for thiocholine is assumed to be the same as k_S for acetylthiocholine. Its calculated value (1.3×10^5 s^{-1}) agreed with the simulated k_{-P} value (*8*) and the fitted k_{-P} value determined here. To obtain the predicted K_S for acetylthiocholine, we employed the fasciculin competition assay in Figure 1B. In this assay, the substrate affinity for the peripheral site is determined from the effect of substrate concentration on the rate of equilibration of fasciculin at the peripheral site. The association of fasciculin with the AChE peripheral site was monitored as a decrease in AChE activity toward acetylthiocholine (*8*). The apparent fasciculin association rate constants k_{on} then were calculated from the rate constants for this activity decrease as a function of the fasciculin concentration, and finally, the dependence of k_{on} on the acetylthiocholine concentration was fitted to eq 7 to obtain K_S. The assay requires a sufficiently low dissociation rate constant k_{-F} for the fasciculin–AChE complex to allow measurement of the initial rate constants for fasciculin association, and our preliminary observations indicated that k_{-F} for fasciculin 2 with human D74G was too high to allow these measurements. Therefore, we turned to fasciculin 3, which was reported to have a K_d nearly 100-fold smaller than that of fasciculin 2 with rat brain AChE (*23*) and which did allow k_{on} determinations with the human D74G. As observed previously for fasciculin 2 and human erythrocyte AChE (*8*), acetylthiocholine only partially blocked the association of fasciculin 3 with recombinant wild-type human AChE (Figure 1B). At high saturating concentrations of acetylthiocholine, k_{on} decreased to about 50% of its extrapolated value in the absence of acetylthiocholine. Fitting the k_{on} values for fasciculin 3 at various concentrations of acetylthiocholine to eq 7 gave a K_S of 1.3 ± 1.0 mM. The precision of the individual k_{on} points made it difficult to decrease the error of this estimate, but this K_S value agreed well with that obtained from the substrate inhibition data (Table 1).

Human AChE Residue D74 Is Important in the Binding of Acetylthiocholine to the Peripheral Site of AChE. The quantitative agreement between the K_S measured by fasciculin competition and that obtained by fitting the substrate inhibition profile provided reassuring support for our model in Scheme 3 and its application to wild-type human AChE. We next investigated whether such agreement would extend to the human D74G mutant. The rationale outlined in the introductory section for focusing on this mutant is that D74 may be the key residue in defining peripheral site binding of acetylthiocholine. If this idea is correct, K_S should increase dramatically in D74G mutants. With the human D74G enzyme in Figure 1A, the extent of substrate inhibition in fact was decreased to such an extent that the three-parameter fit in SCoP was unreliable and sometimes failed to converge with the relation $k_2 < k_{-P}$. Therefore, k_2 was fixed to the value in Table 1 obtained for the wild-type human AChE, and only K_S and k_{-P} were fitted. The assumption that k_2 is the same for human wild-type and D74G AChEs was supported by our observation that these AChEs have the same

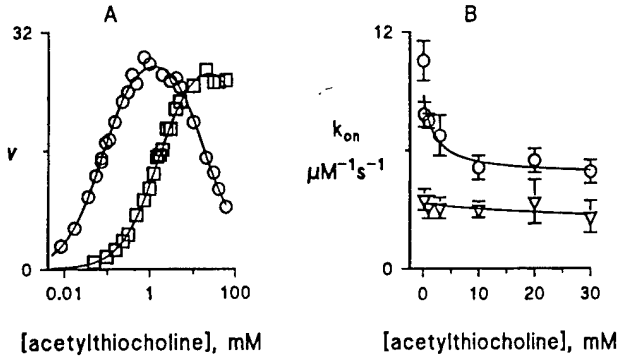

FIGURE 1: Acetylthiocholine binding to the peripheral site of human AChE. Reaction mixtures with varying amounts of acetylthiocholine were supplemented with NaCl such that [S] + [NaCl] = 60 mM to maintain a constant ionic strength. (A) Substrate inhibition with acetylthiocholine. Points represent initial velocities (micromolar per minute) measured at the indicated substrate concentrations with the wild-type (O) or D74G (□) AChE (80 pM) as outlined in Experimental Procedures. Lines were fitted with the SCoP program by employing eqs 2−4. For wild-type AChE, the parameters K_S, k_{-P}, and k_2 were fitted simultaneously, while for the D74G mutant, k_2 was fixed at 1.28×10^4 s^{-1} and K_S and k_{-P} were fitted (see Table 1). Lines fitted with the Haldane equation (eq 1) were virtually superimposable with those shown and gave a K_{app} of 76 ± 2 μM and a K_{SS} of 22 ± 1 mM for wild-type AChE and a K_{app} of 1670 ± 60 μM and a K_{SS} of 300 ± 70 mM for the D74G mutant. (B) Inhibition of fasciculin 3 binding by acetylthiocholine. Association rate constants k_{on} for fasciculin 3 measured at the indicated substrate concentrations with wild-type (O) or D74G (▽) AChE were determined by analysis with eqs 5 and 6 as outlined in Experimental Procedures (data not shown). Points represent a series of k_{on} measurements, and lines were obtained with eq 7 by fixing K_S at the value obtained from substrate inhibition in Table 1 and fitting k_{FP}/k_F to 0.52 ± 0.05 (wild type) or 0.6 ± 0.5 (D74G). A line for the wild-type AChE points fitting all three constants in eq 7 corresponded closely to that shown and gave a K_S of 1.3 ± 1.0 mM and a k_{FP}/k_F of 0.52 ± 0.06.

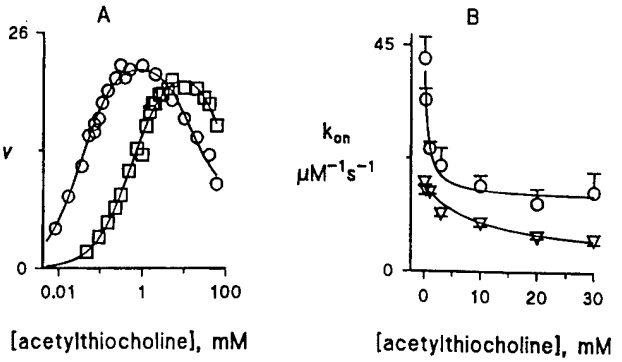

FIGURE 2: Acetylthiocholine binding to the peripheral site of *Torpedo* AChE. Ionic strength was maintained with up to 60 mM NaCl as shown in Figure 1. (A) Substrate inhibition with acetylthiocholine. Assays were conducted as described for Figure 1A with wild-type (O) or D72G (□) AChE (80 pM). Lines were fitted with the SCoP program as in Figure 1A except that for the D72G mutant k_2 was fixed at 0.97×10^4 s^{-1} (see Table 1). Lines fitted with the Haldane equation (eq 1) were close to (wild type) or virtually superimposable with (D72G) those shown and gave a K_{app} of 35 ± 2 μM and a K_{SS} of 39 ± 3 mM for wild-type AChE and a K_{app} of 570 ± 25 μM and a K_{SS} of 140 ± 20 mM for the D72G mutant. (B) Inhibition of fasciculin 2 binding by acetylthiocholine. Association rate constants k_{on} for fasciculin 2 with affinity-purified wild-type (O) or unpurified D72G (▽) AChE were determined as described for Figure 1B (data not shown). Lines were obtained as in Figure 1B with k_{FP}/k_F fitted to 0.33 ± 0.04 (wild type) or 0.15 ± 0.05 (D72G). Lines fitting all three constants in eq 7 corresponded closely to those shown and gave a K_S of 0.40 ± 0.21 mM and a k_{FP}/k_F of 0.32 ± 0.05 for the wild-type points and a K_S of 3.8 ± 1.7 mM and a k_{FP}/k_F of 0.30 ± 0.06 for the D72G points.

k_{cat} value (see Experimental Procedures), and k_2 is a major contributor to k_{cat}. Average fitted values of K_S (33 ± 8 mM) and k_{-P} [$(9 \pm 3) \times 10^4$ s^{-1}] were obtained from the human D74G data in Figure 1B and two additional experiments at slightly different ionic strengths (Table 1). Ionic strength had no effect on k_{-P}, which was nearly unchanged from the value for wild-type AChE. In contrast, K_S increased about 20-fold with the D74G mutant, and the change in this parameter alone was sufficient to nearly abolish substrate inhibition. Of particular importance, this increase in K_S was supported by the fasciculin 3 competition data for the human D74G mutant in Figure 1B. Values of k_{on} did not differ significantly as the acetylthiocholine concentration ranged from 0.1 to 30 mM, and the data could be fitted to eq 7 by assigning a fixed K_S of 33 mM from the substrate inhibition data.

To determine whether D72 was essential for the binding of acetylthiocholine to the peripheral site of AChE from another species, we examined recombinant *Torpedo* AChEs. Wild-type *Torpedo* AChE exhibited substrate inhibition similar to that observed with wild-type human AChE (Figure 2A), and average fitted values of K_S (0.5 ± 0.2 mM) and k_{-P} [$(16 \pm 3) \times 10^4$ s^{-1}] were obtained (Table 1). Both the wild type and D72G AChEs from *Torpedo* had sufficient affinity for fasciculin 2 to conduct fasciculin competition measurements. Acetylthiocholine was slightly more effective in blocking the association of fasciculin 2 with the wild-type *Torpedo* than with the wild-type human AChE, as high saturating concentrations of acetylthiocholine decreased k_{on} to about one-third of its extrapolated value in the absence of acetylthiocholine (Figure 2B). Fitting the k_{on} values to eq 7 gave a K_S of 0.4 ± 0.2 mM (Table 1), in agreement with the K_S obtained from substrate inhibition of wild-type *Torpedo* AChE. Substrate inhibition with the *Torpedo* D72G mutant was more evident than with the human D74G enzyme (Figure 2A). As with human D74G, however, it was necessary to fix k_2 to obtain a K_S of 10 ± 1 mM (Table 1). The fasciculin 2 competition data supported this estimate. Values of k_{on} with the *Torpedo* D72G mutant decreased at least 3-fold as the acetylthiocholine concentration ranged from 0.1 to 30 mM (Figure 2B), and fitting to eq 7 gave a K_S (4 ± 2 mM). The somewhat lower K_S values for the wild-type and D72G *Torpedo* AChEs relative to those of the corresponding human AChEs suggest that residues other than D72 contribute more to the peripheral site for acetylthiocholine in *Torpedo* AChE than in human AChE. For example, residues 72−75 in *Torpedo* AChE are DEQF, while in human AChE they are DTLY; this sequence difference may contribute to greater acetylthiocholine affinities in the peripheral site of the *Torpedo* AChEs.

The effects of the D72G mutation that we observe on the experimental kinetic parameters for acetylthiocholine hydrolysis in eq 1 are consistent with previous analyses of D72 mutants of AChE. We found no significant difference in k_{cat} between human wild-type and D74G AChEs and a slight 25−30% increase in the k_{cat} for *Torpedo* D72G AChE relative to that for the *Torpedo* wild-type enzyme (see Experimental Procedures), in reasonable agreement with a small 40% decrease in the reported k_{cat} values for mouse and human D74N (*14*, *15*). All studies agree that K_{app}

Table 2: Rate Constants for the Phosphorylation of Wild-Type and D72G AChE by Fluorogenic OPs[a]

OP enzyme	inhibitor	k_{OP} (min^{-1})	a	K_{OP} (μM)	k_{OP}/K_{OP} (μM^{-1} min^{-1})	k_{OP}/K_{OP} relative decrease (fold)
EMPC						
wild type[b]						
	none	150 ± 11	–	224 ± 24	0.67 ± 0.03	–
	propidium	570 ± 140[c]	5 ± 2[c]	1260 ± 350[c]	0.45 ± 0.02	1.5
	fasciculin	0.23 ± 0.08	0.002	220 ± 110	0.0011 ± 0.0002	610
D74G						
	none	74 ± 10	–	64 ± 12	1.2 ± 0.1	–
	propidium	710 ± 110	>10	330 ± 70	2.2 ± 0.2	*d*
	fasciculin	19 ± 4	0.24 ± 0.08	1260 ± 320	0.015 ± 0.001	80
DEPQ						
wild type[b]						
	none	1600 ± 200	–	7.5 ± 1.3	205 ± 11	–
	propidium	1200 ± 400[c]	0.7 ± 0.4[c]	85 ± 30[c]	15 ± 1	14
	fasciculin	0.66 ± 0.10	0.0003	700 ± 140	0.0010 ± 0.0001	220000
D74G						
	none	850 ± 140	–	90 ± 20	10 ± 1	–
	propidium	760 ± 300[c]	0.8 ± 0.9[c]	240 ± 130[c]	3.2 ± 0.4	3
	fasciculin	*e*	*e*	*e*	<0.006 ± 0.0004	>1500

[a] Values of k_{OP} and K_{OP} were determined from the dependence of k on [OP] (eq 8), and a (Scheme 1) was calculated by extrapolation to a saturating concentration of inhibitor (*9*). [b] Data from ref *9*. [c] The maximum [OP] employed (30−60% of the estimated K_{OP}) did not exceed 80% of the estimated K_{OP}, and therefore, estimates of k_{OP} and K_{OP} are approximate. [d] k_{OP}/K_{OP} increased by a factor of 1.9. [e] No estimate was possible because of the lower affinity of fasciculin 2 for the D74G mutant, the low reactivity of the complex of fasciculin 2 and D74G with DEPQ, and the near linearity of k with [OP] (eq 8).

increases when D72 is mutated, and our observations of a 22-fold increase in human D74G (Figure 1A) and a 16-fold increase in *Torpedo* D72G (Figure 2A) are consistent with 28- and 5-fold increases reported for mouse (*14*) and human (*15*) D74N, respectively. We also found that K_{SS}, the experimental substrate inhibition constant, increased by factors of 14 with human D74G and 4 with *Torpedo* D72G relative to those of the wild-type enzymes, in reasonable agreement with the 35-fold increase reported in mouse D74N (*14*).

Phosphorylation of Recombinant Human D74G by EMPC and DEPQ in the Presence and Absence of Peripheral Site Ligands. EMPC and DEPQ are fluorogenic OPs that release fluorescent leaving groups when they phosphorylate the AChE acylation site (Scheme 1). As observed previously with wild-type human AChEs (*9*), most of the fluorescence increase on reaction of these OPs with the human D74G mutant occurred with a single rapid exponential time course (data not shown). The dependence of the rate constants on the OP concentrations was analyzed with eq 8. The D74G mutation had little effect on the reaction of EMPC, a neutral OP. The first-order rate constant k_{OP} decreased about 2-fold, and the equilibrium dissociation constant K_{OP} decreased about 4-fold relative to that of wild-type AChE (Table 2). A similar decrease in k_{OP} was observed for DEPQ, a cationic OP, but K_{OP} increased by about an order of magnitude. These changes are consistent with those reported in second-order phosphorylation rate constants (k_{OP}/K_{OP}) for other neutral and cationic OPs with mouse wild-type and D74N AChEs (*16*). These reports showed that k_{OP}/K_{OP} for cationic OPs decreased 35−145-fold in the mutant relative to that of wild-type AChE, in contrast to a 1.4−2.6-fold increase for neutral OPs, and the authors concluded that D74 was responsible for the enhanced reactivity of cationic OPs relative to their uncharged counterparts.

In the presence of peripheral site ligands, interpretation of k_{OP} and K_{OP} in terms of the intrinsic rate constants in Scheme 1 involved extrapolation to a saturating concentration of the ligand (*9*). Since the extrapolation required a known K_I for the ligand, we determined K_I values of 29.5 ± 0.4 μM for propidium and 8.2 ± 0.6 nM for fasciculin 2 with human D74G AChE. These values are about 30- and 300-fold higher, respectively, than the corresponding K_I determinations with wild-type human AChE (*7*, *11*). These increases are somewhat larger than the respective 4- and 30-fold increases in K_I relative to that of the wild type previously reported for propidium and fasciculin 2, with mouse D74N AChE (*14*, *31*). The relatively low affinities of propidium and fasciculin 2 with human D74G AChE made it difficult to extrapolate their precise effects on OP phosphorylation, particularly with DEPQ. Propidium showed no inhibition of the EMPC reaction with this mutant, and both k_{OP} and K_{OP} increased when propidium was introduced (Table 2). The absence of propidium inhibition of EMPC phosphorylation also was seen with wild-type AChE (Table 2) and was noted previously to be consistent with our steric blockade model (*9*). Since this model predicts that a small peripheral site ligand like propidium will have relatively little effect on a substrate like an OP that equilibrates with the acylation site before acylation occurs, the increases in k_{OP} and K_{OP} might appear to require an additional conformational effect induced by bound propidium on the OP reactivity at the acylation site (*32*). However, these increases may arise simply from the fact that steric overlap would occur if both propidium and EMPC or DEPQ were placed in their normal binding sites in the binary AChE complexes (*9*). Molecular movement of the substrate to reduce this overlap can explain the increase in K_{OP} for both EMPC and DEPQ when propidium is bound with either wild-type or D74G AChE (Table 2), and this movement could induce strain in the bond to the OP leaving group to account for the increase in k_{OP} for EMPC (Table 2; *9*). Alternatively, this increase in k_{OP} may result from nonproductive binding of EMPC to the free enzyme, for example, with its leaving group directed inward rather than out of the active site gorge. If bound propidium interfered with EMPC binding in a nonproductive binding

configuration and thereby increased the percentage of EMPC bound in a productive mode, an increase in a (along with a corresponding increase in K_{OP}) would be expected, as seen in Table 2 for the propidium–EMPC ternary complexes. In any event, it is clear that there are mechanisms which could account for this increase in k_{OP} without invoking a propidium-induced conformational change in the acylation site.

In contrast to propidium, fasciculin 2 binding to the peripheral site dramatically decreased the phosphorylation rate constants for EMPC and DEPQ with wild-type AChE by 3–5 orders of magnitude (*9*; Table 2). We interpreted this qualitative difference from propidium to indicate that fasciculin induces a conformational change or a conformational restraint in the acylation site that reduces a (*9*). The D74G mutation appears to have an effect on the ability of fasciculin to induce this conformational change with EMPC. The value of a increased from 0.002 in the wild-type enzyme to 0.24 in D74G AChE (Table 2). Fasciculin 2 clearly inhibited the reaction of DEPQ with D74G AChE, but the maximal inhibition could not be determined. Estimates of k_{OP}/K_{OP} decreased nearly linearly with the fasciculin 2 concentration up to 10 μM, the highest concentration tested (Table 2). Because of the relatively low affinity of fasciculin 2 for the D74G enzyme, the residual free AChE dominated the reaction with DEPQ and prevented extrapolation to the very low rate constants for the reaction of DEPQ with the fasciculin 2 complex.

DISCUSSION

To understand the role of an active site residue in the AChE catalytic pathway, it is useful to determine the contribution of the residue to the affinity of substrates for the peripheral site. While this contribution can be assessed by measurements of K_S from substrate competition with fasciculin as depicted in Figure 1B, such measurements require great precision as well as a high affinity of fasciculin for the peripheral site. To develop an alternative procedure for measuring K_S in AChE mutants as well as in *Drosophila* AChE and BChE with low fasciculin affinities, we examined whether K_S can be measured directly from substrate inhibition curves as shown in Figure 1A. We show in Table 1 that K_S values can be obtained from substrate inhibition curves that agree with those from fasciculin competition if three conditions are met: (1) k_{cat} is determined independently from active site titrations; (2) K_{app} and $[E]_{tot}$ are estimated from an initial fit of the substrate inhibition curve to the Haldane equation (eq 1); and (3) simplifying assumptions are applied to Scheme 3 to decrease the independent rate constants to a number that can be fitted uniquely by a computer-assisted simultaneous equation solver. We impose the simplifying assumptions that several rate constants are unaffected by bound ligands (e.g., $a = b = 1$), are related by previous measurements in the literature (e.g., $k_2 = k_3$), or can be combined into terms (e.g., B and R/R_S) for which K_S is relatively insensitive. As future studies fit multiple v versus [S] data sets with, for example, varying concentrations of specific inhibitors, the number of independent rate constants that can be fitted uniquely should increase and eliminate uncertainties arising from the simplifying assumptions.

As a negatively charged residue in the AChE active site, D72 in principle could affect catalytic activity in several ways. First, it could contribute to a general electrostatic effect that attracts cationic substrates and inhibitors. A high net negative charge near the active site was initially demonstrated by the effects of ionic strength on k_{cat}/K_{app} for cationic substrates and on the association rate constant k_I for cationic inhibitors (*33*). Molecular modeling calculations (*34*, *35*) from the three-dimensional structure supported this notion by suggesting that the AChE catalytic subunit has a dipole moment aligned with the active site gorge that accelerates association rates for cationic ligands. The magnitude of the acceleration can be estimated as the ratio of k_I extrapolated to zero ionic strength to k_I at high ionic strength. For example, this ratio was about 7.5 for the cationic trifluoromethyl ketone TMTFA and mouse AChE (*31*). It remained about 7.1 following mutation of D74 to N, even though this mutation decreased k_I for TMTFA more than 20-fold relative to that of wild-type AChE (*31*). From this comparison, we conclude that D72 contributes very little to a general electrostatic effect on cationic ligands. This conclusion is consistent with other observations which show that negatively charged residues at or near the peripheral site contribute only modestly to the electrostatic field at the active site (*31*, *36*).

A second way in which D72 could affect catalytic activity was recently proposed from molecular modeling studies of AChE (*37*). In these Brownian dynamics simulations, the mutation D74N had little effect on the frequency of cation entry into the peripheral site but significantly decreased the likelihood that a cation in the peripheral site would move to the acylation site. The simulations predicted a 30-fold reduction of k_I for TMTFA in the D74N mutant relative to that of the wild-type enzyme, in excellent agreement with the observed 25-fold reduction. These authors proposed that D72 may act as an electrostatic anchor that traps cationic ligands entering the active site gorge (*37*). A similar proposal based on modeling calculations also has been offered (*38*). Our data provide strong experimental support for this hypothesis by showing that D72 is directly involved in a transient binding of acetylthiocholine at the peripheral site. It is likely that as a consequence of this binding k_{-S} falls below k_I in Scheme 3, ensuring that most substrate molecules that encounter the peripheral site proceed on to hydrolysis. Estimates of K_S, the equilibrium dissociation constant for this binding, can be obtained directly from the partially competitive effect of acetylthiocholine on fasciculin binding, and they can also be obtained indirectly by the application of Scheme 3 to the substrate inhibition curve for acetylthiocholine (Figure 1). Both methods agreed that K_S increased from about 1–2 mM in wild-type human AChE to about 30 mM in the D74G mutant.

The hypothesis that D72 traps entering cationic ligands revives the classic notion of an anionic site in the AChE catalytic pathway (*10*) and suggests that D72 functions as such a site. While K_S is the most direct measure of cationic substrate affinity for this anionic site, analysis according to Scheme 3 indicates that two parameters determined from eq 1, K_{app} and K_{SS}, are closely related to K_S. As noted above, mutation of D72 to G decreased k_{cat}/K_{app} by increasing the effective K_{app} without appreciable effect on k_{cat}. Mutation of D72 to G also increased the K_{SS} for acetylthiocholine and made substrate inhibition less evident. K_{SS} increased in the mutant because the level of substrate binding that gave rise to steric blockade was decreased. Therefore, according to

Scheme 3, mutations such as that in D72G that result in an increase in the K_S for substrate binding in the peripheral site (without an effect on k_{cat}) should give rise to parallel increases in K_{app} and K_{SS}. Furthermore, this loss in affinity should also be reflected in increases in K_I for cationic inhibitors specific to either the peripheral site or the acylation site, as shown by consideration of Scheme 4.

Scheme 4

$$E + I \underset{k_{-I1}}{\overset{k_{I1}}{\rightleftharpoons}} EI_P \underset{k_{-I2}}{\overset{k_{I2}}{\rightleftharpoons}} EI$$

In Scheme 4, an inhibitor first binds to the peripheral site with an equilibrium dissociation constant K_{I1}. Its partitioning between the peripheral site and the acylation site is then given by the equilibrium constant K_{I2} ($=k_{-I2}/k_{I2}$). The experimental $K_I = K_{I1}K_{I2}/(1 + K_{I2})$, and the inhibitor will be specific for the peripheral site if $K_{I2} \gg 1$ ($K_I = K_{I1}$) or for the acylation site if $K_{I2} \ll 1$ ($K_I = K_{I1}K_{I2}$). In either case, K_I is proportional to K_{I1}, and a mutation like that in D72G which we propose to increase only K_{I1} will increase the experimental K_I. Scheme 4 is consistent with experimental results. Mutations of D74 to G or N in human or mouse AChE consistently reduced the affinity of both monoquaternary ligands specific to the acylation site (edrophonium) and of cationic ligands specific to the peripheral site (propidium) by factors of about 5 (*14*, *31*, *39*). Bisquaternary ligands that bind simultaneously to both the peripheral and acylation sites are particularly sensitive to these D72 mutations and showed reductions in affinity of more than 2 orders of magnitude. K_{OP} for OPs is essentially an equilibrium constant equivalent to a K_I, and Table 2 shows that K_{OP} for cationic DEPQ increased about 12-fold for human D74G relative to that for wild-type AChE. Similar decreases in the affinity of cationic ligands for the active site of BChE were observed when D70 was mutated to G (*17*). The affinity of monoquaternary cations decreased about 10-fold relative to that of the wild-type BChE, and that of bisquaternary cations decreased about 100-fold in the D70G mutant relative to that of the wild-type BChE. To account for these data, Masson et al. (*17*) proposed a mechanism in which a cationic ligand first binds to D70 before proceeding to a second site at the base of the active site gorge. Although no data were presented to demonstrate ligand binding near D70, this proposal is very similar to that inferred here for the role of D72 in AChE.

A third possible way that D72 could affect catalytic activity is by mediating a conformational change to the acylation site when a ligand binds to the peripheral site. Such a conformational change has been proposed previously to account for inhibition of substrate hydrolysis by bound peripheral site ligands (*17*, *40*), but in our view, solid evidence supporting this proposal has been obtained for only one peripheral site ligand, fasciculin (*9*). The binding of fasciculin drastically decreased organophosphorylation rate constants for both the neutral EMPC and the cationic DEPQ by factors of nearly 10^3–10^5 (Table 2). Since OPs essentially equilibrate prior to phosphorylation of S*200* in the acylation site (*9*), this inhibition cannot result from steric blockade. We previously rationalized this unique effect of fasciculin (*9*) by referring to crystal structure analyses of fasciculin–AChE complexes (*12*, *13*). These analyses show that fasciculin 2 interacts not only with W*279* and other residues in the peripheral site but also with residues on the outer surface of the C*67*–C*94* ω-loop within 4 Å of W*84* in the acylation site, well beyond the region of the peripheral site occupied by propidium (*7*, *15*). These more extensive surface interactions provide a structural basis for an inhibitory conformational effect on the acylation site when fasciculin but not propidium is bound to the peripheral site. Data in Table 2 indicate that some of this inhibitory conformational effect is mediated by D*72*. In particular, the first-order phosphorylation rate constant in the *E*OPXI$_P$ ternary complex with fasciculin relative to the corresponding rate constant in *E*OPX alone is given by the constant a in Scheme 1, and the low value of a for the wild-type enzyme (0.002) is a direct indication of the inhibitory conformational effect of fasciculin. Since a for EMPC increased about 100-fold to 0.24 in the human D74G mutant relative to that in wild-type AChE, almost all of the inhibitory effect of fasciculin on first-order phosphorylation by EMPC was lost in the mutant. Therefore, even though D*72* does not make direct contact with fasciculin 2 according to the crystal structures, it may be important in maintaining an interaction between fasciculin and the ω-loop that is necessary to transmit the inhibitory conformational effect. Evidence supporting a role for D*72* in this interaction was provided by the 300-fold decrease in fasciculin 2 affinity in the human D74G mutant relative to that in the wild-type enzyme.

ACKNOWLEDGMENT

We are grateful to Drs. Suzanne Bon and Jean Massoulié (CNRS URA 1857, Paris, France) for the construction and expression of the *Torpedo* AChEs. We thank Dr. Pascale Marchot (CNRS Unite Propre de Recherche 9039, Marseille, France) for a sample of highly purified fasciculin 3 (*23*).

REFERENCES

1. Rosenberry, T. L. (1979) *Biophys. J. 26*, 263–290.
2. Rosenberry, T. L. (1975) Acetylcholinesterase. In *Advances in Enzymology* (Meister, A., Ed.) Vol. 43, pp 103–218, John Wiley & Sons, New York.
3. Taylor, P., and Lappi, S. (1975) *Biochemistry 14*, 1989–1997.
4. Sussman, J. L., Harel, M., Frolow, F., Oefner, C., Goldman, A., Toker, L., and Silman, I. (1991) *Science 253*, 872–879.
5. Velan, B., Barak, D., Ariel, N., Leitner, M., Bino, T., Ordentlich, A., and Shafferman, A. (1996) *FEBS Lett. 395*, 22–28.
6. Ollis, D. L., Cheah, E., Cygler, M., Dijkstra, B., Frolow, F., Franken, S. M., Harel, M., Remington, S. J., Silman, I., Schrag, J., Sussman, J. L., Verschueren, K. H. G., and Goldman, A. (1992) *Protein Eng. 5*, 197–211.
7. Szegletes, T., Mallender, W. D., and Rosenberry, T. L. (1998) *Biochemistry 37*, 4206–4216.
8. Szegletes, T., Mallender, W. D., Thomas, P. J., and Rosenberry, T. L. (1999) *Biochemistry 38*, 122–133.
9. Mallender, W. D., Szegletes, T., and Rosenberry, T. L. (1999) *J. Biol. Chem. 274*, 8491–8499.
10. Nachmansohn, D., and Wilson, I. B. (1951) *Adv. Enzymol. 12*, 259–339.
11. Eastman, J., Wilson, E. J., Cervenansky, C., and Rosenberry, T. L. (1995) *J. Biol. Chem. 270*, 19694–19701.
12. Harel, M., Kleywegt, G. J., Ravelli, R. B. G., Silman, I., and Sussman, J. L. (1995) *Structure 3*, 1355–1366.
13. Bourne, Y., Taylor, P., and Marchot, P. (1995) *Cell 83*, 503–512.
14. Radic, Z., Pickering, N. A., Vellom, D. C., Camp, S., and Taylor, P. (1993) *Biochemistry 32*, 12074–12084.

15. Barak, D., Kronman, C., Ordentlich, A., Ariel, N., Bromberg, A., Marcus, D., Lazar, A., Velan, B., and Shafferman, A. (1994) *J. Biol. Chem. 269*, 6296−6305.
16. Hosea, N. A., Radic, Z., Tsigelny, I., Berman, H. A., Quinn, D. M., and Taylor, P. (1996) *Biochemistry 35*, 10995−11004.
17. Masson, P., Legrand, P., Bartels, C. F., Froment, M.-T., Schopfer, L. M., and Lockridge, O. (1997) *Biochemistry 36*, 2266−2277.
18. Kalow, W. (1962) *Pharmacogenetics: heredity and the response to drugs*, pp 69−136, W. B. Saunders Co., Philadelphia.
19. Lockridge, O. (1990) *Pharmacol. Ther. 47*, 35−60.
20. Rosenberry, T. L., and Scoggin, D. M. (1984) *J. Biol. Chem. 259*, 5643−5652.
21. Duval, N., Bon, S., Silman, I., Sussman, J., and Massoulié, J. (1992) *FEBS Lett. 309*, 421−423.
22. Harel, M., Sussman, J. L., Krejci, E., Bon, S., Chanal, P., Massoulié, J., and Silman, I. (1992) *Proc. Natl. Acad. Sci. U.S.A. 89*, 10827−10831.
23. Marchot, P., Khelif, A., Ji, Y.-H., Masnuelle, P., and Bourgis, P. E. (1993) *J. Biol. Chem. 268*, 12458−12467.
24. Karlsson, E., Mbugua, P. M., and Rodriguez-Ithurralde, D. (1984) *J. Physiol. (Paris) 79*, 232−240.
25. Laemmli, U. K. (1970) *Nature 227*, 680−685.
26. Ellman, G. L., Courtney, K. D., Andres, J. V., and Featherstone, R. M. (1961) *Biochem. Pharmacol. 7*, 88−95.
27. Riddles, P. W., Blakeley, R. L., and Zerner, B. (1979) *Anal. Biochem. 94*, 75−81.
28. Haldane, J. B. S. (1930) *Enzymes*, p 84, Longman, New York.
29. Froede, H. C., and Wilson, I. B. (1984) *J. Biol. Chem. 259*, 11010−11013.
30. Bazelyansky, M., Robey, E., and Kirsch, J. F. (1986) *Biochemistry 25*, 125−130.
31. Radic, Z., Kirchhoff, P. D., Quinn, D. M., McCammon, J. A., and Taylor, P. (1997) *J. Biol. Chem. 272*, 23265−23277.
32. Radic, Z., and Taylor, P. (1999) *Chem.-Biol. Interact. 119−120*, 111−117.
33. Nolte, H. J., Rosenberry, T. L., and Neumann, E. (1980) *Biochemistry 19*, 3705−3711.
34. Ripoll, D. R., Faerman, C. H., Axelsen, P. H., Silman, I., and Sussman, J. L. (1993) *Proc. Natl. Acad. Sci. U.S.A. 90*, 5128−5132.
35. Antosiewicz, J., McCammon, J. A., Wlodek, S. T., and Gilson, M. K. (1995) *Biochemistry 34*, 4211−4219.
36. Shafferman, A., Ordentlich, A., Barak, D., Kronman, C., Ber, R., Bino, T., Ariel, N., Osman, R., and Velan, B. (1994) *EMBO J. 13*, 3448−3455.
37. Tara, S., Elcock, A. H., Kirchhoff, P. D., Briggs, J. M., Radic, Z., Taylor, P., and McCammon, J. A. (1998) *Biopolymers 46*, 465−474.
38. Botti, S. A., Felder, C. E., Lifson, S., Sussman, J. L., and Silman, I. (1999) *Biophys. J. 77*, 2430−2450.
39. Shafferman, A., Velan, B., Ordentlich, A., Kronman, C., Grosfeld, H., Leitner, M., Flashner, Y., Cohen, S., Barak, D., and Ariel, N. (1992) *EMBO J. 11*, 3561−3568.
40. Barak, D., Ordentlich, A., Bromberg, A., Kronman, C., Marcus, D., Lazar, A., Ariel, N., Velan, B., and Shafferman, A. (1995) *Biochemistry 34*, 15444−15452.

BI000210O

Protein Science (2000), 9:1063–1072. Cambridge University Press. Printed in the USA.

Three-dimensional structures of *Drosophila melanogaster* acetylcholinesterase and of its complexes with two potent inhibitors

MICHAL HAREL,[1] GITAY KRYGER,[1] TERRONE L. ROSENBERRY,[2] WILLIAM D. MALLENDER,[2] TERENCE LEWIS,[3] RODNEY J. FLETCHER,[3] J. MITCHELL GUSS,[1,5] ISRAEL SILMAN,[4] AND JOEL L. SUSSMAN[1]

[1]Department of Structural Biology, Weizmann Institute of Science, Rehovot 76100, Israel
[2]Department of Pharmacology, Mayo Foundation for Medical Education and Research, Department of Research, Mayo Clinic Jacksonville, Jacksonville, Florida 32224
[3]Zeneca Agrochemicals, Jealott's Hill Research Station, Bracknell, Berkshire RG12 6EY, United Kingdom
[4]Department of Neurobiology, Weizmann Institute of Science, Rehovot 76100, Israel

(RECEIVED January 3, 2000; FINAL REVISION March 24, 2000; ACCEPTED March 30, 2000)

Abstract

We have crystallized *Drosophila melanogaster* acetylcholinesterase and solved the structure of the native enzyme and of its complexes with two potent reversible inhibitors, 1,2,3,4-tetrahydro-*N*-(phenylmethyl)-9-acridinamine and 1,2,3,4-tetrahydro-*N*-(3-iodophenyl-methyl)-9-acridinamine—all three at 2.7 Å resolution. The refined structure of *D. melanogaster* acetylcholinesterase is similar to that of vertebrate acetylcholinesterases, for example, human, mouse, and fish, in its overall fold, charge distribution, and deep active-site gorge, but some of the surface loops deviate by up to 8 Å from their position in the vertebrate structures, and the C-terminal helix is shifted substantially. The active-site gorge of the insect enzyme is significantly narrower than that of *Torpedo californica* AChE, and its trajectory is shifted several angstroms. The volume of the lower part of the gorge of the insect enzyme is ~50% of that of the vertebrate enzyme. Upon binding of either of the two inhibitors, nine aromatic side chains within the active-site gorge change their conformation so as to interact with the inhibitors. Some differences in activity and specificity between the insect and vertebrate enzymes can be explained by comparison of their three-dimensional structures.

Keywords: anticholinesterase; insect acetylcholinesterase; insecticide; insecticide resistance

Acetylcholinesterase (AChE) terminates synaptic transmission at cholinergic synapses by rapid hydrolysis of the neurotransmitter, acetylcholine (Rosenberry, 1975). Due to this crucial role, it serves as the target for a broad range of chemical agents, both natural and man-made (Millard & Broomfield, 1995). These anticholinesterases include drugs for the treatment of myasthenia gravis and acute glaucoma (Taylor, 1996) and, more recently, the first generation of anti-Alzheimer drugs (Davis & Powchik, 1995; Nightingale, 1997); organophosphate (OP) nerve agents (Millard & Broomfield, 1995); and OP and carbamate pesticides, including insecticides (Casida & Quistad, 1998) and anthelmintics (Martin, 1997). Crop losses worldwide due to insects have been estimated to amount to up to 50% of total agricultural output (Shani, 1998), focusing attention on the importance of insecticide development. The rapid appearance of insecticide-resistant strains (Mukhopadhyay et al., 1997) renders insecticide development a constant battle between man and insect. In the case of insecticides directed against AChE, resistance has been shown to be due to mutations in the AChE gene (Yao et al., 1997), resulting in reduced sensitivity to OP and carbamate insecticides. Knowledge of the three-dimensional (3D) structure of insect AChE can yield information crucial both to producing improved versions of existing insecticides and in the search for new candidates. Crop spraying with insecticides exposes agricultural workers to high levels of pesticides, and the WHO estimates that this leads to 220,000 deaths annually from single short-term exposure (Veil, 1992). Chronic insecticide exposure may also have substantial deleterious effects, including psychiatric symptoms and delayed neuropathy (Moretto & Lotti, 1998). Thus, insecticide design must strive for inhibitors of insect AChE that are both efficient and selective for the insect enzyme relative to human AChE (hAChE), as well as to AChEs of other vertebrates. In the following, we

Reprint requests to: Joel L. Sussman, Department of Structural Biology, Weizmann Institute of Science, Rehovot 76100, Israel; e-mail: Joel.Sussman@weizmann.ac.il.
[5]Permanent address: Department of Biochemistry, University of Sydney, Sydney 2006, Australia.

Abbreviations: AChE, acetylcholinesterase; *Dm*AChE, *Drosophila melanogaster* acetylcholinesterase; hAChE, human acetylcholinesterase; PDB, Protein Data Bank; *Tc*AChE, *Torpedo californica* acetylcholinesterase.

report the first 3D structure of an insect AChE, that of the fruit fly, *Drosophila melanogaster* (*Dm*AChE), as well as of its complexes with two members of a novel family of potent inhibitors related to the anti-Alzheimer drug, tacrine. These structures will provide a valuable tool both for insecticide design and for understanding the structural basis for mutagenic resistance to OP and carbamate insecticides. Furthermore, taken in conjunction with our knowledge of the structures of the complexes of *Torpedo californica* AChE (*Tc*AChE) with a variety of AChE inhibitors (Harel et al., 1993, 1996), and the recently reported 3D structures of mouse AChE (mAChE) (Bourne et al., 1995, 1999) and hAChE (Kryger et al., 1998), the *Dm*AChE structure will provide a rational basis for improving the selectivity of new insecticides and, thereby, reducing their toxicity toward humans and other vertebrates.

Results and discussion

Comparison of the DmAChE and TcAChE structures

Three-dimensional structures of the vertebrate AChEs, *Tc*AChE (Sussman et al., 1991), mAChE (Bourne et al., 1995, 1999), and hAChE (Kryger et al., 1998) were determined previously, and the *Dm*AChE structure reported here is the first invertebrate AChE structure to be solved. Despite the lower 36% sequence identity of *Dm*AChE and *Tc*AChE, relative to the 53–54% sequence identity of hAChE or mAChE and *Tc*AChE (Fig. 1), their 3D structures are folded similarly, and their active sites closely overlap. The main structural differences between *Dm*AChE and *Tc*AChE are found in their external loops and in the tilt of the C-terminal helix (Fig. 2A), differences that are unlikely to affect catalytic function directly.

Like the vertebrate AChEs, *Dm*AChE belongs to the α/β hydrolase fold family, with a core of eight β-sheets connected by α-helices (Ollis et al., 1992). The root-mean-square (RMS) difference in the positions of the Cα atoms of the two structures (using 362 out of 575 residues) is 0.8 Å (see Table 1). Some regions in surface loops show up to 8 Å deviation between the *Dm*AChE and *Tc*AChE structures, mostly in areas of insertions or deletions in the sequences, i.e., 22–24, 193–198, 298–301, 353–356, 418–422, and 545–549. The active-site triad (Ser238, His440, Glu367), the oxyanion hole-forming residues (Gly150, Gly151, and Ala239), and the anionic binding site (Trp 83) overlap well with the vertebrate active site. However, the side chains show slightly different conformations than those in *Tc*AChE (Fig. 2B) (for comparison to *Tc*AChE numbering, see Table 2). A change in the shape of the acyl binding pocket results from differences in two important amino acid residues: Leu328 (Phe288 in *Tc*AChE) and Phe440 (Val400 in *Tc*AChE). These changes alter the shape of the acyl pocket, but not the total space available for inhibitors or for the acyl group of the substrate (Fig. 2C).

Table 1. *Cα RMS in Å*

	*Dm*AChE	ZAI complex	ZA complex
*Dm*AChE			
ZAI complex	0.5		
ZA complex	0.7	0.4	
*Tc*AChE[a]	0.8	0.7	0.8

[a]342 Cα used.

In *Dm*AChE, as in *Tc*AChE, the dimer is formed by two symmetry-related monomers associated through a four-helix bundle. Overlapping two helices of the bundle in *Dm*AChE and *Tc*AChE in one subunit shows a slight twist of the dimers relative to each other, with the Cα atoms of *Dm*AChE Gly55 and *Tc*AChE Gly56 being the farthest apart (8.4 Å).

A comparison of insect and vertebrate AChE sequences shows three inserts in the insect sequence (Fig. 1). The two short inserts (residues 192–199 and 297–301) are located in neighboring surface loops, while the long insert (residues 104–139) is located at the surface, adjacent to the N-terminus; only four of its residues, 136–139, are visible in the electron density map, the rest being disordered.

The active-site gorge, which spans from the outer peripheral binding site, near Trp321 (Trp279 in *Tc*AChE), ~20 Å toward the catalytic triad, deep within the molecule, is wider in *Tc*AChE than in *Dm*AChE. Furthermore, the trajectory of the gorge is shifted by several angstroms (Fig. 3). This shift is the result of changes in several amino acid residues. Thus, replacement of Asp72 in *Tc*AChE by Tyr71 in *Dm*AChE, of Tyr121 in *Tc*AChE by Met153 in *Dm*AChE, and of Phe330 in *Tc*AChE by Tyr370 in *Dm*AChE, have a synergistic effect, resulting in the narrow "neck" of the gorge being shifted by up to 4.5 Å (see Figs. 3, 4). The volume of the active-site gorge below this "neck" in *Dm*AChE is about 50% of that of the equivalent portion of the gorge in *Tc*AChE, as assessed by the program VOIDOO (Kleywegt & Jones, 1994). This is due in part to a shift in the position of the indole ring of the principal "anionic" site residue, Trp83 (Figs. 2B, 3) and the replacement of Asp72 in *Tc*AChE by Tyr71 in *Dm*AChE.

The potential surface of *Dm*AChE is similar to that of other AChE molecules (Felder et al., 1997; Botti et al., 1998) and shows grouping of negative charges on the face of the molecule containing the opening to the active-site gorge and of positive charges on the opposite face (Fig. 5A). The direction of the molecular dipole moment is approximately along the axis of the active-site gorge, as is the case in other AChE structures (Fig. 5B).

Binding of inhibitors to insect AChE

The synthetic compound, 1,2,3,4-tetrahydro-*N*-(3-iodophenylmethyl)-9-acridinamine (ZAI, see Fig. 6) is a powerful anticholinesterase, with an apparent K_i = 1.09 nM for the highly homologous *Musca domestica* (house fly) AChE (C. Personeni & T. Lewis, unpubl. obs.). It makes intimate contacts with several aromatic residues in the active-site gorge of *Dm*AChE (Fig. 7A). The tacrine moiety of ZAI occupies a position in the gorge similar to that which it occupies in the *Tc*AChE:tacrine complex (Harel et al., 1993), and makes planar π–π interactions with Trp83 and Tyr370. The interplanar distances are shorter than 3.7 Å. An edge-on 3.4 Å aromatic interaction is formed between Trp472 and the saturated ring of the tacrine moiety, and there is a 3.2 Å interaction between the iodine atom and Phe330. Another π–π planar interaction, with a distance of 3.8 Å, occurs between the phenyl moiety of the inhibitor and Tyr71. An edge-on aromatic interaction of 3.9 Å occurs between the phenyl moiety and Tyr374.

Nine aromatic residues in the active-site gorge change their conformation upon insertion of the inhibitor. The side chains of residues Tyr71, Trp83, Tyr324, Phe330, Tyr370, Phe371, Tyr374, Trp472, and His480 all move so as to permit the inhibitor to be accommodated (Fig. 7B).

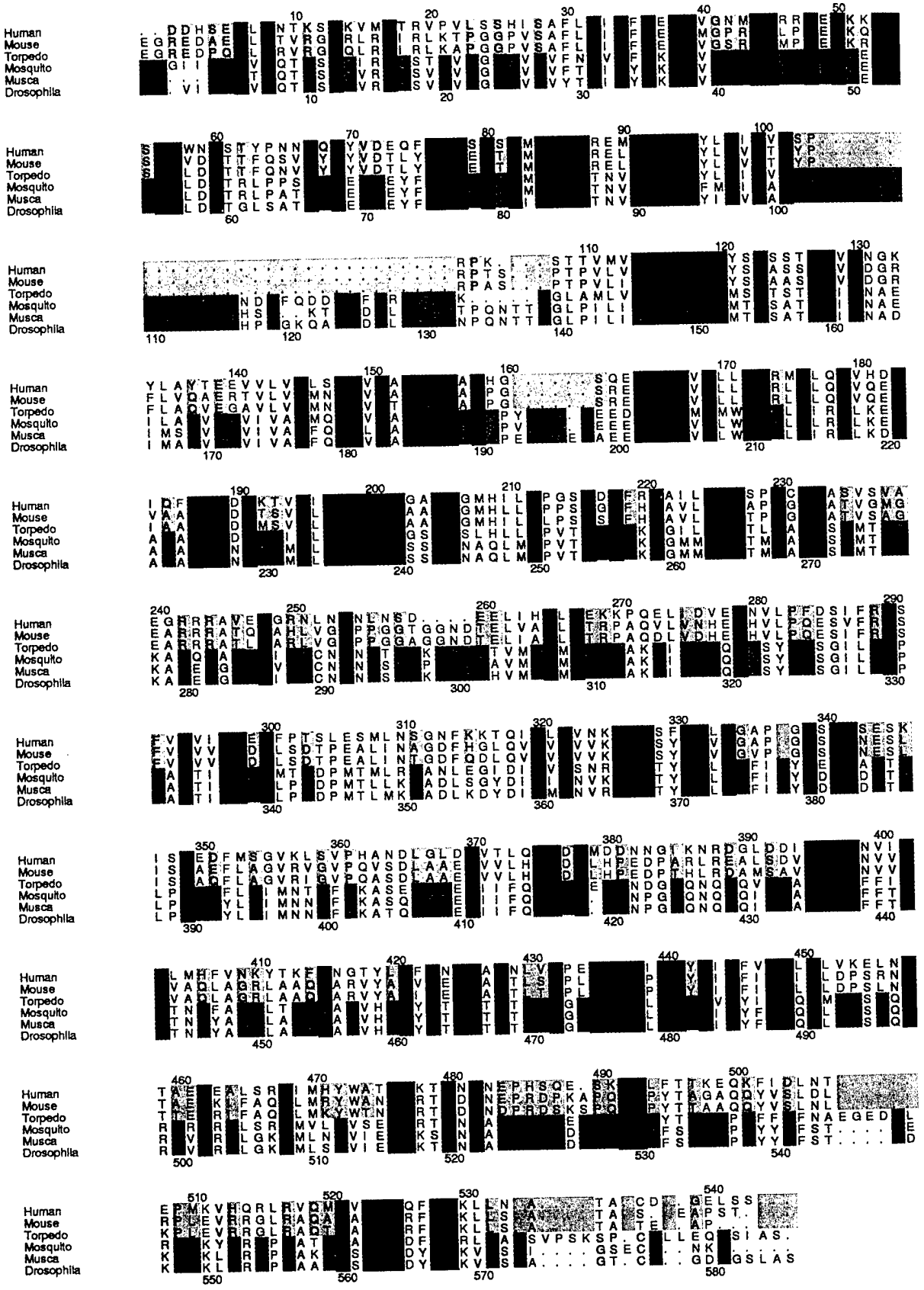

Fig. 1. Alignment of three vertebrate and three insect AChE sequences. Red, insect/vertebrate identity; yellow, insect/vertebrate similarity; blue, vertebrate only identity or similarity; green, insect only identity or similarity; *Tc*AChE numbering shown along the top line, and *Dm*AChE numbering along the bottom.

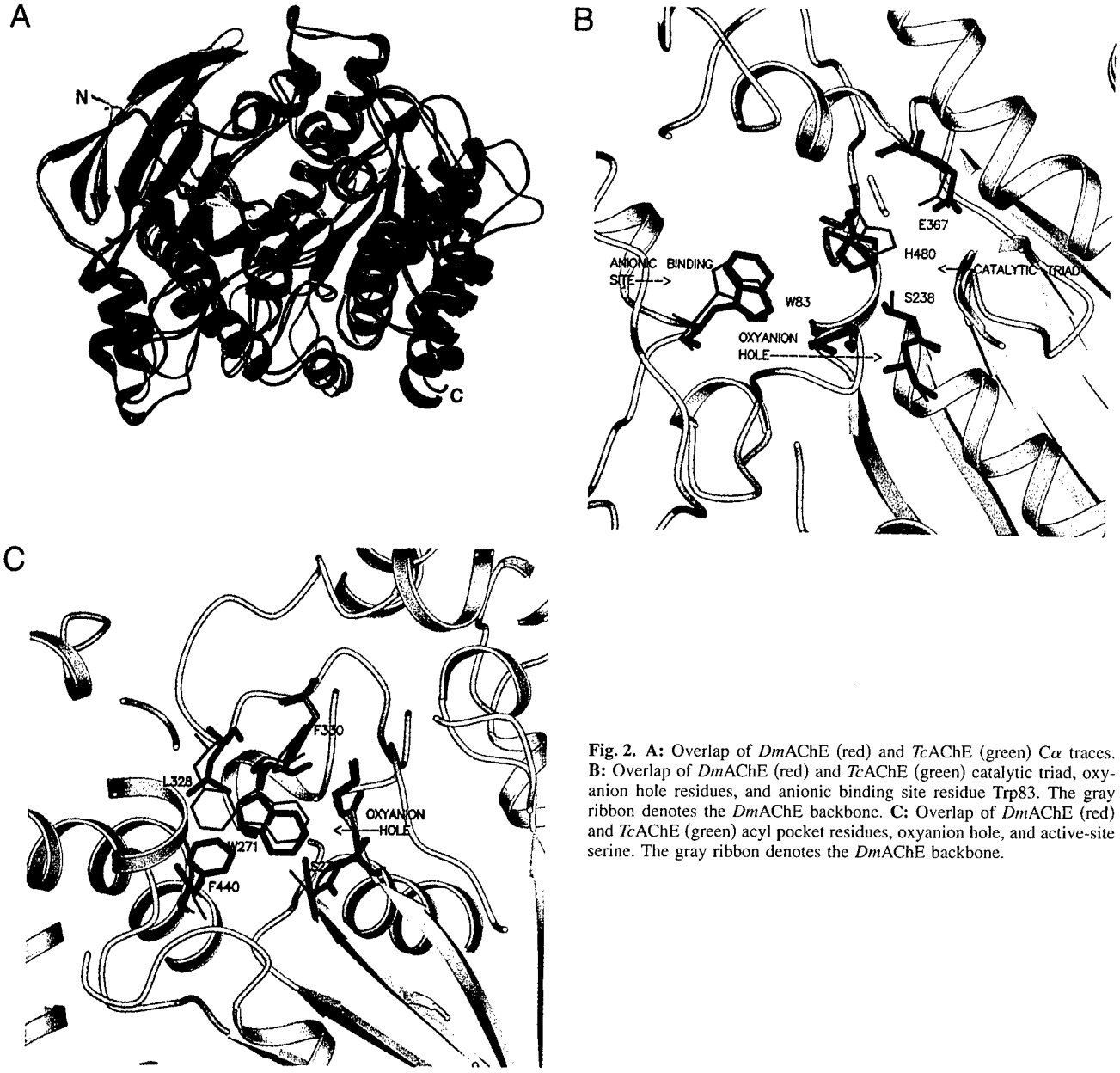

Fig. 2. A: Overlap of *Dm*AChE (red) and *Tc*AChE (green) Cα traces. **B:** Overlap of *Dm*AChE (red) and *Tc*AChE (green) catalytic triad, oxyanion hole residues, and anionic binding site residue Trp83. The gray ribbon denotes the *Dm*AChE backbone. **C:** Overlap of *Dm*AChE (red) and *Tc*AChE (green) acyl pocket residues, oxyanion hole, and active-site serine. The gray ribbon denotes the *Dm*AChE backbone.

Two peaks greater than 3.6σ are seen in the difference electron density map. The first is at the position of the iodine atom on the phenyl ring of ZAI, and the other is 1.8 Å from the catalytic triad residue, Ser238 OG. Upon refinement, the inhibitor iodine displayed a negative difference electron density peak, and a temperature factor much higher than that of the rest of the atoms in the inhibitor. Decreasing the occupancy of the iodine atom to 0.5 eliminated the negative peak and brought the temperature factor close to those of the phenyl ring atoms. This may be interpreted as implying that some of the iodine atoms are being lost. This putative cleavage, resulting in loss of ~50% of the iodine atoms, might be due to the intense X-ray radiation (Beamline XRD, Elettra Synchrotron, Trieste), causing cleavage of the C-I bond in a way analogous to cleavage of the Cys254–Cys265 bond in *Tc*AChE observed on the undulator beamline, ID14-EH4, at the European Synchrotron Radiation Facility (Grenoble) (Weik et al., 2000). We assume that the iodine is replaced by a hydroxyl group rather than by a hydrogen atom. This assumption is based on our finding that, upon refinement of the complex of *Dm*AChE with 1,2,3,4-tetrahydro-*N*-(phenylmethyl)-9-acridinamine (ZA; see Fig. 6), which lacks the iodine atom present in ZAI, the phenyl group occupies a position different from that which it occupies in the ZAI–*Dm*AChE complex, although the tacrine moiety occupies approximately the same position (see Fig. 7C). Furthermore, we do not observe disorder in the position of the iodophenyl group in ZAI–*Dm*AChE. Such disorder would be expected if the iodine were replaced by a proton, thus converting some of the ZAI molecules to ZA. A second argument in favor of I–OH exchange is the fact that in the ZAI–*Dm*AChE complex there is a water molecule 2.54 Å from the iodine atom. This distance is perfect for a –OH···water hydrogen

Table 2. *Active-site gorge residues from the bottom of the gorge to its entrance*

*Dm*AChE	*Tc*AChE
Tyr162	Tyr130
Ile484	Ile444
Tyr148	Tyr116
Glu237	Glu199
Gly481	Gly441
Gly149	Gly117
Ser238	Ser200
Gly155	Gly123
Trp83	Trp84
Gly150	Gly118
His480	His440
Thr 154	Ser122
Gly151	Gly119
Trp472	Trp432
Glu80	Ser81
Trp271	Trp233
Tyr370	Phe330
Met153[a]	Tyr121
Phe371	Phe331
Leu328	Phe288
Phe330	Phe290
Arg70[a]	Val71[a]
Tyr71	Asp72
Glu69	Tyr70
Tyr374	Tyr334
Trp321	Trp279
Glu72	Glu73
Tyr324	Leu282
Tyr73	Gln 74
Asp375	Gly33

[a]Only main-chain atoms flank the gorge.

bond, but too close for an iodine···water bond. A search through the Cambridge Data Base retrieved two well-determined X-ray structures with iodobenzene···water distances of 4.4 Å (T. Steiner, pers. comm.). While Trp83 is in the same conformation in the ZA complex as in the ZAI complex, making a π–π stacking interaction with the tacrine moiety, Tyr370 assumes a different conformation (Fig. 7C). Tyr71 is, however, in the same conformation as in the ZAI complex, though the different position of the phenyl moiety of ZA precludes it from taking part in a π–π interaction. His480 assumes two alternate conformations, both different from its conformation in the native enzyme.

The high positive difference peak seen in the oxyanion hole, near Ser238 OG, when refined as a water molecule, showed excess positive density and a temperature factor of 2 Å^2 (the minimum value specified in CNS (Brünger et al., 1997, 1998)). Although absent in the native *Dm*AChE electron density map, it is present in the ZA as well as in the ZAI complex. It was refined as a noncovalently bound sulfate ion. The assignment of sulfate to this peak was based on its tetrahedral shape and on the fact that sulfate is present in the crystallization medium.

Insect vs. vertebrate AChE: Structure-based differences in activity

The active-site gorge of AChE is coated with aromatic side chains (13 in *Dm*AChE; 14 in *Tc*AChE), which interact with its various inhibitors via noncovalent interactions (Harel et al., 1993, 1996; Kryger et al., 1999). These side chains render the gorge pliable in accommodating inhibitors by swinging to assume different conformations, thus widening or narrowing the gorge to allow passage and lodgment of inhibitors, with little or no concomitant movement of main-chain atoms. This implies that the relative narrowness of the *Dm*AChE gorge (Fig. 3A,B) cannot, as such, be taken advantage of in the design of inhibitors selective for insect AChE.

The primary candidates for achieving inhibitor selectivity are the eight residues clustered near the opening of the gorge, which differ in the insect and vertebrate sequences. The largest differences, which are potential targets for inhibitor selectivity, are in Tyr71, Tyr73, Glu80, and Asp375, which are Asp, Gln, Ser, and Gly, respectively, in vertebrates. However, differences in residues that do not line the gorge, but interact with gorge residues (i.e., second shell), may play a role in influencing selectivity, as discussed below.

One of the known differences between vertebrate and insect AChEs is the latter's ability to hydrolyze substrates with larger acyl moieties, for example, butyrylcholine (Gnagey et al., 1987). A possible reason for this difference is that in the vertebrate acyl binding pocket, the residues equivalent to Leu328 and Phe371 in *Dm*AChE (Phe288 and Phe331 in *Tc*AChE) are both phenylalanines and form a rigid π–π stacking pair. The maximal difference in dihedral angles of residue Phe331 in *Tc*AChE, and in six of its refined complexes, is $\Delta\chi1 = 11°$; $\Delta\chi2 = 13°$. In *Dm*AChE, residue 328 is a leucine, and the rigid π–π stacking is lost (though the total aromatic nature of the pocket is maintained by the "gain" of Phe440). The loss of rigid stacking renders Phe371 more mobile, thus enabling the insect acyl binding pocket to accommodate larger moieties. The corresponding maximum differences in dihedral angles for residue Phe371 in *Dm*AChE, and for four of its refined complexes (these include two recently refined unpublished complexes), are $\Delta\chi1 = 26°$; $\Delta\chi2 = 34°$. Furthermore, mutagenesis of the same residue in hAChE, i.e., Phe295Leu, increased its activity on butyrylcholine, relative to its activity on acetylcholine, by more than 100-fold (Ordentlich et al., 1993; Vellom et al., 1993). Hence, we predict that a Leu328Phe mutation in *Dm*AChE should reduce its capacity to hydrolyze butyrylcholine. This prediction will be tested by site-directed mutagenesis.

Resistance to anticholinesterase insecticides from a structural viewpoint

Four natural mutations have been identified in insect AChEs (Fournier et al., 1993; Yao et al., 1997), which confer resistance to insecticides in both *Drosophila* and in *Musca*: Gly265Ala, Phe330Tyr, Ile161Val, and Phe77Ser. (1) Gly265 is conserved across both insects and vertebrates (see Fig. 1). The Gly265Ala mutation is not in the active-site gorge, but in a second shell. We propose that the additional methyl group points toward the active-site Ser238 and thus affects catalysis. (2) The Phe330Tyr mutation is in the array of aromatics lining the acyl pocket. Phe330 is also conserved throughout other invertebrates as well as vertebrates. The additional OH of Tyr330 would be lodged in the acyl binding pocket, reduce its size, and hence its capacity to bind inhibitors. (3) The

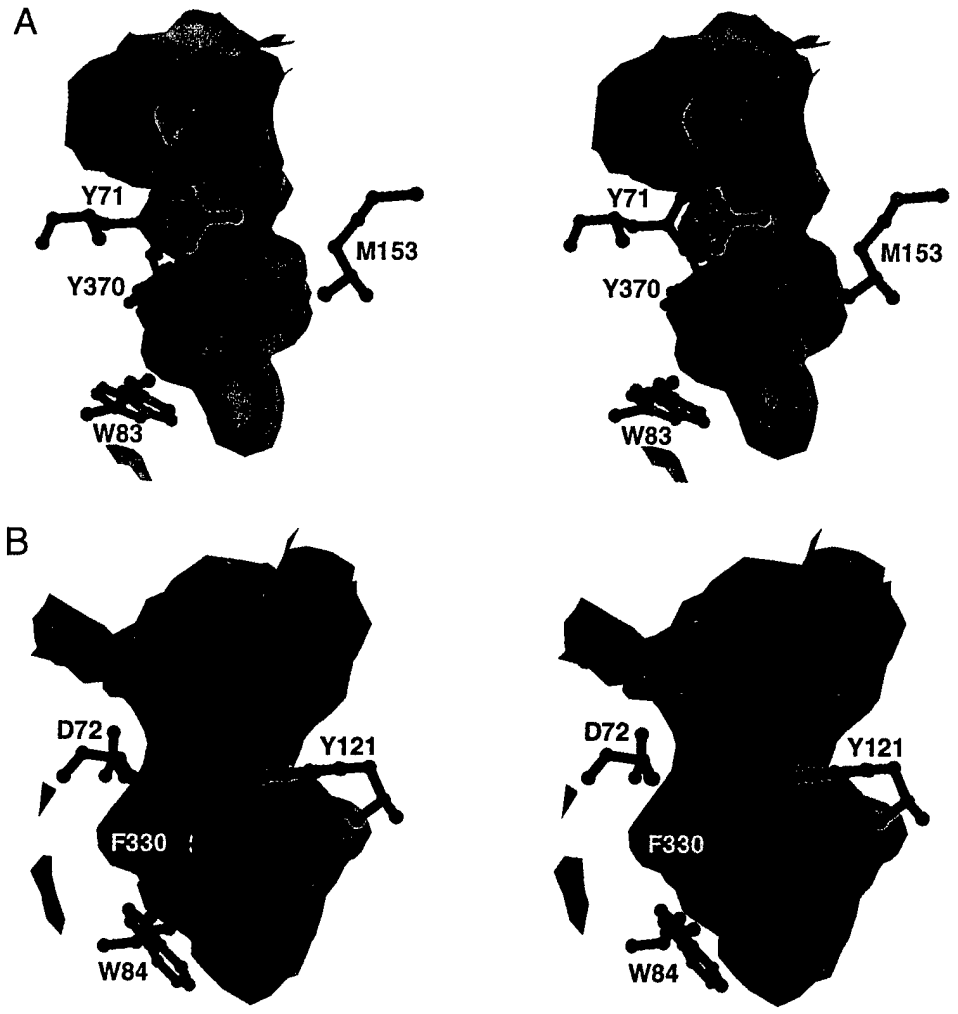

Fig. 3. Stereoviews of the active-site gorges of *Dm*AChE and *Tc*AChE. The accessible surfaces are rendered semi-transparent using the program DINO (Philippsen, 2000). Residues that significantly influence the trajectory and volume (see text) are shown as ball and stick. **A:** The active-site gorge of *Dm*AChE. **B:** The active-site gorge of *Tc*AChE. Residue Phe330 is on the far side of the surface.

Ile161Val mutation is also in the second shell. Valine is found in this position in vertebrates (see Fig. 1). Residue 161 has some interactions with the key "anionic" site residue, Trp83. Comparison of the *Dm*AChE structure with the vertebrate structures shows that the isoleucine is in somewhat closer contact than the valine with Trp83 (3.8 vs. 4.0 Å). This may have an effect on the mobility of Trp83 or on its electrostatic properties. (4) Phe77, which is another residue conserved across species, is also in the second shell. It forms an end-on π–π interaction with the active-site gorge residue Trp472; mutating it to serine eliminates this interaction and, apparently, alters the structure of the active-site gorge.

Materials and methods

Preparation of recombinant DmAChE

Construction of a secreted form of *Dm*AChE, transfection of *Drosophila* Schneider Line 2 cells, and selection of stable cell lines were accomplished as described previously (Incardona & Rosenberry, 1996). The S2-SEC 1/3 clone was maintained at high cell density in Schneider's *Drosophila* medium (Life Technologies, Inc., Rockville, Missouri) for production of secreted *Dm*AChE. Medium was removed every 10–14 days, and *Dm*AChE was purified by two cycles of affinity purification on an acridinium resin (Rosenberry & Scoggin, 1984). Briefly, after loading the *Dm*AChE-medium over a 15–50 mL affinity column, the resin was washed with buffers containing 10 mM sodium phosphate, pH 7, in four stages, to remove impurities. The four buffers consisted of (1) 5–10 column volumes of 10 mM sodium phosphate, pH 7, only; (2) two to three column volumes of buffer with the addition of 500 mM NaCl; (3) 5–10 column volumes of buffer with 50 mM NaCl and 0.1% Triton X-100 added; (4) 5–10 column volumes of buffer with the addition of 20 mM NaCl. Purified *Dm*AChE was eluted from the column by ligand competition, using a solution of 5 mM sodium phosphate, pH 7, containing 5 mM decamethonium bromide (Sigma Chemical Co., St. Louis, Missouri), and 0.1% Triton X-100. Fractions containing purified *Dm*AChE were identified by a spectrophotometric activity assay (Ellman et al., 1961) and pooled for dialysis against 10 mM sodium phosphate, pH 7, to remove the decamethonium. The enzyme was then subjected to a

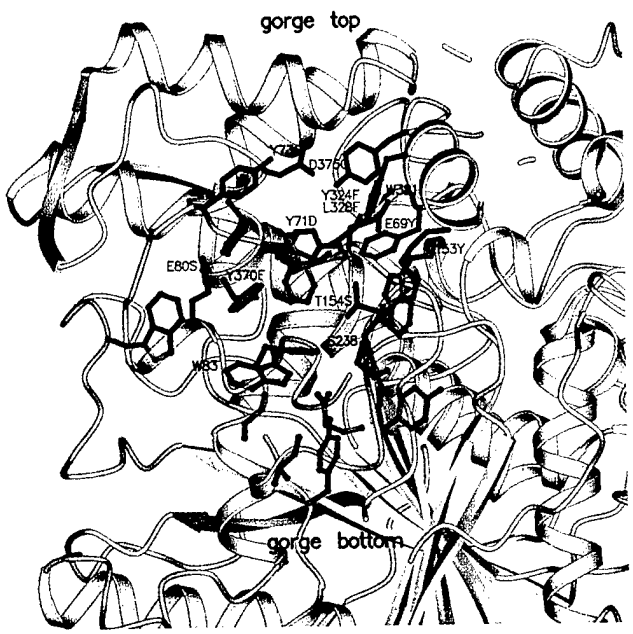

Fig. 4. Active-site gorge flanking residues in *Dm*AChE. Residues identical in vertebrate and insect are shown in green; different residues shown in red. For those residues labeled, the letter preceding the residue number corresponds to *Dm*AChE, and the letter following it corresponds to *Tc*AChE.

second round of affinity purification, using the same washing protocol, but eluting with a decamethonium solution that did not contain Triton X-100. Purified recombinant *Dm*AChE samples analyzed by SDS-polyacrylamide gel electrophoresis (Laemmli, 1970) displayed no detectable contaminants. In the presence of reducing agents, a prominent band of 70 kDa monomer and minor bands corresponding to 55 and 16 kDa fragments were obtained. The smaller fragments are the result of the same proteolytic processing observed for native *Dm*AChE (Gnagey et al., 1987). In the absence of reducing agents, bands of 140 kDa homodimers (viz. two 70 kDa subunits) and 125 kDa heterodimers (viz. one 70 kDa subunit and one 55 kDa fragment) were seen (Incardona & Rosenberry, 1996).

Data collection, structure determination, and refinement

*Dm*AChE crystals were grown by the hanging drop method at 19 °C from a 4 mg/mL protein solution diluted 1:1 with the reservoir solution, whose composition was 13% MPEG2000/0.1 M ammonium sulfate/0.03 M leucine/0.1 M acetate, pH 4.6. Crystals grew in four to five days as trigonal prisms, 0.2 mm in size, space group $P4_32_12$ (enantiomorph chosen from the structure solution). The crystals of the complexes were obtained by cocrystallization. In the case of ZAI (Fig. 6), the mother liquor contained 2% of a saturated solution of the ligand in DMSO; in the case of ZA, it contained 2% of a saturated solution of the ligand in 75% methanol. In both cases, the crystals obtained were isomorphous with the native *Dm*AChE crystals (see Table 3).

X-ray data for the native crystal and for the ZAI complex were collected at the Elettra synchrotron in Trieste, on beamline XRD, at 100 K, using 20% sucrose as cryoprotectant. The data were

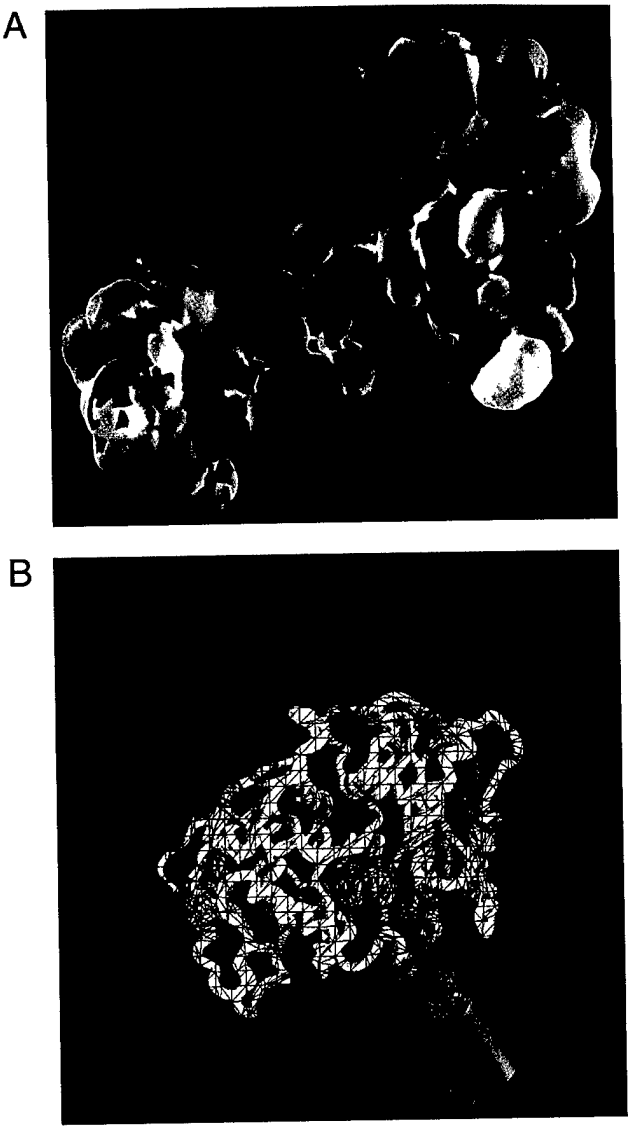

Fig. 5. A: Representation of solvent-accessible molecular surface. The entrance to the active-site gorge is centered within the large red area near the top left. Color coding represents electrostatic potential surfaces: 2.5 kT/e in blue and −2.5 kT/e in red. **B:** Schematic drawing of the ±0.25 kT/e isopotential surface of *Dm*AChE. Orientation is the same as in **A**, and the green arrow denotes the direction of the dipole moment.

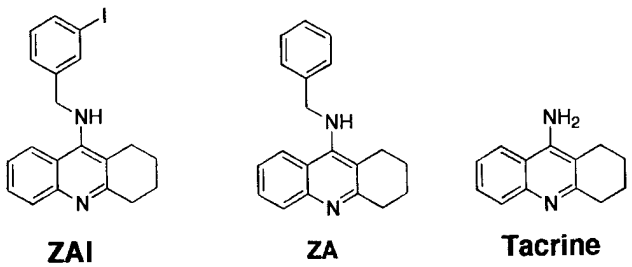

Fig. 6. Chemical formulas of reversible AChE inhibitors: ZAI, ZA, and tacrine.

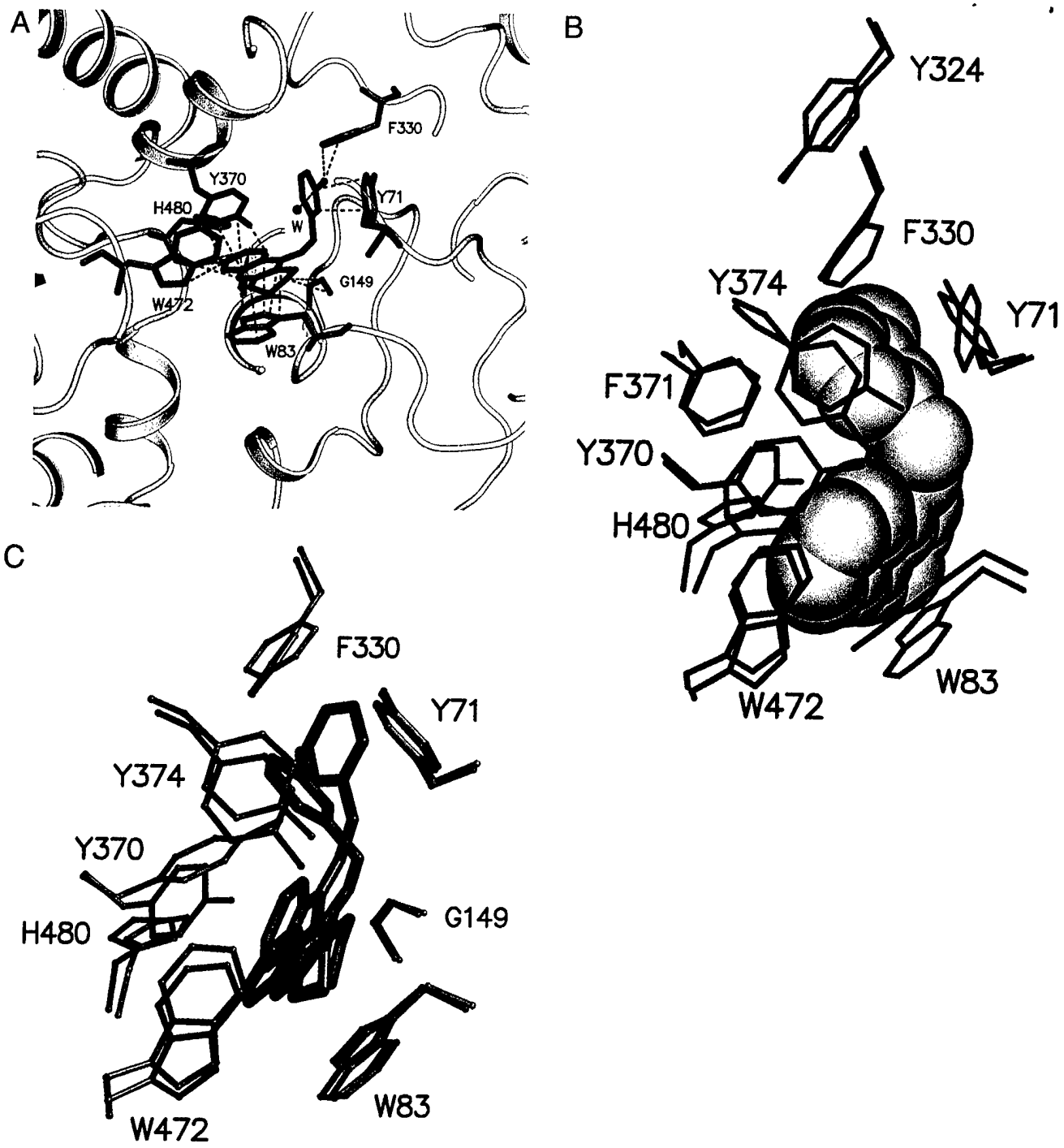

Fig. 7. Representations of interactions of *Dm*AChE with ZAI and ZA. **A:** *Dm*AChE residues (turquoise) interacting with ZAI (red) with distances <3.8 Å. **B:** Nine aromatic residues in native *Dm*AChE (black) change their conformation when ZAI (red), shown with its van der Waals surface, binds to *Dm*AChE. **C:** Overlap of ZAI complex (red) and ZA complex (turquoise). The inhibitors are shown as thick sticks, and the side chains of the principal residues with which they interact as thin sticks.

integrated, scaled, and reduced with DENZO and SCALEPACK (Otwinowski & Minor, 1997). A molecular replacement solution was found using the program AMoRe (Navaza, 1994) of the program suite CCP4 (Bailey, 1994).

The solution, using the *Tc*AChE monomer as a search model, and 10 − 4 Å resolution data, showed a monomer in the asymmetric unit, with *R*-factor = 53%, correlation coefficient = 30%. The packing in space group $P4_32_12$ reveals the familiar AChE dimer (Sussman et al., 1991), with a disulfide bridge between the COOH-terminal Cys577 residues. Despite a sequence identity of *Dm*AChE to *Tc*AChE and to hAChE of 37 and 36%, respectively (Fig. 1), refinement of the *Dm*AChE structure, starting from the

Table 3. *Data collection and refinement*

	Native	Complex ZAI	Complex ZA	Derivative Xe
Space group, mol/AU	$P4_32_12$, 1	$P4_32_12$, 1	$P4_32_12$, 1	$P4_32_12$, 1
Unit cell axes $a = b,c$ (Å)	94.34, 159.0	94.93, 160.02	95.81, 162.03	94.33, 158.9
X-ray source	Elettra, Trieste, XRD	Elettra, Trieste, XRD	NSLS, BNL, X12C	Elettra, Trieste, XRD
Wavelength (Å)	1.0	1.0	0.98	1.0
Resolution range (Å)	30–2.70	30–2.72	30–2.70	30–2.72
Data collection temperature (K)	100	100	100	100
Cryoprotectant	20% sucrose	20% sucrose	20% sucrose	20% sucrose
No. of unique reflections	20,200	19,982	21,076	20,182
Completeness (%)	99.1 (98.8)[a]	96.8 (99.2)[a]	97.7 (84.4)[a]	99.3 (99.9)[a]
R_{sym} (on I) (%)	5.0 (16.1)[a]	6.0 (25.4)[a]	3.8 (27.4)[a]	6.3 (39.5)[a]
$I/\Sigma(I)$	33.5 (5.8)[a]	15.5 (2.4)[a]	24.3 (3.2)[a]	23.7 (3.7)[a]
Rcullis (centric)	—	—	—	73%
Phasing power (centric)	—	—	—	0.87
Rcullis (acentric)	—	—	—	83%
Phasing power (acentric)	—	—	—	1.20
Figure of merit (centric)	—	—	—	0.52
No. of protein atoms	4,216	4,246	4,207	—
No. of solvent atoms	137	165	97	—
No. of sugars	6	5	5	—
No. of sulfate ions	—	1	1	—
R_{fact} (R_{free}) $F > 0\sigma$	25.8% (30.1%)	22.0% (26.5%)	22.0% (26.3%)	—
RMS from ideality[b]				
Bond length (Å)	0.009	0.008	0.007	—
Bond angle (Å)	1.670	1.425	1.463	—
Average B values (Å^2)	53.8	53.3	50.8	—
Ramachandran plot[c]				
Favord	77.2%	84.9%	85.1%	—
Allowed	20.9%	13.7%	13.7%	—
Generously allowed	1.7%	0.9%	0.9%	—
Disallowed	0.2%	0.7%	0.4%	—

[a]Statistics for outer shell 2.8–2.7 Å data in parentheses.
[b]Calculated by program WHATCHECK (Vriend, 1990).
[c]Calculated by program PROCHECK (Laskowski et al., 1993).

*Tc*AChE model (Raves et al., 1997) (PDB IDCode 2ACE), resulted in a model whose R-factor did not refine below 35%.

A single suitable heavy atom derivative was found by immersing a native *Dm*AChE crystal in a chamber containing gaseous xenon at 5 bar pressure for 1 min, as described by Sauer and coworkers (Sauer et al., 1997). X-ray data were collected as described above for the native crystal. The crystal of the Xe derivative was isomorphous with the native crystal (see Table 3). The locations of two Xe atoms were determined with the program FFT and refined with the program MLPHARE, from the program suite CCP4 (Bailey, 1994), and with HEAVY_SEARCH from the program suite CNS (Brünger et al., 1997, 1998). Both programs yielded the same two Xe sites, which were used for the phasing with their anomalous contribution (Table 3). The ZAI complex, which contains iodine, was designed and synthesized to aid in phasing; it did not, however, yield useful heavy atom phasing information and was solved and refined in parallel to the native structure.

The structures were refined in the resolution range of 30–2.7 Å, using the maximum likelihood, slow cooling, and optimum combination of coordinate files that produced a minimum free R-value from the averaged structure factors using the CNS package (Brünger et al., 1997, 1998). The Fobs were scaled anisotropically, and a bulk solvent correction was applied (Brünger et al., 1997, 1998). Of particular help in solution of the structure was the composite anneal omit map produced by CNS (Brünger et al., 1997, 1998).

The structures were fitted into the electron density with the program O (Jones et al., 1991). Residues 1–2, 104–135, 575–586 in the native *Dm*AChE structure, residues 103–135, 574–586 in the ZAI complex structure, and residues 1–2, 103–136, 574–586 in the ZA complex do not lie in any significant electron density. The largest insert in the *Dm*AChE sequence, relative to *Tc*AChE, is residues 104–140 (Fig. 1). No electron density is observed for this insert, except for four residues at its C-terminus.

Because the refined *Dm*AChE-ZAI complex structure showed some unexplained electron density at the active site, a similar inhibitor, ZA, in which the iodine atom had been replaced by a hydrogen (Fig. 6), was cocrystallized with *Dm*AChE. X-ray data were collected on beamline X12C of the NSLS, at Brookhaven National Laboratory, at a wavelength of 0.98 Å, at 100 K, using 20% sucrose as cryoprotectant. This structure was solved by molecular replacement, starting from the *Dm*AChE-ZAI structure.

The refined structures were analyzed with program PROCHECK (Laskowski et al., 1993). The figures were generated with the programs ALSCRIPT (Barton, 1993), MOLSCRIPT (Kraulis, 1991), BOBSCRIPT (Esnouf, 1999), DINO (Philippsen, 2000), GRASP (Nicholls et al., 1991), and RASTER3D (Merritt & Bacon, 1997).

The atomic coordinates and structure factors for the native structure, and for the complexes with ZAI and ZA have been deposited at the PDB and have ID codes 1qo9, 1qon, and 1dx4, respectively.

Acknowledgments

This work was supported by the U.S. Army Medical Research Acquisition Activity under Contract No. DAMD17-97-2-7022, the European Union IVth Framework in Biotechnology, the Kimmelman Center for Biomolecular Structure and Assembly, Israel, the Nella and Leon Benoziyo Center for Neurosciences, the Dana Foundation, and the generous support of Tania Friedman. T.L.R. and W.D.M. acknowledge the support of NIH Grant NS-16577. I.S. is Bernstein–Mason Professor of Neurochemistry. Special thanks to Cristoph Kratky, Oliver Sauer, and Ulrike Wagner (University of Graz), for helping us to obtain the Xe heavy atom derivative, and Ansgar Philippsen for help in preparation of the figures.

References

Bailey S. 1994. The CCP4 suite: Programs for protein crystallography. *Acta Crystallogr D50*:760–763.

Barton GJ. 1993. ALSCRIPT, a tool to format multiple sequence alignments. *Protein Eng 6*:37–40.

Botti SA, Felder CE, Sussman JL, Silman I. 1998. Electrotactins: A class of adhesion proteins with conserved electrostatic and structural motifs. *Protein Eng 11*:415–420.

Bourne Y, Taylor P, Bougis PE, Marchot P. 1999. Crystal structure of mouse acetylcholinesterase. A peripheral site-occluding loop in a tetrameric assembly. *J Biol Chem 274*:2963–2970.

Bourne Y, Taylor P, Marchot P. 1995. Acetylcholinesterase inhibition by fasciculin: Crystal structure of the complex. *Cell 83*:503–512.

Brünger AT, Adams PD, Clore GM, DeLano WL, Gros P, Grosse-Kunstleve RW, Jiang JS, Kuszewski J, Nilges M, Pannu NS, et al. 1998. Crystallography & NMR system: A new software suite for macromolecular structure determination. *Acta Crystallogr D54*:905–921.

Brünger AT, Adams PD, Rice LM. 1997. New applications of simulated annealing in X-ray crystallography and solution NMR. *Structure 5*:325–336.

Casida JE, Quistad GB. 1998. Golden age of insecticide research: Past, present, or future? *Annu Rev Entomol 43*:1–16.

Davis KL, Powchik P. 1995. Tacrine. *Lancet 345*:625–630.

Ellman GL, Courtney KD, Andres V Jr, Featherstone RM. 1961. A new and rapid colorimetric determination of acetylcholinesterase activity. *Biochem Pharmacol 7*:88–95.

Esnouf RM. 1999. Further additions to MolScript version 1.4, including reading and contouring of electron-density maps. *Acta Crystallogr D55*:938–940.

Felder CE, Botti SA, Lifson S, Silman I, Sussman JL. 1997. External and internal electrostatic potentials of cholinesterase models. *J Mol Graphics Modelling 15*:318–327.

Fournier D, Mutero A, Pralavorio M, Bride J-M. 1993. *Drosophila* acetylcholinesterase: Mechanisms of resistance to organophosphates. *Chem Biol Interact 87*:233–238.

Gnagey AL, Forte M, Rosenberry TL. 1987. Isolation and characterization of acetylcholinesterase from *Drosophila*. *J Biol Chem 262*:13290–13298.

Harel M, Quinn DM, Nair HK, Silman I, Sussman JL. 1996. The X-ray structure of a transition state analog complex reveals the molecular origins of the catalytic power and substrate specificity of acetylcholinesterase. *J Am Chem Soc 118*:2340–2346.

Harel M, Schalk I, Ehret-Sabatier L, Bouet F, Goeldner M, Hirth C, Axelsen P, Silman I, Sussman JL. 1993. Quaternary ligand binding to aromatic residues in the active-site gorge of acetylcholinesterase. *Proc Natl Acad Sci USA 90*:9031–9035.

Incardona JP, Rosenberry TL. 1996. Construction and characterization of secreted and chimeric transmembrane forms of *Drosophila* acetylcholinesterase: A large truncation of the C-terminal signal peptide does not eliminate glycoinositol phospholipid anchoring. *Mol Biol Cell 7*:595–611.

Jones TA, Zou J-Y, Cowan SW, Kjeldgaard M. 1991. Improved methods for building protein models in electron density maps and the location of errors in these models. *Acta Crystallogr A47*:110–119.

Kleywegt GJ, Jones TA. 1994. Detection, delineation, measurement and display of cavities in macromolecular structures. *Acta Crystallogr D50*:178–185.

Kraulis P. 1991. MOLSCRIPT: A program to produce both detailed and schematic plots of protein structure. *J Appl Crystallogr 24*:946–950.

Kryger G, Giles K, Harel M, Toker L, Velan B, Lazar A, Kronman C, Barak D, Ariel N, Shafferman A, et al. 1998. 3D Structure at 2.7Å resolution of native and E202Q mutant human acetylcholinesterase complexed with fasciculin-II. In: Doctor BP, Taylor P, Quinn DM, Rotundo RL, Gentry MK, eds. *Structure and function of cholinesterases and related proteins*. New York: Plenum. pp 323–326.

Kryger G, Silman I, Sussman JL. 1999. Structure of acetylcholinesterase complexed with E2020 (Aricept®): Implications for the design of new anti-Alzheimer drugs. *Structure 7*:297–307.

Laemmli UK. 1970. Cleavage of structural proteins during the assembly of the head of bacteriophage T4. *Nature 227*:680–685.

Laskowski RA, MacArthur MW, Moss D, Thornton JM. 1993. PROCHECK: A program to check the stereochemical quality of protein structures. *J Appl Crystallogr 26*:283–291.

Martin RJ. 1997. Modes of action of anthelmintic drugs. *Vet J 154*:11–34.

Merritt EA, Bacon DJ. 1997. Raster3D—Photorealistic molecular graphics. *Methods Enzymol 277*:505–524.

Millard CB, Broomfield CA. 1995. Anticholinesterases: Medical applications of neurochemical principles. *J Neurochem 64*:1909–1918.

Moretto A, Lotti M. 1998. Poisoning by organophosphorus insecticides and sensory neuropathy. *J Neurol Neurosurg Psychiatry 64*:463–468.

Mukhopadhyay AK, Karmakar P, Hati AK, Dey P. 1997. Recent epidemiological status of malaria in Calcutta Municipal Corporation area, West Bengal. *Indian J Malariol 34*:188–196.

Navaza J. 1994. AMoRe—An automated procedure for molecular replacement. *Acta Crystallogr D50*:157–163.

Nicholls A, Sharp K, Honig B. 1991. Protein folding and association: Insights from the interfacial and thermodynamic properties of hydrocarbons. *Proteins Struct Funct Genet 11*:281–296.

Nightingale SL. 1997. Donepezil approved for treatment of Alzheimer's disease. *JAMA 277*:10.

Ollis DL, Cheah E, Cygler M, Dijkstra B, Frolow F, Franken SM, Harel M, Remington SJ, Silman I, Schrag J, et al. 1992. The α/β hydrolase fold. *Protein Eng 5*:197–211.

Ordentlich A, Barak D, Kronman C, Flashner Y, Leitner M, Segall Y, Ariel N, Cohen S, Velan B, Shafferman A. 1993. Dissection of the human acetylcholinesterase active center—Determinants of substrate specificity—Identification of residues constituting the anionic site, the hydrophobic site, and the acyl pocket. *J Biol Chem 268*:17083–17095.

Otwinowski Z, Minor W. 1997. Processing of X-ray diffraction data collected in oscillation mode. *Methods Enzymol 276*:307–326.

Philippsen A. 2000. DINO: Visualizing structural biology. http://www.bioz.unibas.ch/~xray/dino.

Raves ML, Harel M, Pang Y-P, Silman I, Kozikowski AP, Sussman JL. 1997. 3D Structure of acetylcholinesterase complexed with the nootropic alkaloid, (-)-huperzine A. *Nat Struct Biol 4*:57–63.

Rosenberry TL. 1975. Acetylcholinesterase. *Adv Enzymol 43*:103–218.

Rosenberry TL, Scoggin DM. 1984. Structure of human erythrocyte acetylcholinesterase. *J Biol Chem 259*:5643–5652.

Sauer O, Schmidt A, Kratky C. 1997. Freeze-trapping isomorphous xenon derivatives of protein crystals. *J Appl Crystallogr 30*:476–486.

Shani A. 1998. Integrated pest management using pheromones. *Chemtech 28*:30–35.

Sussman JL, Harel M, Frolow F, Oefner C, Goldman A, Toker L, Silman I. 1991. Atomic structure of acetylcholinesterase from *Torpedo californica*: A prototypic acetylcholine-binding protein. *Science 253*:872–879.

Taylor P. 1996. Anticholinesterase agents. In: Hardman JG, Limbird LE, Molinoff PB, Ruddon RW, Gilman AG, eds. *The pharmacological basis of therapeutics*, 9th ed. New York: McGraw-Hill. pp 161–176.

Veil S. 1992. *Our planet, our health*. New York: WHO Commission on Health and Environment, World Health Organization.

Vellom DC, Radic Z, Li Y, Pickering NA, Camp S, Taylor P. 1993. Amino acid residues controlling acetylcholinesterase and butyrylcholinesterase specificity. *Biochemistry 32*:12–17.

Vriend G. 1990. WHAT IF: A molecular modelling and drug design program. *J Mol Graphics Modelling 8*:52–56.

Weik M, Ravelli RBG, Kryger G, McSweeney S, Raves M, Harel M, Gros P, Silman I, Kroon J, Sussman JL. 2000. Specific chemical and structural damage to proteins produced by synchrotron radiation. *Proc Natl Acad Sci USA 97*:623–628.

Yao H, Chuanling Q, Williamson MS, Devonshire AL. 1997. Characterization of the acetylcholinesterase gene from insecticide-resistant houseflies (*Musca domestica*). *Chin J Biotechnol 13*:177–183.

CHAPTER 16

HEAD-TO-TAIL CYCLIC PEPTIDES AND CYCLIC PEPTIDE LIBRARIES

ARNO F. SPATOLA and PETERIS ROMANOVSKIS
Department of Chemistry, University of Louisville

1. INTRODUCTION

Naturally occurring peptides often exist in cyclic, bicyclic, or polycyclic forms.[1] In most cases, the ring structures are formed through the oxidation of cysteine residues to form cystine disulfide bridges. But peptides can form alternative ring structures, through formation of amide bonds or through aryl–aryl linkages, and a variety of other functional group combinations. Most of the latter groups have been found in lower animals and plants. Examples of a few such ring structures are shown in Fig. 16.1.

A common method of classification of amide ring types is by the location of the ring juncture. Thus the link may involve two side-chains, one side-chain and the backbone, or two backbone elements (Fig. 16.2). Head-to-tail cyclic peptides are the most common form of the last group and typically form a ring via amide bond formation through the juncture of the N-terminal amine and the C-terminal carboxylic acid. This type of head-to-tail cyclic peptide is the primary class that will be discussed in this chapter.

1.1. Examples of Synthetic Head-to-Tail Cyclic Peptides

To date, there are no known examples of head-to-tail cyclic peptides in mammals. But such structures have often been discovered in bacteria, fungi, and other lower organisms, and many have unusual biological activities. There is currently great interest in these compounds as potential pharmaceutical agents. In contrast to linear peptides, head-to-tail cyclic peptides are not susceptible to attack by the exopeptidases (amino- and carboxy-peptidases). Furthermore, their constrained nature reduces the entropic penalty and offers the potential for

The Amide Linkage: Selected Structural Aspects in Chemistry, Biochemistry, and Materials Science,
Edited by Arthur Greenberg, Curt M. Breneman, and Joel F. Liebman
ISBN 0-471-35893-2

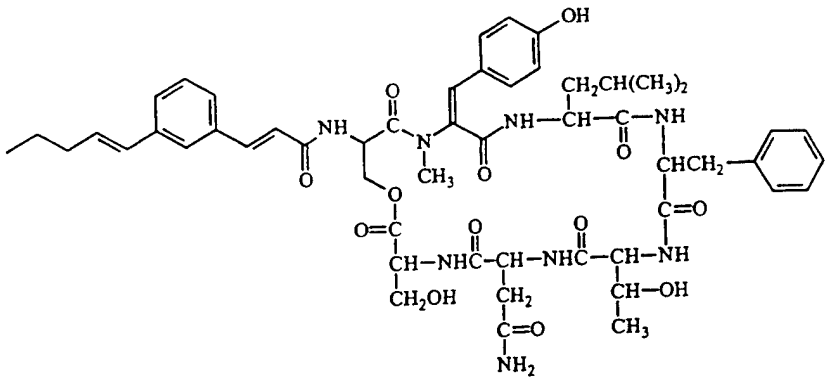

(a)

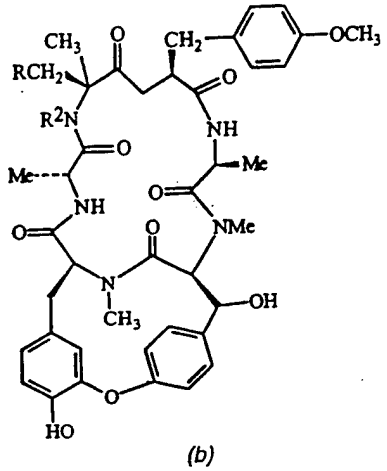

(b)

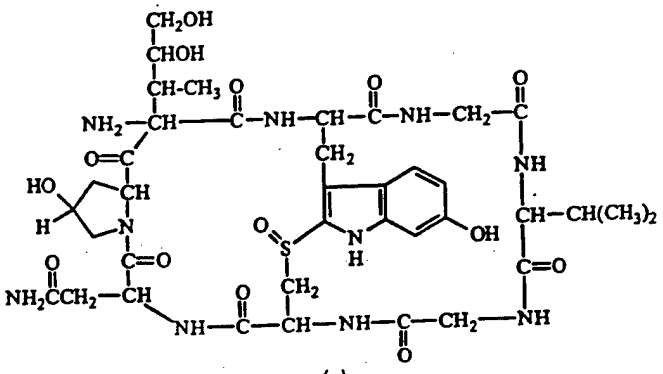

(c)

FIGURE 16.1. Examples of naturally occurring cyclic peptides with amide and nonamide groups in the ring. (*a*) Tachykinin antagonist from *Streptomyces violceonigen*; (*b*) structure of Bouvardins; (*c*) structure of the mushroom-derived toxin α-amantin.

improved binding, and often improved selectivity, toward a given biological receptor. These properties render cyclic peptides more like peptidomimetics in the continuum between peptides and nonpeptides in the perpetual search for potent, orally active, and selective pharmaceuticals.

Natural products have served as a rich source of head-to-tail cyclic peptides. Some of these, such as stylostatin, cyclo(Ala–Ile–Pro–Phe–Asp–Ser–Leu) have been isolated from sea sponges and have reasonably potent activity in an

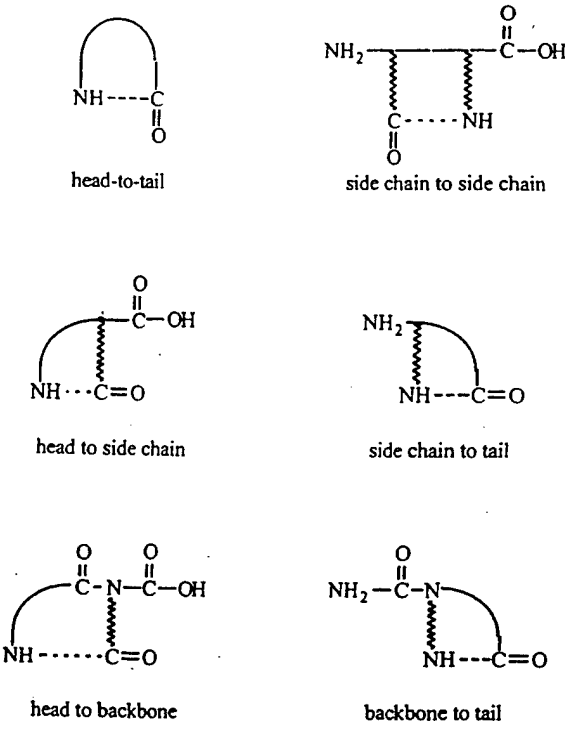

FIGURE 16.2. Various types of peptide monocycle closures that can feature new amide (- - -) formation.

anti-leukemia assay.[2] Lower organisms have yielded compounds with other important biological actions, such as Gramicidin S, (Fig. 16.3(a)) a potent antimicrobial compound,[3] cyclosporin (Fig. 16.3(b)), the clinically important immune suppressant,[4] and the cyclic pentapeptide, BQ-123 (Fig. 16.3(c)), an antagonist to the endothelin peptides with potential utility as an antihypertensive agent.[5] Gramicidin S was originally isolated from a strain of *Bacillus brevis*,[3] while BQ-123 is actually a modified version of the natural product found in Streptomyces broth.[5]

Cyclosporin is a cyclic undecapeptide containing no less than seven *N*-methylated amino acid residues. In one conformer, it contains no amide hydrogens that are not intramolecularly hydrogen bonded.[6] Cyclosporin is a relatively rare example of a fairly large peptide that retains significant oral activity in humans. One possible explanation for this is that the lack of free polar amide functions precludes extensive solvation by water molecules during biological transport and this hydrophobic character facilitates its passage through a variety of nonpolar cell membranes.

Figure 16.3(d) depicts the structure of a somatostatin analog which retains only five of the original amino acids in the 14-residue hypothalamic peptide hormone, somatostatin 14. While somatostatin contains a disulfide bridged ring, the synthetic analog, designed by Merck chemists and referred to as "mini-somatostatin," possesses a head-to-tail all-amide structure.[7] This compound is comparable in activity to its parent and had a brief clinical history before being withdrawn due to unacceptable side effects.

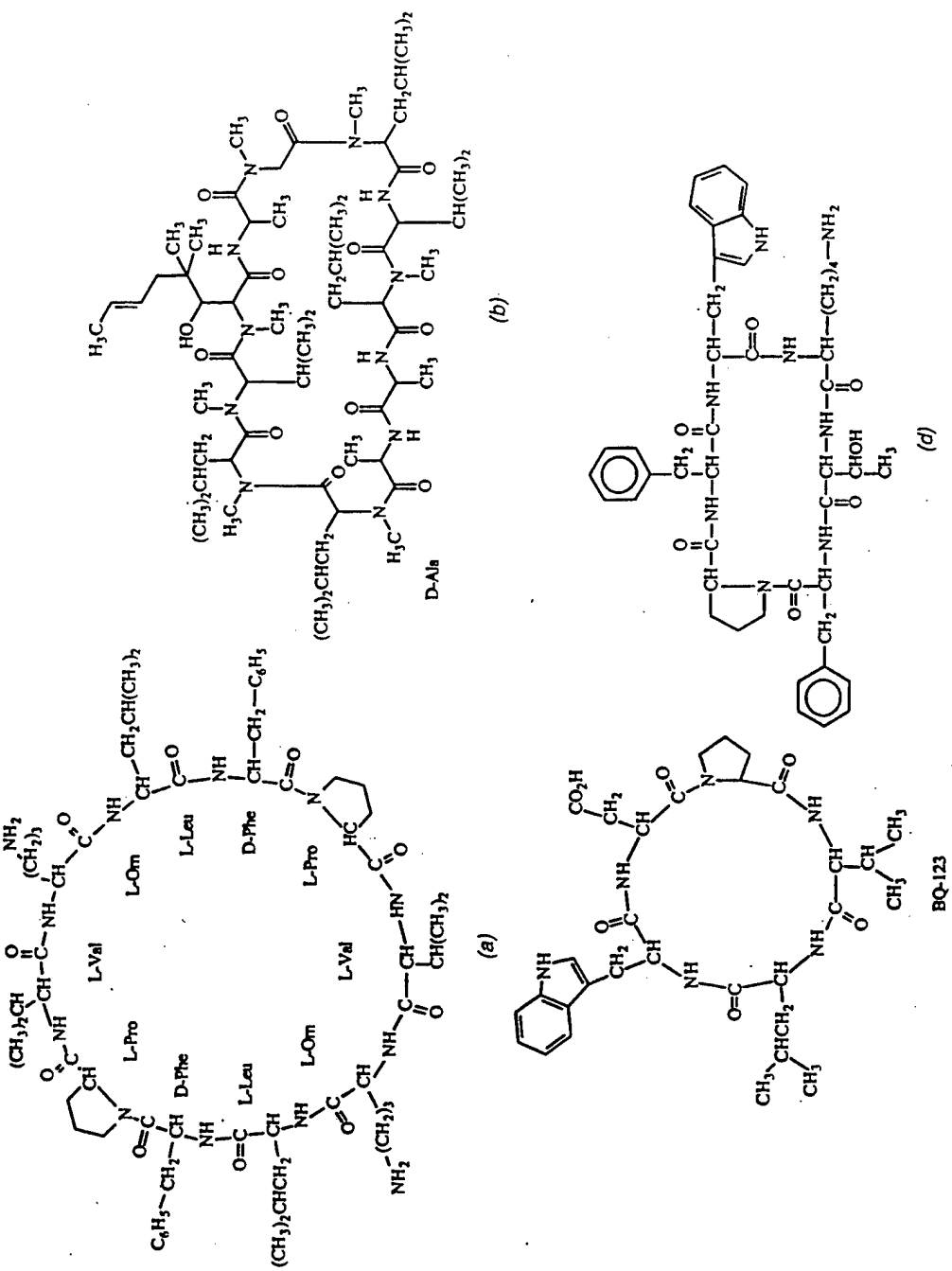

FIGURE 16.3. Examples of potent biologically active cyclic peptides: (*a*) the broad spectrum cyclic peptide anitbiotic, Gramicidin; (*b*) cyclosporin, an immune suppressant; (*c*) the cyclic pentapeptide, BQ-123, an endothelin antagonist; and (*d*) mini-somatostatin, a cyclic hexapeptide inhibitor of growth hormone release.

Current research with cyclic peptides tends to emphasize their potential as pharmaceuticals or to find leads for constrained peptide mimetics. But head-to-tail cyclic peptides provide an imaginative approach for producing new biomaterials and for studying aggregation tendencies. For example, Ghadiri and colleagues have shown that by alternating D and L residues in a cyclic peptide, these compounds can exist in an extended stacked structure referred to as nanotubes.[8] The exploration of these molecules and their derivatives is one of the more exciting areas in a fascinating arena of structural diversity.

2. METHODS OF SYNTHESIS

2.1. General Approaches

Historically, cyclic peptides were synthesized by classical methods of peptide chemistry in solution.[9] Often linear peptides were intramolecularly cyclized using azide methods or by heating linear active esters of peptides (e.g., *p*-nitrophenyl esters) for several hours until cyclization was judged complete. But yields were often low and dimerization and epimerization were significant problems.

Several strategies exist for synthesizing cyclic peptides including side chain-to-side chain, side chain-to-terminal group, and terminal group-to-terminal group (head-to-tail) cyclizations. Head-to-tail cyclizations can be accomplished either in solution[9] or while attached to a solid phase resin using carbodiimide or some other form of chemical coupling agent to form C $\rightarrow$ N terminal amides (Fig. 16.4). Only at the end of 1960s did reports start to appear on the successful synthesis of head-to-tail cyclized peptides on the solid phase.[10,11] An excellent review article[12] covers the present state-of-the-art for synthesizing cyclic peptides on solid phase carriers.

In this chapter, we emphasize new developments on the synthesis of cyclic peptides, primarily head-to-tail cyclic peptides, in which all steps have been carried out in the solid-phase mode and emphasizing work from the authors' laboratory. Nevertheless, when dealing with the synthesis of other types of cyclopeptides (head-to-side chain, side chain-to-side chain, side chain-to-tail), similar tactical considerations involving choice of protecting groups, condensing reagents, and problems of chirality are usually considered.

On-resin head-to-tail cyclization presumes anchoring of the first amino acid to the solid phase carrier through its side chain and features the following steps:

1. side chain anchoring of an initially protected amino acid residue to a polymeric support;
2. stepwise solid-phase assembly of the linear sequence;
3. orthogonal deprotection to liberate selectively a free C-α-carboxylic group and the N-terminal amine for the subsequent cyclization step;
4. efficient activation of the C-α-carboxylic group and its condensation with free N-α-amino group to close the desired head-to-tail ring, taking

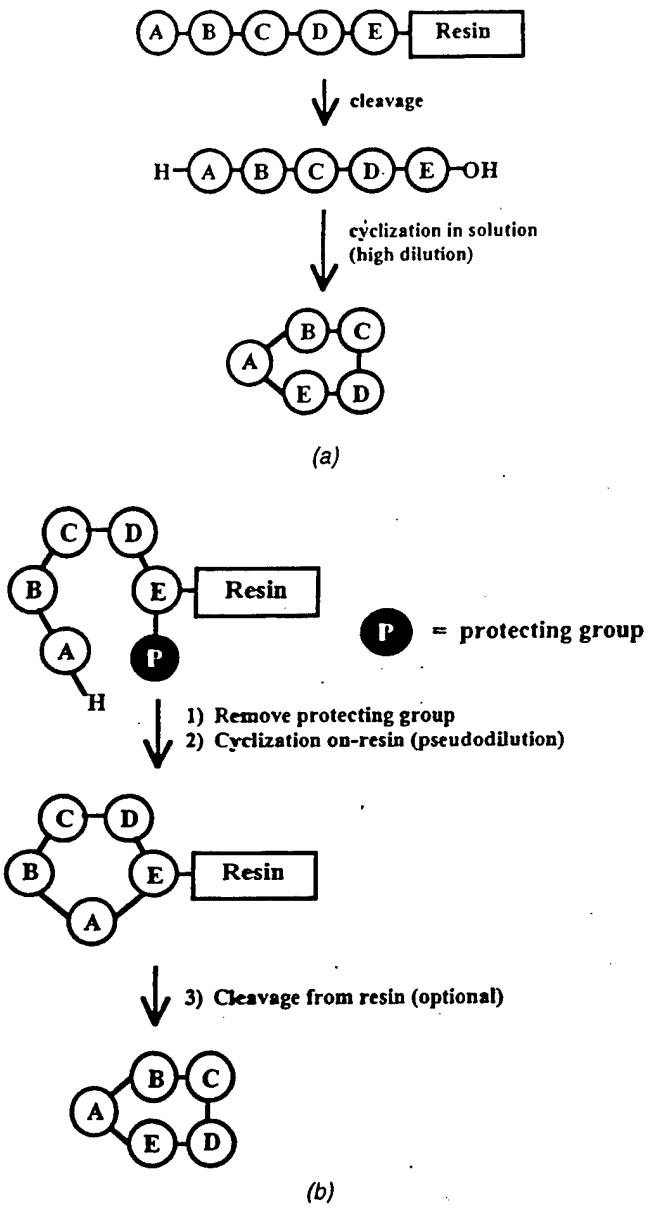

FIGURE 16.4. Representation of head-to-tail cyclic peptides prepared either by (*a*) solution cyclization or via (*b*) on-resin cyclization.

advantage of the pseudo-dilution phenomenon which favors intramolecular resin-bound reactions;[13] and

5. final deprotection and cleavage to release the required free cyclic peptide into solution. Side chain attachment also allows the synthesis of other peptide derivatives that would be otherwise inaccessible by standard solid phase synthesis procedures, e.g., peptide *p*-nitroanilides.

2.2. Examples of Synthetic Strategies Utilizing Orthogonality

Depending on the synthetic goal the anchor bond should be compatible with at least one of the two main peptide synthesis strategies, based on Boc- and/or

Fmoc chemistries. For various trifunctional amino acids, the anchor bond can be represented by an ester bond (Asp, Glu, Ser, Thr), amide bond (Asn, Gln), urethane bond (Lys, Orn [ornithine], Dab [α,γ-diamionbutyric acid]), mixed carbonate (Ser, Tyr, Thr), ether bond (Tyr), thioether bond (Cys), C–N bond in a special case (His), or a sulfamide-based linker (Arg). Simultaneously the anchor bond is expected to provide the protection for the side chain functional group during synthesis. The anchor group must also be orthogonal to the α-carboxyl protecting group: the latter is to be cleaved off selectively under mild conditions at the end of the peptide chain assembly before the cyclization step.

A system for peptide synthesis is defined as orthogonal when two or more kinds of protecting groups are used and each protecting group is removable separately and selectively based on different chemical mechanisms without affecting the other group's stability.[14] In contrast to the synthesis of a linear peptide (demanding two levels of orthogonality—one for the N-terminal amino group, another for the C-terminal carboxyl group and side chains of trifunctional amino acids), design of a cyclopeptide synthesis must include one additional (third) level of orthogonality. The three-dimensional orthogonal strategy is achieved by combining protecting groups that are, for example, cleavable by acid (Boc–), strong acid (benzyl-based), base (Fmoc–), palladium (Aloc,–OAl), fluoride ion (trimethylsilylethyl-based), or with nucleophiles (Dde). Examples of these combinations are collected in Table 16.1 and selected structures are provided in Table 16.2. These demands in turn suggest that a trifunctional amino acid can be attached directly to polystyrene resin (Merrifield resin, hydroxymethyl resin, aminomethyl resin), to the resin through a linker, or to another suitable support such as polyethylene glycol modified polystyrene (TentaGel or PEG-PS), polyamide, or a membrane-based solid. The exact chemistries may be expected to influence the anchor bond stability, chemistry, and the ease of cleavage of the final product from the resin. Usually the most critical decision involves the choice of the C-terminal carboxylic acid protecting group and the nature of the linkage of the side chain functional group to the solid support.

2.2.1. Carboxyl Protecting Groups

2.2.1.1. OFm Esters. A general method for the SPPS of head-to-tail cyclic peptides containing an aspartyl residue in their sequence was proposed by Rovero et al.[15] Synthesis was performed starting from the Asp residue linked to PAM-resin through the β-carboxyl function and protected as its fluorenylmethyl ester on the α-carboxylic acid group. Once the linear precursor had been synthesized by the Boc/benzyl strategy and the Boc protecting group on the N-terminal amino function was removed with TFA, the C-terminal carboxyl group of the Asp residue was selectively deprotected with piperidine and head-to-tail cyclization was easily accomplished by the BOP method. Final HF deprotection of the side chains of trifunctional residues, with concomitant cleavage from the resin, gave the cyclic peptide as a single product of good purity in reasonable yield.

TABLE 16.1. Selected Examples of Orthogonality of Protecting Groups for SPPS of Head-to-Tail Cyclic Peptides

C^{α}–COOH Protection	N^{α}–NH_2 Protection	Side Chain Protection	Anchoring Bond/Cleavages	Resins Used	Amino Acids	References
–OFm	Boc–*	benzyl-based or related	ester, urethane, amide/HF	hydroxymethyl-PAM	Asp, Glu, Lys, Orn, Dab	15, 19
				MBHA	Asn, Gln	19
–ODmb	Fmoc–*	*t*-Bu-based	ester/TFA	4-alkoxybenzyl	Asp, Glu	23
–OAR	Boc–	benzyl-based or related	mixed carbonate/HF	hydroxymethyl-	Ser, Tyr	47
	Fmoc–	*t*-Bu-based	ester, amide, BAL, urethane/TFA	4-alkoxybenzyl	Asp, Glu, Lys	27
				PAL-aminomethyl	Asn, Gln	27
–ONB	Boc–	benzyl-based or related	ester, ether, urethane/HF	hydroxymethyl	Asp, Glu, Tyr, Lys	51
			ester (hemi-succinate linker)/NH_3	aminomethyl-	Ser	51
–ODmab	Fmoc–	*t*-Bu-based	ester/TFA	2-chlorotrityl	Glu, Asp	39

*Boc = *tert*-butyloxycarbonyl; Fmoc – fluorenylmethyloxycarbonyl.

This approach was further developed in our laboratory for the synthesis of head-to-tail cyclic peptide libraries.[16] However, as suggested by Bednarek et al.,[17] the C-terminal-OFm ester is not completely stable under the conditions used for Boc-based solid phase synthesis. The neutralization cycle required before coupling, when Boc- is used on the α-amino group, exposes the –OFm ester protecting the C-terminal α-carboxylic group to the tertiary base diisopropyl-ethylamine (DIPEA) which can result in a small amount of deprotection.[18] Detailed studies revealed that epimerization accompanied chain growth and was therefore most likely caused by premature removal of the C-terminal protecting group during and after the neutralization step.[19] This unintended exposure of the acid function can lead to inappropriate activation by the condensing agent during subsequent stepwise N-terminal elongation and accounts for ever-increasing amounts of epimerization as synthesis proceeds. Nevertheless, we found that in situ neutralization could avert many of these problems; this orthogonality was successfully used for the synthesis of Lys-, Orn-, and Dab-containing cyclic peptides through a similar side chain attachment mode.[20] This side chain attachment approach was successfully applied for the synthesis of a small library of stylostatin analogs[21] as well as a large library of cyclic pentapeptides which included the endothelin antagonist analog BQ-123[22] (Fig. 16.3(c)), discussed later in this chapter.

2.2.1.2. ODmb Esters. In an on-resin cyclization technique developed by McMurray,[23] the first amino acid attached to a 4-alkoxybenzyl-resin was either Fmoc–Asp-α-2,4-dimethoxybenzyl (Dmb) ester or Fmoc–Glu–ODmb ester. The resin-bound Dmb esters are compatible with hydrolysis using 1% TFA in methylene chloride. (See Table 16.2 for descriptions.) The *t*-butyl- and sulfonyl-based side chain protecting groups widely used in solid phase Fmoc chemistry are mostly stable to these conditions. If Asn or Gln residues are desired these amino acid esters can be attached to the acid-labile amide handle such as peptide amide linker (PAL)[24] or the methoxy-substituted benzhydrylamine handles.[25] A comparable Fmoc/ODmb protection strategy was also used by Brugghe et al.[26] to prepare cyclic peptides containing 7–14 amino acid residues as potential synthetic vaccines for bacterial meningitis.

2.2.1.3. OAl Esters. Several authors have applied allyl chemistry to provide the third dimension of orthogonality to the initially anchored Asp or Glu via their α-carboxyl-protected allyl esters.[27,28] The allyl group is stable to the conditions used for removal of most acid and base labile protecting groups. Thus, it is compatible for both Boc and Fmoc methods of peptide synthesis. At the appropriate stage the allyl esters can be selectively deblocked with palladium(0) under nearly neutral conditions. While this is a potentially attractive approach to orthogonality, the homogeneous palladium reagents are air sensitive and can sometimes give rise to greater amounts of side products.[29]

TABLE 16.2. Structures of Common Acid Protecting Groups and Methods for their Removal

	Removed by	Stable to
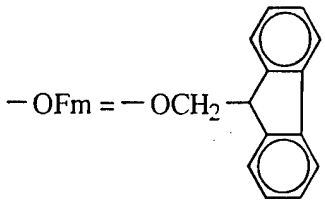	20% piperidine/ DMF	TFA
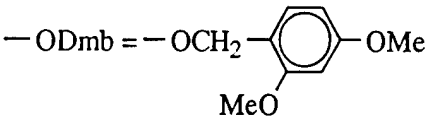	1% TFA/ CH_2Cl_2	20% piperidine/ DMF
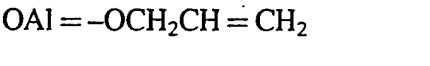	Pd^0/morpholine as allyl acceptor	TFA; 20% piperidine/DMF
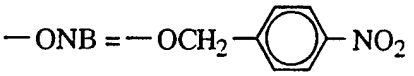	$SnCl_2$/DMF	TFA
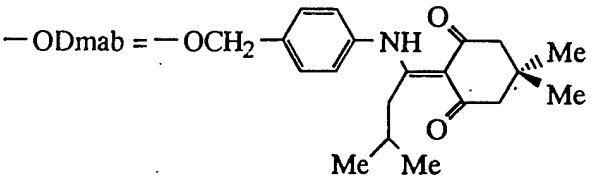	2% hydrazine/ DMF	TFA; 20% piperidine/DMF

2.2.1.4. ONB Esters. *p*-Nitrobenzyl (–ONB) esters are stable to most conditions of peptide synthesis; they can be selectively cleaved in the presence of *t*-butyl and benzyl based protecting groups by reducing agents (Zn in HOAc, Na_2S, $Na_2S_2O_4$ or $SnCl_2$ in aqueous organic solvents).[30] These esters have been used to provide orthogonality for the solution phase synthesis of cyclic analogs of some ACTH/α-MSH linear fragments.[31] However, upon reductive cleavage of ONB esters, quinonimine methide is formed, and this leads to intractable contaminants. Recently, a new approach was suggested[32] for the removal of the reactive intermediate (quinonimine methide) from the reaction mixture based on its reaction with benzene sulfonic acid.[33]

Recently, it has been reported that a new *p*-nitrobenzyl-based linker, 5-hydroxymethyl-2-nitrophenoxy-acetyl (2-NPA), is HF-resistant. By using this group for resin attachment, this provides for the orthogonal cleavage of protected and unprotected peptides from resins in organic and aqueous media using sodium dithionite under very mild reductive conditions.[34] This represents a swap between the groups used for the side chain versus main chain functionalities and suggests that other protecting groups are often similarly reversible as appropriate. This and other examples in which the side chain acid groups can be linked to solid supports by a variety of cleavable linkers are contained in Table 16.3.

TABLE 16.3. Selected Examples of Linkers Attached to Solid Supports by their Carboxylic Acid Function

No.	Linker	Structure (Linker-Resin)	Peptide Released from Linker by	Reference
1	5-hydroxymethyl-2-nitrobenzoic acid	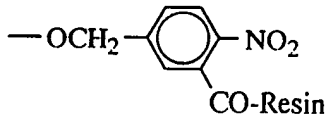	$Na_2S_2O_4$	34
2	5-hydroxymethyl-2-nitrophenoxyacetic acid	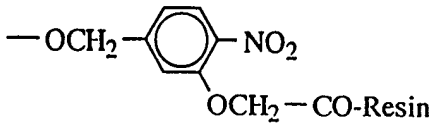	$Na_2S_2O_4$	35
3	4-oxocrotonic acid	$-OCH_2-CH=CH-CO$-Resin	Pd^0/morpholine as allyl acceptor	36
4	N-[(9-hydroxymethyl)-2-fluorenyl]-succinamic acid	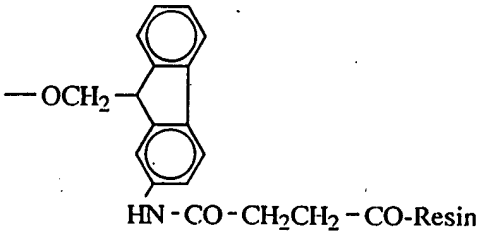	secondary amine	46
5	4-hydroxymethyl-3-nitrobenzoic acid	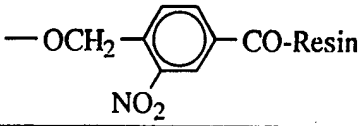	photolysis at 350 nm in TFE-CH_2Cl_2 for 16 h	47

2.2.1.5. ODmab Esters. The Dde group, (1-(4,4-dimethyl-2,6-dioxocyclo-hexylidene)ethyl), typically has been used for side chain amine protection.[37] The Dde group is stable to the acidic reagents used in Boc-based solid phase synthesis. It is mostly stable to 20% piperidine/DMF, but can be removed by treatment with 2% hydrazine in DMF. The compatibility of Dde- and allyl-chemistries has been exploited to provide two "mild" extra orthogonal steps for an otherwise Fmoc/*t*-butyl-based SPPS of an intrachain-branched Lys-based cyclic peptide.[38]

By combining the desirable properties of the N-Dde group with the known lability of 4-aminobenzyl esters, this led to the development of a new carboxyl-protecting group (–ODmab) 4-(N-[1-(4,4-dimethyl-2,6-dioxocyclohexylidene)-3-methylbutyl]amino) benzyl ester (Table 16.2) that retains all the desired chemical properties for masking either the α- or the β(γ-) carboxylic acid groups of Asp/Glu. This group is stable to acidic reagents, and it is also reported to be completely stable to Fmoc-deprotection conditions.[39] Removal can be effected by using 2% hydrazine in DMF, thus providing another approach to orthogonality.

Applications of orthogonality of new systems can lead to further complications, thus removal of the Dde group by hydrazine results in side reactions in peptides containing the allyloxycarbonyl (Aloc) protecting group. The addition of allyl alcohol as scavenger prevents the hydrogenation of the Aloc group. Under these conditions, Dde and Aloc groups can also be used as fully orthogonal protection techniques in solution and SPPS.[40] These precautions may also be required when using the ODmab group together with allyl chemistries.

2.2.2. Side Chain Linkage Methods

2.2.2.1. Ester or Amide Linkages. Most amino acid side chain attachment strategies have involved the use of aspartic acid and glutamic acid residues since the functional group involves the same chemistries as normal α-carboxylic acid solid phase peptide synthesis. If the side chain acid is attached to the resin through a benzyl ester-type linkage, acid cleavage provides the Asp or Glu residues. If ammonolysis is used as the cleavage method or if initial attachment is to a benzhydrylamine or *p*-methylbenzhydrylamine resin, the cleavage will yield the corresponding asparagine or glutamine derivatives (Fig. 16.5).

Choices for the α-carboxylic acid protecting group will be based on the nature of the amine protection (Boc or Fmoc) and on the approach towards orthogonality that is desired. A latter section will describe some of the specific derivatives used for head-to-tail cyclic peptide synthesis.

2.2.2.2. Urethane-based Linkages. Trifunctional amino acids with amino acid side chains such as lysine and ornithine have primarily been attached to a solid support using a benzyloxycarbonyl-type urethane bond. The urethane or carbamate group is compatible with both Boc and Fmoc strategies and can be formed from hydroxymethyl resins with amines. Such resins were first prepared

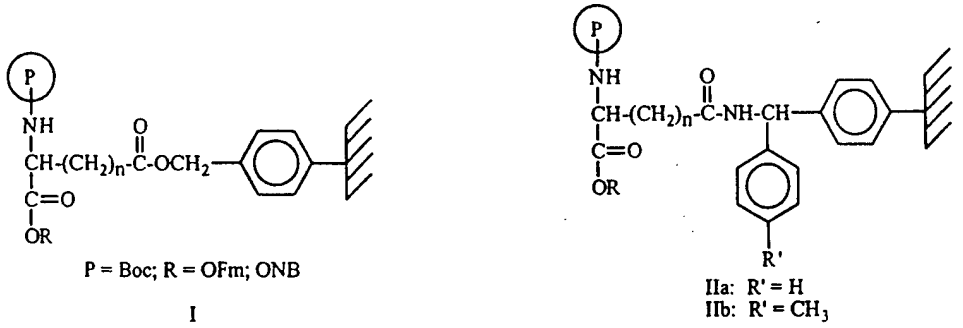

FIGURE 16.5. Side chain attachment of aspartic acid ($n = 1$) or glutamic acid ($n = 2$) to polystyrene resin (I) or to benzhydrylamine; (IIa) $R' = H$ or *p*-methylbenzhydrylamine resin; (IIb) $R' = CH_3$ for formation of Asp, Glu(I) or Asn, Gln(II) containing cyclic peptides.

from the hydroxymethyl derivative of the classical Merrifield resin by reaction with phosgene, to furnish the corresponding chloroformate derivative, which was followed by displacement of halogen by the amine component.[41] Thus, Sklyarov and Shashkova attached a preformed linear tetrapeptide via the δ-amino group of an ornithine residue to a chloroformate derivatized polystyrene support (Scheme 1). After the addition of six more residues, the peptide product, an analog of Gramicidin S, was deprotected at both ends, cyclized on the resin and detached from the resin.[11]

However, the use of phosgene is dangerous and not compatible with more acid labile resins required for orthogonal schemes. Other synthetic pathways useful for preparing the reactive species leading to alkoxycarbonylation of amines involve the preparation of various activated derivatives of alcohols (activated mixed carbonates or chloroformates). Several of these methods have also been used for the preparation of polyethylene glycol derivatives.[42]

Thus, hydroxymethyl resin can be easily converted to activate mixed carbonate in nearly quantitative yield by treatment with *p*-nitrophenyl

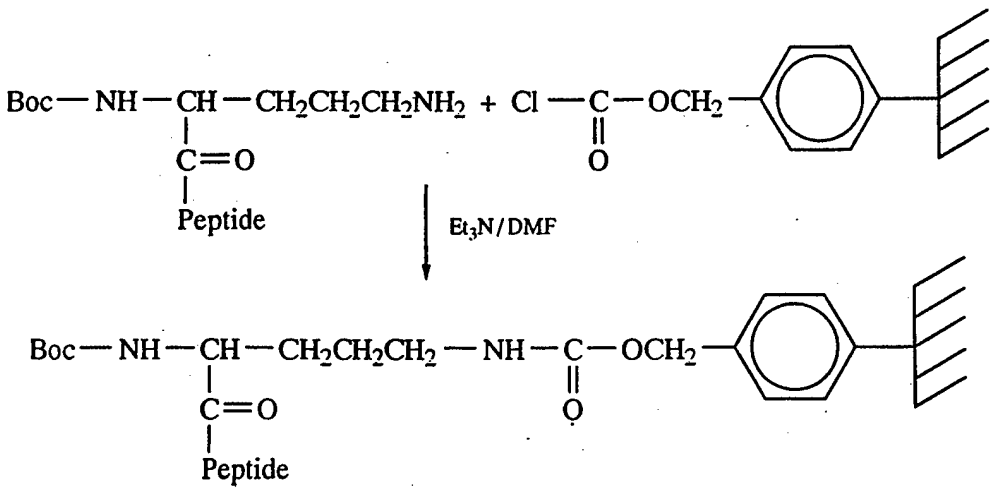

Scheme 1. Attachment of the ornithine side chain to activated polystyrene resin to furnish a urethane linkage.

chloroformate and *N*-methyl morpholine.[43] This activated mixed carbonate is claimed to be a robust polymer-bound reagent well suited for urethane formation as well as for other modifications that can be used for combinatorial library production.

N,N'-disuccinimidyl carbonate (DSC) has recently been proposed as a mild agent for alkyoxycarbonylation of amines from the corresponding alcohols in solution.[44] This method can also be used to prepare the resin-bound urethanes. In a recent comparison of some of the various derivatization agents (Fig. 16.6) used to form activated carbonates from hydroxymethyl resin (*p*-nitrophenyl chloroformate, carbonyldiimidazole, DSC, or di(pentafluorophenyl)carbonate)[45]), DSC and di(pentafluorophenyl)carbonate were the most effective, providing high levels of substitution, reasonable stability and ease of handling. Both showed good reactivity in the subsequent urethane formation processes. Urethane-based side chain attachment has been used with the Fmoc–/–OAl strategy,[46] Boc–/–OFm strategy,[20] and it is also compatible with the Boc–/–ONB strategy.

2.2.2.3. Mixed Carbonate Links. Activated carbonates such as those used for the preparation of urethanes from amines can also be used to form stable links with the hydroxyl side chains of amino acids. For example, the active mixed carbonate resins formed from disuccinimidyl carbonate and hydroxymethyl resins were reported to undergo transesterification with alcohols in the presence of dimethylaminopyridine as catalyst.[47] The resulting asymmetric carbonates are reported to be stable for Boc-based synthesis. Using this chemistry, several model cyclic peptides attached to solid polystyrene-based supports via their hydroxyl (serine) or phenolic (tyrosine) side chains could be prepared with the Boc strategy and with the allyl group used for α-carboxylic acid protection. Cleavage of the products from resin was achieved using either anhydrous HF or with trifluoromethane sulfonic acid.

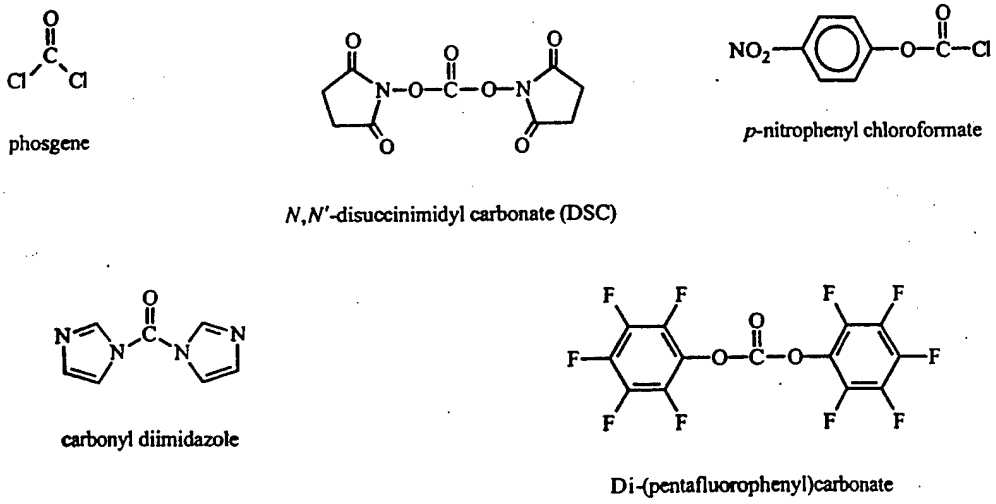

FIGURE 16.6. Structures of reagents used for activation of resin bound alcohols as a first step toward urethane formation.

2.2.3. Examples of Amino Acid Derivatives Used for Cyclic Peptides. Once a suitable orthogonal protection strategy is selected, the head-to-tail cyclic peptides can be conveniently prepared by linking the desired trifunctional amino acid to a solid support via its side chain. In the sections below, we describe methods that have been used for preparation of cyclic peptides using several of the coded trifunctional amino acids and their analogues.

2.2.3.1. Asp, Glu, Asn, Gln. A convenient method for preparing a cyclic peptide with on-resin cyclization is shown in Fig. 16.7. Orthogonality is provided by use of a base-labile fluorenylmethyl ester. Boc–Asp–OFm can be obtained by reacting Boc–Asp–anhydride with 1 equivalent of fluorenylmethanol in the presence of base followed by fractional crystallization from ethyl acetate and hexane to obtain the α-ester. Boc–Glu–OFm could be obtained by reacting commercially-available Boc–Glu(OBzl)–OH with fluorenylmethanol in ethyl acetate in the presence of Boc anhydride and pyridine[48] and removing the γ-benzyl ester by catalytic hydrogenolysis.

Esterification of the β-carboxylic group of Asp to the hydroxymethyl–polystyrene support is achieved through a Mitsunobu reaction[49] mediated

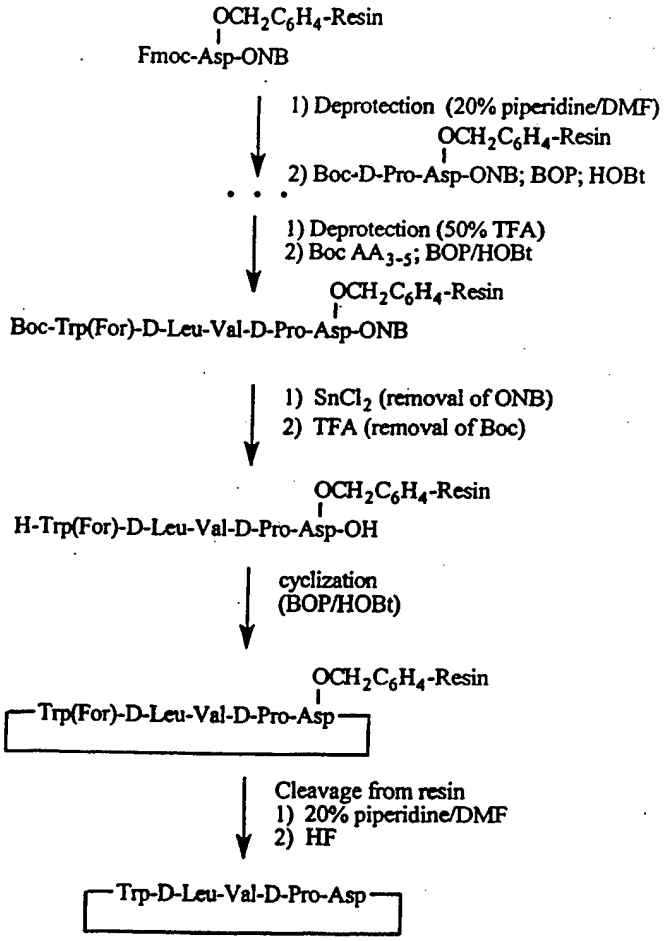

FIGURE 16.7. Synthesis of a model cyclopentapeptide using Asp–ONB for orthogonality.

through triphenylphosphine and diethyl azodicarboxylate in THF or by using Boc_2O/pyridine in methylene chloride. Esterification of the γ-carboxylic group of Glu onto the support can also be accomplished with Boc_2O/pyridine. By coupling the same ω-carboxylic groups with BOP to para-methylbenzhydrylamine resin, Asn and Gln peptides are produced upon cleavage (Table 16.2).

Allyl esters provide a separate approach for orthogonal protection of the α-carboxylic acid. Fmoc–Asp(OH)–OAl and Fmoc–Glu(OH)–OAl were prepared by reacting commercially-available Fmoc–Asp/Glu(OtBu)–OH in neat allyl bromide in the presence of diisopropylethylamine (2 equivalents). Esterification of ω-carboxyls of Fmoc–Asp–OAl and Fmoc–Glu–OAl to *p*-alkoxybenzyl supports was achieved by *N,N'*-diisopropylcarbodiimide (DIC) or TBTU in the presence of 4-dimethylaminopyridine. Coupling of the same ω-carboxyls on amide resin ultimately generates Asn or Gln peptides upon cleavage.[46,50]

Another approach to orthogonality involves the *p*-nitrobenzyl ester as a carboxylic acid protecting group. Fmoc–Asp–ONB could be prepared by reacting Fmoc–Asp internal anhydride with 1 equivalent of *p*-nitrobenzyl alcohol and base.[51] This was followed by fractional crystallization to remove the undesired β-ester. The analogous glutamic acid derivative was prepared by reacting Fmoc–Glu(OtBu)–OH with *p*-nitrobenzyl bromide in the presence of DIPEA with selective OtBu removal by TFA to produce Fmoc–Glu–ONB.

2.2.3.2. Lys, Orn, Dab, Dap. The diamino acids lysine, ornithine, diaminobutyric acid, and diaminopropionic acid can similarly be differentially protected using the corresponding allyl or *p*-nitrobenzyl esters. Fmoc–Lys–OAl can be obtained by refluxing commercially-available Fmoc–Lys(Boc)–OH in neat allyl bromide in the presence of DIPEA. The final product is obtained by removal of the Boc-amino protecting group after which it can be coupled to the solid support.[46] The ONB ester is also obtained by starting with Fmoc–Lys(Boc)OH with removal of the Boc group after esterification.[51] The resulting product, Fmoc–Lys–ONB, can be attached to an activated mixed carbonate resin or other suitably functionalized support to provide a linkage useful for the preparation of head-to-tail cyclic peptides (Fig. 16.8).

Another approach toward the preparation of orthogonally protected diamino acids involves the use of a suitably protected glutamine or asparagine precursor which is subjected to the Hofmann rearrangement.[52,53] Thus, Boc–Gln–OFm can be treated with *bis*(trifluoroacetoxy)iodobenzene to afford the corresponding diamino butyric analog, Boc–Dab–OFm. This derivative is then attached to a solid support via its side chain amine group by using a suitable linker.

2.2.3.3. Ser, Tyr, Thr. One method for preparing cyclic peptides by using the side chain hydroxyl function for resin attachment also involves the allyl group for carboxyl protection (Fig. 16.8(b)). The reaction of DSC with 4-hydroxymethyl-polystyrene resins affords the corresponding active carbonates, which in the presence of base, can react smoothly with compounds containing hydroxyl

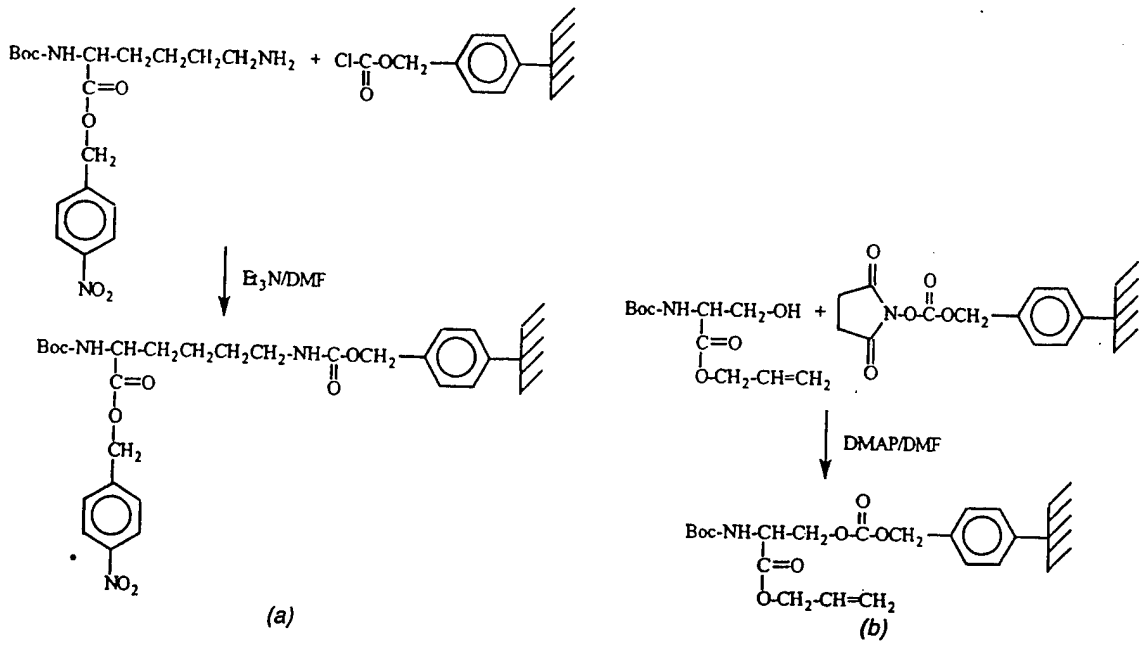

FIGURE 16.8. The *p*-nitrobenzyl and allyl esters can be used for carboxyl protection when attaching lysine (*a*) or serine (*b*) to resin supports.

functions (Boc–Ser–OAllyl, Boc–Tyr–OAllyl and others) to afford the corresponding mixed carbonates.[47]

Another comparable approach developed in our laboratory uses the *p*-nitrobenzyl group (ONB) for acid protection. Thus, Boc–Ser–ONB is prepared from Boc–Ser–OH and the product attached to the support as the Boc–Ser(Suc)–ONB derivative. Using this approach, a serine analog of the BQ-123 endothelin antagonist was prepared in good yield.[20]

The use of an asymmetric carbonate bond for tyrosine side chain attachment has been considered in analogy with serine attachment. We chose an aryl benzyl ether bond to attach Boc–Tyr–ONB to the hydroxymethyl-PS resin through a Mitsunobu reaction[49] (Scheme 2). This reaction has been used successfully to form aryl ethers.[54] More recently Mitsunobu etherification of polymer-supported phenols with alcohols in solution has been studied[55] and conditions for attachment of protected tyrosines to the hydroxymethyl resin using this approach have been developed.[56] We found the Mitsunobu conditions quite useful for etherification: the triphenyl phosphonium activated hydroxymethyl resin, when treated with Boc–Tyr–ONB, in the presence of tertiary amine, formed an aryloxide which, provided a good yield of the side chain attached Tyr derivative.

2.2.3.4. His. Orthogonality for His has been achieved by attaching the amino acid to polystyrene resin through a 2,4-dinitrophenyl-type side chain protecting group. For that purpose, the aminomethyl resin was reacted with excess 1,5-fluoro-2,4-dinitrobenzene to give polymer-bound 1-fluoro-2,4-dinitrobenzene. Reaction of the latter with Boc–His gave Boc–His(DNP) attached to the resin through its side chain (Fig. 16.9(a)). The His-derivatized resin was used for the synthesis of a cyclic hexapeptide with on-resin cyclization. After removal from

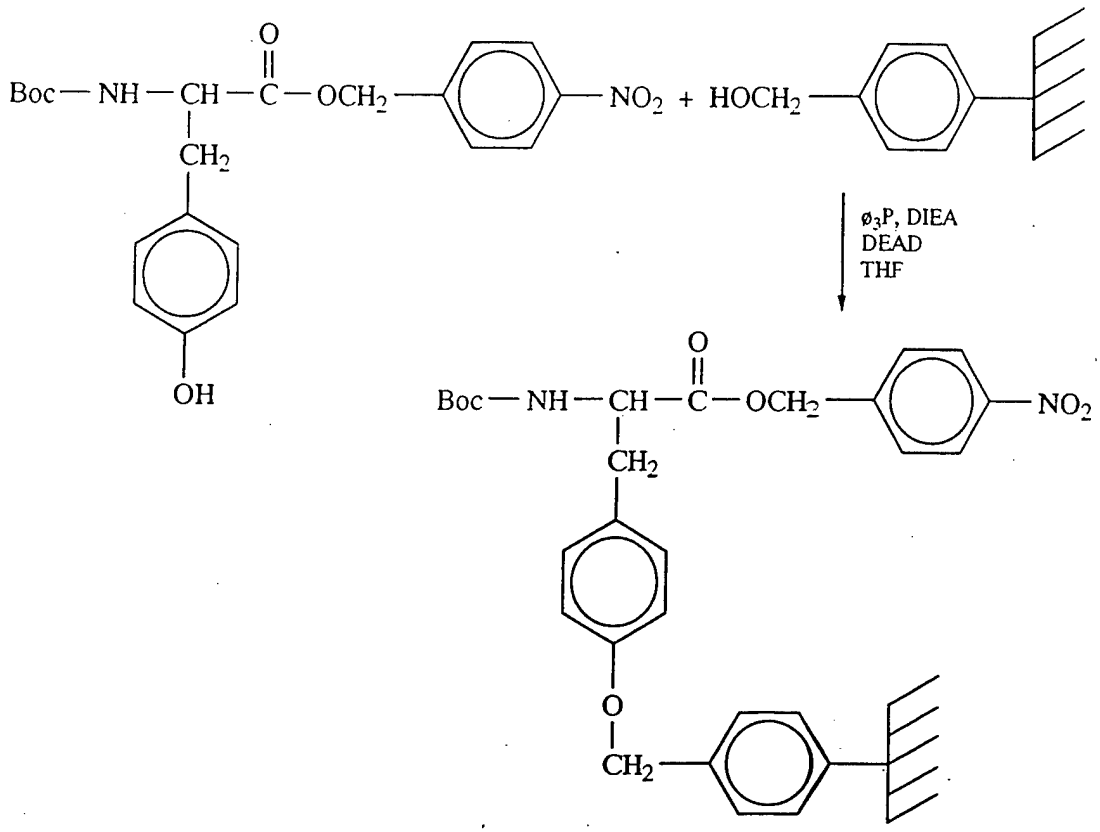

Scheme 2. Use of Mitsunobu reaction conditions to attach tyrosine through its side chain to a hydroxymethyl resin.

the resin by thiophenol/DMF treatment, cyclic $(Gly–His)_3$ was obtained in good yield and purity.[57]

2.2.3.5. Arg. The guanidyl side chain of arginine is typically protected by an aryl sulfonyl derivative such as the 4-methoxy-2,3,6-trimethylbenzenesulfonyl (Mtr) group. Arginine can be attached to a solid support by using a modified form of the Mtr group in which the 4-methoxy group methyl has been replaced by a 4-carboxymethyl moiety. This new linker-protecting group, CMtr, (Fig. 16.9(b)) allows synthesis of Arg-peptides and Arg-peptide derivatives that are inaccessible by current procedures. While the more traditional Mtr group may lead to incomplete cleavage, the use of the modified linkage should result in a purer product.[58] But this approach has not yet been applied to the synthesis of head-to-tail cyclic peptides.

2.2.3.6. Cys. The cysteine residue provides an interesting challenge for side chain attachment strategies. Sulfur is a good leaving group and there is always a danger of a β-elimination reaction. One approach is to use an indirect attachment to a solid support via an intervening linker or handle. Using this approach, C-terminal cysteines with an Fmoc-group for N-α-protection and *t*-butyl or allyl groups for C-α-protection have been attached to solid supports using an S-xanthenyl (2-Xal) handle[59] (Fig. 16.9(c)). By using this anchoring handle, a

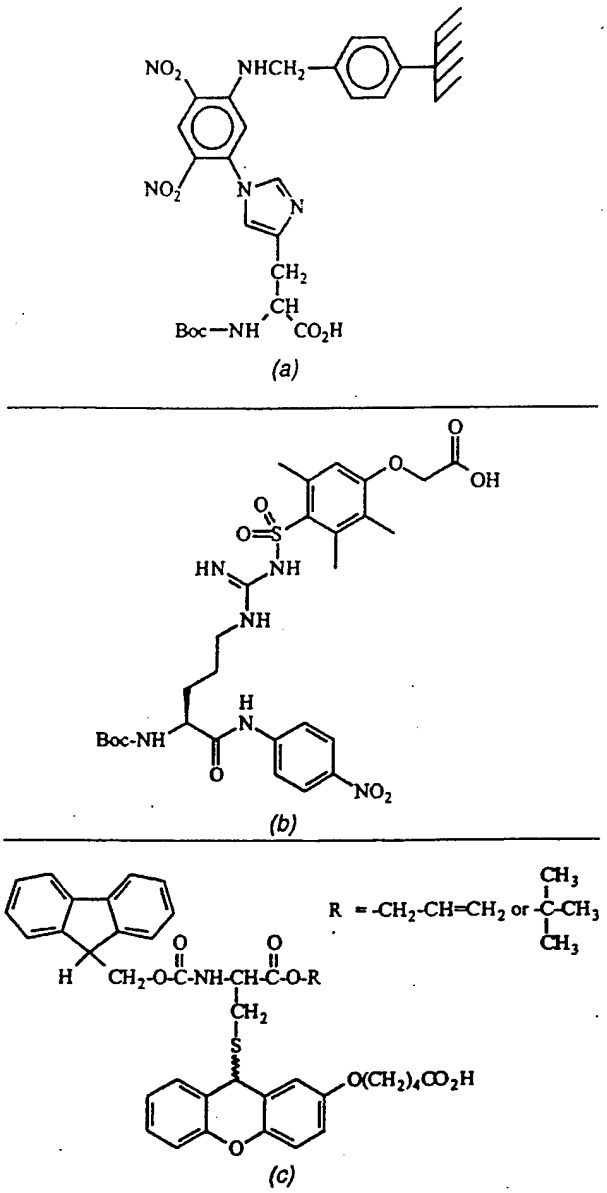

FIGURE 16.9. Amino acid derivatives used for side chain attachment of glutamic acid; (a) histidine; (b) arginine; (c) and cysteine (d).

common side reaction during the base deprotection step, involving formation of a dehydroalanine intermediate followed by piperidine addition,[60] is circumvented. Cleavage of the S-(2-Xal) by an acidolytic or oxidative mechanism in concert with appropriate protecting groups for the C-α-carboxyl acid provides options for the preparation of free or protected disulfide containing peptides.[59]

Attachment of cysteine through its side chain can be exploited to provide the elimination products. It has been shown that a polymer-bound cysteine, protected at its N-terminus, can be readily esterified or coupled with an amine or amino acid ester. Oxidation of the corresponding sulfides with m-chloroperbenzoic acid furnishes the desired sulfone derivative attached to the resin. (Scheme 3) In this case, dehydroalanine derivatives are obtained by treating the

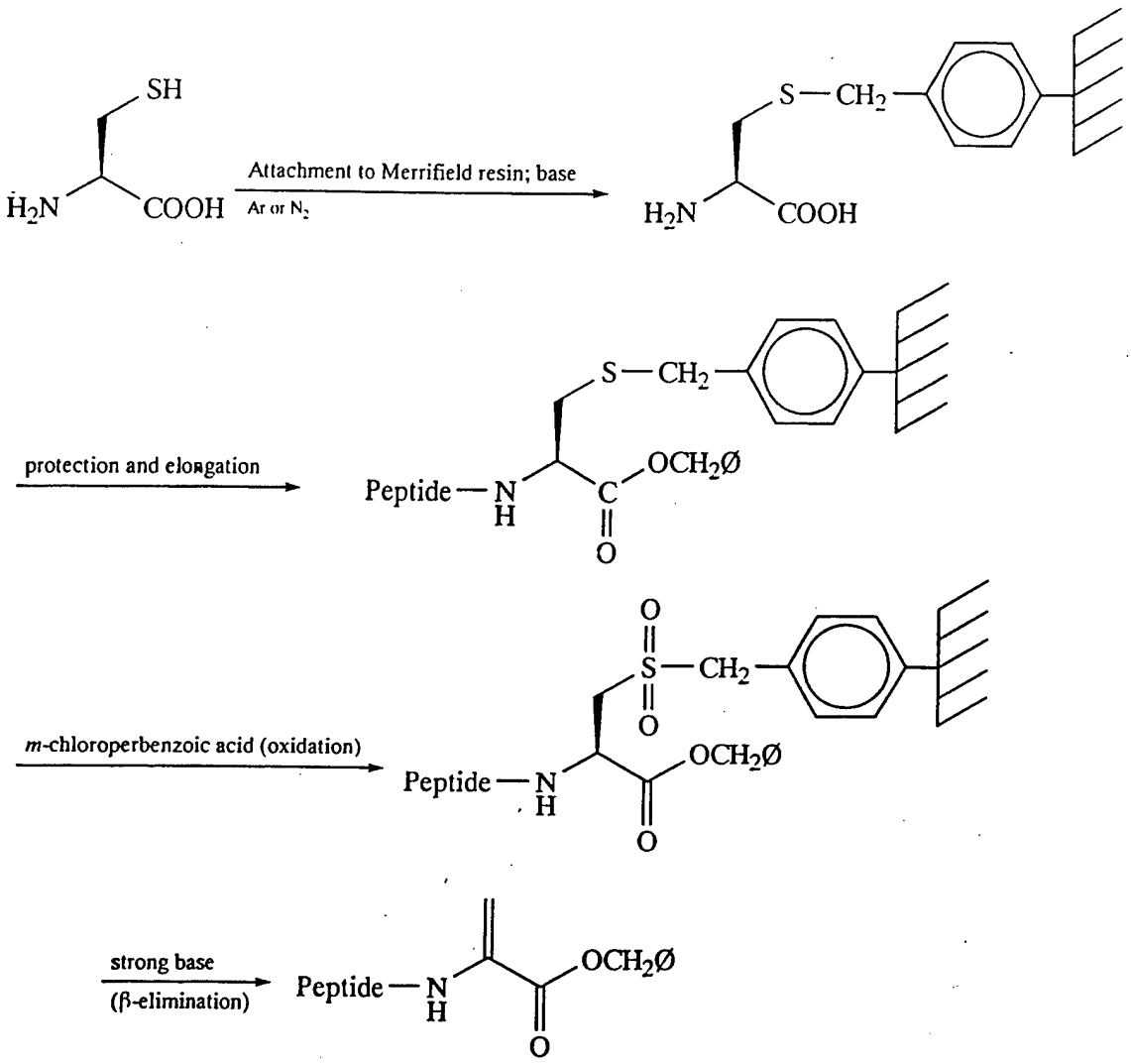

Scheme 3. Synthesis of dehydroalanine peptides based on cysteine side chain attachment.

sulfone derivatized resin with an equimolar amount of the strong base DBU (1,8-diazabicyclo[5.4.0]undec-7-ene) in CH_2Cl_2.[61]

2.2.4. Cyclic Peptides from Amide (NH) Attachment to Resin. The attachment of amino acids to solid supports through their side chains leads to the consideration of alternative approaches. Alkoxybenzaldehyde-based linkers have been used for the temporary protection of amide nitrogens.[62] These same derivatives allow anchoring of the first amino acid residue for SPPS through the amide nitrogen of the peptide backbone (Fig. 16.10). Initially an aldehyde precursor to PAL was coupled through a reductive amination procedure to the α-amine of the prospective C-terminal amino acid, which was protected as a *tert*-butyl, methyl, or allyl ester, or modified to a dimethyl acetal.[63] The resultant intermediates, all secondary amines, were treated with Fmoc–Cl or Fmoc–succinimide to give the corresponding protected amino acid preformed handle

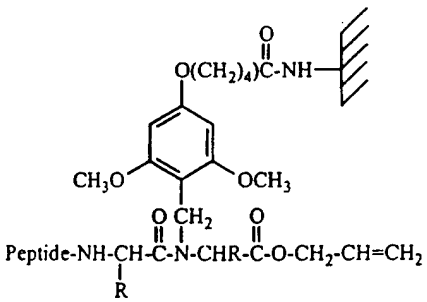

FIGURE 16.10. Structure of a peptide attached to a solid support through a backbone amide linker (BAL) and with an allyl ester for C-terminal protection.

derivatives in 40–70% yields. These preformed handles are then ready to attach to PEG-PS supports through a BOP/HOBt mediated coupling.

The Fmoc-preformed BAL handle derivative of Gly–OAllyl has been coupled onto polystyrene resin and extended (including the modified protocol to avoid diketopiperazine formation) to generate the protected peptide-resin Fmoc–Pro–Tyr–Leu–Ala–(Bal–PS)Gly–OAl. Cleavage with 5% trifluoroacetic acid provided the protected peptide Fmoc–Pro–Tyr–Leu–Ala–Gly–OAl in greater than 85% purity and 90% yield. In a preliminary experiment, the allyl ester was removed selectively from the BAL-anchored peptide with Pd(0), and the Fmoc group was then removed with piperidine/DMF (1 : 4). On-resin cyclization using BOP/HOBt/DIPEA gave the expected five-residue head-to-tail cyclic peptide as the main product.

More recent work has focused on improved handles which can be prepared more readily and which provide a wider array of amide derivatives.[64,65]

In conclusion, the backbone amide linker (BAL) anchoring has been applied to the solid phase synthesis of linear peptides with a considerable range of C-terminal modifications, and appears to provide an alternative general approach for the synthesis of head-to-tail cyclic peptides.

2.3. Coupling Agents

The azide method has often been used for the solution cyclization of linear peptides, primarily due to its relatively low danger of racemization as compared to other methods. Azide formation and cyclization are carried out in separate stages following removal of the N-α-protecting group of the linear precursor (Scheme 4). Azide formation proceeds so fast that the α-amino group is not affected by deamination. Cyclization is generally conducted at high dilution (for a review, see Ref. 66). A related compound that generates an azide intermediate, diphenylphosphoryl azide, has been the reagent of choice for linear peptide cyclization in solution since its introduction for that purpose in 1979,[67] and has been combined with dimethylaminopyridine and hydroxybenzotriazole to accelerate the rate of cyclization.[68] 2-Ethoxy-1-ethoxycarbonyl-1,2-dihydroquinoline (EEDQ)[69] has been used for solid phase hexapeptide cyclization (presumably through the formation of an intermediate mixed anhydride).[57]

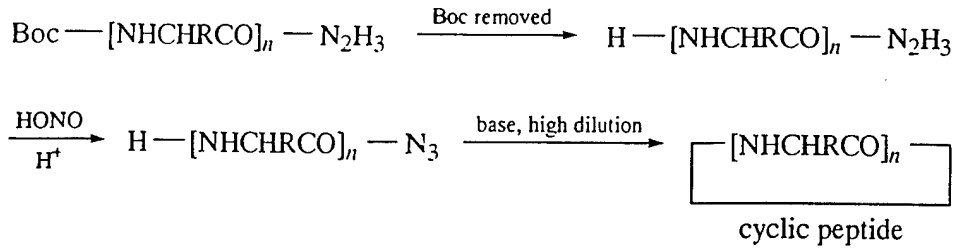

Scheme 4. Intramolecular cyclization of a peptide in solution using azide generation from a linear precursor.

Dicyclohexylcarbodiimide (DCC), first described in the 1950s,[70] is still one of the most popular activating agents in peptide cyclizations; it is used either in conjunction with hydroxybenzotriazole (HOBt) or with other activated hydroxyl compounds for active ester generation.[71] Addition of HOBt to carbodiimide-mediated activations is beneficial: intermediate hydroxybenzotriazole esters are generated. They need not be isolated, the reaction is extremely fast, the method counteracts racemization, and other side reactions are few.[72] Another variant, diisopropylcarbodiimide (DIC), is considered advantageous as it forms a derivative, diisopropylurea, that is more soluble than dicyclohexylurea (DCU).[73] Recent results indicate that HOAt, a 4-nitrogen containing variant, is a very effective coupling additive, more efficient than HOBt for solution or solid-phase synthesis.[74] Both HOBt and HOAt effectively catalyze the active ester aminolysis.

Phosphonium and uronium (a urea-derived carbocation)-based reagents (BOP, PyBOP, PyBroP, HBTU, TBTU, HAPyU, and others) have become popular in recent years.[74–77] Structures of these analogues are shown in Fig. 16.11. They couple quickly and smoothly even with sterically hindered amino acids.[78] The manufacture of BOP involves hexamethylphosphoric triamide that is highly carcinogenic. However, in most cases, BOP can be substituted by PyBOP without loss of performance.

On investigating coupling efficiencies and rates for several reagents and esters they were arranged in the following order BOP/HOBt > DIC/HOBt > DIC/HOPfp.[79] Uronium and phosphonium derivatives of HOAt, namely, HATU and PyAOP are even better coupling agents.[80] X-ray structure analysis of HATU and HBTU has revealed that the solid phase structures of these compounds are not the *N,N,N′,N′*-tetramethyluronium salts as commonly presented in the literature, but rather the guanidinium N-oxides[81] (Fig. 16.12). Also, the existence of HAPyU in the form of its guanidinium N-oxide in the solid state has been confirmed by X-ray analysis, as well as by ^{13}C NMR spectroscopy in solution.[82] It has been noted that uronium-based coupling reagents can sometimes interact with the amino group leading to linear guanidino-derivatives instead of the expected cyclic products.[83–85] Therefore, PyAOP has been recommended for the synthesis of cyclic peptides. This reagent precludes guanidinium formation that can occur when uronium salts such as HATU or HBTU react with the amino groups during a slow coupling reaction.

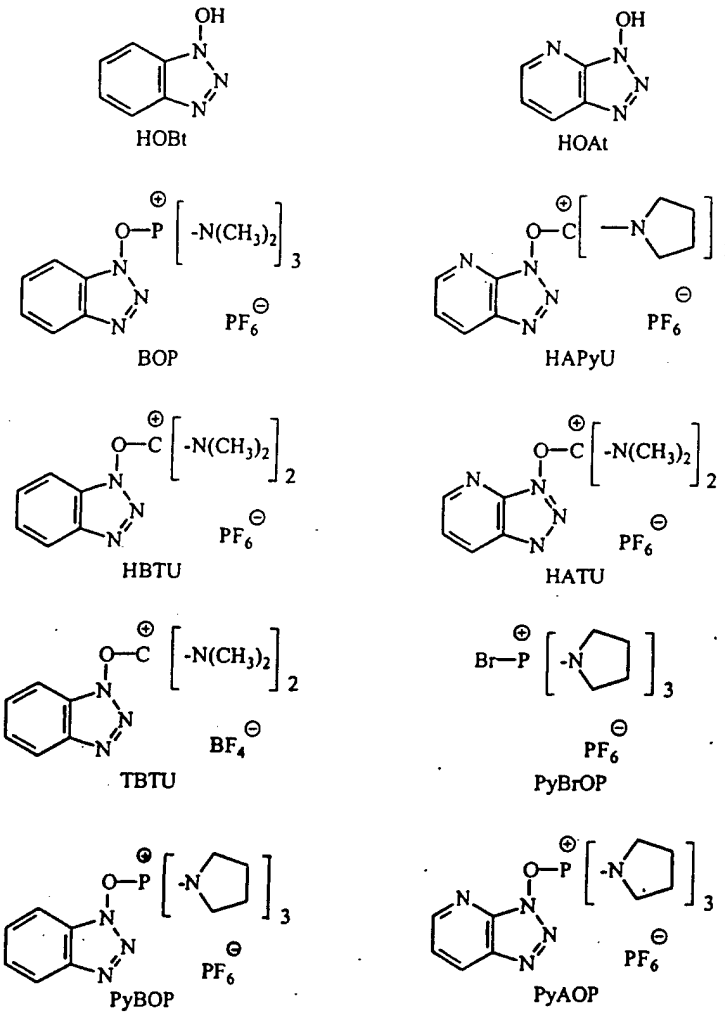

FIGURE 16.11. Common coupling agents used for the peptide cyclization step and their abbreviations.

2.4. Cyclization Techniques

Once a peptide has been synthesized on a solid support via side chain attachment, it can be intramolecularly condensed to form the desired head-to-tail cyclic product. Several approaches have been developed to carry out the cyclization reaction.

2.4.1. Cyclization in Solution. In this method of preparing head-to-tail cyclic peptides, the linear precursors are assembled either by classical methods in solution or cleaved after SPPS from the resin, purified and the cyclization reactions are carried out in solution. Most reactions are carried out under conditions of high dilution (10^{-5} M or less) and this can complicate subsequent reaction work-up.

2.4.2. Resin-bound Active Esters as Peptide Anchoring Groups for End-to-End Cyclization. In this approach, the C-terminal attachment point on the resin is turned into an active ester and upon cyclization, the product is released into

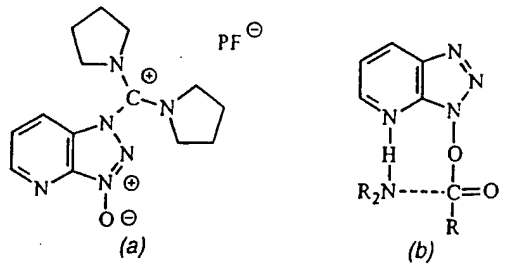

FIGURE 16.12. Structure of the condensing agent HAPyU as the guanidinium N-oxide in the solid state (*a*) as contrasted to the postulated reactive intermediate in solution during coupling where the adjacent 7-azabenzotriazole additive (*b*) can assist in amide bond formation via intramolecular base catalysis.

solution. Various groups including resin-bound *o*-nitrophenol,[10] *p*-sulfonylphenol[86] or *p*-nitrobenzophenone oxime[87] have been used as anchoring groups; their esterification with N-protected peptides produced polymeric active esters. After cleavage of the amino protecting group the resin-bound peptide active ester spontaneously cyclizes in the presence of tertiary amine, simply in suspension in highly swelling solvents (CH_2Cl_2, DMF, or pyridine).

2.4.3. On-resin Cyclization. There are two approaches currently available for the on-resin preparation of the head-to-tail cyclic peptides: the first involves selective deprotection of the C-terminal carboxylic group, activation of the liberated carboxyl function by converting it into an active ester[88]—either by carbodiimide/phenol or transesterification reagent, e.g., pentafluorophenyl trifluoroacetate[89] or *p*-nitrophenyl trifluoroacetate[90] and subsequent liberation of the amino function with cyclization initiated upon neutralization by organic base. The other approach involves simultaneous or concomitant liberation of both the C-terminal carboxylic and N-terminal amino groups and creating the lactam bridge by use of the highly effective phosphonium or uronium-based coupling reagents.[91] Both these methods retain the advantage of the pseudodilution effect provided by the resin carrier which concomitantly simplifies the reaction work-up step.

2.4.4. Enzyme-assisted Cyclization. Enzyme assisted cyclization of linear peptide esters is a relatively new but promising approach for the preparation of head-to-tail cyclic peptides.[92] Due to the entropic barriers for cyclization reactions and competing intermolecular oligomerization, chemical methods are considered largely inefficient for cyclization of longer peptides. Several head-to-tail cyclic peptides (12–25 residues in length) have been obtained via enzymatic cyclization of linear peptide C-terminal glycolate phenylalanylamide using the enzyme, subtiligase. In this particular case, cyclization efficiency appeared to depend primarily on peptide sequence and not concentration. No side chain protection was necessary because the subtiligase enzyme does not accept the ε-amino group of Lys as a substrate and thus this ensures the desired head-to-tail ligation.

2.5. Analytical Techniques

Cyclization reactions in solution can be conveniently monitored by analytical reversed-phase C_{18} HPLC typically using the familiar 0.05% TFA/acetonitrile gradients. Alternatively, on-resin cyclization reactions can be monitored by the qualitative and quantitative ninhydrin reaction (Kaiser test)[93] or the bromophenol blue test for support-bound amines.[94,95] Following the cyclization step, the reaction products are typically isolated by preparative reversed phase HPLC. The identity and purity of all isolated products can be confirmed by various mass spectrometry techniques (FABMS, ESMS, MALDI-TOF and others).[84,85,96–98] Cyclic peptides are identified as those products having a mass of 18 mass units less than their linear counterparts due to the loss of water upon cyclization. The UV-extinction coefficients of starting peptides and cyclic products usually are identical, while dimerization products have extinction coefficients twice those of the corresponding monomers.

2.6. Side Reactions in Cyclization

Oligomerization and C-terminal amino acid epimerization are two major side reactions that affect on-resin cyclization. The first variant occurs from the intermolecular condensation of neighboring peptide molecules to form dimers or oligomers, a phenomenon observed during side chain-to-side chain as well as head-to-tail cyclizations.[99] This is caused by the condensation of peptides adjacent to each other on the same polymer strand or by condensation of peptides on different strands of polymer that are within bonding distance. Racemization is not an unexpected phenomenon since it is also observed as a result of activation of the carboxyl termini of peptides in fragment condensations.

Side reactions are naturally more prevalent when cyclizations are slow. Thus, during the cyclization of an all L-hexapeptide in DMF solution, significant amounts of by-products were observed.[100] These included higher molecular weight masses such as + 60 amu (*N*-α-acetylated linear peptides; acetic acid is sometimes found as an impurity in acetonitrile); + 87 amu (*N*-α-acetylated linear peptide dimethylamides from DMF); and an additional impurity at + 166 amu was seen but not identified. Linear piperidine amides (+ 85 amu) are often observed if piperidine is used during synthesis, e.g., for Fmoc deprotection. Small amounts of piperidine can be difficult to remove through normal washes and can couple to the activated C-terminus when intramolecular cyclizations are slow. Another common impurity observed when uronium condensing reagents are used is the C-terminal guanidinium derivatized by-product (+ 98 amu). This was observed during the synthesis of small ring cyclic opioid peptide analogues.[83]

Aspartic acid and glutamic acid groups in peptides are often the cause of common side reactions. Loss of 18 mass units can be due to imide formation, but dehydration of asparagine and glutamine residues, while less common, can also be a problem. When aspartic acid is linked to a resin through its side chain, the possibility of an α-aspartyl to β-aspartyl rearrangement is often a possibility.

Among major side products observed while cyclizing glutamic acid-containing peptides in side chain to tail or side chain to side chain derivatives in 5-mer to 14-mer epitopes were the linear peptides modified at their Glu side chain carboxylic groups. Thus a +27 amu peak was attributed to a linear peptide adduct formed with dimethylamine, a trace impurity found in DMF. And a +69 amu peak resulted from an adduct formed with morpholine, a possible trace component in *N*-methylmorpholine, a base often used with difficult cyclization sequences.[101]

Sometimes, side reactions can be misinterpreted as evidence of difficult cyclization sequences. Unusually long cyclization times using BOP/HOBt/DIPEA in DMF, as monitored by the ninhydrin test appeared to be due to a reluctance to form the ring. But upon FABMS analysis of the reaction products, a major side product was seen that turned out to be a linear piperidide (+85 amu). This common derivative,[16] reported also by others[27] would result in a continuous positive ninhydrin test, since there would no longer be a carboxylic acid available for amide formation. This difficulty was overcome by more extensive washes in order to effect complete removal of residual piperidine salts that form following N-Fmoc- or C-OFm cleavage using 20% piperidine/DMF before cyclization.

3. EXAMPLES OF CYCLIC PEPTIDES OF VARYING RING SIZE

3.1. Lactams

While peptide cyclization normally implies the presence of at least two amino acids, lactam rings can often form from side chain to backbone processes that may also be in competition with oligomerization or with the formation of larger ring sizes.

The γ-, δ-, and ε-amino acids ($NH_2(CH_2)_nCO_2H$, where $n=3-5$), bound as active esters to the resin support, provided only the 5-, 6-, and 7-membered lactam rings on cyclization with no or only slight oligomerization.[102] Resin-bound β-alanine gave mainly the cyclic tri- and tetrapeptides, less cyclopentapeptide and very little eight-membered cyclodipeptide as well as some macrocyclic hexa- and heptapeptides. ε-Aminoundecanoic acid and ω-aminododecanoic acid yield mainly cyclic diamides (24 or 26 ring atoms, respectively) and decreasing amounts of higher rings up to hexamers. Lactams with unfavorable ring sizes (4-, 12-, and 13-membered rings) are not formed at all during ring-closure of the polymer-bound ω-amino acids.[102] It seems that steric isolation of the grafted polymer chains leading to monomeric rings only occurs to a minor degree. Instead very large rings (up to about 300–400 ring atoms) are formed.[102]

Polystyrene-based resins have been suggested to act chemically as a rigid lattice,[103] separating the loci of polypeptide growth. When insoluble cross-linked poly-4-hydroxy-3-nitro-styrene was used as a phenol component for a

peptide active ester, condensation between the active peptide moieties was markedly reduced and internal aminolysis led to the formation of the desired cyclic peptides[10] which were released from the insoluble carrier. It has been suggested that the enhanced preference for cyclization over open-chain coupling of peptides bound to high molecular-weight polystyrene—2% divinylbenzene based resins takes place due to separation of the specific reaction sites in the rigid lattice, an effect equivalent to high dilution (pseudodilution factor). However, convincing evidence has appeared that complete intra-resin site separation is not achieved: in fact, it has been unambiguously demonstrated that even moderately cross-linked polymers (up to 8% divinylbenzene) must be regarded as rather flexible entities, and that steric hindrance due to the polymer backbone can be discounted as a significant factor in preventing intermolecular reactions.[104]

3.2. Cyclodipeptides

Diketopiperazines (DKP) or dioxopiperazine analogs of amino acids are the simplest form of head-to-tail cyclic peptide. Diketopiperazines are frequently observed as unwanted side products, arising from intramolecular aminolysis at the dipeptide level in both solution and SPPS. DKP formation is favored by the presence in either the first or second positions of amino acids (Gly, Pro, or *N*-alkyl) that can easily adopt a cis-configuration in the resulting amide bond. Another favorable combination is to have one L- and one D-amino acid in the dipeptide, due to the minimal steric interference between the two side chains. Furthermore, rates of DKP formation differ considerably depending on the nature of the peptide–resin linkages or the structure of the C-terminal carboxyl protecting group. For example, when solid phase syntheses were performed with BAL-anchored amino acid allyl or *n*-alkyl esters, the authors[63] observed an almost quantitative side reaction due to DKP formation during Fmoc group removal at the dipeptide level. Interestingly, DKP products formed in this fashion have been exploited as scaffolds for combinatorial chemistry, with simultaneous ring formation and release from the resin. The structures themselves provided a large variety of DKP derivatives since they provided at least three different points of diversity: both amino acid side chains and one (of the two) amide bonds.[105]

3.3. Cyclic Tripeptides and Tetrapeptides

Triproline can be cyclized on a polymeric support to give the nine-membered cyclotriprolyl ring.[102] With other amino acids, cyclic tri- and tetrapeptides are formed only to a small or even negligible extent when polymer-bound *p*-sulfophenyl esters are used as the anchoring groups for end-to-end cyclization.[102] All the tripeptide sequences studied yielded oligomeric products featuring a homologous series of cyclopeptides containing up to eight tripeptide residues, i.e., 72 ring atoms. In the case of resin-bound trisarcosine, a sequential

set of cyclic peptides with up to 27 sarcosine residues could be identified by ge chromatography.[102]

While investigating the tetrapeptide [4-alanine]-chlamydocin cyclo(Aib Phe–D–Pro–Ala) precursor cyclization in solution, it was reported[106] that on of the four sequences, namely, H–Ala–Aib–Phe–D–Pro–OH (activated as it ONSu ester), produced the desired product in a much higher (at least an order o magnitude) yield than what was obtained from cyclization of the other linea tetrapeptides. This result again supports a strong sequence dependence on th nature of products formed during a cyclization step.

In cyclic diprolines and cyclic triprolines, both the smaller ring size and th proline side chains contribute to the relative rigidity of the backbone, restrictin the peptide to an all-*cis* conformation.[107] Cyclic tetrapeptides serve as usefu model compounds to study the relatively slow *cis–trans* isomerization equili- bria, *cis/trans* isomerization determined conformations, energy barriers betwee them, and their interconversions as well as the relative tendencies of the linea precursors to cyclize.[107]

In another study examining the effect of ring size, on-resin cyclization wa studied with variable length side-chain amino and carboxyl groups on the firs and fourth residues in a model tetrapeptide[108] (Fig. 16.13). BOP reagent wa used as the condensing agent to generate lactams containing 14–18 atoms. Afte cleavage from the resin, the desired cyclic tetrapeptide and a major side produc were obtained. It was found that the degree of cyclization difficulty increased significantly as the ring size of the lactam decreased from 18 to 14 atoms. Complete lactam formation required repeated condensations by using 3 equiv of BOP reagent. Thus, an 18-membered ring was formed after four couplings during a period of nearly two days; in contrast, the 14-membered ring required 14 couplings of 12 h each to reach completion as judged by the ninhydrin test. The major side product was identified as a cyclic dimer, obtained as a conse- quence of interchain cyclization on the resin.

When there is no turn-inducing structural feature (*N*-methyl amino acid, proline, or D-amino acid) present in the peptide, the linear precursor of a cyclopeptide may be unfavorably disposed toward cyclization. In the latter case, a reversible chemical modification of the peptide main chain favoring the cisoid conformation can help. Tetra(phenylalanine) whose preferred linear and rigid conformation is unfavorable for cyclization was used as a test compound for this approach. Three *t*-Boc groups were introduced as substituents on the main chain nitrogen atoms and this altered the molecule enough to allow induction of a

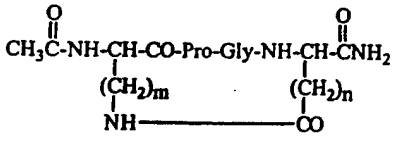

FIGURE 16.13. Structure of a tetrapeptide ($m = 4-1$; $n = 2,1$) with ring sizes from 14 to 18 subjected to cyclization. Cyclization times range from two days (18-membered ring) to one week (14-membered ring).

conformation with extremities close enough together for cyclization. Cyclization yields increased from less than 1–27% after this chemical modification.[109] On the other hand, cyclic tri-, tetra-, penta-, and hexacarbamates (with correspondingly, 13, 18, 23, and 28 ring atoms) were obtained in high yield and purity by a solid phase synthesis of side chain protected linear derivatives followed by a cyclization reaction by TBTU/HOBt in CH_2Cl_2 solution.[110]

3.4. Cyclizations of Medium Sized Rings

Medium sized rings typically contain 5–8 amino acid residues, and most studies have thus far focused at the lower range of cyclic penta- and hexapeptides. The monocyclization of peptides is often controversial and can still be regarded as an unsettled problem. Theoretical studies predict that intramolecular head-to-tail cyclizations are dependent on peptide length and can also be heavily influenced by side chain configurations. Thus, a DLDLDL hexapeptide is predicted to cyclize intramolecularly while the all-L sequence should resist head-to-tail ring closure, according to these predictions. It has been suggested that cyclization reactions of linear penta- or hexapeptides that do not contain turn-inducing amino acids such as Gly, Pro, or a D-amino acid may be extremely slow and give rise to side reactions such as epimerization and cyclodimerization even at high dilutions (10^{-3}–10^{-4}M).[111]

Significant variations of cyclization yield with sequence were observed in the DPPA mediated condensation of three different linear hexapeptides that were designed to produce the same cyclic product.[112] Cyclo-(Phe–Pro–Phe–Pro–Phe–Pro) was isolated in only 2% yield from the linear all-L-peptide H-(Phe–Pro)$_3$-OH, and low yields were also obtained from two linear diastereomers (Table 16.4). In contrast, the cyclization yield from the diastereomeric linear precursor, H–D–Phe–Pro–Phe–Pro–Phe–Pro–OH, was 57%. From their observations the authors concluded that the best precursor of a cyclic hexapeptide containing a D-amino acid residue is the sequence with the D-residue at the amino terminus.

In another instructive example involving the thymopentin pentapeptide H–Tyr–Arg–Lys–Glu–Val–Tyr–OH, cyclization in solution was performed starting from H–Tyr–Arg–Lys–Glu–Val–OH and using carbodiimide/DMAP. This resulted in a product of high yield and purity, better than obtained using the azide method. However, the strong activation conditions led to complete

TABLE 16.4. Cyclic Hexapeptide Yields Vary Greatly Depending on Configurations Present

Linear Sequence	Yield of Cyclic Peptide (%)
1. H–D-Phe–Pro–Phe–Pro–Phe–Pro–OH	57
2. H–Phe–Pro–D-Phe–Pro–Phe–Pro–OH	2
3. H–Phe–Pro–Phe–Pro–D-Phe–Pro–OH	1
4. H–Phe–Pro–Phe–Pro–Phe–Pro–OH	2

inversion of the C-terminal valine in those cases. This problem was not seen when the linear precursors contained a C- or N-terminal D-amino acid. It was suggested that the presence of a D-amino acid in one of these positions favored a conformation in the linear precursor that would lead to rapid cyclization in good yield.[113] In the absence of such a favorable conformation, the strong and long-lasting activation would lead to racemization at the C-terminus, in which case the now LLLLD linear peptide could undergo cyclization readily.[113]

On the other hand, synthesis of the same cyclic thymopentin pentapeptide from a different linear precursor, H–Arg–Lys–Asp–Val–Tyr–OH, using DPPA with in situ azide formation and a different point of cyclization (Tyr) provided only one product: the all-L-amino acid cyclic pentapeptide. Determination of the chirality of all five amino acids confirmed the absence of racemization.[114] Surprisingly, when the highly effective cyclization agent HAPyU was used, no intermolecular reactions were observed, even at high peptide concentrations (0.1–0.2 M), indicating that at least for the head-to-tail and side chain cyclizations studied, application of the principle of dilution is not required.[115] Attempts to cyclize a thymopentin-related hexapeptide analogue, H–Val–Arg–Lys(Ac)–Ala–Val–Tyr–OH (0.01 M in solution) using BOP and its HOBt-based analogues yielded 5–25% of the desired cyclic peptide. However, the process was accompanied by extensive racemization of the C-terminal tyrosine residue. In contrast, using HAPyU, the all-L-cyclohexapeptide was formed in 55% yield within 30 minutes; and less than 0.5% of the D-Tyr isomer was detected in the reaction mixture. But even HAPyU was not able to effect cyclization of the corresponding all-L pentapeptide without racemization.

In another instructive example, a set of six diastereomeric cyclic hexapeptides of the sequence H–Leu–Tyr–Leu–Gln–Ser–Leu–OH, in which each residue was serially replaced with the D-amino acid, was synthesized (classical methods in solution) and cyclized via their azides.[116] The authors found no significant difference in the cyclization yields with respect to the position of the D-residue, and they could not confirm that a β-turn inducing subunit (a DL pair) needed to be placed only at the center or only at the ends of the peptide chain in order to induce mono-cyclization. Nevertheless, the corresponding all-L-hexapeptide, H–Leu–Tyr–Leu–Gln–Ser–Leu–OH, failed to cyclize when using the azide method or with water-soluble carbodiimide (EDCI).

When two isomeric linear hexapeptides, H–Leu–Met–Gln–Trp–Phe–Gly–OH and H–Met–Gln–Trp–Phe–Gly–Leu–OH (the two linear sequences did not coelute in RP-HPLC) were submitted to cocyclization (PyBOP, DIPEA, DMF), only a single cyclic product was obtained, indicating that both peptides cyclized independently in a head-to-tail fashion to form the same structure. No dimers or polymeric sequences were detected by HPLC or FABMS.[117]

Often the imino acid proline is included to help induce β-turn structure and facilitate cyclization. However, whereas the pentapeptide, H–Arg–Lys(Ac)–Ala–Val–Tyr–OH, underwent cyclization at room temperature (HAPyU, DIPEA, 0.001 M in DMF) to give a mixture of 33% cyclomonomer and 38% cyclodimer in only 10 min, the presence of Pro, regardless of its position in the

linear sequence, dramatically hindered formation of cyclomonomers.[118] Similarly, the cyclization probability of hexapeptides was nearly abolished by the presence of proline.[118] In contrast to proline, a single D-amino acid, glycine or *N*-methylamino acid, or just the backbone-modified 2-hydroxy-4-methoxybenzyl (Hmb) -derivatized Ala residues dramatically increased the formation of cyclic pentapeptide monomer.[118]

Oligomer formation during cyclizations of peptides attached to a solid support has been investigated by numerous groups. Again, results have been mixed. In a detailed study of longer peptide sequences by McMurray, the amount of dimer content was uniformly high, and this was not significantly affected by changes in the resin type, resin load, solvent, or coupling agents.[119] In contrast to these results, our group's experience with smaller cyclic pentapeptides has been more positive. Only minimal amounts of dimer content could be found in several studies when using a side-chain attachment, on-resin head-to-tail cyclization approach.[21] A possible explanation for this dichotomy may relate to β-sheet formation.[21,104,120] Longer peptides may be more likely to form anti-parallel β-sheet dimers while still attached to the solid support and this may facilitate intermolecular dimer formation. In contrast, with shorter linear sequences, this type of β-sheet structure may be less prevalent, comparable to the behavior of linear peptides in solution, and thus intermolecular reactions may be entropically disfavored. In any case, the tendencies of compounds to form dimers and higher oligomers is almost certainly sequence specific. The cyclization rules governing product monomer/dimer ratios are likely to resist a facile discovery for some time to come.

3.5. Larger Cyclic Peptides

An interesting study regarding the relationship between primary structure and cyclization efficiency was conducted on a 14-residue cyclic peptide that, when correctly cyclized takes on an amphipathic β-sheet form. A set of purified linear peptides, prepared by solid phase methods, were head-to-tail cyclized in DMF with BOP or HBTU reagents. HPLC analysis of the cyclization products convincingly demonstrated that:

1. Low yields and significant racemization (up to 40%) can occur during cyclization reactions, especially when the carboxyl terminus is not proline;
2. peptides which cyclized more slowly showed greater amounts of racemization;
3. the reaction conditions used had a major influence on the amount of racemization.[121]

The synthesis of a series of 25 11-residue side chain-to-side chain lactam cyclized peptides of related sequences with ring sizes ranging from 15 to 39-

atoms was also investigated.[88] The highest yields of the target cyclic peptides were observed with ring sizes of 21–30 atoms, corresponding to ring sizes of seven to ten amino acid residues. Good yields were also reported for some of the smaller ring sizes. However, the largest cyclic lactams were obtained with only poor yields of the desired monocyclic peptides, with cyclodimers being the major contaminants.

Side chain-to-side chain and side chain-to-tail lactam formation on a TentaGel resin was studied using peptides of varying length and based on a 12-mer sequence, H–Glu–Gly–Val–Gln–Gln–Glu–Gly–Ala–Gln–Gln–Pro–Ala–OH. Among the cyclic peptides studied, the 8-mer sequence gave the highest yield. When yields were low, the major side products observed included the linear peptides modified at their Glu side chain carboxyl groups, and intermolecularly cross-linked dimers. When ring sizes were larger than 11 amino acids or smaller than six amino acids, dimers and linear peptide adducts were more common.

Since the ring-size dependence of cyclization efficiency may be specific to the epitope sequence and Pro has been reported to assist peptide cyclizations, a series of oligoalanyl peptides with the sequence H–$(Ala)_n$–Pro–Ala–Glu(OAl)–β–Ala–β–Ala–Lys–Met–TentaGel ($n = 2–11$) were synthesized and subsequently cyclized in a head-to-side chain (Glu) fashion on TentaGel resin. The results indicated that the cyclization of the oligoalanyl peptides larger than eight amino acids was poor. Peptides with deletion sequences were detected and became problematic with increasing length, even though double couplings were employed during the synthesis.[101]

Enzymes represent a potentially attractive way to produce cyclic peptides through an efficient catalytic condensation process. Enzyme assisted cyclization of peptide C-terminal glycolate phenylalanylamide esters using the enzyme, subtiligase, revealed a minimum length requirement of 12 residues. Peptides shorter than 12 residues hydrolyzed or dimerized but did not cyclize, presumably because the enzyme could not accommodate both ends in a productive binding geometry. As the length of the peptides increased, the cyclization efficiency also increased while dimerization and hydrolysis decreased. No dimerization was observed for peptides greater than 14 residues in length, indicating that intramolecular cyclization is much faster than the corresponding intermolecular dimerization.[92]

4. PROPERTIES OF HEAD-TO-TAIL CYCLIC PEPTIDE

By forming a new amide bond between the N-terminal amine and the C-terminal carboxylate, the resulting cyclic peptide acquires new physical characteristics. The elimination of two ionizable groups renders the cyclic peptide more hydrophobic with commensurably longer retention times on most reversed phase-high performance liquid chromatography columns. The cyclic peptides

are naturally resistant to exopeptidases and in general can be expected to be more stable to most proteolytic enzymes although this is not necessarily an absolute tendency.[122]

When assayed for their biological activities, cyclic peptides are often more potent than their linear counterparts. This behavior has been exploited through the preparation of cyclic analogs of the Arg–Gly–Asp cell-adhesion motif, cyclo(Arg–Gly–Asp–Phe–Pro–),[123] by the synthesis of a cyclic hexapeptide analogue of somatostatin, cyclo(Phe–Pro–Phe–D-Trp–Lys–Thr–),[7] and by a constrained analog of leucine enkephalin, Tyr-cyclo(D-Lys–Gly–Phe–Leu–), known as the DiMaio–Schiller compound.[124] The latter case involved ring formation from the side chain of D-lysine to the C-terminal acid, since the N-terminal amine group is known to be part of the essential pharmacophore for this opioid analog. Cyclic compounds often possess the added bonus of receptor selectivity. For example, the DiMaio–Schiller analog was found to be much more potent towards the μ versus the δ class of opioid receptors. Interestingly, an even more constrained analog with a 13-atom ring, Tyr-cyclo(D-Lys–Phe–Ala–), was even more potent, with subnanomolar IC_{50}s towards both receptor classes, but was therefore surprisingly nonselective.[125]

While cyclic peptides might appear to be ideal drug lead candidates because of their stabilized structure, they tend to exhibit limited bioavailability.[122] Through the study of transport properties of peptides, several workers have concluded that the problem may devolve to the nature of the amide bond itself. Because of its hydrogen bonding potential, the amide groups accumulate waters of hydration that inhibit transport through membrane barriers.[126] The resulting "desolvation penalty" is a significant energy cost which is a reasonable rationale for the lack of oral activity of even relatively constrained, small ring cyclic peptides.

The cyclic undecapeptide immune-suppressant cyclosporin provides a spectacular exception to this limited bioavailability. Cyclosporin actually retains significant oral activity and has been a mainstay of postsurgical transplant regimens. But cyclosporin's structure contains seven *N*-methyl amides which precludes any role as hydrogen bond donors. And in one of its known multiple low-energy conformers, cyclosporin's remaining four amides are each involved in a pair of *intra*molecular hydrogen bonds.[127]

The lessons from cyclosporin could serve as models for future structure–function studies. The first steps would involve a strategy to use cyclic peptides first to find biologically active lead candidates for a given biological response. Then, in analogy with cyclosporin, the parent structure might be modified with amide bond replacements, and/or other conformational constraints designed to enhance membrane transport while inhibiting enzymatic degradation. This general approach has led to considerable research for suitable amide bond surrogates that go beyond *N*-methylation. These efforts are supplemented by studies with other backbone modifications including β-turns and γ-turn mimics.[128]

5. CYCLIC PSEUDOPEPTIDES

Pseudopeptides have been defined as peptides with one or more amide bond replacements (referred to as amide bond surrogates).[129] Examples of these replacements include ketomethylene ($COCH_2$), reduced carbonyl (CH_2NH), retroamide (NHCO), thioamide (CSNH), alkene (CH=CH), thiomethylene (CH_2S), and hydroxyethylene ($CHOHCH_2$).[129,130] Several of these can be readily prepared using solid phase methods of synthesis as shown in Scheme 5. Some of the earliest examples of pseudopeptides were intended as inhibitors of such enzymes as collagenase[131] and renin[132] and have more recently found applications for inhibition of HIV aspartyl protease.[130] Reviews have appeared which cover the "psi-bracket" nomenclature of pseudopeptides and the breadth of backbone changes found in nature and synthetic analogs of peptides.[129,133,134]

Cyclic pseudopeptides represent a natural extension of backbone-modified linear peptides; they combine the inherently greater resistance of cyclic peptides toward enzyme attack with one or more enzyme resistant amide replacements. In those cases where pseudopeptide backbone changes introduce unwanted flexibility in linear peptides, small cyclic peptides represent better hosts by providing increased conformational constraint.[135,136]

While the conformational properties of the amide bond have been extensively studied, there is less known about the ability of well-known structural features such as helices, loops, β-turns and β-sheets to coexist with a plethora of possible backbone modifications. One way to study this question is by introducing an amide surrogate as a "guest" in one or more positions of a cyclic peptide "host."[137] For example, the well-studied cyclic pentapeptides, cyclo(Gly–Pro–Gly–D-Xxx–Pro), were shown to form a relatively common stabilized structure, consisting of two intramolecular hydrogen bonds (Fig. 14(a)), using four of the five amide bonds, participating either as H-bond donors or H-bond acceptors.[139,140] This cyclic peptide was thus recognized as a suitable model system to ask whether various amide bond replacements could coexist with the

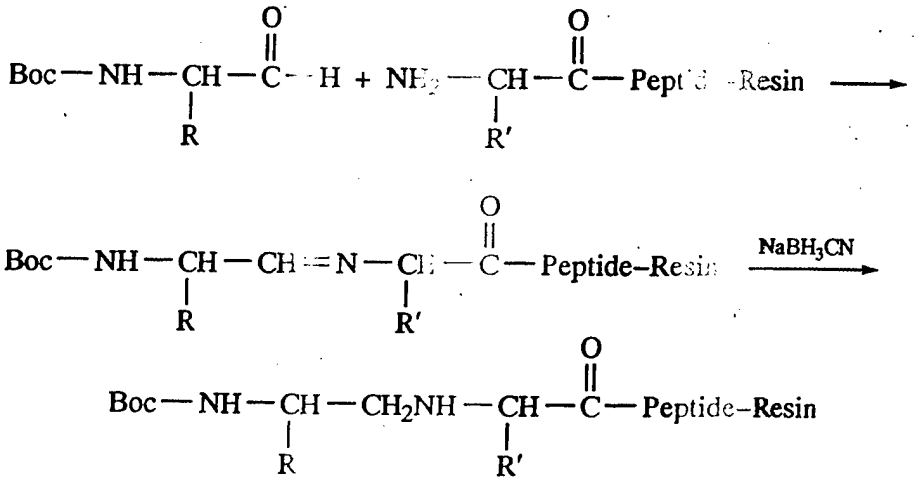

Scheme 5. Solid phase synthesis of a ψ[CH_2NH] pseudopeptide.

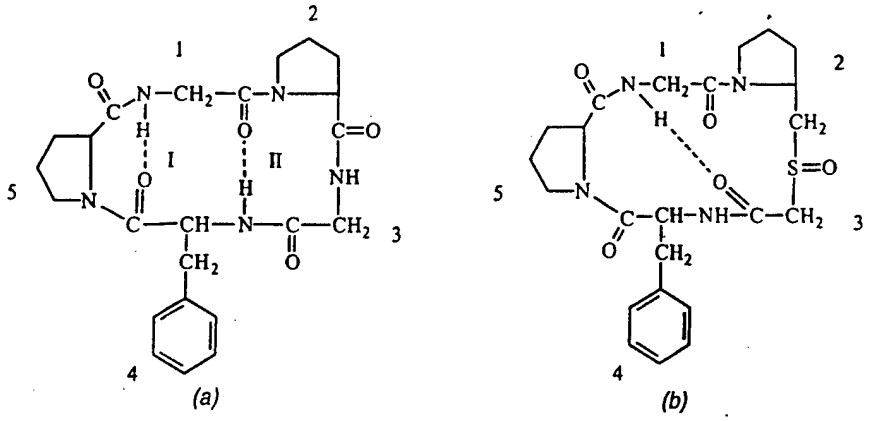

FIGURE 16.14. Structure of a cyclic pentapeptide (*a*) and a cyclic ψ[CH_2S] pseudopentapeptide (*b*) showing shift of intramolecular β-turn.

intramolecular β- and γ-turns found in the parent molecule.[137] Remarkably, the sulfoxide group, normally an excellent hydrogen bond acceptor, does not form any inter- or intramolecular hydrogen bond in the solid state.

As shown in Table 16.5, a variety of amide bond surrogates were introduced into the model pentapeptides at several positions. NMR spectrometry was used to assess the presence of intramolecular hydrogen bonding using chemical shift, temperature dependence and solvent dependence data. While analysis was often complicated by the presence of two or more rapidly interconverting conformers, especially in the solvent dimethylsulfoxide, it is clear that the different amide

TABLE 16.5. Amide Bond Replacements Within the Cyclic Peptide cyclo(Gly–Pro ψ[XX]Gly–D-Phe–Pro) and cyclo(Pro ψ[YY]Gly–Pro–Gly–D-Phe)

	Amide Bond Replacement	$CDCl_3$	DMSO	Reference
XX =				
ψ[CONH]	Amide	+	+	139
ψ[CH_2S]	Thiomethylene ether	+	+	137, 138
ψ[CH_2SO]	Thiomethylene ether sulfoxide (R or S)	±	±	142
ψ[CH_2NH]	Reduced carbonyl	±	−	143
ψ[CH_2NH] · TFA	Reduced carbonyl (protonated)	−	−	143
ψ[CSNH]	Thioamide	+	+	141
YY =				
ψ[CONH]	Amide	+	+	139
ψ[CH_2S]	Thiomethylene ether	+	+	137, 138
ψ[CH_2SO]	Thiomethylene ether sulfoxide (R or S)	−	+	143
ψ[CH_2NH]	Reduced carbonyl	±	±	143
ψ[CH_2NH] · TFA	Reduced carbonyl (protonated)	±	±	143

+ = compatible with turns; − = not compatible with turns.
± = compatible with only one turn or alters structure.

replacements can exhibit a wide range of conformational disruptions. For example, with a single ψ[CH_2SO] replacement in the original β-turn position, an intramolecular hydrogen bond is observed in the solid state but it is now in an altered relative position (Fig. 16.14(b)). Remarkably, the sulfoxide group, normally an excellent hydrogen bond acceptor, does not form any inter- or intramolecular hydrogen bond in the solid state. It will be of interest to investigate the effects of amide surrogates in rings both larger and smaller than cyclic pentapeptides (15 atoms) and to establish the sequence dependence of these structural modifications.

The thioamide replacement, ψ[CSNH], represents a particularly subtle amide bond surrogate. It was first introduced into a head-to-tail cyclic peptide in the model cyclopentapeptides, cyclo[Proψ[CSNH]Gly–Pro–Gly–D-Phe] and cyclo[Pro–Gly–Proψ[CSNH]Gly–D-Phe][141] and soon thereafter in a biologically active cyclic enkephalin (but in a side chain-to-tail analogue).[144] The reduced electronegativity of sulfur places higher electron density on the thioamide nitrogen, resulting in its potentially improved H-bond donor ability. In fact, when the thioamide was introduced into a cyclic hexapeptide model system, cyclo(Pro–Phe–Val–Phe–Phe–Gly) at the Phe–Phe position, the molecule altered its parent conformation, presumably to favor the donor ability of the thioamide[145] (Fig. 16.15). In contrast, within a cyclic pentapeptide, cyclo-(Proψ[CSNH]Gly–Pro–Gly–D-Phe), where the thioamide NH would have been the donor contributor to an intramolecular γ turn, this feature was *not* observed. This was attributed to a steric clash between the bulkier sulfur of the thioamide and the adjacent proline side chain.[141]

Pseudopeptides can also be prepared in which two or more amide bonds are replaced: this can give rise to unique forms of macrocycles, especially if the building blocks incorporate chiral amino acids with defined side chains. One of the first examples of such pseudopeptide macrocycles was the cyclic pseudohexapeptide, (Glyψ[CH_2S]Phe)$_3$.[146] Similar head-to-tail cyclic analogues containing ψ[CH_2NH] amide bond replacements were also prepared using solid phase methods of synthesis, and some were shown to bind metal ions, presumably via the basic amine backbone moieties.[147]

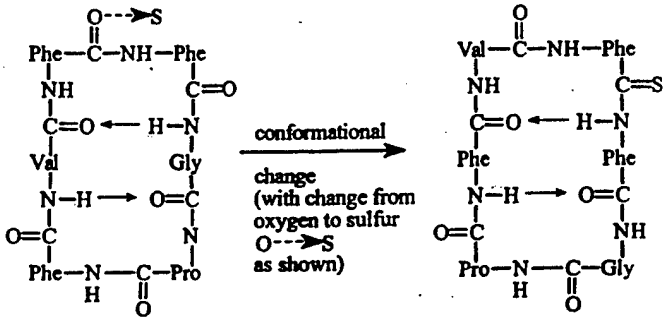

FIGURE 16.15. Conformational change accompanies thionation of a more sterically accessible Phe–Phe amide to form the Pheψ[CSNH]Phe-containing pseudopeptide. This leads to a new hydrogen bonded structure with thioamide participation as a donor. Nevertheless all structures displayed significant conformational heterogeneity.

The combination of flexible amide replacements with rigid amino acids represents further evidence of the evolution of cyclic peptide analogs. One such structure is represented by the compound, D-Phe[1]–Cys–Tyrψ[CH_2N]D-Tca–Lys–Thr–Pen–Thr–NH_2, where Tca represents a constrained β-carboline-related tryptophan analog.[148] This analog of somatostatin is a significant departure from the original hypothalamic-derived tetradecapeptide. Unlike mini-somatostatin,[7] the head-to-tail cyclic hexapeptides developed by the Merck group, this structure retains the disulfide bridge of somatostatin, but in a much smaller, 18-atom ring. Furthermore, the ring contains both a ψ[CH_2NH] amide replacement as well as the highly constrained amino acid derivative, tetrahydro-β-carboline. Remarkably, many of these somatostatin analogues possess opioid activity although the reduced potency and lack of selectivity seen with the pseudopeptides compared to their all-amide parents were attributed to the flexible ψ[CH_2N] unit. It is significant that such flexibility appears to persist in spite of the presence of the constrained Tca residue within the ring portion of the molecule.

6. LIBRARIES OF HEAD-TO-TAIL CYCLIC PEPTIDES

In 1991, a number of groups revealed their detailed research involving methods to generate and test mixtures or arrays of linear peptides known as peptide libraries.[149–153] Soon thereafter, the field became known as combinatorial chemistry. Thus, the pioneering work of Mario Geysen with linear peptides[154] was expanded to include a much wider group of organic molecules including carbohydrates, nucleic acids, and rigid peptidomimetic heterocycles such as the benzodiazepines. Numerous reviews of this approach have recently appeared,[155–161] as well as several texts,[162–165] and a useful on-line listing of references to the field is maintained.[166]

In 1993, our group reported one of the initial efforts to extend this field to include head-to-tail cyclic peptides.[16] A year earlier, DeGrado and colleagues had impressively demonstrated, using disulfide bridged cyclic peptides prepared on bacterial viruses known as phages, that cyclic peptides can provide analogues that are 2–3 orders of magnitude more potent than their linear counterparts in their bioassays.[167] This finding accelerated efforts by several groups to prepare more constrained peptides, pseudopeptides and peptidomimetic structures, both individually and in library (mixture) formats. For example, Houghten's group reported that while linear peptides tended to yield a higher percentage of active structures or "hits," their cyclic counterparts yielded fewer but higher quality candidates, overcoming the entropic penalty of the more flexible linear chains.[28]

The same San Diego group reported an imaginative approach toward molecular diversity in a cyclic scaffold by introducing diversity in the side chains of a cyclic oligolysine precursor.[168] Thus, the central ring can be composed of cyclo(Gly–Lys)$_n$ and the ε-amino groups of the three lysines can be used to attach additional functional groups in a combinatorial fashion (Fig. 16.16(a)).

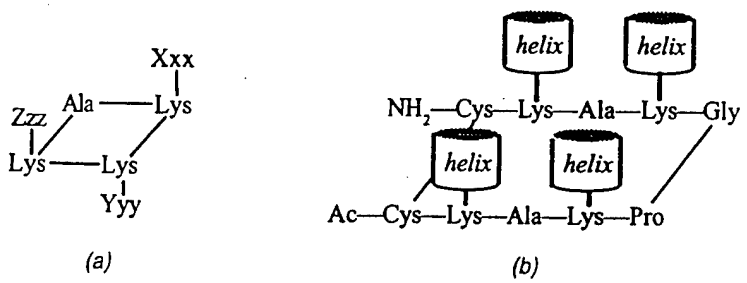

FIGURE 16.16. Structure of a cyclic peptide library template and comparison with the TASP template for the synthesis of protein mimics.

This structure is reminiscent of a relatively rigid "TASP" template introduced by Mutter and co-workers[169] to prepare protein mimics with relatively constrained linear peptides tethered to the oligolysine core (Fig. 16.16(b)).

In our approach, we exploited known chemistries for preparing cyclic peptides using a side chain resin attachment Fmoc strategy as described earlier.[15] While this tactic fixes the linkage point, the remaining positions may be substituted by small or large mixtures of amino acids or their analogues. By adopting the positional scan approach,[170] we were able to prepare an 80,000-component library (with about 20,000 nonredundant cyclic peptides) in 48 separate vials with two fixed positions represented in each vial (the D-aspartic acid attachment link and one other). (Fig. 16.17.) Once these mixtures were assayed for binding against an endothelin receptor, the most active vials corresponded exactly to the four residues of a potent endothelin antagonist,

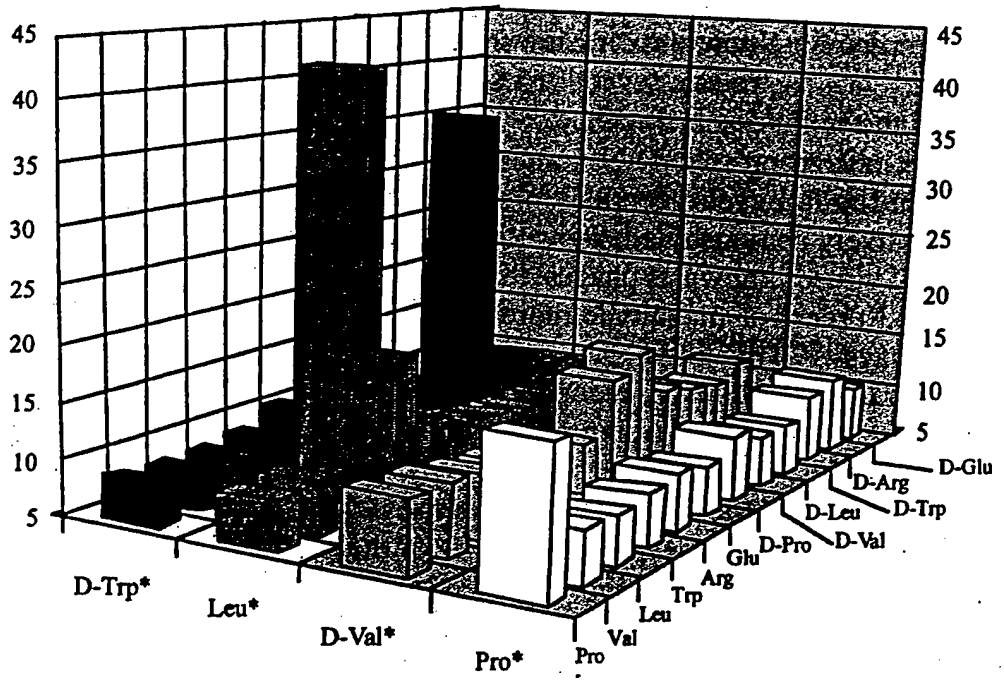

FIGURE 16.17. Endothelin antagonist bioactivity profiles for a set of 48 cyclic pseudopeptide "library" mixtures incorporating the positional scan approach.

cyclo(Phe–D-Val–Leu–D-Trp–D-Asp–).[22] This experiment supported the utility of mixtures for lead discovery by providing a positive control. It also demonstrated the effectiveness of the positional scan approach to find rather quickly a few lead compounds after a single set of assays.

A solid phase strategy with concomitant cyclization and cleavage using *p*-nitrobenzophenone oxime resin has been utilized to obtain a cyclic pentapeptide library cyclo(Arg–Gly–Asp–Xxx–Aca), where Xxx = Ser, Lys, Gln, Ala, Glu, Pro, Val, Tyr, Phe, Trp(CHO), and Aca = ω-aminocaproic acid.[171] The oxime resin procedure was effective at producing nearly equivalent peptide mixtures when using either a separate coupling protocol for the individual amino acids or by a mixed coupling in which the 10 amino acids were represented by equivalent molar quantities.

Using a solution cyclization approach, a set of more than 400 head-to-tail cyclic hexapeptides were prepared having the sequence RGDSPXxx, where Xxx = all usual L- and D-amino acids and Gly and RZzzDSZzzY, where Zzz = all possible combinations of the 20 L-amino acids, analogues were studied.[100] It was found that L- and D-amino acids in the C-terminal position have no influence on the cyclization of the hexapeptide analogues. Ile, Val, Thr (D- or L-) in the C-terminal position reduced cyclization yields. This finding is in contrast to prior reports[13] that suggested that the presence of either Gly, Pro or a D-configuration amino acid residue in the sequence is an essential prerequisite for ring closure of linear hexapeptides.

These methods for cyclic library production should also be amenable for the synthesis of related peptidomimetics. In fact, libraries of cyclopseudopeptides have been prepared in which dipeptide units in the ring were substituted with either Proψ[CH_2S]Gly pseudodipeptides or by Xxxψ[CH_2NH]Yyy pseudopeptide units.[172] In the latter case, the cyclic analogs were prepared on the solid support by coupling an amino aldehyde to the resin bound amine followed by sodium cyanoborohydride reduction of the Schiff base intermediate (Scheme 5). Following cleavage, the pseudopeptides containing one or more ψ[CH_2NH] units were cyclized in solution to furnish several head-to-tail cyclic peptides including cyclo(D-Pheψ[CH_2NH]Xxx–Arg–Gly–Asp),[172] cyclo(Glyψ[CH_2NH]Phe)$_3$ and cyclo(Glyψ[CH_2NH]Phe)$_4$.[147] Alternatively, using side chain attachment, this approach can be adapted for the synthesis of cyclic ψ[CH_2NH] pseudopeptides via on-resin cyclization.

Future applications of cyclic peptides can be envisaged in which they can be used for drug discovery, for the production of novel biomaterials, and even for use in affinity separations. In many cases, their use may not require cleavage from the solid support in which case more options are available for permanent attachment of side chain functional groups to a solid support.[173] Resin bound cyclic peptide libraries have been described and cyclic peptides attached to photolabile linkers provide an additional approach to orthogonality. It may be anticipated that additional innovations will involve cyclic peptides as important contributors to the quest for practical applications of molecular diversity.

REFERENCES

1. Ovchinnikov, Y. A.; Ivanov, V. T. In *The Proteins*, Neurath, H.; Hill, R. L. Eds.; Academic Press; New York, 1982, p. 307.
2. Pettit, G. R.; Srirangam, J. K.; Herald, D. L.; Erickson, K. L.; Doubek, D. L.; Schmidt, J. M.; Tackett, L. P.; Bakus, G. J. *J. Org. Chem.* 1992, **57**, 7217.
3. Gause, G. F.; Brazhnikova, M. G. *Lancet* 1994, **247**, 715.
4. Hassan, M. A.; Al-Yahya, M. A. In *Analytical Profiles of Drugs Substances, 16*, Florey, K. Ed.; Academic Press: New York, 1987, p. 145.
5. Ihara, M.; Noguchi, K.; Saeki, T.; Fukuroda, T.; Tsuchida, S.; Kimura, S.; Fukami, T.; Ishikawa, K.; Nishibe, M.; Yano, M. *Life Sciences* 1992, **50**, 247.
6. Fesik, S. W.; Gampe, Jr., R. T.; Holzman, T. F.; Egan, D. A.; Edalji, R.; Luly, J. R.; Simmer, R.; Helfrich, R.; Kishore, V.; Rich, D. H. *Science* 1990, **250**, 1400.
7. Veber, D. F.; Freidinger, R. M.; Perlow, D. S.; Paleveda, W. J.; Holly, F. W.; Strachen, R. G.; Nutt, R. F.; Arison, B. H.; Hommick, C.; Randall, W. C.; Giltzer, M. S.; Saperstein, R.; Hirschmann, R. *Nature* 1981, **292**, 55.
8. Ghadiri, M. R.; Granja, J. R.; Buehler, L. K. *Nature* 1994, **369**, 301.
9. Schroder, E.; Lubke, K. In *The Peptides, Vol. II. Synthesis, Occurrence and Action of Biologically Active Polypeptides*, Academic Press: New York, 1966.
10. Fridkin, M.; Patchornik, A.; Katchalski, E. *J. Am. Chem. Soc.* 1965, **87**, 4646.
11. Sklyarov, L. Y.; Shashkova, I. V. *J. Gen. Chem.* 1969, **39**, 2778.
12. Kates, S. A.; Solé, N. A.; Albericio, F.; Barany, G. In *Peptides: Design, Synthesis and Biological Activity*; Basava, C.; Anantharamaiah, G. M. Eds.; Birkhauser: Boston, 1994, p. 39.
13. Mazur, S.; Jayalekshmy, P. *J. Am. Chem. Soc.* 1978, **101**, 677.
14. Barany, G.; Merrifield, R. B. In *The Peptides*, Vol. II, Gross, E.; Meienhofer, J. Eds.; Academic Press: New York, 1979, p. 1.
15. Rovero, P.; Quartara, L.; Fabbri, G. *Tetrahedron Lett.* 1991, **32**, 2639.
16. Darlak, K.; Romanovskis, P.; Spatola, A. In *Peptides: Chemistry, Structure, and Biology*; Hodges, R.; Smith, J. Eds.; ESCOM: Leiden, 1994, p. 981.
17. Bednarek, M.; Bodanszky, M. *Int. J. Peptide Protein Res.* 1983, **21**, 196.
18. Bodanszky, M.; Deshmane, S. S.; Martinez, J. *J. Org. Chem.* 1979, **49**, 1622.
19. Spatola, A. F.; Darlak, K.; Romanovskis, P. *Tetrahedron Lett.* 1996, **37**, 591.
20. Romanovskis, P.; Spatola, A. F. In *Peptides 1996*; Ramage, R.; Epton, R. Eds.; 1998, p. 761.
21. Spatola, A. F.; Romanovskis, P. In *Combinatorial Peptide and Nonpeptide Libraries*; Jung, J. Ed.; VCH: Weinheim, 1996, p. 327.
22. Spatola, A. F.; Crozet, Y.; deWit, D.; Yanagisawa, M. *J. Med. Chem.* 1996, **39**, 3842.
23. McMurray, J. S. *Tetrahedron Lett.* 1991, **32**, 7679.
24. Albericio, F.; Kneib-Cordonier, W.; Biancalana, S.; Gero, L.; Madada, R. I.; Hudson, D.; Barany, G. *J. Org. Chem.* 1990, **55**, 3730.
25. Matsueda, G.; Stewart, J. *Peptides* 1991, **2**, 45.
26. Brugghe, H. F.; Timmermans, H. A. M.; Vanunen, L. M. A.; Jan Ten Hove, G.; van De Werken, G.; Poolman, J. T.; Hoogerhout, P. *Int. J. Peptide Protein Res.* 1994, **43**, 166.

27. Kates, S. A., Solé, N. A.; Johnson, C. R.; Hudson, D.; Barany, G.; Albericio, F. *Tetrahedron Lett.* 1993, **34**, 1549.
28. Eichler, J.; Lucka, A. W.; Pinilla, C.; Houghten, R. A. *Molecular Diversity* 1996, **1**, 233.
29. Valero, M. L.; Giralt, E.; Andreu, D. *Tetrahedron Lett.* 1996, **37**, 4229.
30. Guibe-Jampel, E.; Wakselman, M. *Synthetic Commun.* 1982, **12**, 219.
31. Romanovskis, P. J.; Syskov, I. V.; Liepkaula, I. K.; Porunkevich, J. A.; Ratkevich, M. P. in *Peptides: Synthesis, Structure, Function*; Gross, E.; Rich, D. Eds.; Pierce Chem. Co.: Rockford, 1981, p. 229.
32. Hocker, M. D.; Caldwell, C. G.; Macsata, R. W.; Lyttle, M. H. *Peptide Res.* 1995, **8**, 310.
33. Hinsberg, O.; Himmelschein, A. *Chem. Ber.* 1896, **29**, 2019.
34. Pande, C. S.; Gupta, S. K.; Glass, J. D. *Indian J. Chem.* 1987, **26B**, 957.
35. Kulikov, S. V.; Selivanov, R. S.; Ginak, A. I. In *Peptides: Chemistry, Structure and Biology*; Kaumaya, P. T. P.; Hodges, R. S. Eds.; Mayflower Scientific Ltd.: 1966, p. 48.
36. Birr, C. In *Innovation and Perspectives in Solid Phase Synthesis*; Epton, R. Ed.; Oxford, 1994, p. 83.
37. Bycroft, B. W.; Chan, W. C.; Chhabra, S. R.; Hone, N. D. *J. Chem. Soc. Chem. Commun.* 1993, 778.
38. Bloomberg, G. B.; Askin, D.; Gargaro, A. R.; Tanner, M. J. A. *Tetrahedron Lett.* 1993, **34**, 4709.
39. Chan, W. C.; Bycroft, B. W.; Evan, D. J.; White, P. *J. Chem. Soc. Chem. Commun.* 1995, 2209.
40. Rohwedder, B.; Mutti, Y.; Dumy, P.; Mutter, M. *Tetrahedron Lett.* 1998, **39**, 1175.
41. Letsinger, R. L.; Kornet, M. J. *J. Am. Chem. Soc.* 1963, **85**, 3045.
42. Zalipsky, S. *Bioconjugate Chem.* 1995, **6**, 150.
43. Dressman, B. A.; Spangle, L. A.; Kaldor, S. W. *Tetrahedron Lett.* 1996, **37**, 937.
44. Ghosh, A. K.; Duong, T. T.; McKee, S. P.; Thompson, W. J. *Tetrahedron Lett.* 1992, **33**, 1775.
45. Medvedkin, V. N.; Mitin, Y. V.; Klimenko, L. V.; Podgornova, N. N.; Bystrychenko, A. I.; Zabolotskikh, V. F.; Korobeinikova, L. I.; Pozdeeva, V. V. *Bioorg. Khim (in Russian)* 1989, **15**, 460.
46. Alsina, J.; Rabanal, F.; Giralt, E.; Albericio, F. *Tetrahedron Lett.* 1994, **35**, 9633.
47. Alsina, J.; Chiva, C.; Ortiz, M.; Rabanal, F.; Giralt, E.; Albericio, F. *Tetrahedron Lett.* 1997, **38**, 883.
48. Pozdnev, V. F. *Int. J. Peptide Protein Res.* 1992, **40**, 407.
49. Mitsunobu, O. *Synthesis* 1981, **1**, 1.
50. Trzeciak, A.; Bannwarth, W. *Tetrahedron Lett.* 1992, **33**, 4557.
51. Romanovskis, P.; Spatola, A. F. *J. Peptide Res.* 1998, **52**, 356.
52. Waki, M.; Kitajima, Y.; Izumiya, N. *Synthesis* 1981, 266.
53. Loudon, G. M.; Radhakrishna, A. S.; Almond, M. R.; Blodgett, J. K.; Boutin, R. H. *J. Org. Chem.* 1984, **49**, 4272.
54. Bittner, S.; Assaf, Y. *Chem. and Ind.* 1975, 281.

55. Krchňák, V.; Flegelova, Z.; Weichsel, A. S.; Lebl, M. *Tetrahedron Lett.* 1995, **36**, 6193.
56. Richter, L. S.; Gadek, T. R. *Tetrahedron Lett.* 1994, **35**, 4705.
57. Isied, S. S.; Kuehn, C. G.; Lyon, J. M.; Merrifield, R. B. *J. Am. Chem. Soc.* 1982, **104**, 2632.
58. Urban, J.; Dattilo, J. W. In *15th APS (American Peptide Symposium), Abstracts*; June 14–19, 1997, Nashville, TN, p. 131.
59. Han, Y.; Barany, G. *J. Org. Chem.* 1997, *62*, 3841.
60. Lukszo, J.; Patterson, D.; Albericio, F.; Kates, S. A. *Letters in Peptide Sci.* 1996, **3**, 157.
61. Yamada, M.; Miyajima, T.; Horikawa, H. *Tetrahedron Lett.* 1998, **39**, 289.
62. Johnson, T.; Quibell, M.; Owen, D.; Sheppard, R. C. *J. Chem. Soc. Chem. Commun.* 1993, 369.
63. Jensen, K. J.; Songster, M. F.; Vagner, V.; Alsina, J.; Albericio, F.; Barany, G. *J. Am. Chem. Soc.* 1998, **120**, 5441.
64. Fivush, A. M.; Wilson, T. M. *Tetrahedron Lett.* 1997, **38**, 7151.
65. Sarantakis, D.; Bicksler, J. J. *Tetrahedron Lett.* 1997, **38**, 7325.
66. Meienhofer, J. In *The Peptides*; Gross, E.; Meienhofer, J. Eds.; Academic Press: New York, 1979, Vol. 1, p. 197.
67. Shioiri, T.; Ninomiya, K.; Yamada, S. *J. Am. Chem. Soc.* 1972, **94**, 6203.
68. Spatola, A. F.; Anwer, M. K.; Rockwell, A. L.; Gierasch, L. M. *J. Am. Chem. Soc.* 1986, **108**, 825.
69. Belleau, B.; Malek, G. *J. Am. Chem. Soc.* 1968, **90**, 1651.
70. Sheehan, J. C.; Hess, G. P. *J. Am. Chem. Soc.* 1955, **77**, 1067.
71. Rich, D. H.; Singh, J. In *The Peptides* Gross, E.; Meienhofer, J. Eds.; Academic Press: New York, 1979, Vol. 1, p. 241.
72. Koenig, W.; Geiger, R. *Chem. Ber.* 1970, **105**, 788.
73. Sarantakis, D.; Teichman, J.; Lien, E. L.; Fenichel, R. L. *Biochem. Biophys. Res. Commun.* 1976, **73**, 336.
74. Carpino, L. A. *J. Am. Chem. Soc.* 1993, **115**, 4397.
75. Castro, B.; Dormoy, J. R.; Evin, G.; Selve, C. *Tetrahedron Lett.* 1975, 1219.
76. Henklein, P.; Beyermann, M.; Bienert, M.; Knorr, R. In *Peptides 1990*; Giralt E.; Andreu, D. Eds.; ESCOM, 1991, p. 67.
77. Carpino, L. A.; El-Faham, A.; Minor, C. A.; Albericio, F. *J. Chem. Soc. Chem. Commun.* 1994, 201.
78. Coste, J.; Frérot, E.; Dufour, M. N.; Pantaloni, A.; Jouin, P. In *Peptides 1990*; Giralt, E.; Andreu, D. Eds.; ESCOM, 1991, p. 76.
79. Hudson, D. *J. Org. Chem.* 1988, **53**, 617.
80. Carpino, L. A.; El-Faham, A.; Truran, G. A.; Minor, C. A.; Kates, S. A.; Griffin, G. W.; Shroff, H.; Triolo, S. A.; Albericio, F. In *Innovations and Perspectives in Solid Phase Synthesis*; Epton, R. Ed.; Mayflower: Birmingham, 1994, p. 95.
81. Abelmoty, I.; Albericio, F.; Carpino, L. A.; Foxman, B. M.; Kates, S. A. *Lett. Peptide Sci.* 1994, **1**, 57.

82. Henklein, P.; Costisella, B.; Wray, V.; Domke, T.; Carpino, L.; El-Faham, A.; Kates, S. A.; Abdelmoty, I.; Foxman, B. M. In *15th American Peptide Symposium, Abstracts*; June 14–19, 1997, Nashville, TN, p. 173.
83. Story, S. C.; Aldrich, J. V. *Int. J. Peptide Protein Res.* 1994, **43**, 292.
84. Delforge, D.; Dieu, M.; Delaive, E.; Art, M.; Gillon, B.; Devreese, B.; Raes, M.; Van Beeumen, J.; Remacle, J. *Lett. Peptide Sci.* 1996, **3**, 89.
85. Artmangkuls, S.; Arbogast, B.; Barofsky, D.; Aldrich, J. V. *Lett. Peptide Sci.* 1996, **3**, 357.
86. Flanigan, E.; Marshall, G. R. *Tetrahedron Lett.* 1970, 506.
87. DeGrado, W. F.; Kaiser, E. T. *J. Org. Chem.* 1980, **45**, 1295.
88. Tumelty, D.; Needels, M. C.; Antonenko, V. V.; Bovy, P. R. In *Peptides: Chemistry, Structure and Biology*; Kaumaya, P. T. P.; Hodges, R. S. Eds.; Mayflower, 1966, p. 121.
89. Green, M.; Berman, J. *Tetrahedron Lett.* 1990, **41**, 5851.
90. Sakakibara, S.; Inukai, N. *Bull. Chem. Soc. Japan* 1964, **37**, 1231.
91. Hruby, V.; Meyer, J. -P. In *Bioorganic Chemistry: Peptides and Proteins*, Hecht, S. M. Ed.; Oxford University Press: New York, 1998, p. 27.
92. Jackson, D. Y.; Burnier, J. P.; Wells, J. A. *J. Am. Chem. Soc.* 1995, **117**, 819.
93. Kaiser, E.; Colescott, R.; Bossinger, C.; Cook, P. *Anal. Biochem.* 1970, **34**, 595.
94. Krchnak, V.; Vagner, J.; Lebl, M. *Int. J. Peptide Protein Res.* 1988, **32**, 415.
95. Krchnak, V.; Vagner, J.; Safar, P.; Lebl, M. *Coll. Czech. Chem. Commun.* 1988, **53**, 2542.
96. Schnölzer, M.; Jones, A.; Alewood, P. F.; Kent, S. B. H. *Anal. Biochem.* 1992, **204**, 335.
97. Metzger, J. W.; Kempter, C.; Weismüller, K. H.; Fung, G. *Anal. Biochem.* 1994, **219**, 261.
98. Eckart, K. *Mass. Spectrometry Rev.* 1994, **13**, 23.
99. McMurrary, J. S.; Lewis, C. A.; Obeyesekere, N. U. *Peptide Res.* 1994, **7**, 195.
100. Feiertag, S.; Weismüller, K. H.; Nicholson, G. J.; Jung, G. In *Peptides: Chemistry, Structure and Biology*; Kaumaya, P. T. P.; Hodges, R. S. Eds.; Mayflower, 1996, p. 693.
101. Yu, H.; Yu, C.; Chu, Y. *Tetrahedron Lett.* 1998, **39**, 1.
102. Rothe, M.; Lohmüller, Fischer, W.; Taibe, W.; Breuksch, U. In *Solid Phase Synthesis* Epton, R. Ed.; SPCC (UK) Ltd.: Birmingham, 1990, p. 551.
103. Regen, S.; Lee, D. P. *J. Am. Chem. Soc.* 1974, **96**, 294.
104. Rothe, M.; Alt, A.; Taiber, W.; Berginski, R.; Bernard, H. In *Solid Phase Synthesis*; Epton, R. Ed.; Mayflower: Birmingham, 1994, p. 111.
105. del Fresno, M.; Alsina, J.; Royo, M.; Barany, G.; Albericio, F. *Tetrahedron Lett.* 1998, **39**, 2639.
106. Pastuszak, J.; Gardner, J. H.; Singh, J.; Rich, D. H. *J. Org. Chem.* 1982, **47**, 2982.
107. Link, U.; Mästle, W.; Rother, M. *Int. J. Peptide Protein Res.* 1993, **42**, 475.
108. Rao, M. H.; Yang, W.; Joshua, H.; Becker, J. M.; Naider, F. *Int. J. Peptide Protein Res.* 1995, **45**, 418.

109. Cavelier-Frontin, F.; Achmad, S.; Verducci, J.; Jacquier, R.; Pepe, G. *J. Mol. Structure (Theochem)* 1993, **286**, 125.

110. Warrass, R.; Wiesmüller, K. H.; Jung, G. *Tetrahedron Lett.* 1998, **39**, 2715.

111. Mutter, M. *J. Am. Chem. Soc.* 1977, **99**, 8307.

112. Brady, S. F.; Varga, S. L.; Freidinger, R. M.; Schwenk, D. A.; Mendlowski, M.; Holly, F. W.; Veber, D. F. *J. Org. Chem.* 1979, **44**, 3101.

113. Kessler, H.; Kutscher, B. *Liebigs Ann. Chem.* 1986, 869.

114. Heavner, G.; Audhya, T.; Doyle, D.; Tjoeng, S.; Goldstein, G. *Int. J. Peptide Protein Res.* 1991, 37, 198.

115. Ehrlich, A.; Rothemund, S.; Brudel, M.; Beyermann, M.; Carpino, L. A.; Bienert, M. *Tetrahedron Lett.* 1993, **34**, 4781.

116. Kessler, H.; Hasse, B. *Int. J. Peptide Protein Res.* 1992, **39**, 36.

117. Sowemimo, V.; Scanlon, D.; Jones, P.; Craik, D. J. *J. Protein Chem.* 1994, **13**, 339.

118. Ehrlich, A.; Klose, J.; Heyne, H. U.; Beyermann, M.; Carpino, L. A.; Bienert, M. In *Peptides: Chemistry, Structure and Biology*, Kaumaya, P. T. P.; Hodges, R. S. Eds.; Mayflower, 1996, p. 75.

119. McMurray, J. S.; Lewis, C. A.; Obeyesekere, N. U. *Peptide Res.* 1994, **7**, 195.

120. Plaue, S. *Int. J. Peptide Protein Res.* 1990, **35**, 510.

121. Kondejewski, L. H.; Semchuk, P. D.; Daniels, L.; Wilson, I.; Hodges, R. S. In *15th APS Abstracts*; June 14–19, 1997, Nashville, TN, p. 193.

122. Hirschmann, R. *Angew. Chem. Int. Ed. Engl.* 1991, **30**, 1278.

123. Kessler, H.; Diefenbach, B.; Finsinger, D.; Geyer, A.; Gurrath, M.; Goodman, S. L.; Holzemann, G.; Haubner, R.; Jonczyk, A.; Muller, G.; Graf von Roedern, E.; Wermuth, J. *Lett. Peptide Sci.* 1995, **2**, 155.

124. Schiller, P. W.; DiMaio, J. *Nature* 1982, **297**, 79.

125. Ro, S.; Zhu, Q.; Lee, C. W.; Goodman, M.; Darlak, K.; Spatola. A. F.; Chung, N. N.; Schiller, P. W.; Malmberg, A. B.; Yakksh, T. L.; Burks, T. F. *J. Peptide Sci.* 1995, **1**, 157.

126. Conrad, R. A.; Hilgers, A. R.; Ho, N. F. H.; Burton, P. S. *Pharmaceutical Res.* 1992, **9**, 435.

127. Wenger, R. M. *Angew Chem. Int. Ed. Engl.* 1985, **24**, 77.

128. Gillespie, P.; Cicariello, J.; Olson, G. L. *Biopolymers (Peptide Sci.)* 1997, **43**, 191.

129. Spatola, A. F. In *Chemistry and Biochemistry of Amino Acids, Peptides and Proteins*; Vol. VII, Weinstein, B. Ed.; Marcel Dekker: New York, 1983, p. 267.

130. Sawyer, T. K. In *Structure-Based Drug Design: Diseases, Targets, Techniques and Developments*; Veerpandian, P. Ed.; Marcel Dekker: New York, 1997, p. 559.

131. Yankeelov, Jr., J. A.; Fok, K. F.; Carothers, D. J. *J. Org. Chem.* 1978, **43**, 1623.

132. Szelke, M.; Leckie, B.; Hallett, A.; Jones, D. M.; Sueiras, J.; Atrash, B.; Lever, A. F. *Nature* 1982, **299**, 533.

133. Gante, J. *Angew. Chem. Int. Ed. Engl.* 1994, **33**, 1699.

134. Goodman, M.; Ro, S. In *Burger's Medicinal Chemistry and Drug Discovery*; Vol. I, Wolff, M. E. Ed.; Wiley: New York, 1995, p. 803.

135. Gero, T. W.; Spatola, A. F.; Torres-Aleman, I.; Schally, A. V. *Biochem. Biophys. Res. Commun.* 1984, **120**, 840.

136. Spatola, A. F.; Edwards, J. V. *Biopolymers* 1986, **25**, S229.
137. Spatola, A. F.; Anwer, M. K.; Rockwell, A.; Gierasch, L. *J. Am. Chem. Soc.* 1986, **108**, 825.
138. Spatola, A. F.; Gierasch, L.; Rockwell, A. *Biopolymers* 1983, **22**, 147.
139. Pease, L. G.; Watson, C. *J. Am. Chem. Soc.* 1978, **100**, 1279.
140. Karle, I. *J. Am. Chem. Soc.* 1978, **100**, 1286.
141. Sherman, D. B.; Spatola, A. F. *J. Am. Chem. Soc.* 1990, **112**, 433.
142. Ma, S.; Richardson, J.; Spatola, A. F. *J. Am. Chem. Soc.* 1991, **113**, 8529.
143. Ma, S.; Spatola, A. F. *Int. J. Peptide Protein Res.* 1992, **41**, 204.
144. Sherman, D. B.; Spatola, A. F.; Wire, W. S.; Burks, T. F.; Nguyen, T. M. D.; Schiller, P. W. *Biochem. Biophys. Res. Commun.* 1989, **162**, 1126.
145. Kessler, H.; Geyer, A.; Matter, H.; Köck, M. *Int. J. Peptide Protein Res.* 1992, **40**, 25.
146. Spatola, A. F.; Darlak, K. *Tetrahedron* 1988, **44**, 821.
147. Chen, J. J.; Teesch, L. M.; Spatola, A. F. *Lett. Peptide Sci.* 1996, **3**, 17.
148. Kazmierski, W. M.; Ferguson, R. D.; Knapp, R. J.; Lui, G. K.; Yamamura, H. I.; Hruby, V. J. *Int. J. Peptide Protein Res. I* 1992, **39**, 401.
149. Geysen, H. M.; Meloen, R. H.; Barteling, S. J. *Proc. Natl. Acad. Sci., U.S.A.* 1984, **81**, 3998.
150. Furka, A.; Sebestyen, F.; Asgedom, M.; Dibo, G. *Int. J. Peptide Protein Res.* 1991, **37**, 487.
151. Houghten, R. A.; Pinilla, C.; Blondelle, S. E.; Appel, J. R.; Dooley, C. T.; Cuervo, J. H. *Nature* 1979, **354**, 84.
152. Nikolaiev, V.; Stierandova, A.; Krchnak, V.; Seligmann, B.; Lam, K. S.; Salmon, S. E.; Lebl, M. *Peptide Research* 1993, **6**, 161.
153. Fodor, S.; Read, J. L.; Pirrung, M. C.; Stryer, L.; Lu, A. T.; Solus, D. *Science* 1991, **251**, 767.
154. Geysen, A. M.; Roddo, S. J.; Mason, T. J. *Molecular Immunology* 1986, **23**, 709.
155. Bunin, B. A.; Plunkett, M. J.; Ellman, J. A. *Proc. Natl. Acad. Sci., U.S.A.* 1994, **91**, 4708.
156. Hobbs-DeWitt, S.; Kiely, J. S.; Stankovic, C. J.; Schroeder, M. C.; Cody, D. M. R.; Pavia, M. R. *Proc. Natl. Acad. Sci., U.S.A.* 1993, **90**, 6909.
157. Gallop, M. A.; Barrett, R. W.; Dower, W. J.; Fodor, S. P. A.; Gallop, M. A. *J. Med. Chem.* 1994, **37**, 1233.
158. Gordon, E. M.; Barrett, R.; Dower, W. J.; Fodor, S. P. A.; Gallop, M. A. *J. Med. Chem.* 1994, **37**, 1385.
159. Terrett, N. K.; Gardner, M.; Gordon, D. W.; Kobylecki, R. J.; Steele, J. *Tetrahedron* 1995, **51**, 8135.
160. Thompson, L. A.; Ellman, J. A. *Chem. Rev.* 1996, **96**, 555.
161. Lam, K. S.; Lebl, M.; Krchnak, V. *Chem. Rev.* 1997, **97**, 411.
162. Jung, G. *Combinatorial Peptides and Nonpeptide Libraries* VCH: Weinheim; 1996.
163. Bunin, B. *The Combinatorial Index*, Academic Press, 1998.

164. *Combinatorial Chemistry: Synthesis and Applications*; Wilson, S. R.; Czarnik, A. W. Eds.; John Wiley, 1998.
165. *Combinatorial Peptide Library Protocols. Methods in Molecular Biology*; Vol. 87, Cabily, S. H. Ed.; Academic Press, 1997.
166. Lebl, M. *Molecular Diversity References* http//:www.5z.com.
167. O'Neil, K. T.; Hoess, P. H.; Jackson, S. A.; Ramachandran, N.; Mousa, S. A.; DeGrado, W. F. *Proteins* 1992, **14**, 509.
168. Eichler, J.; Lucka, A. W.; Houghten, R. A. *Peptide Res.* 1994, 7, 300.
169. Sila, U.; Mutter, M. *J. Mol. Recog.* 1995, **8**, 29.
170. Dooley, C. T.; Houghten, R. A. *Life Sci.* 1993, **52**, 1509.
171. Mihara, H.; Yamabe, S.; Niidome, T.; Aoyagi, H.; Kumagai, H. *Tetrahedron Lett.* 1995, **36**, 4837.
172. Wen, J. J.; Spatola, A. F. *J. Peptide Res.* 1997, **49**, 3.
173. Winkler, D.; Schuster, A.; Hoffmann, B.; Schneider-Mergener, J. In *Peptides 1994*; Maia, H. L. S. Ed.; Escom: Leiden, 1994, 485.

INHIBITORS OF THE ACETYLCHOLINESTERASE PERIPHERAL SITE MAY PROTECT AGAINST ORGANOPHOSPHATE TOXICITY.

Terrone L. Rosenberry[#], William D. Mallender[#], Bernadette Cusack[#], Tivadar Szegletes[†], Peter Romanovskis*, and Arno F. Spatola*

[#] Mayo Clinic Jacksonville, Department of Pharmacology, Jacksonville, FL 32224.
* University of Louisville, Department of Chemistry, Louisville, KY 40292.
[†] Proctor and Gamble, Budapest, Hungary.

Acetylcholinesterase (AChE) is one of the most efficient enzymes known. The AChE active site consists of a narrow gorge with two separate ligand binding sites: an *acylation site* at the bottom of the gorge where substrate hydrolysis occurs and a *peripheral site* at the gorge mouth. In recent studies, we showed that ligands which bind specifically to the peripheral site can slow the rates at which other ligands enter and exit the acylation site, a feature we denoted steric blockade. We also demonstrated that cationic substrates can form a low affinity complex at the peripheral site that accelerates catalytic hydrolysis at low substrate concentrations but results in substrate inhibition at high concentrations because of steric blockade of product release. AChE is inactivated by organophosphates in pesticides and chemical warfare agents because organophosphates can pass through the peripheral site and phosphorylate the catalytic serine in the acylation site. We are investigating the design of cyclic inhibitors that will bind specifically to the peripheral site and present a pronounced steric blockade to organophosphates while allowing selective passage of acetylcholine to the acylation site. Cyclic inhibitors with affinities for the peripheral site in the sub-micromolar range have been identified.

This work was supported by the U.S. Army Medical Research and Materiel Command under Grant DAMD 17-98-2-8019, by grant NS16577 from the National Institutes of Health, and by grants from the Muscular Dystrophy Association of America.

Introduction

The primary physiological role acetylcholinesterase (AChE)[1] is to hydrolyze the neurotransmitter acetylcholine at cholinergic synapses (*1*). AChE is one of the most efficient enzymes known (*2*), and recent studies have focused on the structural basis of its high catalytic efficiency. Ligand binding studies (*3*) and X-ray crystallography (*4*) revealed a narrow active site gorge some 20 Å deep with two separate ligand binding sites. The acylation site at the bottom of the gorge contains residues involved in a catalytic triad (H*440*, E*327*, S*200*)[2] and W*84*, which binds to the trimethylammonium group of acetylcholine. The peripheral site at the mouth of the gorge includes, among others, residue W*279*. AChE, like other members of the α/β-hydrolase family, contains an ω loop with boundaries set by a disulfide bond (C*67* – C*94*) (*5*; *6*). Residues from Y*70* through W*84* in this loop extend along one side of the gorge from the peripheral site to the acylation site. This segment includes residue D*72*, which is positioned near a constriction at the boundary between the peripheral site and the acylation site.

In a series of recent publications, we have focused on clarifying the role of the peripheral site in the catalytic pathway for AChE (*7* – *10*). The three-dimensional structure indicates that ligands specific for the acylation site must first pass through the peripheral site on their way to

the acylation site. Other cationic ligands, including the phenanthridium derivative propidium and the fasciculins, a family of nearly identical snake venom neurotoxins, are specific for the peripheral site and do not proceed further. Initial information about the peripheral site was obtained by studying the formation of ternary complexes with AChE. Such complexes, involving the binding of different ligands to the acylation and peripheral sites, showed little thermodynamic interaction between the bound ligands (*3*). However, the binding of small cationic ligands like propidium to the peripheral site slowed the rate constants for ligand entry into and exit from the acylation site by factors of up to 400 (*7*). We termed this effect steric blockade and demonstrated that it was responsible for pronounced propidium inhibition when substrate hydrolysis is near diffusion controlled.

In this paper we review the evidence that steric blockade by substrate bound to the peripheral site is responsible for the phenomenon of substrate inhibition (*11*), a decrease in hydrolysis rates at high substrate concentration. Our analysis revealed that substrate inhibition occurs because low affinity binding of acetylthiocholine near residue D74 in the peripheral site slows the rate of dissociation of product thiocholine from the acylation site, making it rate limiting at high substrate concentrations (*8*). Our studies also indicated that initial binding of acetylthiocholine to the peripheral site accelerated hydrolysis rates at low substrate concentrations. The acceleration is probably the most important contribution of the peripheral site to the catalytic process. We also report the effects of bound fasciculin on the organophosphorylation of human wild type and D74G AChE. Fasciculin is the only peripheral site ligand identified to date that inhibits reactions at the acylation site by a mechanism in addition to steric blockade or simple steric overlap in the ternary complex. Finally, we present preliminary data on cyclic peptides that are designed to bind specifically to the AChE peripheral site. Our long-term goal is to optimize the structure of cyclic inhibitors to selectively block the access of organophosphates (OPs) to the AChE acylation site. Such inhibitors may useful as protective agents against OP poisoning.

Methods

Materials. Recombinant human "wild type" and D74G AChE were expressed as secreted dimeric forms in *Drosophila* S2 cells in culture (*9*; *10*) and purified by two cycles of affinity chromatography on acridinium resin (*12*). Fasciculin 2 was obtained from Dr. Carlos Cervenansky at the Instituto de Investigaciones Biologicas, Clementa Estable, Montevideo, Uruguay (*13*), while fasciculin 3 was obtained from Dr. Pascale Marchot at the Laboratoire de Biochimie, Faculté de Médicine, Université d'Aix-Marseille II, Marseille, France (*14*). DEPQ and EMPC were synthesized as previously described (*9*). Propidium iodide was purchased from Calbiochem.

Steady state measurements of AChE-catalyzed substrate hydrolysis. Hydrolysis of acetylthiocholine was monitored with a spectrophotometric Ellman assay (*15*). Assay conditions and data analysis methods were identical to those described previously (*7*; *10*). Active site concentrations were determined from V_{max}/k_{cat}, and k_{cat} was established in titrations with DEPQ monitored by fluorometric assays (*9*; *10*).

Determination of rate constants in Scheme 2. To estimate key rate constants, we solved the corresponding steady state rate equations numerically with the program SCoP (version 3.51) (*8*; *10*). This solution avoids equilibrium assumptions and allows examination of rates in the

context of our steric blockade model, which postulates that bound peripheral site ligand has no effect on k_2 or k_3 but decreases k_{-P} by a factor of 100 (*10*). The current treatment also postulates that product bound to the acylation site does not alter k_3, that k_{-P} for product dissociation from the acetylated enzyme is identical to that from free enzyme, and that peripheral site binding is unaffected by the binding of ligands to the acylation site (*10*).

Slow equilibration of fasciculin in the presence of peripheral site inhibitors. Apparent association rate constants k_{on} for fasciculin binding to the AChE peripheral site were measured by a procedure used previously (*13*; *8*). Each series of binding measurements included reactions at a fixed acetylthiocholine concentration ([S]) and four to ten fasciculin concentrations ([F]). We assume that ligand binding to the peripheral site is unaffected by the presence of ligands or an acyl group at the acylation site and that fasciculin reacts with E with an intrinsic association rate constant k_F and with ES_P (Scheme 2) with an intrinsic association rate constant k_{FP},(*8*). Then k_{on} is given by eq. 1, where K_S is the equilibrium dissociation constant for S at the peripheral site (*8*).

$$k_{on} = \frac{k_F + k_{FP}\frac{[S]}{K_S}}{1 + \frac{[S]}{K_S}} \qquad \text{(eq. 1)}$$

To obtain estimates of K_S, values of k_{on} obtained at each [S] were fitted to eq. 1 by nonlinear regression analysis (Fig.P, BioSoft, Version 6) in which k_{on} values were weighted by the reciprocal of their variance.

Phosphorylation of AChE by fluorogenic OPs. Reaction of AChE with EMPC or DEPQ was monitored by the appearance of their fluorescent leaving groups by stopped flow fluorometry (*9*; *10*). The release of product from each OP occurred primarily in one large phase that was fitted to an exponential time course with rate constant k (*9*). Data was analyzed according to Scheme 1.

Scheme 1

$$\begin{array}{ccccccc}
\mathrm{OPX} + E & \overset{K_O}{\rightleftharpoons} & E\mathrm{OPX} & \overset{k_2}{\longrightarrow} & \mathrm{X} + E\mathrm{OP} & \overset{k_3}{\longrightarrow} & E + \mathrm{OPOH} \\
+ & & + & & + & & \\
\mathrm{I} & & \mathrm{I} & & \mathrm{I} & & \\
K_I \Updownarrow & & K_{SI} \Updownarrow & & K_{AI} \Updownarrow & & \\
\mathrm{OPX} + E\mathrm{I_P} & \overset{K_{O2}}{\rightleftharpoons} & E\mathrm{OPXI_P} & \overset{ak_2}{\longrightarrow} & \mathrm{X} + E\mathrm{OPI_P} & \overset{k_3}{\longrightarrow} & E\mathrm{I_P} + \mathrm{OPOH}
\end{array}$$

In this scheme, OPX is the intact OP with leaving group X; EOPX is the initial complex of the OP with AChE, characterized by the equilibrium dissociation constant $K_O = k_{-O}/k_O$ (*9*).); and EOP is the phosphorylated enzyme. The ligand I can bind to the peripheral site in each of the enzyme species (as denoted by the subscript P). OPs were assumed to equilibrate with the AChE

acylation site even when inhibitors were bound to the peripheral site, and the dephosphorylation rate constant k_3 was assumed to be negligible. The dependence of k on the OP concentration was analyzed by weighted nonlinear regression analysis (assuming constant percent error in k) according to eq. 2 to give k_{OP} and k_{OP}/K_{OP}, the respective first- and second-order rate constants of phosphorylation.

$$k = \frac{k_{OP}\,[OP]}{K_{OP} + [OP]} \qquad \text{(eq. 2)}$$

In the absence of I, $k_{OP} = k_2$ and $K_{OP} = K_O$. In the presence of I, the relative intrinsic first order rate constant a for phosphorylation in Scheme 1 was calculated from k_{OP}, K_{OP} and the competitive inhibition constant K_I for the inhibitor as outlined previously (*9*; *10*).

Synthesis of cyclic peptides and screening for AChE inhibition. Cyclic peptides were prepared by peptide synthesis on amino acids attached to resin by carboxylate side chains. Peptide products were purified to homogeneity by reversed phase HPLC with various polarity solvents (i.e. water with increasing acetonitrile). Product purity and identity was confirmed by MALDI-TOF and ESI mass spectrometry and amino acid analysis. Peptides were analyzed for AChE binding activity and inhibition with two assays formatted for high throughput screening in a microtiter plate reader. First, each peptide was assayed for inhibition of steady-state acetylthiocholine hydrolysis in a standard AChE activity assay (*15*). Second, each product was tested for the ability to compete with fasciculin and decrease fasciculin association rates in a continuous AChE activity assay where fasciculin association rates are examined (*8*). Inhibitors with higher levels of inhibition at 10 μM concentrations were characterized by determination of the competitive inhibition constant (K_I) for AChE (*8*).

Results

A mechanistic model for substrate inhibition of AChE. Traditional catalytic pathways for AChE propose the binding of an ester substrate S to the acylation site to form an *E*S complex, followed by formation of the acylated enzyme intermediate *E*A and deacylation to regenerate the free enzyme *E*. We recently obtained evidence that the catalytic pathway for AChE should be extended by making explicit two new classes of intermediates (*8*). One class includes enzyme species with the initial product of hydrolysis, the alcohol leaving group P (*e.g.*, thiocholine), still bound to the acylation site. These intermediates are denoted *E*AP and *E*P in Scheme 2.

Scheme 2

$$\begin{array}{ccccccccccc} & & & & & & & \xrightarrow{k_{-P}} & & & \\ & & & & & & \mathrm{Ac} + E\mathrm{P} & & \mathrm{P} + E & & \\ & & & & & & \uparrow k_3 & & & & \\ E + \mathrm{S} & \underset{k_{-S}}{\overset{k_S}{\rightleftharpoons}} & E\mathrm{S_P} & \underset{k_{-1}}{\overset{k_1}{\rightleftharpoons}} & E\mathrm{S} & \xrightarrow{k_2} & E\mathrm{AP} & \xrightarrow{k_{-P}} & \mathrm{P} + E\mathrm{A} & \xrightarrow{k_3} & E + \mathrm{Ac} \end{array}$$

The second includes intermediates in which S is bound to the AChE peripheral site, indicated by the subscript P as in ES_P in Scheme 2. Substrate initially binds in ES_P and then slides into the acylation site to give *E*S. While intermediates like *E*AP and *E*P can often be ignored in kinetic analyses at substrate concentrations below that at the maximum hydrolysis rate (*8*, *10*), these intermediates become important at high substrate concentrations when substrate inhibition is observed. Substrate inhibition requires a model in which a second molecule of substrate interacts with at least one of the intermediates in Scheme 2. In theory, substrate inhibition could arise if substrate binding to *E*S or *E*P blocked acylation or deacylation, but there is no evidence that the binding of a small ligand like acetylthiocholine to the peripheral site can inhibit these steps. In contrast, we have shown directly that the binding of the small peripheral site ligands propidium or gallamine creates a steric blockade that decreases the association and dissociation rate constants for ligand binding to the acylation site by factors of 10 to 400 (*7*). Substrate binding to the peripheral site to give an EPS_P complex then might also be expected to present a steric blockade that would reduce the rate constant for product dissociation from this complex.

We recently examined whether this scheme could account quantitatively for substrate inhibition profiles with human AChE (*8*; *10*). A nonequilibrium simulation of the substrate inhibition profile was in excellent agreement with the observed profile (*8*), but our goal was to actually fit the two key kinetic parameters in Scheme 2, K_S and k_{-P}, with substrate inhibition data. To achieve this, we reduced eleven rate constant variables that arise when substrate is allowed to bind to the peripheral site in all the complexes in Scheme 2 to three parameters, K_S, k_{-P} and k_2, which were fitted in the program SCoP (*10*). The profile of *v vs.* [S] for acetylthiocholine with recombinant wild type human AChE showed the bell shape that is the hallmark of pronounced substrate inhibition, and this profile was fitted precisely with the SCoP program. Fitted values of $K_S = 1.9 \pm 0.7$ mM and $k_{-P} = 6 \pm 1 \times 10^4$ s^{-1} were obtained, in agreement with our previous simulations (*8*). We selected K_S and k_{-P} as parameters to be fitted because they can be compared to independent experimentally predicted values. The predicted k_{-P} was calculated indirectly from the relationship $k_{-P} = K_P k_P$, where K_P is the measured equilibrium dissociation constant for thiocholine inhibition of AChE and the association rate constant k_P for thiocholine is assumed to be the same as k_S for acetylthiocholine. Its calculated value (1.3×10^5 s^{-1}) (*8*) agreed reasonably with the fitted k_{-P} value here. To obtain the predicted K_S for acetylthiocholine, we employed the fasciculin competition assay in Fig. 1B. In this assay, substrate affinity for the peripheral site is determined from the effect of substrate concentration on the rate of equilibration of fasciculin at the peripheral site. The association of fasciculin with the AChE peripheral site was monitored as a decrease in AChE activity toward acetylthiocholine (*8*). The apparent fasciculin association rate constants k_{on} then were calculated from the rate constants for this activity decrease as a function of the fasciculin concentration, and finally the dependence of k_{on} on the acetylthiocholine concentration was fitted to eq. 1 to obtain K_S. As observed previously for fasciculin 2 and human erythrocyte AChE (*8*), acetylthiocholine only partially blocked the association of fasciculin 3 with recombinant wild type human AChE (Fig. 1B). At high saturating concentrations of acetylthiocholine, k_{on} decreased to about one-half of its extrapolated value in the absence of acetylthiocholine. Fitting the k_{on} values for fasciculin 3 at various concentrations of acetylthiocholine to eq. 1 gave $K_S = 1.3 \pm 1.0$ mM. The precision of the individual k_{on} points made it difficult to decrease the error of this estimate, but this K_S value agreed well with that obtained from the substrate inhibition data.

The quantitative agreement between the K_S measured by fasciculin competition and that obtained by fitting the substrate inhibition profile provided reassuring support for our steric blockade model. We next investigated whether such agreement would extend to the human D74G mutant. D74 may be the key residue in defining peripheral site binding of acetylthiocholine (*10*). If this idea is correct, K_S should increase dramatically in D74G mutants. With the human D74G enzyme in Fig. 1A, substrate inhibition in fact was decreased to such an extent that the three-parameter fit in SCoP was unreliable and sometimes failed to converge with $k_2 < k_{-P}$. Therefore, k_2 was fixed to the value obtained for wild type human AChE and only K_S and k_{-P} were fitted. The assumption that k_2 is the same for human wild type and D74G AChEs was supported by our observation that these AChEs have the same k_{cat} value (*10*), and k_2 is a major contributor to k_{cat}. Average fitted values of K_S = 33 ± 8 mM and k_{-P} = (9 ± 3) × 10^4 s^{-1} were obtained from the human D74G data in Fig. 1B and two additional experiments. The 20-fold increase in K_S with the D74G mutant was sufficient to nearly abolish substrate inhibition. Of particular importance, this increase in K_S was supported by the fasciculin 3 competition data for the human D74G mutant in Fig. 1B. Values of k_{on} did not differ significantly as acetylthiocholine ranged from 0.1 to 30 mM, and the data could be fitted to eq. 1 by assigning a fixed K_S of 33 mM from the substrate inhibition data. The correlation between K_S obtained by fitting substrate inhibition curves with K_S determined by competition with fasciculin was also examined with purified AChEs from *Torpedo* (*10*). For wild type *Torpedo* AChE these respective K_S values were 0.5 ± 0.2 mM and 0.4 ± 0.2 mM, while for D72G *Torpedo* AChE these respective K_S values were 10 ± 1 mM and 4 ± 2 mM. The agreement between K_S values determined by the two procedures provides strong support for the application of the steric blockade model to substrate inhibition data. Furthermore, the increase in K_S observed for D72G *Torpedo* AChE indicates that D72 is also an important residue for the binding of acetylthiocholine to the peripheral site in *Torpedo* AChE.

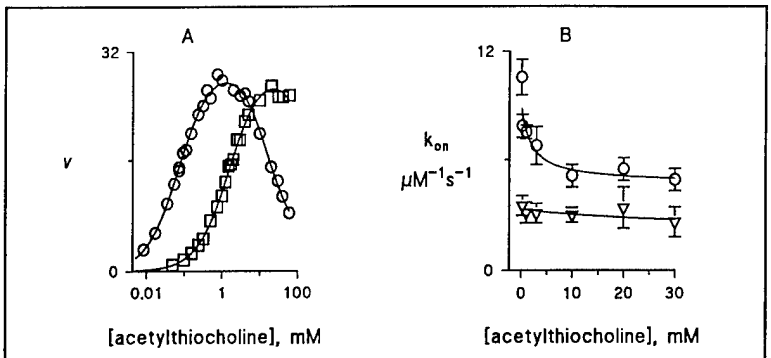

Fig. 1. Acetylthiocholine binding to the peripheral site of human AChE ([Mallender, 2000 #395]). Reaction mixtures with varying amounts of acetylthiocholine were supplemented with NaCl such that [S] + [NaCl] = 60 mM to maintain constant ionic strength. *Panel A*. Substrate inhibition with acetylthiocholine. Points represent initial velocities (uM/min) measured at the indicated substrate concentrations with wild type (-O-) or D74G (-□-) AChE (80 pM). Lines were fitted with the SCoP program. *Panel B*: Inhibition of fasciculin 3 binding by acetylthiocholine. Points represent a series of measurements of association rate constants k_{on} for fasciculin 3 measured at the indicated substrate concentrations with wild type (-O-) or D74G (-∇-) AChE. Lines were obtained with eq. 1 by fixing K_S at the value obtained from substrate inhibition and fitting k_{FP}/k_F to 0.52 ± 0.05 (wild type) or 0.6 ± 0.5 (D74G). A line for the wild type AChE points fitting all three constants in eq. 1 corresponded closely to that shown and gave K_S = 1.3 ± 1.0 mM and k_{FP}/k_F = 0.52 ± 0.06.

Phosphorylation of human AChEs by EMPC and DEPQ in the presence and absence of peripheral site ligands. EMPC and DEPQ are fluorogenic OPs that release fluorescent leaving groups when they phosphorylate the AChE acylation site (Scheme 1). With both wild type and D74G AChE, most of the fluorescence increase on reaction of these OPs with the human D74G

mutant occurred with a single rapid exponential time course (*9*; *10*). The dependence of the rate constants on the OP concentrations was analyzed with eq. 2. The D74G mutation had little effect on the reaction of EMPC, a neutral OP. The first order rate constant k_{OP} decreased about two-fold and the equilibrium dissociation constant K_{OP} decreased about 4-fold relative to wild type AChE (Table 1). A similar decrease in k_{OP} was observed for DEPQ, a cationic OP, but K_{OP} increased by about an order of magnitude. These changes are consistent with those reported in second-order phosphorylation rate constants (k_{OP}/K_{OP}) for other neutral and cationic OPs with mouse wild type and D74N AChEs (*16*).

Table 1. Rate constants for the phosphorylation of wild type and D72G AChE by fluorogenic OPs

OP / Enzyme	Inhibitor	k_{OP} min^{-1}	a	K_{OP} uM	k_{OP}/K_{OP} $uM^{-1}min^{-1}$	k_{OP}/K_{OP} Relative decrease
EMPC						
Wild type						
	None	150±11	—	224±24	0.67±0.03	—
	Propidium	570±140 [a]	5±2 [a]	1260±350 [a]	0.45±0.02	1.5
	Fasciculin	0.23±0.08	0.002	220±110	0.0011±0.0002	610
D74G						
	None	74±10	—	64±12	1.2±0.1	—
	Propidium	710±110	>10	330±70	2.2±0.2	*b*
	Fasciculin	19±4	0.24±0.08	1260±320	0.015±0.001	80
DEPQ						
Wild type						
	None	1600±200	—	7.5±1.3	205±11	—
	Propidium	1200±400 [a]	0.7±0.4 [a]	85±30 [a]	15±1	14
	Fasciculin	0.66±0.10	0.0003	700±140	0.0010±0.0001	220000
D74G						
	None	850±140	—	90±20	10±1	—
	Propidium	760±300 [a]	0.8±0.9 [a]	240±130 [a]	3.2±0.4	3
	Fasciculin	*c*	*c*	*c*	< 0.006±0.0004	>1500

[a] The maximum [OP] employed (30 - 60 % of the estimated K_{OP}) did not exceed 80% of the estimated K_{OP}, and therefore estimates of k_{OP} and K_{OP} are approximate.

[b] k_{OP}/K_{OP} increased by a factor of 1.9.

[c] No estimate was possible because of the lower affinity of fasciculin 2 for the D74G mutant, the low reactivity of the complex of fasciculin 2 and D74G with DEPQ, and the near linearity of k with [OP] (eq. 2).

In the presence of peripheral site ligands, interpretation of k_{OP} and K_{OP} in terms of the intrinsic rate constants in Scheme 1 involved extrapolation to a saturating concentration of the ligand (*9*). The relatively low affinities of propidium and fasciculin 2 with human D74G AChE made it difficult to extrapolate their precise effects on OP phosphorylation, particularly with DEPQ. Propidium showed no inhibition of the EMPC reaction with this mutant, and both k_{OP} and K_{OP} increased when propidium was introduced (Table 1). The absence of propidium inhibition of EMPC phosphorylation also was seen with wild type AChE (Table 1) and is consistent with our steric blockade model (*9*). This model predicts that a small peripheral site ligand like propidium will have relatively little effect on a substrate like an OP that equilibrates with the acylation site before acylation occurs. The mechanistic basis for the increases in k_{OP} and K_{OP} are unclear. These increases may arise from a shift in bound OP to reduce steric overlap with propidium or from nonproductive binding of EMPC to the free enzyme (*10*), or they might reflect an additional conformational effect induced by bound propidium on the OP reactivity at

the acylation site (*17*).

In contrast to propidium, fasciculin 2 binding to the peripheral site dramatically decreased the phosphorylation rate constants for EMPC and DEPQ with wild type AChE by three to five orders of magnitude (Table 1). We interpret this qualitative difference from propidium to indicate that fasciculin induces a conformational change or a conformational restraint in the acylation site that reduces the acylation rate constant (*a* in Scheme 1) for bound OP (*9*). The D74G mutation appears to have an effect on the ability of fasciculin to induce this conformational change with EMPC. The value of *a* increased from 0.002 in the wild type enzyme to 0.24 in D74G AChE (Table 1). Fasciculin 2 clearly inhibited the reaction of DEPQ with D74G AChE, but the maximal inhibition could not be determined. It is important to understand the mechanism by which fasciculin induces this effect on *a* at the acylation site and the role played by D74. If the effect can be mimicked with synthetic peripheral site inhibitors and tailored to be specific for organophosphorylation, it may become a useful strategy for protection against OP toxicity.

Cyclic ligands as selective inhibitors of organophosphorylation. One strategy suggested by our characterization of AChE peripheral site inhibition is to design an inhibitor that will bind to the peripheral site and impose a steric blockade that is selective for OPs and thus protective against OP toxicity. Such an inhibitor must exclude OPs from the acylation site while interfering minimally with acetylcholine passage. Our search for such ligands has focused on cyclic peptide and pseudopeptide compounds. Cyclic molecules have a variety of advantages that we intend to exploit during the course of our studies. First, a cyclic molecule is a ring with a pore that in theory can be designed to exclude passage of bulky OPs while allowing smaller acetylcholine to pass. Relatively small cyclic compounds consisting of 6 to 8 amino acids possess the necessary space to permit passage of acetylcholine. Second, the incorporation of both natural and unnatural amino acids using combinatorial methods allows for synthesis of an enormous number of cyclic compounds in libraries of various size. Furthermore, cyclic peptides are conformationally constrained, an asset in molecular modeling studies.

Our initial efforts focused on large libraries of several hundred cyclic peptides with random amino acid sequences. We examined the effect of ring size (5- to 9- member cyclic peptides), peptide backbone (D- amino acids, L- amino acids, unnatural peptide linkages (thioether, aminosubstituted)), and amino acid side chain composition (charge, hydrophobicity, and aromaticity). Several sets of peptides indicated AChE binding at high total peptide concentrations (100 μM), and common features began to emerge. First, most of the libraries that gave positive results possessed amino acid sequences with positively charged residues. Second, there was a clear preference in binding and inhibitory activity for libraries with 7- and 8- residue cyclic peptides. The diversity of libraries identified in this screening procedure was very encouraging, as it demonstrated that numerous different amino acid sequences have potential as AChE peripheral site specific inhibitors.

With the information gained from our initial screening of random peptide libraries, we initiated the directed design of the next series of cyclic compound libraries using fasciculin as a prototype. Fasciculin serves as an excellent example of the kind of AChE inhibitor that would be necessary for the protection of the enzyme from OPs. Fasciculin is specific for the peripheral site and displays an impressive affinity for the enzyme (K_D ~ 10 - 20 pM) (*13; 18*). Furthermore, the structure of fasciculin consists of three finger-like loops protruding from a central disulfide linked core (Fig. 2) (*19*). Previous studies have shown that

disulfide linked cyclic peptides based on the loops of fasciculin could bind to AChE and inhibit enzyme activity, but with low affinities (~15 μM) that were 10^5 times smaller than the natural toxin (*20*). We have employed molecular modeling using the crystal structure of the AChE-fasciculin complex (*21; 22*) to design individual cyclic peptides and peptide mixtures based on the primary amino acid sequence of loop II of fasciculin (Fig. 2). This loop displays the greatest area of contact with the AChE peripheral site. Our initial efforts focused on cyclic peptides based on the fasciculin primary sequence of cyclo[Arg-Arg-His-Pro-Pro-Lys-Met-Xxx], where Xxx is the cyclization residue (Asp, Asn, Glu, or Gln). Closer examination of the AChE-fasciculin crystal structure indicated that Arg^2, Lys^6, and Xxx do not make direct contact with the enzyme surface. We varied these residues to evaluate the effect of different side chains or peptide linkages on cyclic peptide activity. In addition, novel amino acids (nor-leucine (Nle) and napthylalanine (Nal)) were inserted in an attempt to improve inhibitor potency by altering peptide hydrophobicity and conformational flexibility. Inhibitory peptides identified as promising candidates from initial screening assays were analyzed to determine their K_I for AChE (Table 2). Results indicated that cyclic peptide structures with a net positive charge, a Gln cyclization residue and a napthylalanine residue at position 2 or 7 displayed the best inhibitory activity on AChE. Furthermore, cyclic peptides outperformed linear molecules, and our screening assay accurately predicted the rank-order of K_I values measured for active peptide inhibitors (Table 2).

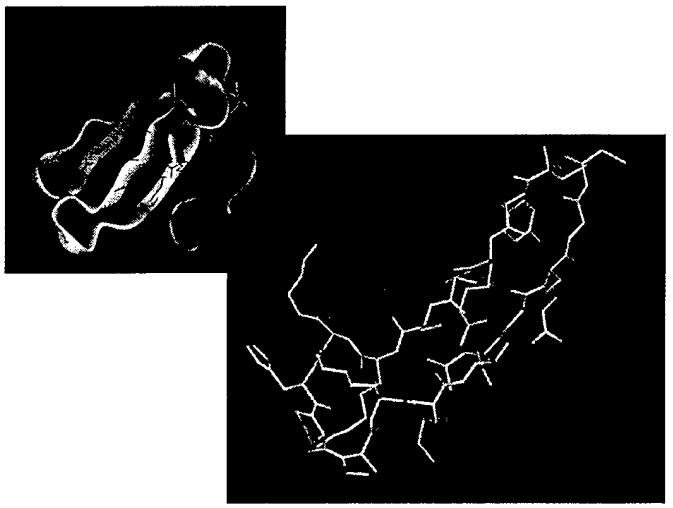

Figure 2. Structure of fasciculin and fasciculin loop II as taken from the AChE-fasciculin crystal structure. Upper panel, structure of fasciculin with individual loops colored in green, yellow and red. Lower panel, structure of loop II of fasciculin with degree of buried surface area indicated by color (blue represents solvent exposed, yellow and orange represent partially buried and red represents total buried in the AChE-fasciculin interface.

Table 2. Octapeptide inhibitors at the AChE peripheral site

Peptide Sequence								Percent Inhibition, Initial Screen				Ki
								Activity		Fas Binding		
1	2	3	4	5	6	7	8	10 μM	1 μM	10 μM	1 μM	μM
Fasciculin												
R	R	H	P	P	K	M						
cyclic peptides												
R	L-Nal	H	P	P	K	M	Q	79	40	52	14	0.2
R	A	H	P	P	K	L-Nal	Q	78	28	62	23	1
R	A	H	P	P	K	D-Nal	Q	68	21	50	7	1.5
R	D-Nal	H	P	P	K	M	Q	65	27	54	27	1.1
R	A	H	P	P	K	M	Q	51	16	53	36	2
R	A	H	P	P	K	M	N	29	5	15	0	6.4
linear peptide												
R	A	H	P	P	K	Nle	Q	18	12	20	26	14.4

As shown in Table 2, by using information from fasciculin in the directed design of novel, cyclic peripheral site AChE inhibitors, we have generated a class of compounds with low micromolar to high nanomolar affinity for the enzyme peripheral site. We will next focus our efforts on improving peptide inhibitor affinity for AChE. New individual peptide and peptide mixtures will be synthesized that incorporate alternate amino acid sequences and chemistries to search for compounds with great affinity for the AChE peripheral site. These new peptides will also include molecules that have chemical structures that are more conformationally restrained (using substituted amino acids or disulfide bonds). We will also include the use of positional scanning and library deconvolution to assess the effect of amino acid composition. These methods have been used previously to rediscover a naturally occurring peptide ligand from large combinatorial libraries (*23*). Equilibrating acylation site inhibitors will be used to determine how these cyclic peptide molecules inhibit AChE activity. Information on the mechanism of cyclic peptide inhibition of AChE will be crucial when we begin active screening of candidate cyclic inhibitors for effectiveness in blocking OP penetration into the AChE active site.

Footnotes

[1] Abbreviations: AChE, acetylcholinesterase; OP, organophosphate; EMPC, 7-[(methylethoxyphosphonyl)oxy]-4-methylcoumarin; DEPQ, 7-[(diethoxyphosphoryl)oxy]-1-methylquinolinium iodide.

[2] Throughout this paper, italicized residue numbers refer to the *Torpedo* AChE sequence. D74 in the human and mouse AChE sequences corresponds to D*72* in *Torpedo* AChE.

References

1. Rosenberry, T. L. (1979). *Biophys. J.* **26**: 263-290.
2. Rosenberry, T. L. (1975). Acetylcholinesterase. In: **Advances in Enzymology, 43** (Meister, A., ed.), John Wiley & Sons, New York, pp. 103-218
3. Taylor, P. and Lappi, S. (1975). *Biochemistry* **14**: 1989-1997.
4. Sussman, J. L., Harel, M., Frolow, F., Oefner, C., Goldman, A., Toker, L. and Silman, I. (1991). *Science* **253**: 872-879.
5. Velan, B., Barak, D., Ariel, N., Leitner, M., Bino, T., Ordentlich, A. and Shafferman, A. (1996). *FEBS Lett.* **395**: 22-28.
6. Ollis, D. L., Cheah, E., Cygler, M., Dijkstra, B., Frolow, F., Franken, S. M., Harel, M., Remington, S. J., Silman, I., Schrag, J., Sussman, J. L., Verschueren, K. H. G. and Goldman, A. (1992). *Protein Eng.* **5**: 197-211.
7. Szegletes, T., Mallender, W. D. and Rosenberry, T. L. (1998). *Biochemistry* **37**: 4206-4216.
8. Szegletes, T., Mallender, W. D., Thomas, P. J. and Rosenberry, T. L. (1999). *Biochemistry* **38**: 122-133.
9. Mallender, W. D., Szegletes, T. and Rosenberry, T. L. (1999). *J. Biol. Chem.* **274**: 8491-8499.
10. Mallender, W. D., Szegletes, T. and Rosenberry, T. L. (2000). *Biochemistry, in press*
11. Nachmansohn, D. and Wilson, I. B. (1951). *Adv. Enzymol.* **12**: 259-339.
12. Rosenberry, T. L. and Scoggin, D. M. (1984). *J. Biol. Chem.* **259**: 5643-5652.

13. Eastman, J., Wilson, E. J., Cervenansky, C. and Rosenberry, T. L. (1995). *J. Biol. Chem.* **270**: 19694-19701.

14. Marchot, P., Khelif, A., Ji, Y.-H., Masnuelle, P. and Bourgis, P. E. (1993). *J. Biol. Chem.* **268**: 12458-12467.

15. Ellman, G. L., Courtney, K. D., Andres, J., V. and Featherstone, R. M. (1961). *Biochem. Pharmacol.* **7**: 88-95.

16. Hosea, N. A., Radic, Z., Tsigelny, I., Berman, H. A., Quinn, D. M. and Taylor, P. (1996). *Biochemistry* **35**: 10995-11004.

17. Radic, Z. and Taylor, P. (1999). *Chem.-Biol. Interact.* **119-120**: 111-117.

18. Karlsson, E., Mbugua, P. M. and Rodriguez-Ithurralde, D. (1984). *J. Physiol. (Paris)* **79**: 232-240.

19. le Du, J. H., Marchot, P., Bourgis, P. E. and Fontecilla-Camps, J. C. (1992). *J. Biol. Chem.* **267**: 22122-22130.

20. Falkenstein, R. J. and Pena, C. (1997). *Biochem. Biophys. Acta* **1340**: 143-151.

21. Bourne, Y., Taylor, P. and Marchot, P. (1995). *Cell* **83**: 503-512.

22. Harel, M., Kleywegt, G. J., Ravelli, R. B. G., Silman, I. and Sussman, J. L. (1995). *Structure* **3**: 1355-1366.

23. Spatola, A. F., Crozet, Y., deWit, D. and Yanagisawa, M. (1996). *J. Med. Chem.* **39**: 3842-3846.

THE JOURNAL OF BIOLOGICAL CHEMISTRY
Vol. 276, No. 26, Issue of June 29, pp. 23282–23287, 2001

Printed in U.S.A.

Thioflavin T Is a Fluorescent Probe of the Acetylcholinesterase Peripheral Site That Reveals Conformational Interactions between the Peripheral and Acylation Sites*

Received for publication, October 20, 2000, and in revised form, April 18, 2001
Published, JBC Papers in Press, April 19, 2001, DOI 10.1074/jbc.M009596200

Giancarlo V. De Ferrari‡, William D. Mallender§¶, Nibaldo C. Inestrosa‡, and Terrone L. Rosenberry§‖

From the §Department of Pharmacology and Program in Neurosciences, Mayo Foundation for Medical Education and Research, Mayo Clinic Jacksonville, Jacksonville, Florida 32224 and the ‡Centro de Regulación Celular y Patología, Departamento de Biología Celular y Molecular, Facultad de Ciencias Biológicas, Pontificia Universidad Católica de Chile, Alameda 340, 114-D Santiago, Chile

Three-dimensional structures of acetylcholinesterase (AChE) reveal a narrow and deep active site gorge with two sites of ligand binding, an acylation site at the base of the gorge, and a peripheral site near the gorge entrance. Recent studies have shown that the peripheral site contributes to catalytic efficiency by transiently binding substrates on their way to the acylation site, but the question of whether the peripheral site makes other contributions to the catalytic process remains open. A possible role for ligand binding to the peripheral site that has long been considered is the initiation of a conformational change that is transmitted allosterically to the acylation site to alter catalysis. However, evidence for conformational interactions between these sites has been difficult to obtain. Here we report that thioflavin T, a fluorophore widely used to detect amyloid structure in proteins, binds selectively to the AChE peripheral site with an equilibrium dissociation constant of 1.0 μM. The fluorescence of the bound thioflavin T is increased more than 1000-fold over that of unbound thioflavin T, the greatest enhancement of fluorescence for the binding of a fluorophore to AChE yet observed. Furthermore, when the acylation site ligands edrophonium or *m*-(*N*, *N*,*N*-trimethylammonio)trifluoroacetophenone form ternary complexes with AChE and thioflavin T, the fluorescence is quenched by factors of 2.7–4.2. The observation of this partial quenching of thioflavin T fluorescence is a major advance in the study of AChE for two reasons. First, it allows thioflavin T to be used as a reporter for ligand reactions at the acylation site. Second, it indicates that ligand binding to the acylation site initiates a change in the local AChE conformation at the peripheral site that quenches the fluorescence of bound thioflavin T. The data provide strong evidence in support of a conformational interaction between the two AChE sites.

Acetylcholinesterase (AChE)[1] hydrolyzes the neurotransmitter acetylcholine at extremely high catalytic rates (1). Ligand binding studies (2) and x-ray crystallography (3) have revealed a narrow active site gorge some 20 Å deep with two separate ligand binding sites. During catalytic hydrolysis, the substrate acyl group is transferred briefly to residue Ser-200[2] in the acylation site at the bottom of the gorge. This site contains residues involved in a catalytic triad (His-440, Glu-327, Ser-200) and Trp-84, which binds to the trimethylammonium group of acetylcholine. The peripheral site near the mouth of the gorge includes, among others, residues Asp-72 and Trp-279. Recent investigations have shown that the peripheral site contributes to catalytic efficiency by transiently binding substrates on their way to the acylation site (4–6).

The question of whether the peripheral site plays additional roles in the catalytic process has long been of interest. Changeux (7) was among the first to appreciate that AChE contained two distinct ligand binding sites and that there may be allosteric interactions between ligands bound at these sites involving conformational changes in the protein molecule. Ligands bound to the peripheral site can inhibit or accelerate reactions at the acylation site, and these effects have often been attributed to conformational interactions between the sites (8, 9). However, direct evidence for such conformational interactions has been difficult to obtain. For example, three-dimensional structures of AChE complexes with two ligands specific for the acylation site, edrophonium and the cationic trifluoromethylketone TMTFA, showed no changes in the structure of the peripheral site (10, 11). In this report we show that thioflavin T (Fig. 1) binds specifically to the AChE peripheral site and is one of the most useful fluorescent probes of AChE yet discovered.

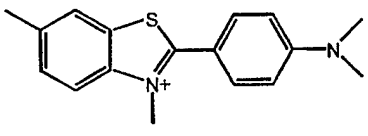

FIG. 1. **Structure of thioflavin T.**

This fluorophore frequently is used to detect amyloid structure in proteins (12), but the three-dimensional structure of the AChE peripheral site shows no indication of the extensive β

* This work was supported by Grant NS-16577 from the National Institutes of Health, Grant DAMD 17-98-2-8019 from the United States Army Medical Research Acquisition Activity, grants from the Muscular Dystrophy Association of America (to T. L. R.), Grant FONDAP N 13980001 and a Presidential Chair in Science from the Chilean Government (to N. C. I.), and Grant FONDECYT N 4000030 (to G. V. D.). The costs of publication of this article were defrayed in part by the payment of page charges. This article must therefore be hereby marked "*advertisement*" in accordance with 18 U.S.C. Section 1734 solely to indicate this fact.

¶ Current address: Millennium Pharmaceuticals, Inc., Cambridge, MA 02139.

‖ To whom correspondence should be addressed. Tel.: 904-953-7375; Fax: 904-953-7370; E-mail: rosenberry@mayo.edu.

[1] The abbreviations used are: AChE, acetylcholinesterase; TMTFA, *m*-(*N*,*N*,*N*-trimethylammonio)trifluoroacetophenone.

[2] Throughout this paper we number residues according to the *Torpedo* AChE sequence. For example, Trp-84 and Ser-200 in this sequence correspond to Trp-86 and Ser-203, respectively, in mammalian AChE.

sheet structure characteristic of amyloid. The intense fluorescence of thioflavin T bound to AChE is partially quenched by the binding of acylation site ligands in ternary complexes, and this quenching appears to result from a conformational interaction between the two sites.

EXPERIMENTAL PROCEDURES

Materials—Recombinant human AChE (13) was purified as outlined previously, and active site AChE concentrations were determined by assuming 450 units/nmol (6).[3] Thioflavin T chloride (Sigma) concentrations were assigned as 70% of the dry weight. Thioflavin T chloride recrystallized from water gave an extinction coefficient $\epsilon_{412\ nm}$ of 36,000 $M^{-1}\ cm^{-1}$. Concentrations of propidium iodide (Calbiochem) were determined with an extinction coefficient $\epsilon_{493\ nm}$ of 5900 $M^{-1}\ cm^{-1}$ (2), and concentrations of edrophonium chloride (ethyl(3-hydroxyphenyl)dimethylammonium chloride; Sigma) were determined with $\epsilon_{271\ nm}$ of 3400 $M^{-1}\ cm^{-1}$ from the dry weight (14). TMTFA (kindly provided by Dr. Daniel Quinn, University of Iowa) concentrations were calibrated by titration with AChE.

Steady State Inhibition of Enzyme-catalyzed Substrate Hydrolysis—Substrate hydrolysis rates v were measured in buffer (20 mM sodium phosphate and 0.02% Triton X-100 at pH 7.0) at 25 °C after addition of small aliquots of thioflavin T, acetylthiocholine, and 5,5′-dithiobis-(2-nitrobenzoic acid) (to a final concentration of 0.33 mM) in a total volume of 1.0 ml. An Ellman assay (15) was used to measure formation of the thiolate dianion of 5,5′-dithiobis-(2-nitrobenzoic acid) at 412 nm ($\Delta\epsilon_{412\ nm}$ = 14.15 $mM^{-1}\ cm^{-1}$; (16)) for 1–3 min on a Varian Cary 3A spectrophotometer, and substrate concentrations were corrected for substrate depletion resulting from hydrolysis during this interval. It was assumed that acetylthiocholine concentrations were maintained at low enough values (<1.0 mM) to ignore substrate inhibition in the absence of inhibitors (4). In this case, a simplified scheme for inhibition by peripheral site ligands is given in Scheme 1.

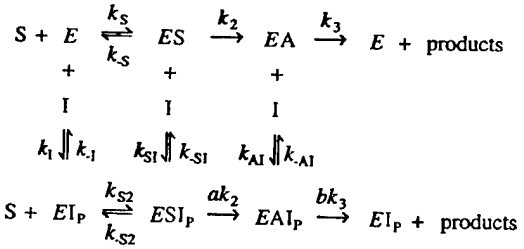

SCHEME 1

In this scheme, inhibitor (I) can bind to each of the three enzyme species: E, ES, and EA. For example, ESI_P represents a ternary complex with substrate (S) at the acylation site and I at the peripheral site (denoted by the subscript P). The acylation rate constant k_2 is altered by a factor α in this ternary complex. Reciprocal plots of v^{-1} versus $[S]^{-1}$ at all I concentrations here were linear, a result consistent with Scheme 1 (4, 17), and slopes of these plots were calculated by weighted linear regression analyses that assumed that v has a constant percent error. Plots of these slopes *versus* inhibitor concentration were fitted to Equation 1 by nonlinear regression analyses (Fig.P (BioSoft) version 6.0) with slope values weighted by the reciprocal of their variance (17).

$$\frac{\text{slope } (v^{-1}\ vs.\ [S]^{-1})}{K_{app}/V_{max}} = \frac{\left(1+\frac{[I]}{K_I}\right)}{\left(1+\frac{\alpha[I]}{K_I}\right)} \qquad \text{(Eq. 1)}$$

K_I is the equilibrium dissociation constant for I with E, and the experimental parameter α is simply the ratio of the second order rate constant with saturating I to that in the absence of I (17).

If thioflavin T (I1) can form a ternary complex with a second inhibitor (I2) and AChE, the residual concentration of free enzyme $[E]$ in the presence of both inhibitors relative to the concentration of free enzyme ($[E]_{[I2]=0}$) when only I1 is present is given by Equation 2 (18).

$$\frac{[E]}{[E]_{[I2]=0}} = \frac{K_2\left(1+\frac{[I1]}{K_1}\right)}{K_2\left(1+\frac{[I1]}{K_1}\right)+[I2]\left(1+\frac{[I1]}{K_{12}}\right)} \qquad \text{(Eq. 2)}$$

In this equation, K_1 is the equilibrium dissociation constant for I1 with E, K_2 is the equilibrium dissociation constant for I2 with E, and K_{12} is the equilibrium dissociation constant for I1 with the $EI2$ complex. The concentrations $[E]$ and $[E]_{[I2]=0}$ are proportional to the second order rate constants for substrate hydrolysis. Their ratio here was estimated from the relative v at 19 μM acetylthiocholine, a concentration sufficiently below the K_{app} of 50 μM for acetylthiocholine (17), to justify the approximation that substrate hydrolysis was second order.

Fluorescence Determinations of the Binding of Thioflavin T and Propidium to AChE—The fluorescence of either thioflavin T or propidium is enhanced when these ligands bind to the AChE peripheral site. Fluorescence was monitored on a Perkin-Elmer LS-50B luminescence spectrometer in 20 mM sodium phosphate buffer (pH 7.0) and 0.02% Triton X-100 thermostated at 23 ± 1 °C. Thioflavin T fluorescence was measured with excitation at 450 nm and emission from 470 to 500 nm with excitation and emission slits of 10 nm. Propidium fluorescence was monitored with excitation at 500 nm and emission from 590 to 630 nm with slits of 10 nm (2, 18). Total areas under the fluorescence emission curves (F) were calculated (unless otherwise noted), and fluorescence contributions from scatter in the buffer and enzyme were subtracted.

In some experiments values of F were fitted by nonlinear regression analysis (Fig.P) to Equation 3 (18).

$$F = f_L L_{tot} + 0.5(f_{EL} - f_L)\left[D - \sqrt{D^2 - 4E_{tot}L_{tot}}\right] \qquad \text{(Eq. 3)}$$

In Equation 3, f_L is the fluorescence intensity coefficient for free ligand, f_{EL} is the fluorescence intensity coefficient for bound ligand, E_{tot} is the total enzyme concentration, L_{tot} is the total ligand concentration, K_D is the equilibrium dissociation constant, and $D = E_{tot} + L_{tot} + K_D$. Data were fitted by nonlinear regression analysis (Fig.P) to Equation 3, either with L_{tot} as the independent variable and E_{tot} fixed or with the calculated E_{tot} as the independent variable and L_{tot} fixed, to give K_D, f_{EL}, and in some cases f_L. In these analyses, values of F were weighted by assuming constant percent error.

In other experiments, Scheme 2 was employed to evaluate interactions in ternary complexes involving thioflavin T and a second ligand in fluorescence assays. In this scheme the affinity of thioflavin T (L) at the peripheral site (denoted by subscript P) of AChE (E) is characterized by the dissociation constant K_L in the absence of an acylation site ligand (I) and by K_{L2} when I occupies the acylation site. When I was edrophonium, the binding of I to E and EL_P was assumed to reach equilibrium instantaneously with dissociation constants K_I and K_{I2}, respectively. Binding of I to E and EL_p was much slower when I was TMTFA and occurred with association rate constants k_I and k_{I2} and dissociation rate constants k_{-I} and k_{-I2}, respectively. The program SCoP (Simulation Resources, Inc., Redlands, CA; version 3.51) was applied directly to the

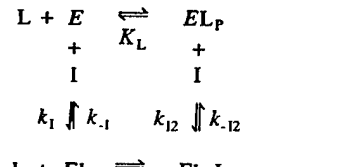

SCHEME 2

rate equations corresponding to Scheme 2 (17). This program solves differential equations with numerical solvers and allowed fitting of F at various inhibitor concentrations and/or times. The total concentrations E_{tot}, L_{tot}, and I_{tot}, as well as f_L, were inserted into the program as fixed input parameters. With edrophonium, the program simultaneously fit the fluorescence areas F to the edrophonium concentrations to determine five parameters: the three equilibrium constants (K_L, K_I, and K_{L2}), f_{EL}, and f_{EIL}, the fluorescence intensity coefficient for the ternary complex. With TMTFA, K_I also was fixed, and the program simulta-

[3] One unit of AChE activity corresponds to 1 umol of acetylthiocholine hydrolyzed/min under standard pH-stat assay conditions, and these conditions correspond to maximal AChE activity at pH 8 (31). Our conventional spectrophotometric assay at 412 nm is conducted in pH 7 buffer with 0.5 mM acetylthiocholine, conditions that result in 4.8 $\Delta A_{412\ nm}$/min with 1 nM AChE (or about 76% of the maximal activity).

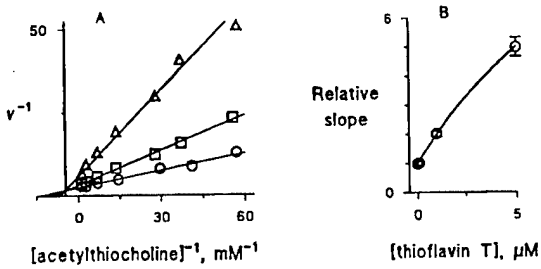

FIG. 2. **Steady state inhibition of AChE hydrolysis by thioflavin T.** *A*, reciprocal plots of initial velocities ($\Delta A_{412\ nm}$/min) and acetylthiocholine concentrations were analyzed by linear regression analysis. Thioflavin T concentrations were 0 (○), 1 μM (□), and 5 μM (△). *B*, the slopes of plots in *A* were normalized by dividing by the slope in the absence of inhibitor and plotted against the inhibitor concentration according to Equation 1 to derive $K_I = 0.90 \pm 0.13$ μM and $\alpha = 0.05 \pm 0.03$.

neously fit the time courses of fluorescence emission intensity at 480 nm (F_{480}) to the time after mixing to determine K_L, K_{L2}, f_{EL}, and f_{EIL} plus two additional parameters, k_I and k_{I2}.

RESULTS

Thioflavin T Inhibits Substrate Hydrolysis by AChE in a Manner Similar to Other Peripheral Site Inhibitors—A conventional steady state analysis of thioflavin T inhibition of AChE is shown in Fig. 2. Increasing concentrations of thioflavin T increase the slopes of the reciprocal plots in Fig. 2*A*, and a plot of these slopes *versus* thioflavin T concentration shows a slight curvature (Fig. 2*B*), consistent with a nonzero value of α in Equation 1. In the classical equilibrium analysis of Scheme 1, α is less than 1 when $aK_S/K_{S2} < 1$. However, we have recently shown that a nonequilibrium analysis provides a more accurate interpretation, and in this analysis α is less than 1 when $k_{S2} < k_S$ (17). The substrate association rate constant k_{S2} becomes smaller than k_S when the bound peripheral site ligand slows the entry of substrate to the acylation site, an effect we have termed steric blockade. The value of α of 0.05 obtained for thioflavin T here is similar to those found for the prototypic peripheral site inhibitors propidium and gallamine ($\alpha = 0.02$) (17), indicating that with bound thioflavin T k_{S2}/k_S is less than 0.05. In addition to demonstrating a substantial steric blockade by thioflavin T, the data in Fig. 2 indicate a competitive inhibition constant K_I for thioflavin T of 0.90 μM.

Thioflavin T Binds to the Peripheral Site, and Its Affinity Is Not Altered by the Binding of Edrophonium to the Acylation Site—To demonstrate that thioflavin T binds to the peripheral site, we measured the ability of two ligands to competitively inhibit thioflavin T binding in a substrate hydrolysis assay (18). Propidium is specific for the AChE peripheral site (2), whereas edrophonium is specific for the AChE acylation site (10), and both inhibited substrate hydrolysis in the absence of thioflavin T, as shown by the *open circles* and *dashed lines* in Fig. 3. If either of these ligands was completely competitive with thioflavin T such that no ternary complex could form, the decrease in v would correspond to the *dotted lines* in Fig. 3. This is essentially the case with propidium in Fig. 3*A*. The affinity of thioflavin T in the ternary complex decreased by a factor of 35 relative to its affinity in the free enzyme, a large change that was not significantly different from complete competition at the ligand concentrations employed. In contrast, the affinity of thioflavin T was no different in the ternary complex with edrophonium and in the free enzyme, and the *fitted line* with both inhibitors was superimposed on the *dashed line* for edrophonium alone in Fig. 3*B*. These data indicate that thioflavin T binds to the AChE peripheral site in a fashion that is essentially competitive with propidium.

The Fluorescence Enhancement of Thioflavin T Bound to AChE Is Much Larger than That of Propidium Bound to AChE—The fluorescence of thioflavin T was strikingly enhanced when it bound to AChE. An excitation peak at 448 nm and an emission peak at 486 nm became apparent, spectral characteristics similar to those of thioflavin T bound to Aβ amyloid (excitation maximum at 448 nm; emission maximum at 480 nm) (also see Ref. 12). To appreciate the fluorescence enhancement of thioflavin T when bound to the peripheral site of AChE, we compared it to the fluorescence enhancement observed with propidium bound to AChE. Prior to this report, propidium has been the fluorophore with the best reported fluorescence enhancement with AChE, and it is widely used as a reporter of ligand affinity at the AChE peripheral site (2, 9, 18). However, when AChE was titrated with varying concentrations of the two fluorophores (Fig. 4), the fluorescence enhancement f_{EL}/f_L for thioflavin T bound to AChE was greater than 1000, whereas that for propidium was about 7 (in agreement with a value of 10 obtained for propidium with *Torpedo* AChE (19)). Clearly, thioflavin T will be a more sensitive and versatile fluorescent reporter of ligand interactions with AChE than propidium has been. The titration in Fig. 4*A* also gave a K_D for thioflavin T binding of 0.89 μM, in good agreement with the K_I obtained in Fig. 2. Repeating this titration and analysis

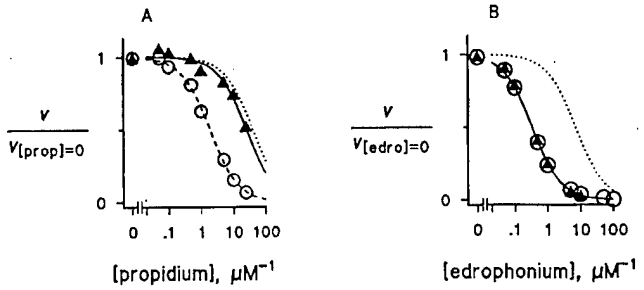

FIG. 3. **Determination of the relative affinity of thioflavin T in the propidium-AChE complex (*A*) or the edrophonium-AChE complex (*B*) by inhibition of substrate hydrolysis.** Mixtures of AChE (○, 25 pM; ▲, 200 pM), the indicated concentration of propidium or edrophonium without (○) or with (▲) thioflavin T (20 μM), 5,5′-dithiobis-(2-nitrobenzoic acid), and 20 μM acetylthiocholine were assayed over a 3–4-min interval. Hydrolysis rates v were normalized by the corresponding v obtained at the same thioflavin T concentration in the absence of propidium ($v_{[prop]=0}$) or edrophonium ($v_{[edro]=0}$). *Lines* correspond to normalized v obtained by fitting the experimental data to Equation 2. In these analyses K_1 for thioflavin T was assumed to be 1.0 μM (from Fig. 1). From the fitted curves without thioflavin T (*dashed lines*), K_2 for propidium was determined to be 1.87 ± 0.09 μM, and K_2 for edrophonium was determined to be 335 ± 14 nM. Ratios of K_{12}/K_1 from the fitted curves with 20 μM thioflavin T (*solid lines*) were 35 ± 9 with propidium and 1.01 ± 0.05 with edrophonium. The *dotted lines* correspond to the curves calculated when no ternary complex forms ($1/K_{12} = 0$).

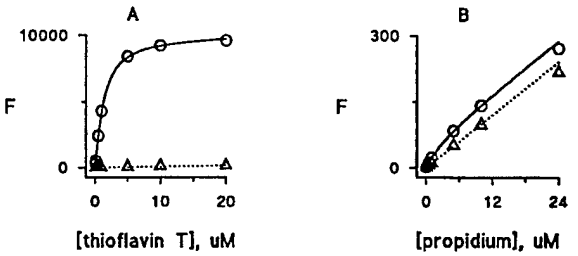

FIG. 4. **Fluorescence titrations of AChE with thioflavin T (*A*) and propidium (*B*).** Fluorescence values (F) were measured as outlined under "Experimental Procedures" at the indicated concentration of ligand (L_{tot}). The fluorescence intensity coefficients for the free ligands (f_F) were obtained from the slope of F *versus* L_{tot} in the absence of AChE (△). The fluorescence F in the presence of a fixed concentration of AChE (0.87 μM) (○) was then fitted to Equation 3 to obtain the fluorescence intensity coefficient for bound ligand (f_{EL}) and K_D for the ligand-AChE complex. For thioflavin T, $K_D = 0.89 \pm 0.05$ μM and $f_{EL}/f_L = 1300 \pm 100$; for propidium, $K_D = 2.4 \pm 0.9$ μM and $f_{EL}/f_L = 6.9 \pm 1.5$.

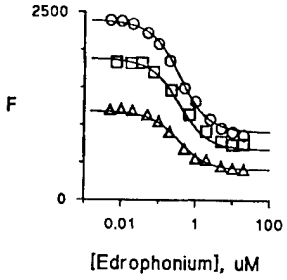

FIG. 5. **Edrophonium binding decreases the fluorescence of AChE-bound thioflavin T.** The fluorescence values (F) of mixtures of AChE (182 ± 20 nM), thioflavin T (○, 10 μM; □, 3 μM; △, 1 μM), and the indicated concentration of edrophonium were determined. The fluorescence intensity coefficient for free thioflavin T (f_L) was taken from Fig. 4 (8.8 units/μM), and F values from all three data sets were fitted with the SCoP program simultaneously, as outlined under "Experimental Procedures." The fitting gave K_L = 1.08 ± 0.03 μM for thioflavin T, K_I = 250 ± 10 nM for edrophonium, K_{L2}/K_L = 1.12 ± 0.02, f_{EL}/f_L = 1600 ± 200, and f_{EL}/f_{EIL} = 2.76 ± 0.02. Most of the standard error magnitudes arose from uncertainty in the AChE concentrations.

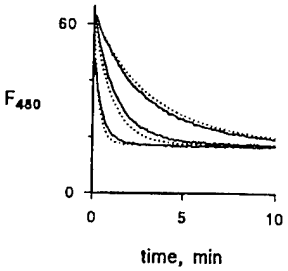

FIG. 6. **Thioflavin T fluorescence monitors the binding of TMTFA to the AChE acylation site.** Reactions were initiated by addition of TMTFA (1, 3, or 10 μM final concentration) to a mixture of AChE (182 ± 20 nM) and thioflavin T (1, 3, or 10 μM) and immediately transferred to the fluorometer, where the emission was monitored at 480 nm (F_{480}), as outlined under "Experimental Procedures." The time courses of F_{480} for each of the nine combinations of TMTFA and thioflavin T were fitted with the SCoP program simultaneously, as outlined under "Experimental Procedures" with K_I for TMTFA fixed at 49 pM (17). The fitting gave the following: K_L = 1.0 μM for thioflavin T; K_{L2}/K_L = 0.56; f_{EL}/f_L = 1600; f_{EL}/f_{EIL} = 4.2; k_I = 3.1 $\mu M^{-1}m^{-1}$; and k_I/k_{I2} = 60. Shown are the three time courses observed at 10 μM thioflavin T and 1 μM (*upper solid line*), 3 μM (*middle solid line*), and 10 μM (*lower solid line*) TMTFA and the corresponding fitted lines (*dotted*).

with a higher fixed concentration of AChE (10 μM) confirmed a 1:1 stoichiometry in the AChE-thioflavin T fluorescent complex (data not shown). Titrations also were conducted with a fixed concentration of thioflavin T (0.2 μM) and varying concentrations of AChE (10 nM–20 μM), and analysis with Equation 3 (18) again indicated a K_D of 0.8–0.9 μM (data not shown). Propidium (100 μM) was strongly competitive with thioflavin T in this titration protocol, because the apparent K_D for thioflavin T increased by at least a factor of 50.

The Binding of Acylation Site Ligands to the AChE-Thioflavin T Complex Decreases the Fluorescence Enhancement of Bound Thioflavin T—According to Fig. 3*B*, a ternary complex of thioflavin T and edrophonium can form with AChE without a loss in affinity of either ligand for its AChE site. We therefore asked whether the binding of an acylation site ligand altered the fluorescence of bound thioflavin T. We first examined the effect of increasing edrophonium concentrations and observed a decrease in the fluorescence as edrophonium saturated the acylation site (Fig. 5). Fitting of the data to Scheme 2 gave values of K_L for thioflavin T and K_I for edrophonium that were in agreement with those from Figs. 2–4 and again indicated almost no change in the affinities of these ligands for AChE in the ternary complex (K_{L2}/K_L = 1.12 ± 0.02, in agreement with K_{I2}/K_I = 1.01 ± 0.05 from Fig. 3*B*). However, the binding of edrophonium decreased the fluorescence of thioflavin T in the ternary complex by a factor of 2.8. The observation of this partial quenching of thioflavin T fluorescence is a major advance in the study of AChE for two reasons. First, it allows thioflavin T to be used as a reporter for ligand reactions at the acylation site. Second, it indicates that ligand binding to the acylation site alters the environment or the configuration of thioflavin T bound to the peripheral site, a point that we return to below.

To illustrate the first point we examined TMTFA, which forms a hemiketal with Ser-200 in the acylation site that is an analog of the transition state formed by acetylcholine (11, 20, 21). The high affinity of TMTFA in this complex allows the time course of its binding to be monitored over a wide range of TMTFA concentrations. Fluorescence traces for nine combinations of TMTFA and thioflavin T concentrations were recorded, and three representative reactions are shown in Fig. 6. The nine reaction time courses were fitted simultaneously to Scheme 2 with the SCoP program. Over this range of association rates the TMTFA concentrations were too high to evaluate K_I for TMTFA; so K_I was fixed at 49 pM as determined previously (17), and six remaining parameters were determined. A wealth of information was obtained. First, a K_L of 1.0 μM for thioflavin T and an enhancement in fluorescence of bound thioflavin T (f_{EL}/f_L) of 1600 were obtained, consistent with data in Figs. 4 and 5. Second, the affinities of thioflavin T and TMTFA in the ternary complex with AChE were at least as high as the affinities in their respective binary complexes (K_{L2}/K_L = K_{I2}/K_I = 0.56), in agreement with the previous observations for edrophonium in Figs. 3 and 5. Third, steric blockade of TMTFA binding by bound thioflavin T was evident (k_I/k_{I2} = 60), although the magnitude of the blockade was somewhat smaller than the nearly 400-fold decrease in association rate constant for TMTFA when propidium was bound to the peripheral site (17). Fourth, the binding of TMTFA decreased the fluorescence of thioflavin T in the ternary complex by a factor of 4.2. The extent of this quenching appears to be somewhat larger than that observed with edrophonium in Fig. 5, suggesting that the quenching of bound thioflavin T in ternary complexes with AChE may depend on the structure of the acylation site ligand. A quenching smaller than that obtained with either edrophonium or TMTFA was observed when Ser-200 was acylated with a methylethoxyphosphonyl group (data not shown), indicating that the acylation site ligand need not be cationic to quench the fluorescence of bound thioflavin T.

DISCUSSION

The discovery that the fluorescence of the AChE-thioflavin T complex is partially quenched when a ligand binds to the acylation site is of both practical and conceptual importance. In practical terms, this fluorescence change can be monitored to report on reactions at the acylation site. We illustrate this with TMTFA in Fig. 6, but similar protocols should allow the reactions of acylating agents like organophosphates to be measured over time courses as short as milliseconds. Conceptually, the partial quenching on the binding of acylation site ligands is the strongest evidence to date of conformational interaction between the peripheral and acylation sites of AChE. Although such conformational interaction has been widely invoked to account for a range of experimental data, close analysis indicates that previous evidence for such interactions is inconclusive.

A frequent assertion is that ligand binding to the peripheral site alters the conformation of the acylation site to reduce the efficiency of acylation or deacylation by substrates. This explanation has been offered to account for inhibition of substrate

hydrolysis by peripheral site ligands (9) and, when the substrate itself can bind to the peripheral site, for substrate inhibition at high substrate concentrations (22). As noted by Taylor and Radic (23), ligand association with the peripheral site also may prevent access of a cationic substrate to the acylation site by physically obstructing substrate entry or by charge repulsion between ligand and substrate. Before an allosteric interaction can be invoked, contributions from these other factors must be eliminated. Over the past 3 years, we have demonstrated that bound peripheral site ligands do physically obstruct the entry of substrates as well as of other ligands into the acylation site. Bound propidium decreases the association and dissociation rate constants for the acylation site ligands huperzine A and TMTFA by factors of 10–400. We have termed this effect steric blockade (17) and shown that similar decreases in the association rate constants for substrates and the dissociation rate constants for the alcohol products of substrate hydrolysis (*e.g.* thiocholine) are sufficient to account for the inhibition of substrate hydrolysis by peripheral site ligands (4, 17) as well as for substrate inhibition (4). Steric blockade in our terminology is strictly a kinetic effect, and it can have no influence on substrate affinity or hydrolysis by slowly reacting substrates like organophosphates that equilibrate with AChE before acylation. However, 5- to 10-fold decreases in organophosphate affinity for propidium-bound AChE were observed with both a cationic and a neutral organophosphate, indicating an additional type of interaction (6, 13). Molecular modeling calculations indicate that an organophosphate with a large leaving group would overlap with propidium if both ligands were placed in their expected sites in free AChE (13), and we have attributed these decreases in affinity to adjustments that accommodate both ligands in the ternary complex (6, 13). Modeling calculations indicate that such steric overlap is not a factor in ternary complexes involving propidium-AChE and either huperzine A or TMTFA; yet ligand affinities in the ternary complexes also are 5- to 7-fold lower than in the corresponding binary complexes (17). We have suggested that the decreased affinities arise from electrostatic interactions between these cationic ligands (17). In summary, experimental data indicate that the binding of a peripheral site ligand to AChE can result in steric blockade, steric overlap, and/or electrostatic interaction that inhibits substrate hydrolysis or reduces ligand affinity at the acylation site. With small peripheral site ligands like propidium and gallamine, we see no evidence of an additional allosteric conformational effect that contributes to inhibition.

More compelling indications of conformational interaction between the peripheral and acylation sites of AChE have come from two other experimental approaches. First, the spectral properties of a pyrenebutyl methylphosphono group attached to Ser-200 in the acylation site are altered slightly by the binding of gallamine to the peripheral site (24). The authors attributed these alterations to an increase in polarizability of the pyrenebutyl environment, perhaps due to torsional movements of aromatic side chains in the vicinity of the pyrenebutyl moiety induced by the binding of the peripheral site ligand. Second, bound peripheral site ligands can accelerate the reaction of acylating agents with Ser-200 in the acylation site. Gallamine accelerated the acylation of AChE by dimethylcarbamyl fluoride (25), and peripheral site inhibitors including propidium and gallamine increased the first order phosphorylation rate constants for neutral organophosphates with AChE (6, 13, 26). This rate constant reflects the transfer of the organophosphate group to Ser-200 in the binary or ternary complexes (equivalent to k_2 and ak_2, respectively, in Scheme 1). Before these effects can be attributed to a conformational change in the acylation site induced by ligand binding to the peripheral site, however, other explanations again must be eliminated. Foremost among alternative explanations is steric overlap as denoted above. One of the neutral organophosphates with accelerated first order phosphorylation when propidium is bound was also shown by molecular modeling to bind with AChE in a way that partially overlapped with the propidium binding site (13). We have argued that movement of the organophosphate to eliminate this overlap in the ternary complex could potentially induce strain in the bond to the organophosphate leaving group and thereby increase the phosphorylation rate constant (6). In like fashion, preliminary molecular modeling suggests that the pyrenebutyl methylphosphono group attached to Ser-200 is bulky enough to overlap partially with the peripheral site. Although the affinities of gallamine and propidium were similar for this modified AChE and for free AChE, a large thermodynamic interaction between the ligands is not necessary for there to be spectral changes due to the ligand proximity. Steric overlap thus remains a concern when conformational interactions between the peripheral and acylation sites are proposed. However, several pairs of peripheral site ligands and organophosphates (some with quite small leaving groups) showed the acceleration phenomenon (26). Because steric overlap is unlikely to generate the acceleration in all of these cases, it appears reasonable to infer a conformational change that promotes phosphorylation on ligand binding to the peripheral site.

Our data here are the first to indicate that ligand binding to the acylation site can alter the conformation of the peripheral site. The partial quenching of the fluorescence of bound thioflavin T when a ligand binds to the acylation site cannot result from fluorescence resonance energy transfer, because there is no spectral overlap between thioflavin T and either of the acylation site ligands edrophonium or TMTFA. However, the fluorescence of thioflavin T has been shown to depend on solvent viscosity (27), with a relationship previously described for a class of fluorescent dyes called molecular rotors (28, 29). These dyes show increased fluorescence when introduced into high viscosity media, due to a decreased torsional relaxation. Binding to the AChE peripheral site could reduce the torsional mobility of thioflavin T and account for its enhanced fluorescence. It is less clear how the binding of an acylation site ligand could partially quench this fluorescence in the ternary complex, but the quenching would appear to require an increase in the torsional mobility of bound thioflavin T induced by a change in the local AChE conformation that is initiated in the acylation site. The exact location of thioflavin T when bound to the AChE peripheral site remains to be determined, but it is unlikely that simple proximity to the acylation site ligand could account for the quenching. Crystal structures of bound edrophonium and bound TMTFA show that both ligands bind near the base of the acylation site, well away from the region that defines the peripheral site (10, 11). Furthermore, these ligands show no decrease in affinity in their ternary complexes with propidium-AChE, indicating no steric overlap. Ideally, one would like to support this proposed conformational interaction with additional data, but the conformational changes involved appear to be very small. Crystal structures of AChE and the TMTFA-AChE complex show a root mean square deviation of only 0.4 Å between equivalent C_α positions and no changes in the structure of the peripheral site (11). Electron paramagnetic resonance of AChE labeled with a spin-labeled organophosphate at Ser-200 gave no change in signal when propidium was bound to the peripheral site, although a small change was observed with monoclonal antibodies or the neurotoxin fasciculin, both of which bind to a larger surface area extending beyond the pe-

ripheral site (30). Therefore, we conclude that the quenching of the fluorescence of AChE-bound thioflavin T by acylation site ligands is the only method to date that is sensitive enough to reveal a conformational interaction between the two sites. This interaction may provide a mechanism for bound peripheral site ligands to accelerate acylation site reactions.

Acknowledgments—We express our gratitude to Samuel Pickett for maintenance of cell cultures and purification of recombinant human AChE and to Dr. Joseph Johnson and Matthew Davies for assistance with TMTFA reactions.

REFERENCES

1. Rosenberry, T. L. (1975) in *Advances in Enzymology* (Meister, A., ed.) Vol. 43, pp. 103–218, John Wiley & Sons, Inc., New York
2. Taylor, P., and Lappi, S. (1975) *Biochemistry* **14,** 1989–1997
3. Sussman, J. L., Harel, M., Frolow, F., Oefner, C., Goldman, A., Toker, L., and Silman, I. (1991) *Science* **253,** 872–879
4. Szegletes, T., Mallender, W. D., Thomas, P. J., and Rosenberry, T. L. (1999) *Biochemistry* **38,** 122–133
5. Tara, S., Elcock, A. H., Kirchhoff, P. D., Briggs, J. M., Radic, Z., Taylor, P., and McCammon, J. A. (1998) *Biopolymers* **46,** 465–474
6. Mallender, W. D., Szegletes, T., and Rosenberry, T. L. (2000) *Biochemistry* **39,** 7753–7763
7. Changeux, J.-P. (1966) *Mol. Pharmacol.* **2,** 369–392
8. Hucho, F., Jarv, J., and Weise, C. (1991) *Trends Pharmacol. Sci.* **12,** 422–426
9. Barak, D., Ordentlich, A., Bromberg, A., Kronman, C., Marcus, D., Lazar, A., Ariel, N., Velan, B., and Shafferman, A. (1995) *Biochemistry* **34,** 15444–15452
10. Harel, M., Schalk, I., Ehret-Sabatier, L., Bouet, F., Goeldner, M., Hirth, C., Axelsen, P. H., Silman, I., and Sussman, J. L. (1993) *Proc. Natl. Acad. Sci. U. S. A.* **90,** 9031–9035
11. Harel, M., Quinn, D. M., Nair, H. K., Silman, I., and Sussman, J. L. (1996) *J. Am. Chem. Soc.* **118,** 2340–2346
12. LeVine, H., III (1999) in *Methods in Enzymology* (Wetzel, R., ed) Vol. 309, pp. 274–284, Academic Press, Orlando, FL
13. Mallender, W. D., Szegletes, T., and Rosenberry, T. L. (1999) *J. Biol. Chem.* **274,** 8491–8499
14. Sharp, T. R., and Rosenberry, T. L. (1982) *J. Biochem. Biophys. Methods* **6,** 159–172
15. Ellman, G. L., Courtney, K. D., Andres, J. V., and Featherstone, R. M. (1961) *Biochem. Pharmacol.* **7,** 88–95
16. Riddles, P. W., Blakeley, R. L., and Zerner, B. (1979) *Anal. Biochem.* **94,** 75–81
17. Szegletes, T., Mallender, W. D., and Rosenberry, T. L. (1998) *Biochemistry* **37,** 4206–4216
18. Camps, P., Cusack, B., Mallender, W. D., El Achab, R., Morral, J., Muñoz-Torrero, D., and Rosenberry, T. L. (2000) *Mol. Pharmacol.* **57,** 409–417
19. Taylor, P., Lwebuga-Mukasa, J., Lappi, S., and Rademacher, J. (1974) *Mol. Pharmacol.* **10,** 703–708
20. Brodbeck, U., Schweikert, K., Gentinetta, R., and Rottenberg, M. (1979) *Biochim. Biophys. Acta* **567,** 357–369
21. Nair, H. K., Lee, K., and Quinn, D. M. (1993) *J. Am. Chem. Soc.* **115,** 9939–9941
22. Radic, Z., Reiner, E., and Taylor, P. (1991) *Mol. Pharmacol.* **39,** 98–104
23. Taylor, P., and Radic, Z. (1994) *Annu. Rev. Pharmacol. Toxicol.* **34,** 281–320
24. Berman, H. A., Becktel, W., and Taylor, P. (1981) *Biochemistry* **20,** 4803–4810
25. Kitz, R. J., Braswell, L. M., and Ginsburg, S. (1970) *Mol. Pharmacol.* **6,** 108–121
26. Radic, Z., and Taylor, P. (1999) *Chem. Biol. Interact.* **119–120,** 111–117
27. Friedhoff, P., Schneider, A., Mandelkow, E.-M., and Mandelkow, E. (1998) *Biochemistry* **37,** 10223–10230
28. Kung, C. E., and Reed, J. K. (1986) *Biochemistry* **25,** 6114–6121
29. Loutfy, R. O., and Arnold, B. A. (1982) *J. Phys. Chem.* **86,** 4205–4211
30. Sentjurc, M., Pecar, S., Stojan, J., Marchot, P., Radic, Z., and Grubic, Z. (1999) *Biochim. Biophys. Acta* **1430,** 349–358
31. Rosenberry, T. L., and Scoggin, D. M. (1984) *J. Biol. Chem.* **259,** 5643–5652

CHARACTERIZATION OF A HUMAN ACETYLCHOLINESTERASE MUTANT THAT EXHIBITS SUBSTRATE ACTIVATION KINETICS

Johnson, J.L., Davies, M.P., Venkatasubban, K.S., Cusack, B., Mallender, W.D., and Rosenberry, T.L.

Biophys J. **80**, 279a.

Acetylcholinesterase (AChE) is responsible for terminating nerve impulses at cholinergic synapses by hydrolyzing acetylcholine. Examination of AChE and closely related butyrylcholinesterase (BChE) crystal structures from a number of different organisms reveals a common architecture, but their kinetic profiles can vary. All characterized AChEs exhibit classic substrate inhibition: as the substrate concentration rises, the activity increases, peaks, and then declines (Panel A). However, substrate activation (higher activity than predicted at a given substrate concentration) has only been observed with native BChE and *Drosophila* AChE.

W86 is key in orienting the choline tail prior to substrate hydrolysis. In the W86F mutant, substrate activation is observed for the first time with human AChE. Eadie-Hofstee plots for wild type AChE and D74G show only substrate inhibition while W86F

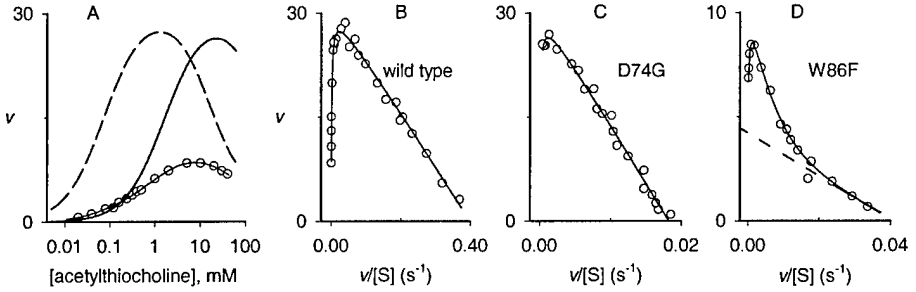

(Panel A) v vs. [S] curves for 80 pM wild type (– –), D72G (—), and W86F (–O–) AChE. *(Panels B-D)* Lines in Panel A were transformed to clarify the substrate activation, which corresponds to the deviation from the dashed line.

exhibits both features, as evidenced by the deviation from linearity (Panels B-D). We will expand our current AChE kinetic model to account for the observed substrate activation.

BIOGRAPHICAL SKETCH

Provide the following information for the key personnel in the order listed for Form Page 2.
Photocopy this page or follow this format for each person.

NAME	POSITION TITLE
Terrone L. Rosenberry	Consultant and Professor of Pharmacology

EDUCATION/TRAINING *(Begin with baccalaureate or other initial professional education, such as nursing, and include postdoctoral training.)*

INSTITUTION AND LOCATION	DEGREE *(if applicable)*	YEAR(s)	FIELD OF STUDY
Oberlin College, Oberlin, Ohio	A.B.	1965	Chemistry
University of Oregon, Eugene, Oregon	Ph.D.	1969	Biochemistry

RESEARCH AND PROFESSIONAL EXPERIENCE: Concluding with present position, list, in chronological order, previous employment, experience, and honors. Include present membership on any Federal Government public advisory committee. List, in chronological order, the titles, all authors, and complete references to all publications during the past three years and to representative earlier publications pertinent to this application. If the list of publications in the last three years exceeds two pages, select the most pertinent publications. **DO NOT EXCEED TWO PAGES.**

Professional Experience:

1965-1966	Teaching Assistant, Department of Chemistry, University of Eugene, OR
1969-1972	Research Associate, Department of Neurology, Columbia University, New York, NY
1975	NATO Senior Fellow, Max-Planck-Institute for Biophysical Chemistry, Gottingen, Germany
1977	Visiting Scientist, Max-Planck-Institute for Biochemistry, Martinsried near Munich, Germany
1972-1979	Assistant Professor of Biochemistry, Dept.of Neurology, Columbia University, New York, NY
1979-1985	Associate Professor of Pharmacology Case Western Reserve University, Cleveland, OH
1986-1987	Senior International Fellow (Fogarty Center, NIH) Institut Pasteur, Paris, France
1985-1996	Professor of Pharmacology, Case Western Reserve University, Cleveland, OH
1996-present	Professor of Pharmacology, Department of Neuroscience, Mayo Clinic Jacksonville, Jacksonville, FL

Honors:

1961-1965	Alfred P. Sloan Scholarship, Oberlin College
1965	Society of Sigma Xi
1965-1969	National Science Foundation Graduate Trainee, Dept. of Chemistry, Univ. of Oregon
1975	NATO Senior Fellowship in Science (NSF)
1979-1984	Journal of Biological Chemistry, Editorial Board
1985-1988	NIH Study Section (Neurology C)
1986-1987	Fogarty Senior International Fellowship (NIH)
1989-1996	Javits Neuroscience Investigator Award (NIH)
1994	Visiting Professor, University of Paris, Ecole Normale Superieure, Paris, France
1999	NIH Study Section, Chair (Molecular, Cellular and Developmental Neurobiology - 6)

Research Projects Ongoing or Completed in the last 3 years:

Interactions in the Active Site of Acetylcholinesterase — Principal Investigator: T. L. Rosenberry
Agency: NIH — Type: R01 NS 16577 — Period: 4/1/98-3/31/01
Assess the role of ligand binding to a peripheral site at the entrance to the AChE active site. Employ kinetic analysis of wild-type AChE and site-directed mutants and interpret by reference to the known AChE three-dimensional structure.

New Inhibitors of the Peripheral site in Acetylcholinesterase that Specifically Block Organophosphorylation
Principal Investigator: T. L. Rosenberry
Agency: U.S. Army Medical Research and Materiel Command — Type: USAMRMC Log No: 97027002
Period: 8/1/98-7/31/01
Design site-directed mutants and peripheral site ligands in which the rate of organophosphorylation of the active site is decreased much more than the rate of substrate hydrolysis.

Interactions in the Active Site of Acetylcholinesterase
Principal Investigator: T. L. Rosenberry
Agency: Muscular Dystrophy Assoc., USA Research Grant Period: 1/1/01-12/31/03
Assess the role of ligand binding to peripheral sites near the AChE active site gorge by kinetic analysis.

Expression and Purification of β-Secretase
Principal Investigator:.I.: T. L. Rosenberry
Alzheimer's Association Research Grant Period: 10/1/00-9/31/02
Express a truncated form of β-secretase (BACE), which generates Aβ peptides from the amyloid precursor protein, in our S2 insect cell expression system. Provide purified protein for crystallization by our collaborators at the Weizmann Institute.

Inhibitors of *in vitro* Amyloid Fibril Formation
Principal Investigator: R. C. Petersen
Subproject Director: T. L. Rosenberry
Agency: NIH Type: P50 AG16574 Period: 05/1/99-04/30/04
Examine the process of Aβ protofibril elongation and dissociation. Identify inhibitors of elongation or promoters of dissociation as potential drugs for the treatment of Alzheimer's disease.

Select Publications (from a total of 122):

Deeg, M.A., Humphrey, D.R., Yang, S.H., Ferguson, T.R., Reinhold, V.N., and Rosenberry, T.L. (1992). Glycan components in the glycoinositol phospholipid anchor of human erythrocyte acetylcholinesterase. Novel fragments produced by trifluoroacetic acid. *J. Biol. Chem.* **267**, 18573-18580.

Deeg, M.A., Murray, N.R., and Rosenberry, T.L. (1992). Identification of glycoinositol phospholipids in rat liver by reductive radiomethylation of amines but not in H4IIE hepatoma cells or isolated hepatocytes by biosynthetic labeling with glucosamine. *J. Biol. Chem.* **267**, 18581-18588.

Sevlever, D., and Rosenberry, T.L. (1993). Mannosamine inhibits the synthesis of putative glycoinositol phospholipid anchor precursors in mammalian cells without incorporating into an accumulated intermediate. *J. Biol. Chem.* **268**, 10938-10945.

Deeg, M.A., Brass, E.P., and Rosenberry, T.L. (1993). Inositol glycan phosphate derived from human erythrocyte acetylcholinesterase glycolipid anchor and inositol cyclic 1,2-phosphate antagonize glucagon activation of glycogen phosphorylase. *Diabetes* **42**, 1318-1323.

Mohney, R.P., Knez, J.J., Ravi, L., Sevlever, D., Rosenberry, T.L., Hirose, S. and Medof, M.E. (1994). Glycoinositol phospholipid anchor-defective K562 mutants with biochemical lesions distinct from those in Thy-1 murine lymphoma mutants. *J. Biol. Chem.* **269**, 6536-6542.

Haas, R. and Rosenberry, T.L. (1995). Protein denaturation by addition and removal of acetonitrile: Application to tryptic digestion of acetylcholinesterase. *Analyt. Biochem.* **224**, 425-427.

Sevlever, D., Humphrey, D.R. and Rosenberry, T.L. (1995). Compositional analysis of glucosaminyl(acyl)phosphatidyl-inositol accumulated in HeLa S3 cells. *Eur. J. Biochem.* **233**, 384-394.

Wongkajornsilp, A. and Rosenberry, T.L. (1995). Uptake of exogenous *sn*-1-acyl-2-*lyso*-phosphatidylinositol into HeLa S3 cells. Reacylation on the cell surface and metabolism to glucosaminyl(acyl)phosphatidylinositol. *J. Biol. Chem.* **270**, 9147-9153.

Eastman, J., Wilson, E.J., Cervenansky, C. and Rosenberry, T.L. (1995). Fasciculin 2 binds to a peripheral site on acetylcholinesterase and inhibits substrate hydrolysis by slowing a step involving proton transfer during enzyme acylation. *J. Biol. Chem.* **270**, 19694-19701.

Haas, R., Jackson, B.C., Reinhold, B., Foster, J.D. and Rosenberry, T.L. (1996). Glycoinositol phospholipid anchor and protein C-terminus of bovine erythrocyte acetylcholinesterase: Analysis by mass spectrometry and by protein and DNA sequencing. *Biochem.J.***314**, 817-25.

Wilson, E.J., Massoulie, J., Bon, S., and Rosenberry, T.L. (1996). The rate of thermal inactivation of *Torpedo* acetylcholinesterase is not reduced in the C231S mutant. *FEBS Lett.* **379**, 161-164.

Rosenberry, T.L., Rabl, C.R., and Neumann, E. (1996). Binding of the neurotoxin fasciculin 2 to the acetylcholinesterase peripheral site drastically reduces the association and dissociation rate constants for N-methylacridinium binding to the active site. *Biochemistry* **35**, 685-690.

Incardona, J.P. and Rosenberry, T.L. (1996). Construction and characterization of secreted and chimeric transmembrane forms of *Drosophila* acetylcholinesterase: A large truncation of the C-terminal signal peptide does not eliminate glycoinositol phospholipid anchoring. *Mol. Biol. Cell* **7**, 595-611.

Incardona, J.P. and Rosenberry, T.L. (1996). Replacement of the glycoinositol phospholipid anchor of *Drosophila* acetylcholinesterase with a transmembrane domain does not alter sorting in neurons and epithelia but results in behavioral defects. *Mol. Biol. Cell* **7**, 613-630.

Sevlever, D., Schiemann, D., Guidubaldi, J., Medof, M.E., and Rosenberry, T.L. (1997). Accumulation of glucosaminyl(acyl)phosphatidylinositol in an S3 HeLa subline expressing normal dolicholphosphomannose synthase activity. *Biochem. J.* **321**, 837-844.

Szegletes, T., Mallender, W.D., and Rosenberry, T.L. (1998). Nonequilibrium analysis alters the mechanistic interpretation of inhibition of acetylcholinesterase by peripheral site ligands. *Biochemistry* **37**, 4206-4216.

Szegletes, T., Mallender, W.D., Thomas, P.J., and Rosenberry, T.L. (1999). Substrate binding to the peripheral site of acetylcholinesterase initiates enzymatic catalysis. Substrate inhibition arises as a secondary effect. *Biochemistry* **38**, 122-133.

Mallender, W.D., Szegletes, T., and Rosenberry, T.L. (1999). Organophosphorylation of acetylcholinesterase in the presence of peripheral site ligands: Distinct effects of propidium and fasciculin. *J. Biol. Chem.* **274**, 8491-8499.

Sambamurti, K., Sevlever, D., Koothan, T., Refolo, L.M., Pinnix, I., Gandhi, S., Onstead, L., Younkin, L., Prada, C.M., Yager, D., Ohyagi, Y., Eckman, C.B., Rosenberry, T.L., and Younkin, S.G. (1999). Glycosylphosphatidylinositol anchored proteins play an important role in the biogenesis of the Alzheimer's amyloid β protein. *J. Biol. Chem.* **274**, 26810-26814.

Sevlever, D., Pickett, S., Mann, K.J., Sambamurti, K., Medof, M.E., and Rosenberry, T.L. (1999). Glycosylphosphatidylinositol anchor intermediates associate with Triton-insoluble membranes in subcellular compartments that include the endoplasmic reticulum. *Biochem J.* **343**, 627-635.

Camps, P., Cusack, B., Mallender, W.D., El Achab, R., Morral, J., Muñoz-Torrero, D., and Rosenberry, T.L. (2000). Huprine X is a novel high affinity inhibitor of acetylcholinesterase that is of interest for the treatment of Alzheimer's disease. *Mol. Pharmacol.* **57**, 409-417.

Harel, M., Kryger, G., Rosenberry, T.L., Mallender, W.D., Lewis, T., Fletcher, R.J., Guss, J.M., Silman, I., and Sussman, J.L. (2000). 3D structure of *Drosophila Melanogaster* acetylcholinesterase and of its complexes with putative insecticides. *Protein Sci.* **9**, 1063-1072.

Mallender, W.D., Szegletes, T., and Rosenberry, T.L. (2000). Acetylthiocholine binds to Asp74 at the peripheral site of human acetylcholinesterase as the first step in the catalytic pathway. *Biochemistry* **39**, 7753-7763.

Perrier, A., Cousin, X., Boschetti, N., Haas, R., Chatel, J.-M., Bon, S., Roberts, W.L., Pickett, S.R., Massoulié, J., Rosenberry, T.L., and Krejci, E. (2000). Two distinct proteins are associated with tetrameric acetylcholinesterase on the cell surface. *J. Biol. Chem.* **275**, 34260-34265.

Mallender, W.D., Yager, D. Onstead, L., Nichols, M.R., Eckman, C., Sambamurti, K., Kopcho, L.M., Marcinkevicience, J., Copeland, R.A., and Rosenberry, T.L. (2001). Characterization of recombinant, soluble β-secretase from an insect cell expression system. *Mol. Pharmacol.* **59**, 619-626.

Massiah, M.A., Viragh, C., Reddy, P.M., Kovach, I.M., Johnson, J., Rosenberry, T.L., and Mildvan, A.S. (2001). Short, strong hydrogen bonds at the active site of human acetylcholinesterase. Proton NMR studies. *Biochemistry* **40**, 5682-5690.

De Ferrari, G.V., Mallender, W.D., Inestrosa, N.C., and Rosenberry, T.L. (2001). Thioflavin T is a fluorescent probe of the acetylcholinesterase peripheral site that reveals conformational interactions between the peripheral and the acylation sites. *J. Biol. Chem.* **276**, 23282-23287.

Premkumar, D.R.D., Fukuoka, Y., Sevlever, D., Brunschwig, E., Rosenberry, T.L., Tykocinski, M.L., and Medof, M.E. (2001). Properties of exogenously added GPI-anchored proteins following their incorporation into cells. *J. Cell. Biochem.* **82**, 234-245.

Wongkajornsilp, A., Sevlever, D., and Rosenberry, T.L. (2001). Metabolism of exogenous *sn*-1-alkyl-*sn*-2-*lyso*-glucosaminyl-phosphatidylinositol in HeLa D cells: accumulation of glucosaminyl(acyl)phosphatidylinositol in a metabolically inert compartment. *Biochem J.*, **359**, 305-313.

BIOGRAPHICAL SKETCH

Provide the following information for the key personnel listed on the budget page.

NAME	POSITION TITLE
ARNO F. SPATOLA	PROFESSOR OF CHEMISTRY AND BIOCHEMISTRY

EDUCATION/TRAINING (Begin with baccalaureate or other initial professional education, such as nursing, and include post-doctoral training).

INSTITUTION AND LOCATION	DEGREE (IF APPLICABLE)	YEAR(S)	FIELD OF STUDY
Cornell University, Ithaca, NY	A.B.	1966	Chemistry
University of Michigan, Ann Arbor, MI	M.S.	1969	Chemistry
University of Michigan, Ann Arbor, MI	Ph.D.	1971	Chemistry
University of Arizona, Tucson, AZ	Postdoctoral	1973	

RESEARCH AND PROFESSIONAL EXPERIENCE: Concluding with present position, list in chronological order, previous employment, experience, and honors. Include present membership on any Federal Government public advisory committee. List in chronological order, the titles, all authors, and complete references to all publications during the past 3 years and to representative earlier publication pertinent to this application. If the list of publications in the last 3 years exceeds 2 pages, select the most pertinent publications. PAGE LIMITATIONS APPLY. DO NOT EXCEED 3 PAGES FOR THE ENTIRE BIOGRAPHICAL SKETCH PER INVESTIGATOR.

PROFESSIONAL EXPERIENCE

1983 – Present Professor of Chemistry, University of Louisville
1990 – Present Professor of Biochemistry, University of Louisville
1978 – 1983 Associate Professor, University of Louisville
1975 – 1990 Associate in Biochemistry, University of Louisville
1973 – 1978 Assistant Professor, University of Louisville
1971 – 1973 Postdoctoral Research Associate, University of Arizona, Tucson, AZ

ADMINISTRATIVE EXPERIENCE

1988 – 1992 Vice Chair, Department of Chemistry, University of Louisville
1998 – Present Director, Institute for Molecular Diversity and Drug Design, University of Louisville

AWARDS AND HONORS

University of Louisville Exceptional Performance Award 1998-1999
University of Louisville Trustees Research Recognition Award 1990
Delphi Award (U of L Dental School Research Award)
Planning Committee, American Peptide Symposium, 1985-91; Program 1995; 1997
Gordon Research Conference on the Chemistry and Biology of Peptides, Co-Chairman, 1990
Devoe-Raynolds Co. Faculty Award in Chemistry, 1990
American Peptide Society, Councilor (1999-05); elected Secretary 99-01

EDITORIAL BOARDS *Journal of Peptide Research*
Letters in Peptide Science

RESEARCH INTERESTS: Rational drug design; cyclic peptides and pseudopeptides; macrotorials, MMP inhibitors; solid phase synthesis and library deconvolution methods; diketopiperizines; peptide hormone analogs; peptidomimetics; NMR and molecular modeling; MALDI-TOF MS antitumor and antimicrobial agents.

PUBLICATIONS

Sougen Ma, John F. Richardson, Arno F. Spatola, "Solution and Solid State Structures of a Cyclic □[CH_2SO] Pseudopentapeptide," *J. Am. Chem. Soc.*, **113**, 8529-8530 (1991).

RESEARCH AND PROFESSIONAL EXPERIENCE (CONTINUED). PAGE LIMITATIONS APPLY.

DO NOT EXCEED 3 PAGES FOR THE ENTIRE BIOGRAPHICAL SKETCH PER INVESTIGATOR.

Mohmed K. Anwer, Arno F. Spatola, "Phase Transfer Catalyzed Cleavage of Peptides Linked to Merrifield Resins," *Tetrahedron Lett.*, **33**, 3121-3124 (1992).

Sougen Ma, Arno F. Spatola, "Conformation of □[CH_2NH] Pseudopeptides: Cyclo[Gly–Pro□[CH_2NH]Gly–D–Phe–Pro]–TFA and Cyclo[Gly–Pro□[CH_2NH]Gly–D–Phe–Pro]," *Int. J. Peptide Protein Res.*, **41**, 204-206 (1992).

Leszek Lankiewicz, C. Y. Bowers, G. A. Reynolds, V. Labroo, S. Vonhof, Arno F. Spatola, "Biological Activities of Thionated Thyrotropin-Releasing Hormone Analogs," *Biochem. Biophys. Res. Commun.*, **184**, 359-366 (1992).

Arno F. Spatola, "Synthesis of Pseudopeptides," in *Methods in Neurosciences*, Vol. 13 (P. Michael Conn, ed.), Academic Press, San Diego, pp. 19-42, 1993.

Ma, John F. Richardson, Arno F. Spatola, "Crystal Structures of Two Cyclic Pseudopentapeptides Containing □[CH_2SO] Backbone Surrogates, *Biopolymers*, **33**, 1101-1110 (1993).

Arno F. Spatola, "Posterior Pituitary Hormones," *Kirk-Othmer Encyclopedia of Chemical Technology*, vol. 13, 1995, pp. 391-406.

S. Rajagopal, A. F. Spatola, "The Mechanism of Palladium-Catalyzed Transfer Hydrogenolysis of Aryl Chlorides by Formate Salts," *J. Org. Chem.*, **60**, 1347-1355 (1995).

Arno F. Spatola, Krzysztof Darlak, Peteris Romanovskis, "Cyclic Peptide Libraries: Reducing Epimerization in Medium Sized Rings During Solid Phase Synthesis," *Tetrahedron Letters*, **37**, 591-594 (1996).

A. F. Spatola, P. Romanovskis, "Cyclic Peptide Libraries: Recent Developments" in *Peptide and Non-Peptide Libraries—A Handbook for the Search of Lead Structures*, G. Jung, ed., VCH Publishers, Weinheim, 1996, Chapter 11.

Arno F. Spatola, Y. Crozet, P. Romanovskis, E. Valente, "Cyclic Peptide Libraries," *Peptides, Chemistry, Structure and Biology, Proceedings of the Fourteenth American Peptide Symposium*, P. T. P. Kaumaya and R. S. Hodges, Eds., Mayflower Scientific Ltd., England, 1996, 281-282.

Jian J. Chen, Lynn M. Teesch, Arno F. Spatola, "Using Cyclic Peptide Mixtures as Probes for Metal Ion Host-Guest Interactions," *Letters in Peptide Science*, **3**, 17-24 (1996).

Bruce Walcheck, Julius Kahn, Joseph M. Fisher, Bruce B. Wang, R. Spencer Fisk, Donald G. Payan, Carol Feehan, Raj Betageri, Krzysztof Darlak, Arno F. Spatola, Takashi Kei Kishimoto, "Neutrophil rolling altered by inhibition of L-selectin shedding *in vitro*," *Nature*, **380**, 720-723 (1996).

Arno F. Spatola, Yvon Crozet, Damiane deWit, Masashi Yanagisawa, "Rediscovering BQ-123 (Endothelin Antagonist): A Self-Deconvoluting Cyclic Pentapeptide Library," *J. Med. Chem.*, **39**, 3842-3846 (1996).

Arno F. Spatola, "Combinatorial Chemistry and Molecular Diversity Course at the University of Louisville—A Description," *Network Science*, **2**, Issue 6, June, 1996.

James J. Wen, Arno F. Spatola, "A Systematic Approach for the Solid Phase Synthesis of Linear and Cyclic Pseudopeptide Libraries Containing □[CH_2NH] Amide Bond Surrogates," *J. Peptide Res.*, **49**, 3-14, (1997).

Jack J. Chen, Arno F. Spatola, "Solid Phase Synthesis of Peptide Hydroxamic Acids," *Tetrahedron Lett.*, **38**, 1511-1514 (1997).

A. F. Spatola, "Peptide Hormones," book chapter in *Peptides and Proteins*, Sidney M. Hecht, ed., Oxford Press: New York, 1998 p. 367-394.

Yvon Crozet, James J. Wen, Rachel O. Loo, Philip C. Andrews, Arno F. Spatola, "Synthesis and Characterization of Cyclic Pseudopeptide Libraries Containing Thiomethylene and Thiomethylene-sulfoxide Amide Bond Surrogates," *Molecular Diversity*, **3**, 261-267, 1998.

Peteris Romanovskis, Arno F. Spatola, "Preparation of Head-to-Tail Cyclic Peptides via Side Chain Attachment: Implications for Library Synthesis," *J. Peptide Research*, **52**, 356-374, 1998.

Peteris Romanovskis and Arno F. Spatola, "Head-to-Tail Cyclic Peptides and Cyclic Peptide Libraries," In: *The Amide Linkage: Significance in Chemistry, Biochemistry, and Materials Science*, Arthur Greenberg, Curt Breneman, and Joel F. Liebman, Editors, John Wiley, 2000, pp. 519-564.

John E. Burden, Peg Davis, Frank Porreca, and Arno F. Spatola, "Synthesis and Biological Activities of Position One and Three Transposed Analogs of the Opioid Peptide YKFA," *Bioorg. Med. Chem. Lett.* 9, 3441-3446 (1999).

William D. Mallender, Wanli Ma, Arno F. Spatola, Terrone L. Rosenberry, "Directed design of novel high affinity, peripheral site acetylcholinesterase ligands to defend the enzyme against inactivation by organophosphates," *Faseb J.* **13**, A1350 (1999).

Arno F. Spatola, Krzysztof Darlak, Peteris Romanovskis, "Synthesis of peptides with sulfur containing amide bond replacement," in: *Synthesis of Peptides and Peptidomimetics*, Houben-Weyl, Stuttgart, in press.

BIOGRAPHICAL SKETCH

Provide the following information for the key personnel in the order listed for Form Page 2.
Photocopy this page or follow this format for each person.

NAME	POSITION TITLE
Joseph L. Johnson, Ph.D.	Postdoctoral Fellow

EDUCATION/TRAINING *(Begin with baccalaureate or other initial professional education, such as nursing, and include postdoctoral training.)*

INSTITUTION AND LOCATION	DEGREE *(if applicable)*	YEAR(s)	FIELD OF STUDY
Brigham Young University, Provo, UT	B.S.	1995	Molecular Biology
Brigham Young University, Provo, UT	Ph.D.	1999	Biochemistry

RESEARCH AND PROFESSIONAL EXPERIENCE: Concluding with present position, list, in chronological order, previous employment, experience, and honors. Include present membership on any Federal Government public advisory committee. List, in chronological order, the titles, all authors, and complete references to all publications during the past three years and to representative earlier publications pertinent to this application. If the list of publications in the last three years exceeds two pages, select the most pertinent publications. **DO NOT EXCEED TWO PAGES.**

Professional experience

1994-1995	Undergraduate Research Assistant, Brigham Young University, Provo, UT
1995-1999	Graduate Research Assistant, Brigham Young University, Provo, UT
2000-present	Postdoctoral Research Fellow, Mayo Clinic, Department of Pharmacology, Jacksonville, FL

Awards, Fellowships and Honors

1990-1995	Trustee's scholar, BYU
1994	Office of Creative Work and Research scholarship
1996	Graduate Teaching Assistant Fellowship
1997,1999	Graduate Research Assistant Fellowship
1997	Best session presentation – Micro ACS Spring Research Conference
1997-1999	BYU Department of Chemistry and Biochemistry Travel Awards
1999	ASBMB Graduate Student Travel Award for 1999 Meeting
1999	Delbert A. Greenwood Award for the Outstanding Graduating Biochemist
2001-2003	NIH Postdoctoral Fellowship

Research Projects Ongoing or Completed in the last 3 years:

Acetylcholinesterase Inhibition by Fasciculin — Principal Investigator: J. L. Johnson
Agency: NIH — Type: F32 NS 41828 — Period: 5/1/01-4/30/03
Investigate the allosteric mechanism of fasciculin inhibition of AChE. Generate AChE and fasciculin site-directed mutants in order to elucidate the residues in the AChE ω-loop and loop 1 of fasciculin that are responsible for the allosteric effect.

Publications

Pead, S., Durrant, E., Webb, B., Larsen, C., Heaton, D., **Johnson, J.**, and Watt, G.D. (1995) Metal Ion Binding to Apo, Holo, and Reconstituted Horse Spleen Ferritin. *J. Inorg. Biochem.* 59, 15-27.

Johnson, J.L., Tolley, A.M., Erickson, J.A., and Watt, G.D. (1996) Steady-State Kinetic Studies of Dithionite Utilization, Component Protein Interaction, and the Formation of an Oxidized Iron Protein Intermediate during *Azotobacter vinelandii* Nitrogenase Catalysis. *Biochemistry* 35, 11336-11342.

Johnson, J.L., Norcross, D.C., Arosio, P., Frankel, R.B., and Watt, G.D. (1999) Redox Reactivity of Apo Animal Ferritins and Heteropolymers Assembled from Recombinant Heavy and Recombinant Light Human Chain Ferritins. *Biochemistry* 38, 4089-4096.

Johnson, J.L., Cannon, M., Frankel, R.B., and Watt, G.D. (1999) Forming the Phosphate Layer in Reconstituted Horse Spleen Ferritin and the Role of Phosphate in Promoting Core Surface Redox Reactions. *Biochemistry* 38, 6706-6713.

Erickson, J.A., Nyborg, A.C., **Johnson, J.L.**, Truscott, S.M., Gunn, A., Nordmeyer, F.R., and Watt, G.D. (1999) Enhanced Efficiency of ATP Hydrolysis during Nitrogenase Catalysis Utilizing Reductants That Form the All-Ferrous Redox State of the Fe Protein. *Biochemistry* 38, 14279-14285.

Nyborg, A.C., Erickson, J.A., **Johnson, J.L.**, Gunn, A., Truscott, S.M., and Watt, G.D. (2000) Reactions of *Azotobacter vinelandii* Nitrogenase Using Ti(III) as Reductant. *J. Inorg. Biochem.* 78, 371-381.

Nyborg, A.C, Erickson, J.A., **Johnson, J.L.**, and Watt, G.D. (2000) Reductant-Dependent ATP Utilization During Nitrogenase Catalysis: Studies Using Ti(III). In **Nitrogen Fixation: From Molecules to Crop Productivity** (Pedrosa, F.O., Hungria, M., Yates, M.G., and Newton, W.E.; Eds.), Kluwer Academic Publishers, Boston. pp.41-42.

Johnson, J.L., Nyborg, A.C., Wilson, P.E., Tolley, A.M., Nordmeyer, F.R., and Watt, G.D. (2000) Analysis of Steady State Fe and MoFe Protein Interactions during Nitrogenase Catalysis. *Biochim. Biophys. Acta* 1543, 24-35.

Johnson, J.L., Nyborg, A.C., Wilson, P.E., Tolley, A.M., Nordmeyer, F.R., and Watt, G.D. (2000) Mechanistic Interpretation of the Dilution Effect for *Azotobacter vinelandii* and *Clostridium pasteurianum* Nitrogenase Catalysis in Terms of Two Iron Proteins Interacting Cooperatively with the MoFe Protein. *Biochim. Biophys. Acta* 1543, 36-46.

Nyborg, A.C., **Johnson, J.L.**, Gunn, A., and Watt, G.D. (2000) Evidence for a Two-Electron Transfer Using the All-Ferrous Fe Protein during Nitrogenase Catalysis. *J. Biol. Chem.* 275, 39307-39312.

Massiah, M.A., Viragh, C., Reddy, P.M., Kovach, I.M., **Johnson, J.L.**, Rosenberry, T.L., and Mildvan, A.S. Short, Strong Hydrogen Bonds at the Active Site of Human Acetylcholinesterase: Protein NMR Studies. *Biochemistry*, 40, 5682-5690.

Posters and Presentations

Experimental Biology 2001, Orlando (2001) – "Characterization of a Human Acetylcholinesterase Mutant that Exhibits Substrate Activation Kinetics"

Biophysical Society Meeting, Boston (2001) – "Characterization of a Human Acetylcholinesterase Mutant that Exhibits Substrate Activation Kinetics"

International Congress on Nitrogen Fixation, Iguassu Falls, Brazil (1999) – "Nitrogenase Kinetics"

International Congress on Nitrogen Fixation, Iguassu Falls, Brazil (1999) – "Reductant-Dependant ATP Utilization During Nitrogenase Catalysis: Studies Using Ti(III)"

International Congress on Nitrogen Fixation, Iguassu Falls, Brazil (1999) – "Nitrogenase Activity Using Ti(III) as Reductant"

ASBMB Biochemistry and Molecular Biology '99, San Francisco (1999) – "Characterization of a Ferritin from *Clostridium pasteurianum*"

Micro ACS Spring Research Conference, BYU (1998) – "Characterization of a Ferritin from *Clostridium pasteurianum*"

Inorganic Biochemistry Summer Workshop, Athens, Georgia (1998) – "Kinetics of Nitrogenase"

Micro ACS Spring Research Conference, BYU (1998) – "Characterization of a Ferritin from *Thermus Aquaticus*"

International Conference of Iron in Biology and Medicine, St. Malo, France (1997) – "Properties of Phosphate Reconstituted HoSF Ferritin Cores"

Micro ACS Spring Research Conference, BYU (1997) – "Kinetics of Nitrogenase"

Micro ACS Spring Research Conference, BYU (1997) – "Iron Uptake by HoSF Ferritin"

Micro ACS Spring Research Conference, BYU (1997) – "Redox Properties of Ferritins"

Micro ACS Spring Research Conference, BYU (1996) – "Non-Redox Iron Release from Ferritin"

Rocky Mountain Regional ACS Meeting, Park City, UT (1995) – "Role of Phosphate in Ferritin"

Micro ACS Spring Research Conference, BYU (1995) – "Role of Phosphate in Ferritin"

BIOGRAPHICAL SKETCH

Provide the following information for the key personnel in the order listed for Form Page 2.
Photocopy this page or follow this format for each person.

NAME	POSITION TITLE
Bernadette Cusack, MAT	Senior Research Analyst, Level V

EDUCATION/TRAINING *(Begin with baccalaureate or other initial professional education, such as nursing, and include postdoctoral training.)*

INSTITUTION AND LOCATION	DEGREE *(if applicable)*	YEAR(s)	FIELD OF STUDY
Emmanuel College, Boston, MA	B.A.	1969	Biology
The Johns Hopkins University, Baltimore, MD	M.A.T.	1970	Biology

RESEARCH AND PROFESSIONAL EXPERIENCE: Concluding with present position, list, in chronological order, previous employment, experience, and honors. Include present membership on any Federal Government public advisory committee. List, in chronological order, the titles, all authors, and complete references to all publications during the past three years and to representative earlier publications pertinent to this application. If the list of publications in the last three years exceeds two pages, select the most pertinent publications. **DO NOT EXCEED TWO PAGES.**

Professional experience

1970-1972	Laboratory Assistant, Joslin Diabetes Center, Harvard Medical School, MA
1972-1976	Clinical Research Center Laboratory Supervisor, Massachusetts Institute of Technology, MA
1976-1980	Laboratory of Neuroendocrinology Supervisor, Massachusetts Institute of Technology, MA
1989-1992	Research Technologist, Mayo Clinic Jacksonville, Department of Pharmacology, FL
1992-present	Associate in Research, Mayo Clinic Jacksonville, Department of Pharmacology, FL
1997-present	Senior Research Analyst Level V, Mayo Clinic Jacksonville, Department of Pharmacology, FL
1997-present	Adjunct Professor of Natural Sciences, University of North Florida, FL

Awards, Fellowships and Honors

1969	Chairman for Eastern NewEngland Biological Conference, Spring
1969-1970	Full Fellowship, The Johns Hopkins University
1998	Gold Star Recipient of Mayo Clinic Above and Beyond Award for leading a group project (Women in Science Symposium)

Publications (from past 5 years)

Cusack, B., Jansen, K., McCormick DJ, Chou T, Pang Y, Richelson E. (2000). A single amino acid of the human and rat neurotensin receptors (subtype 1) determining the pharmacological profile of a species-selective neurotensin agonist. *Biochem Pharmacol.* **60,** (6)793-801.

Boules, M., **Cusack, B.**, Zhao, L., Fauq, A., McCormick, D.J. and Richelson, E. (2000). A novel neurotensin peptide given extracranially decreases food intake in rodents. *Brain Research.* **865,** 35-44.

Cusack, B., Boules, M., Tyler, B.M., Fauq, A., McCormick, D.J. and Richelson, E. (2000). Effects of a novel neurotensin peptide analog given extracranially on CNS behaviors mediated by apomorphine and haloperidol. *Brain Research.* **856,** (1-2) 48-54.

Camps, P., **Cusack, B.,** Mallender, W.D., El Achab, R., Morrral, J. Munoz-Torrero, D., and Rosenberry, T.L. (2000). Huprine X is a novel high affinity inhibitor of acetylcholinesterase that is of interest for the treatment of Alzheimer's Disease. *Molecular Pharmacology.* **57,** 409-417.

Cusack, B., Chou, T., Jansen, K., McCormick, D.J. and Richelson, E. (2000). Analysis of binding sites and efficacy of a species specific peptide at the rat and human neurotensin receptors. *J. Peptide Res.* **55,** (1) 72-80.

Tyler, B.M., Douglas, C.L., Fauq, A., Pang, Y-P., Stables, J.A., **Cusack, B.,** McCormick, D.J., and Richelson, E. (1999). *In Vitro* Binding and CNS Effects of Novel Neurotensin Agonists that Cross the Blood Brain Barrier. *Neuropharmacology.* **38,** (7) 1027-1034.

Tyler, B.M., Jansen, K., McCormick, D.J., Douglas, C.L., Boules, M., Stewart, J.A., Zhao, L., Lacy, B., **Cusack., B.,** Fauq, A. and Richelson, E. (1999). Peptide nucleic acids targeted to the neurotensin receptor and administered i.p. cross the blood-brain barrier and specifically reduce gene expression. *Proceedings of the National Academy of Sciences, USA*. **96,** 7053-7058.

Fauq A.H., Hong, F., **Cusack, B.,** Tyler, B.M., Ping-Pang, Y. and Richelson, E. (1998). Synthesis of (2S)-2-amino-3-(1H-4-indolyl)propanoic acid, a novel tryptophan analog for structural modification of bioactive peptides. *Tetrahedron-Asymmetr.* **9**, (23) 4127-4134.

Tyler, B.M., **Cusack, B.,** Douglas, C.L., Souder, T. and Richelson, E. (1998). Evidence for additional neurotensin receptor subtypes: Neurotensin analogs that distinguish between neurotensin-mediated hypothermia and antinociception. *Brain Research.* **792,** 246-252.

Tyler, B.M., Groshan, K., **Cusack, B**., and Richelson, E. (1998). *In vivo* studies with low doses of levocabastine and diphenhydramine, but not pyrilamine, antagonize neurotensin-mediated antinociception. *Brain Research.* **787,** 78-84.

Tyler, B.M., McCormick, D.J., Hoshall, C.V., Douglas, C.L., Groshan, K., Lacy, B.W., **Cusack, B**. and Richelson, E. (1998). Peptide nucleic acids cross cell membranes *in vivo*: demonstration by specific blockade of protein expression. *FEBS Letters.* **421,** 280-284.

Hong, F., Zaidi, J., Pang, Y-P., **Cusack, B.** and Richelson, E. (1997). Design, synthesis, and pharmacological evaluation of active pyrrole based, nonpeptidic analogs of neurotensin(8-13). *Journal of Chemical Society, Perkin Transactions 1.* **20,** 2997-3004.

Hong, F., **Cusack, B.,** Fauq, A. and Richelson, E. (1997). Peptidic and non-peptidic neurotensin analogs. *Current Medicinal Chemistry.* **4,** 421-434.

Hong, F., Pang, Y-P., **Cusack, B.** and Richelson, E. (1997). Design, synthesis, and pharmacological test of a quinoline based, nonpeptidic analog of neurotensin(8-13). *Journal of Chemical Society, Perkin Transactions.* 2083-2088.

Cusack, B., Groshan, K., McCormick, D.J., Pang, Y-P., Perry, R., Phung, C-T., Souder, T. and Richelson, E. (1996). Chimeric rat/human neurotensin receptors localize a region of the receptor sensitive to binding of a novel, species specific, picomolar affinity peptide. *Journal of Biological Chemistry.* **271,** (25) 15054-15059.

Pang, Y-P., **Cusack, B.,** Groshan, K., and Richelson, E. (1996). Proposed Ligand Binding Site of the Transmembrane Receptor for Neurotensin(8-13). *Journal of Biological Chemistry.* **271,** (25) 15060-15068.

Appendix 16

BIOGRAPHICAL SKETCH

Provide the following information for the key personnel listed on the budget page.

NAME	POSITION TITLE
PETERIS ROMANOVSKIS	SENIOR RESEARCH ASSOCIATE

EDUCATION/TRAINING (Begin with baccalaureate or other initial professional education, such as nursing, and include post-doctoral training).

INSTITUTION AND LOCATION	DEGREE (IF APPLICABLE)	YEAR(S)	FIELD OF STUDY
Polytechnical Institute of Riga, Riga, Latvia	M.S.	1961-65	Chemistry
Institute of Organic Synthesis, Riga, Latvia	Ph.D.	1966-80	Chemistry
Institute of Organic Synthesis, Riga, Latvia	D.Sc.	1990	Chemistry

RESEARCH AND PROFESSIONAL EXPERIENCE: Concluding with present position, list in chronological order, previous employment, experience, and honors. Include present membership on any Federal Government public advisory committee. List in chronological order, the titles, all authors, and complete references to all publications during the past 3 years and to representative earlier publication pertinent to this application. If the list of publications in the last 3 years exceeds 2 pages, select the most pertinent publications. PAGE LIMITATIONS APPLY. DO NOT EXCEED 3 PAGES FOR THE ENTIRE BIOGRAPHICAL SKETCH PER INVESTIGATOR.

PROFESSIONAL EXPERIENCE

1991 – Present University of Louisville, Studies on Cyclic Peptide Libraries
1980 – 1992 Experimental Plant, Institute of Organic Synthesis, Riga, Latvia, Production of synthetic peptide hormones
1966 – 1980 Institute of Organic Synthesis, Latvian Academy of Science, Riga, Latvia, Synthesis, structure-function organization of peptide bioregulators

PUBLICATIONS

Krzysztof Darlak, Peteris Romanovskis, and Arno F. Spatola, "Cyclic Peptide Libraries," Peptides, Chemistry, Structure and Biology, Proceedings of the Thirteenth American Peptide Symposium, Robert S. Hodges and John A. Smith, eds., ESCOM, Leiden, 1994, pp. 981-983.

Arno F. Spatola, Krzysztof Darlak, and Peteris Romanovskis, "Cyclic Peptide Libraries: Reducing Epimerization in Medium Sized Rings During Solid Phase Synthesis," Tetrahedron Letters, 37, 591-594 (1996).

A. F. Spatola and P. Romanovskis, "Cyclic Peptide Libraries: Recent Developments" in Peptide and Non-Peptide Libraries—A Handbook for the Search of Lead Structures, G. Jung, ed., VCH Publishers, Weinheim, 1996, Chapter 11, p. 327-347.

Arno F. Spatola, Y. Crozet, P. Romanovskis, and E. Valente, "Cyclic Peptide Libraries," Peptides, Chemistry, Structure and Biology, Proceedings of the Fourteenth American Peptide Symposium, P. T. P. Kaumaya and R. S. Hodges, Eds., Mayflower Scientific Ltd., England, 1996, 281-282.

Peteris Romanovskis and Arno F. Spatola, "Expanding Diversity in Cyclic Peptide Libraries: Side Chain Attachment Using Asp, Glu, Asn, Gln, Lys, Ser, and Tyr for Initial Peptide Resin Linkage," Peptides 1996, Proceedings of the European Peptide Symposium, 1998, pp. 761-762.

Arno F. Spatola, Yvon Crozet, Peteris Romanovskis, and David Vogel, "Expanding molecular diversity with pseudopeptides and macrotorials. Synthesis, characterization, and biological activities of macrocyclic combinatorial libraries," Peptides: Frontiers of Peptide Science. Proceedings of the 15th American Peptide Symposium, (James P. Tam and Pravin T. P. Kaumaya, Eds.) Kulwar Academic Publishers, 1999, pp. 28-30.

Peteris Romanovskis, David Mendel, Martin J. O'Donnell, William C. Scott, Arno F. Spatola, and Changyou Zhou, "Unnatural peptide synthesis (UPS): a positional scan study," Peptides: Frontiers of Peptide Science. Proceedings of the 15th American Peptide Symposium, (James P. Tam and Pravin T. P. Kaumaya, Eds.) Kulwar Academic Publishers, 1999, pp. 319-320.

Peteris Romanovskis and Arno F. Spatola, "Preparation of Head-to-Tail Cyclic Peptides via Side Chain Attachment: Implications for Library Synthesis," J. Peptide Research, 52, 356-374, 1998.

Peteris Romanovskis and Arno F. Spatola, "Head-to-Tail Cyclic Peptides and Cyclic Peptide Libraries," In: The Amide Linkage: Significance in Chemistry, Biochemistry, and Materials Science, Arthur Greenberg, Curt Breneman, and Joel F. Liebman, Editors, John Wiley, 2000, pp. 519-564.

RESEARCH AND PROFESSIONAL EXPERIENCE (CONTINUED). PAGE LIMITATIONS APPLY.

DO NOT EXCEED 3 PAGES FOR THE ENTIRE BIOGRAPHICAL SKETCH PER INVESTIGATOR.

Arno F. Spatola, Krzysztof Darlak, and Peteris Romanovskis, "Synthesis of peptides with sulphur containing amide bond replacement," in: Synthesis of Peptides and Peptidomimetics, Houben-Weyl, Stuttgart, submitted.

Peteris Romanovskis, Ned Smith, William E. Pierce, and Arno F. Spatola, "Simplified By-Product Analysis Using a Combination of MALDI-TOF Mass Spectrometry and Manual Parallel Solid Phase Synthesis of Cyclic Peptides," 26th European Peptide Symposium, Montpellier, France, September 10 – September 15, 2000.